

Analysis of Phosphatidylinositol Metabolism and ER-Mitochondria Contact Sites in the PINK1/Parkin Pathway

Thesis submitted in fulfilment of the degree of
Doctor of Philosophy at the University of Sheffield



By

Emma Wilson

Department of Biomedical Science University of
Sheffield

March 2018

LIST OF FIGURES.....	6
ABSTRACT.....	9
ACKNOWLEDGEMENTS.....	10
ABBREVIATIONS.....	12
1. INTRODUCTION.....	14
1.1 Parkinson's disease.....	15
1.1.1 Lewy Body Pathology.....	16
1.1.2 The Degeneration of Dopaminergic Neurones.....	16
1.2 Aetiology of PD.....	18
1.2.1 Genetics of PD.....	18
1.2.1.1 Autosomal Dominant familial Parkinson's disease.....	19
1.2.1.1.1 <i>SNCA</i> - α -Synuclein (<i>PARK1/4</i>).....	19
1.2.1.1.2 <i>LRRK2</i> – Leucine-Rich-Repeat kinase 2 (<i>PARK8</i>).....	20
1.2.1.2 Autosomal Recessive Familial Parkinson's disease (AR-JP).....	21
1.2.1.2.1 <i>Parkin</i> (<i>PARK2</i>).....	21
1.2.1.2.2 <i>PINK1</i> (<i>PARK6</i>).....	21
1.2.1.2.3 Synaptojanin 1 (<i>SYNJ1</i>) (<i>PARK20</i>).....	22
1.2.1.3 Genetics of Sporadic PD.....	23
1.2.2 Environmental risk factors of PD.....	23
1.3 Mechanisms of Disease in PD.....	24
1.3.1 Oxidative stress.....	24
1.3.2 Protein aggregation.....	25
1.3.3 Mitochondrial dysfunction.....	26
1.4 Mitochondrial quality control.....	28
1.4.1. Fission and Fusion.....	28
1.4.2 Mitophagy.....	30
1.4.2.1 PINK1 and Parkin Dependent Mitophagy.....	30
1.4.2.2 PINK1 and Parkin independent Mitophagy.....	36
1.4.2.3 Mitochondrial derived vesicles.....	37
1.5 ER-mitochondrial contact sites.....	38
1.5.1 Functions of ER-mitochondrial Contact sites.....	38
1.5.1.1 Lipid transfer and synthesis.....	38
1.5.1.2 Ca^{2+} Homeostasis.....	39
1.5.1.3 Mitochondrial morphology.....	40
1.5.1.4 Autophagy.....	40
1.5.1.5 Unfolded Protein Response (UPR).....	41
1.5.2 The Molecular Basis of ER-Mitochondria contact sites.....	42
1.5.2.1 ERMES.....	42
1.5.2.2 IP3R, Grp75 and VDAC.....	42
1.5.2.3 Mfn2.....	43
1.5.2.4 VAPB and PTPIP51.....	43
1.6 Phosphatidylinositol (PI) metabolism.....	44
1.6.1 Phosphatidylinositol 4 kinase III β (PI4KB).....	45
1.6.1.1 PI4KB Functions.....	47
1.6.2 Synaptojanin (Synj).....	49
1.7 Hypothesis and Aims.....	52
2: MATERIALS AND METHODS.....	53
2.1 <i>Drosophila</i> Genetics.....	54
2.1.1 <i>Drosophila</i> Husbandry.....	54
2.1.2 <i>Drosophila</i> lines.....	54
2.1.3 Climbing Assay.....	55
2.1.4 Flight Assay.....	56
2.2 Cell Culture Techniques.....	57

2.2.1 <i>Drosophila</i> Cell Lines.....	57
2.2.2 <i>Drosophila</i> Cell Culture.....	57
2.2.3 Human Cell lines	57
2.2.4 Cell Culture	57
2.2.5 Freezing down cells.....	58
2.3 Transfecting <i>Drosophila</i> cells lines	58
2.4 Transfecting Human Cell lines	59
2.4.1 Effectine transfection	59
2.4.2 Polyethylenimine, linear (PEI) Transfection.....	59
2.4.3 Transfecting CV1 Cells.....	59
2.4.4 Plasmids	60
2.5 Western Blotting.....	60
2.5.1 Cell Lysis	60
2.5.2 Protein quantification	61
2.5.3 SDS PAGE	61
2.5.4 Transfer	62
2.5.5 Blocking, Antibodies and Detection	63
2.6 Immunofluorescence	64
2.7 Antibodies and Dyes	65
Primary antibodies.....	65
Secondary antibodies and Fluorescent dyes.....	65
2.8 Gene Knockdown	65
2.8.1 Production of dsRNA	65
2.8.2 dsRNA mediated knockdown	66
2.8.3 siRNA acquisition	66
2.8.4 siRNA mediated knockdown.....	67
2.9 Methods of Analysis.....	68
2.9.1 Analysis of Parkin translocation and mitophagy	68
2.9.2 Analysis of mitochondrial morphology in <i>Drosophila</i> cells.....	68
2.9.3 Analysis of Mitochondrial Morphology in Human cells	68
2.9.4 Analysis of fluorescent intensity.	68
2.10 Fluorescence microscopy	69
2.10.1 Deltavision RT Deconvolution widefield Microscope	69
2.10.2 Olympus FV1000 Fluoview confocal Microscope.....	69
2.10.3 Olympus IX73 Microscope.....	69
2.11 Quantitative Real-Time PCR (qRT-PCR).....	70
2.11.1 RNA extraction	70
2.11.2 Reverse transcription of cDNA synthesis	70
2.11.3 Quantitative real time polymerase chain reaction.....	70
2.11.4 Melt Curve Analysis.....	71
2.11.5 Relative fold change analysis	71
2.12 Molecular DNA Techniques	73
2.12.1 Polymerase Chain Reaction (PCR).....	73
2.12.2 Ethidium bromide (EtBr) agarose gels.....	73
2.12.3 PCR clean up and agarose Gel extraction	73
2.12.4 Digestion.....	74
2.12.5 Ligation	74
2.12.6 Transformation	74
2.12.7 Colony PCR.....	75
2.12.8 Extraction of Plasmids	75
2.12.9 Sequencing.....	75
3. ANALYSIS OF <i>SYNJ</i> AND <i>FWD</i> IN <i>DROSOPHILA</i>	76
3.1 Background.....	77
3.2 Hypothesis and Aims	78

3.3 Genetic interactions of <i>synj</i> and <i>fwd</i> with <i>pink1</i> and <i>parkin</i>	79
3.3.1: The knockdown of <i>fwd</i> results in an expression dependent decrease in motor ability	79
3.3.2: The overexpression of <i>fwd</i> results in minimal effects of climbing ability	81
3.3.3 Mutations in <i>fwd</i> result in severe climbing but not flight defects.....	82
3.3.4: <i>fwd</i> does not genetically interact with mitochondrial fission/fusion genes	84
3.3.5: The knockdown of <i>fwd</i> and <i>synj</i> does not alter Mitochondrial morphology in S2R+ <i>Drosophila</i> cells.	87
3.3.6: The overexpression of <i>GFP-fwd</i> and <i>GFP-synj</i> does not alter Mitochondrial morphology in S2R+ <i>Drosophila</i> cells.	90
3.3.7: The overexpression of <i>synj</i> results in a minimal effect on climbing ability.	93
3.3.8: The knockdown of <i>synj</i> results in an expression dependent decrease in motor ability.	94
3.3.9: <i>synj</i> does not genetically interact with <i>pink1^{B9}</i> or <i>park²⁵</i>	95
3.3.10: The reduction or loss of <i>fwd</i> does not result in any change to the motor phenotype of a <i>pink1^{B9}</i> or <i>park²⁵</i> mutant <i>Drosophila</i>	98
3.3.11: The overexpression of <i>fwd</i> partially suppresses climbing defects in <i>pink1^{B9}</i> and <i>park²⁵</i> mutants.	102
3.4 Discussion	104
4. THE ANALYSIS OF <i>PI4KB</i> AND <i>SYNJ</i> IN YFP-PARKIN HELA CELLS	108
4.1 Background	109
4.2 Hypothesis and Aims	110
4.3 Investigation of <i>PI4KB</i>, <i>SYNJ</i> loss in the <i>PINK1</i>/<i>Parkin</i> pathway	110
4.3.1: The transfection of <i>PI4KB</i> , <i>SYNJ1</i> or <i>SYNJ2</i> <i>siRNA</i> in YFP-Parkin HeLa cells results in an efficient knockdown in mRNA levels.	110
4.3.2: The silencing of <i>PI4KB</i> or <i>SYNJ</i> in YFP-Parkin HeLa cells does not alter mitochondrial morphology	112
4.3.3: The knockdown of <i>PI4KB</i> in YFP-Parkin HeLa cells slows Parkin translocation	115
4.3.4: The knockdown of <i>SYNJ</i> in YFP-Parkin HeLa cells results in reduced Parkin translocation.	119
4.3.5: The <i>SYNJ1</i> constructs are readily expressed in HeLa, YFP-HeLa and HEK cells.	124
4.3.6 The overexpression of <i>SYNJ1</i> in YFP-Parkin HeLa cells causes no change in Parkin translocation	126
4.3.7 The knockdown of <i>PI4KB</i> in YFP-Parkin HeLa cells results in a mitophagy defect.	130
4.3.8: The knockdown of <i>SYNJ</i> in YFP-Parkin HeLa cells results in a mitophagy defect	134
4.4 Discussion	136
5. VISUALISATION OF ER-MITOCHONDRIA CONTACT SITES	141
5.1 Background	142
5.2 Hypothesis and Aims	142
5.3 Two novel systems to visualise ER-Mitochondrial contact sites	143
5.3.1: A new system for looking at ER-mitochondria contact sites: Bimolecular Fluorescence Complementation (BiFC)	143
5.3.1.1: The BiFC constructs express in HeLa cells.....	146
5.3.1.2: Co-expression of VC155-VAPBTM with PTPIP51TM-VN155 produces mVenus fluorescence at ER-mitochondria contacts.....	150
5.3.1.3: The BiFC system reports on an increase in ER-Mitochondrial contact sites.	153

5.3.1.4: Decreasing ER-mitochondria contact sites does not result in a decrease in BiFC mVenus fluorescence.....	162
5.3.2: Dimerization dependent GFP (ddGFP) as a reporter of ER-mitochondria contact.....	166
5.3.2.1: Expression and localisation of the ddGFP ER-mitochondria contact probes.....	169
5.3.2.2: The ddGFP ER-mitochondria contact probes report on ER-mitochondria contact.....	173
5.4 Discussion	175
6.DISCUSSION	180
6.1: Phosphatidylinositol metabolism	181
6.1.1 Phosphatidylinositol metabolism in neurodegeneration	181
6.2.2 Phosphatidylinositol metabolism in mitochondrial quality control.....	181
6.2: Synaptic vesicle trafficking and PD.....	182
6.3 Mitochondrial quality control, ER-mitochondria contact sites and PD	184
6.4 Current methods to visualise ER-mitochondrial contact sites.....	188
6.4.1 Electron microscopy (EM), confocal microscopy, super resolution microscopy	188
6.4.2 Fluorescent protein based systems.....	189
6.5 Further work.....	191
7. REFERENCES	193

LIST OF FIGURES

Figure 1.1: Parkinson's disease pathology.....	18
Figure 1.2: Mitochondrial fission and fusion.....	29
Figure 1.3: Mitochondrial fission and fusion.....	30
Figure 1.4: PINK1 degradation.....	31
Figure 1.5: PINK1 and Parkin dependent mitophagy.....	35
Figure 1.6: Lipid metabolism at ER mitochondrial contact sites.....	39
Figure 1.7: Molecular component functions of ER-mitochondrial contact sites.....	44
Figure 1.9: The localisation of PI4K isoforms and the processes they regulate.....	47
Figure 1.10: Synaptojanin isoforms and functions.....	50
Figure 2.1: Climbing apparatus.....	55
Figure 3.1: The knockdown of <i>fwd</i> results in an expression dependent decrease in motor ability.....	80
Figure 3.2: The overexpression of <i>fwd</i> has minimal effects on climbing and flight ability.....	81
Figure 3.3: Mutations in the <i>fwd</i> gene result in sever climbing defects that can be rescued by the overexpression of <i>fwd</i>	83
Figure 3.4: Loss of <i>Opa1</i> ^{s3475} rescues the climbing defect of <i>pink1</i> ^{B9} mutants.....	85
Figure 3.5: The genetic manipulations to increase mitochondrial fission has no effect on the <i>fwd</i> phenotype.....	86
Figure 3.6: Mitochondrial Morphology scoring scale.....	88
Figure 3.8: The overexpression of <i>fwd</i> or <i>synj</i> does not alter mitochondrial morphology in S2R+ <i>Drosophila</i> cells.....	91
Figure 3.9: The overexpression of <i>synj</i> results in minimal effects of climbing ability:.....	93
Figure 3.10: The knockdown of <i>synj</i> results in an expression dependent decrease in motor ability.....	94
Figure 3.11: The depletion of <i>synj</i> in a <i>pink1</i> ^{B9} or <i>park</i> ²⁵ mutant background has no effect on climbing but does show a minimal rescue of flight.....	97
Figure 3.12: The depletion of <i>fwd</i> in a <i>pink1</i> ^{B9} or <i>park</i> ²⁵ mutant background has no effect on climbing or flight:.....	99
Figure 3.13: The depletion of <i>fwd</i> in a <i>pink1</i> ^{B9} or <i>park</i> ²⁵ mutant background has no effect on climbing or flight:.....	100
Figure 3.14 The overexpression of <i>fwd</i> results in a rescue of both <i>pink1</i> ^{B9} and <i>park</i> ²⁵ mutant climbing ability.....	103
Figure 4.1: The qPCR analysis <i>PINK1</i> , <i>PI4KB</i> , <i>SYNJ1</i> and <i>SYNJ2</i>	111

Figure 4.2: The knockdown of PI4KB or SYNJ in YFP-Parkin HeLa cells does not result in changes to mitochondrial morphology	114
Figure 4.3: Parkin translocation scoring system.....	115
Figure 4.4: The knockdown of <i>PI4KB</i> in YFP-Parkin HeLa cells results in a Parkin translocation defect	118
Figure 4.5: The knockdown of <i>SYNJ1</i> in YFP-Parkin HeLa cells results in a slowing of Parkin translocation	121
Figure 4.6: The double knockdown of <i>SYNJ1</i> and <i>SYNJ2</i> in YFP-Parkin HeLa cells result in a Parkin translocation defect	123
Figure 4.7: SYNJ1-145, SYNJ1-170 and SYNJ1-145 R219Q FLAG tagged constructs express in YFP-Parkin HeLa and HEK293 cells	125
Figure 4.8: The overexpression of SYNJ1 in YFP-Parkin HeLa cells results in no Parkin translocation defect:	129
Figure 4.9: The mitophagy scoring system	131
Figure 4.10: The knockdown of <i>PI4KB</i> in YFP-Parkin HeLa cells results in slowing of mitophagy:.....	133
Figure 4.11: The knockdown of <i>SYNJ</i> in YFP-Parkin HeLa cells results in slowing of mitophagy	135
Figure 5.1: The BiFC system.....	145
Figure 5.2: The BiFC constructs express in HeLa cells	147
Figure 5.3: Myc-PTPIP51 TM -VN155 localises to mitochondria	148
Figure 5.4: VC155-VAPB TM localises to the ER	149
Figure 5.5: The HA-VC155-VAPB TM and Myc-VN155-PTPIP51 TM probes are functional in HeLa cells.....	152
Figure 5.6: Increasing ER-mitochondria contacts using an OMM-ER linker does not increase in BiFC mVenus fluorescence	156
Figure 5.7: Increasing ER-mitochondria contacts using HA-PTPIP51 does not increase in BiFC mVenus fluorescence:	158
Figure 5.8: Increase ER-mitochondria contact by inducing ER stress results in an increase in BiFC mVenus fluorescence	161
Figure 5.9: Knockdown of PTPIP51 or VAPB does not affect BiFC mVenus fluorescence	164
Figure 5.10: The ddGFP system	168
Figure 5.11: Expression of ddGFP ER-mitochondria contact probes in HEK293 cells	170
Figure 5.12: PTPIP51 TM -ddGFP ^A and PTPIP51 TM -ddGFP ^B localise to the mitochondria	171

Figure 5.13: ddGFPB-VAPBTM and ddGFPA-VAPBTM localise to the ER.....	172
Figure 5.14. The ddGFP ER-mitochondria contact probes report on ER-mitochondria contact	174
Figure 5.15: The expression of RFP-Linker or HA-PTPIP51 disrupts binding of VN155 to VC155 VAPBTM.....	177
Figure 6.1: Hypothetical model for the relationship between PI metabolism and mitochondrial quality control.....	187

ABSTRACT

PINK1 and *Parkin* are two genes which are commonly mutated in autosomal-recessive juvenile PD (AR-JP). They function in a common mitochondrial quality control pathway to regulate mitochondrial homeostasis. Under mitochondrial depolarization *PINK1*, a serine/threonine kinase, is stabilized on the outer mitochondrial membrane (OMM) where it recruits *Parkin*, an E3 ubiquitin ligase, from the cytosol. *Parkin* then ubiquitinates OMM proteins to aid in the recruitment of the phagophore to the mitochondria and the process of mitophagy. More recently reports have suggested that *PINK1* and *Parkin* are also present at ER-mitochondrial contact sites and may contribute to mitochondrial homeostasis by altering contacts. *SYNJ1*, a neuronal phosphatidylinositol phosphatase, is also mutated in AR-JP and *fwd*, a phosphatidylinositol kinase, was reported to alter mitochondrial morphology in *Drosophila* cells. Together *SYNJ1/synj* and *PI4KB/fwd* act to modulate the phosphatidylinositol balance, therefore it was hypothesized that PI metabolism may be a regulatory factor in the *PINK1/Parkin* pathway and mitochondrial quality control. To examine the effects of manipulating *synj* or *fwd*, *Drosophila* and YFP-*Parkin* HeLa cells models were used to investigate genetic interactions with *pink1* and *parkin*. A further aim was to develop a new tool to visualize ER-mitochondrial contact sites in real time, which would allow visualization of dynamic functions of ER-mitochondrial contact sites. This study found that the loss of *fwd* *in vivo* caused a significant decrease in climbing but not flight ability in adult *Drosophila*. This was not thought to be attributed to changes in mitochondrial morphology. However, the overexpression of *fwd* resulted in a partial rescue of *pink1*^{B9} and *park*²⁵ climbing defect. The silencing of *PI4KB* and *SYNJ1* in YFP-*Parkin* HeLa cells slowed *Parkin* translocation and mitophagy however loss of *SYNJ2* did not. Furthermore, Bimolecular Fluorescence complementation (BiFC) and dimerization dependent GFP (ddGFP) were tested for visualizing of ER-mitochondrial contact sites. Both systems were functional producing fluorescence when co-expressed. The BiFC probes could report on increases in ER-mitochondrial contact sites, however, changes in mitochondrial morphology were observed and suggested that the BiFC and ddGFP systems has some degree of irreversibility, increasing ER-mitochondrial contact sites. This study reveals an interesting link between phosphoinositide metabolism and mitochondrial quality control and high lights a new tool to potentially investigate this further.

ACKNOWLEDGEMENTS

I would like to take this opportunity to thank a number of people who have helped me through this exciting yet challenging period of my life.

Firstly, I would like to send a huge thank you to my supervisor Dr Alexander Whitworth for giving me the opportunity to do a PhD and for his continual guidance throughout the 4 years. He did all he could to help me with my scientific writing, which I find particularly difficult and for that I am very grateful. I would also like to say thank you to Dr Kurt De Vos who adopted me into his lab un-expectantly half way through my PhD. Since then has been a great driving force in developing my skills as a scientist.

I would also like to thank Dr Alvaro Sanchez-Martinez who was the first post doc I worked with. I appreciate his patience and advice both professionally and personally throughout my PhD. I would also like to thank Dr Rachael Ivatt who worked closely with me in the initial stages of my project. She truly was an inspiration and someone to aspire to be like. I would also like to extend a big thank you to all Whitworth lab members who also helped get me through my project including Vinay Godena, Caspar Baldwin, Simon Sattler and Roberta Tufi.

I would also like to separately say thank you to the De Vos and Grierson lab who welcomed me into their lab making the transition from Firth Court to SITraN easier. In particular, I would like to thank Miss Becky Cohen who has not only spell checked most of my thesis but also has become a life-long friend and supported me throughout the last 2 years. I could not have got this far without her. Additionally, I'd like to thank Miss Emma Smith who was always the person I'd turn to if I had any questions. Thank you for being so patient.

My time doing my PhD has been turbulent I don't feel I would have coped without the support of my friends so I want to say a huge thank you to them.

In particular, those friends I made at Sheffield University Jiu Jitsu club who, on multiple days of the week, allow me to repeatedly slam them into the ground I would not have retained my sanity without having that stress relief. Specifically, I would like to thank Miss Clara Alvarez-Lopez and Dr Mary Snape for helping spell check my thesis and for always being available for a drink and chat if I needed it.

I would also like to extend a special thank you to Amy Keerie who was there for me when I was hospitalised with a pulmonary embolism last year. I could not have got through it without her.

ABBREVIATIONS

[Ca ²⁺] - Calcium concentration	IBR - Inbetween RING
AP2 - Adaptor protein 2	IMM - Inner mitochondrial membrane
AR-JP - Autosomal Recessive – Juvenile Parkinson's disease	IMS - Intermembrane space
ATP - Adenosine Tri-Phosphate	IP ₃ R - inositol 1,4,5 triphosphate receptor
Ca ²⁺ - Calcium	L -DOPA - L-3,4-dihydroxyphenylalanine
CCCP - Carbonyl cyanide m-chlorophenyl hydrazine	LB - Luria-Bertani [broth]
CERT - Ceramide transport protein	LIR - LC3-interacting region
CL- Cardiolipin	<i>LRK2</i> - Leucine-Rich-Repeat kinase 2
CME - Clathrin mediated endocytosis	MDV - Mitochondrial derived vesicles
COR - C-terminus of ROC	MEF - Mouse embryonic fibroblast [cells]
DAQ - Dopamine-quinones	MEM - Modified Eagle's Media
DMSO - Dimethyl sulfoxide	Mfn1 - Mitofusin 1
dsRNA - Double-stranded RNA	Mfn2 - Mitofusin 2
ER - Endoplasmic reticulum	MPP - Mitochondrial processing peptidase
ERMES - ER-mitochondrial encounter structure	MPTP - 1-methyl-4-phenyl-1,2,3,6-tetrahydropyridine
ETC - Electron Transport Chain	mtDNA - Mitochondria DNA
FAPP2 - four-phosphate adaptor protein 2	MTS - Mitochondrial targeting sequence
FBS - Fetal bovine serum	OMM - Outer mitochondrial membrane
FOV - Field of view	Opa1 - Optic atrophy 1
fwd – Four wheel drive	ORP9L - OSBP-related proteins 9
GABA - γ-Aminobutyric acid	OSBP - Oxysterol-binding protein 1
<i>GBA</i> - acid beta glycosidase	PA - phosphatidic acid
GO - glucose oxidase	PARL - Presenilin-associated rhomboid-like
GOLPH3 - Golgi phosphoprotein 3	PBS - Phosphate Buffered Saline
GOLPH3L - Golgi phosphoprotein 3 like	PC - Phosphatidylcholine
GTP - Guanosine-5'-triphosphate	PD - Parkinson's disease
H ₂ O ₂ - Hydrogen peroxide	
HDAC6 - Histone deacetylase 6	
HeLa - Henrietta Lacks [cells]	

PE - Phosphatidylethanolamine	SNpc - Substantia Nigra pars compacta
PEMT - PE- <i>N</i> -methyltransferase	SNPs - single nucleotide polymorphisms
PERK - Protein kinase RNA-like endoplasmic reticulum kinase	SRSF - Sheffield RNAi Screening Facility
PI - Phosphatidylinositol	SYNJ2BP - SYNJ2 binding proteins
PI(4,5)P ₂ - phosphatidylinositol 4, 5 bisphosphate	TGN - Trans Golgi network
PI4K - PI kinase	TIM - Translocase of the inner membrane complex
PI4P - phosphatidylinositol 4-phosphate	TMD - Transmembrane domain
PRR- proline rich region	TOM - Translocase of the outer member complex
PS - Phosphatidylserine	UPS - ubiquitin proteasome system
Psd - PS decarboxylase	UBL - Ubiquitin-like
Pss1/2 - phosphatidylserine synthase	UPR - Unfolded protein response
RBR - RING-between-RING	VDRC - Vienna Drosophila RNAi Centre
reactive oxygen species (ROS)	VDAC - Voltage dependent anion channel
RING - Really interesting new gene	VMAT2 - Vesicular monoamine transporter 2
ROC - Ras of Complex	VMP1 Vacuole Membrane Protein 1
ROS - Reactive oxygen species	
S2R+ - Schneider 2 receptor plus [cells]	
Sac1 - Suppressor of actin 1	
SH3 - Src Homology 3	
siRNA - Small interfering RNA	

1. INTRODUCTION

1.1 Parkinson's disease

Parkinson's disease (PD) is the second most common neurodegenerative disorder, affecting 1/5000 people worldwide. It has a mean age of onset of 55, with incidences of PD increasing with age, from 1% of 65 year olds to 5% of 85 year olds (Lill, 2016). It was first characterised in 1817 by James Parkinson as a progressive movement disorder in his paper titled 'An Essay on The Shaking Palsy' (Kempster et al., 2007). PD presents with slowness of movement (bradykinesia), muscular rigidity, tremor and postural instability, thus indicating an inability to initiate movement (Kalia and Lang, 2015). Typically, PD is diagnosed by the presence of at least one of these motor symptoms, with responsiveness to L-3,4-dihydroxyphenylalanine (L-DOPA) supporting evidence of the diagnosis. More recently however, non-motor symptoms, which often precede characteristic motor symptoms, have also been associated with PD. These include depression, constipation, sleep disorders, hallucinations and sensory disturbances. These non-motor symptoms have become increasingly important as they offer a way to predict PD and allow for an earlier diagnosis, opening up different avenues of treatment (Chaudhuri et al., 2006). However, diagnosis of PD currently requires confirmation post mortem with the presence of proteinaceous inclusions, known as Lewy bodies, within the Substantia Nigra pars compacta (SNpc).

Currently there is no cure and limited treatment for PD with the gold standards being either L-DOPA or dopamine agonists. L-DOPA, the precursor to dopamine, acts to increase striatal dopamine to compensate for the degeneration of dopaminergic neurones in the SNpc. Over a 3-month period of L-DOPA treatment, a prominent improvement in motor symptoms is seen. However, long term use of L-DOPA has been reported to produce motor complications such as involuntary movement (dyskinesia) due to excess dopamine within the motor system. Following this, dopamine receptor agonists were employed to stimulate dopamine receptors, alleviating motor symptoms but also reducing the amount of free striatal dopamine and any unwanted dyskinesia (Rascol et al., 2000a). Long term use can result in increased non-motor side effects including psychosis, nausea, vomiting, fatigue and defects in impulse control, making them an imperfect treatment (Rascol et al., 2000b; Smith et al., 2012a). Alternative therapies are available that include deep brain stimulation (DBS), which targets the subthalamic nucleus with high frequency stimulation, restoring basal activity. The surgery involved with DBS is low risk and produces significantly better results than dopamine treatment in some atypical PD patients (Smith et al., 2012b).

1.1.1 Lewy Body Pathology

Lewy body pathology is a hallmark of PD pathology. Lewy bodies are insoluble intra-neuronal proteinaceous inclusions found predominantly in the SN and are typically 8-30 μm in diameter, spherical with a dense core and tell-tale peripheral halo (Forno, 1996). Braak et al. classified a pathological staging system of Lewy bodies in PD based on the progression of Lewy body pathology through the brain from the dorsal vagal nucleus to the midbrain and from the neostriatum to the neocortex. It has been shown that incidence of Lewy bodies correlates with PD progression where stages 1-2 represent incidental Lewy body disease while stages 3-4 show motor impairment and stages 5-6 show cognitive impairment (Braak et al., 2003, 2004, 2006). Furthermore the presence of Lewy bodies correlates with neurodegeneration, where the higher incidence of Lewy bodies produces greater neurodegeneration (Wakabayashi et al., 2013). Lewy bodies are found in both sporadic and familial forms of PD; but are notably absent in a small number of familial PD patients, including most cases of *parkin* and *PINK1*-related autosomal recessive PD (Hardy, 2010; Klein et al., 2012)

Lewy bodies contain over 90 proteins with α -Synuclein, neurofilaments and ubiquitin being the most prominent (**Fig 1.1C**) (Wakabayashi et al., 2007a). α -Synuclein oligomers and proto-fibrils have been suggested to be cytotoxic and contribute to neurodegeneration (Winner et al., 2011), while fibrillary α -Synuclein, as seen in post mortem brain tissue of PD patients, has been hypothesized to be cyto-protective (Olanow et al., 2004). Lewy bodies can be considered a protective mechanism where cytotoxic proto-fibrils are aggregated to produce fibrillary bundles to be removed by the proteasome system, similar to the function of the aggresome (Olanow et al., 2004) (Conway et al., 2001; Volles and Lansbury, 2003). However, others have suggested that if the cell keeps producing toxic protein then Lewy bodies will continue to grow and accumulate protein, resulting in cell death (Wakabayashi et al., 2007b).

1.1.2 The Degeneration of Dopaminergic Neurones

Another prominent feature of PD is the degeneration of dopaminergic neurones in the SNpc, a dark region of basal ganglia which forms part of the midbrain. The dark pigmentation is due to the high levels of neuromelanin, found in catecholaminergic neurones such as dopaminergic neurones. The majority of dopaminergic neurones reside within the ventral mesencephalon but have projections to many areas of the

brain including, the prefrontal cortex, amygdala, hippocampus and striatum. These projections make up three main dopaminergic pathways including the nigrostriatal dopaminergic pathway, which projects from the cell bodies of the SNpc to the putamen and caudate nucleus in the dorsal striatum, forming two motor loops: direct and indirect (**Fig 1.1A and B**). It is the balance of these two pathways which controls the initiation of movement. In PD, loss of these dopaminergic neurones alters the balance between the direct and indirect pathways, resulting in activation of inhibitory GABAergic neurones and thus preventing initiation of movement (Magrinelli et al., 2016).

Why dopaminergic neurones are selectively targeted has been a big question in the field, with many ideas revolving around the energy dependency of the dopaminergic neurones or the production of reactive oxygen species (ROS). One factor that is thought to contribute to the specific degeneration of the dopaminergic neurones is their morphology. The neurones within the SNpc have predominantly long, unbranched and un-myelinated axons which travel long distances to innervate many targets via approximately 370,000 synapses (Braak et al., 2004). The energy intensive cellular characteristics of dopaminergic neurones can put a large metabolic burden on mitochondria, thus enhancing intracellular ROS, resulting in protein, lipid and nucleic acid damage (Sulzer and Zecca, 2000). Furthermore, dopaminergic neurones have intrinsic autonomous pacemaker ability, where the dopaminergic neurones in the SNpc fire both burst or individual impulses at regular intervals, generated by intrinsic calcium (Ca^{2+}) dependent oscillations (Surmeier et al., 2010). These oscillations are essential for voluntary movement control and are thought to maintain a steady supply of dopamine to the striatal regions. However, maintaining a low intracellular Ca^{2+} level again comes at a high metabolic cost, overburdening ATP production and generating ROS (Chan et al., 2009; Grace and Bunney, 1983; Liss et al., 2001).

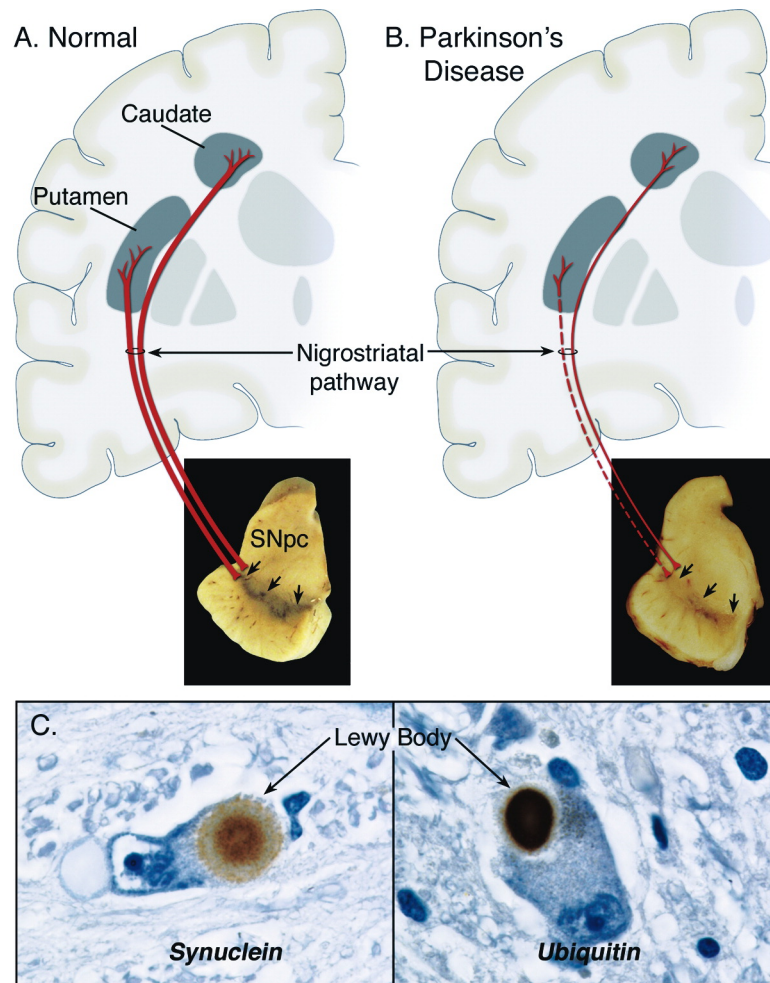


Figure 1.1: Parkinson's disease pathology. Schematic representation of the Nigrostriatal pathway (Red) connecting the SNpc to the putamen and caudate nucleus. The photograph shows the basal ganglia and the dark pigmented dopaminergic neurones within the SNpc under normal conditions (A) and within PD (B). (C) Immunohistochemical labelling of proteinaceous inclusions present in PD. Lewy bodies stained for Synuclein and ubiquitin showing the peripheral halo and dense core (Dauer and Przedborski, 2003).

1.2 Aetiology of PD

The majority of PD cases are sporadic with 90% of patients showing no clear genetic cause. The remaining 10% have a mono-genetic inheritance of highly penetrant mutations segregating with the disease in families. In the past 20 years, many genetic forms of PD have been revealed, which has led to a greater understanding of the disease pathways conserved in sporadic forms of PD.

1.2.1 Genetics of PD

Currently there are over 20 genetic loci of PD classified (**Table 1.1**) which have been assigned the annotation *PARK1-21*. These genetic forms contain a range of autosomal dominant forms of PD such as *SNCA* and *LRRK2* as well as autosomal

recessive forms of PD such as *PARK2* and *PARK6*. Many advances have been made in understanding the disease mechanism of PD by investigating the mono-genetic forms of PD.

Symbol	Gene	Disorder	Inheritance	References
PARK1	<i>SNCA</i> (<i>Point mutations</i>)	Early onset PD	AD	(Polymeropoulos et al., 1997)
PARK2	<i>Parkin</i>	Early onset PD	AR	(Kitada et al., 1998a)
PARK3	<i>Unknown</i>	Classical PD	AD	(Gasser et al., 1998)
PARK4	<i>SNCA</i> (<i>Duplications</i>)	Early onset PD	AD	(Singleton et al., 2003)
PARK5	<i>UCHL1</i>	Classical PD	AD	(Leroy et al., 1998)
PARK6	<i>PINK1</i>	Early onset PD	AR	(Valente, 2004)
PARK7	<i>DJ-1</i>	Early onset PD	AR	(Bonifati et al., 2003)
PARK8	<i>LRRK2</i>	Classical PD	AD	(Paisán-Ruiz et al., 2004)
PARK9	<i>ATP13A2</i>	Kufor-Rakeb syndrome; atypical PD with dementia, spasticity, and supranuclear gaze palsy	AR	(Ramirez et al., 2006)
PARK10	Unknown	Classical PD	Risk Factors	(Hicks et al., 2002)
PARK11	Unknown	Late-onset PD	AD	(Pankratz et al., 2003a)
PARK12	Unknown	Classical PD	Risk Factors	(Pankratz et al., 2003b)
PARK13	<i>HTRA2</i>	Classical PD	AD	(Strauss et al., 2005)
PARK14	<i>PLA2G6</i>	Early-onset dystonia-parkinsonism	AR	(Paisan-Ruiz et al., 2009)
PARK15	<i>FBXO7</i>	Early-onset Parkinsonism pyramidal syndrome	AR	(Di Fonzo et al., 2009)
PARK16	Unknown	Classical PD	Risk Factor	(Satake et al., 2009)
PARK17	<i>VPS35</i>	Classical PD	AD	(Lill, 2016)
PARK18	<i>EIF4G1</i>	Classical PD	AD	(Chartier-Harlin et al., 2011)
PARK19	<i>DNAJC6</i>	Juvenile onset, Atypical PD	AR	(Edvardson et al., 2012)
PARK20	<i>SYNJ1</i>	Juvenile onset, Atypical PD	AR	(Krebs et al., 2013a; Quadri et al., 2013a)
PARK21	<i>DNAJCL3</i>	Late onset PD	AD	(Vilariño-Güell et al., 2014)

Table 1.1: The *PARK* Loci and genes associated with genetic forms of PD: *PARK* Locus with related genes, equivalent disorder and mode of inheritance. Autosomal dominant (AD), autosomal recessive (AR). Adapted from (Kalinderi et al., 2016)

1.2.1.1 Autosomal Dominant familial Parkinson's disease

1.2.1.1.1 *SNCA* - α -Synuclein (*PARK1/4*)

The first mono-genetic form of PD was discovered in 1997 in Italian and Greek families which found a missense mutation (A53T) in the gene *SNCA*, which confers autosomal dominant inheritance. Following the initial discovery of the A53T mutation only 4 other mutations in *SNCA* have been determined: A30P (Krüger et al., 1998), E46K (Zarranz et al., 2004), G51D (Kiely et al., 2013; Lesage et al.,

2013) and H50Q (Appel-Cresswell et al., 2013; Proukakis et al., 2013). In addition to point mutations, *SNCA* can confer pathogenesis through gene duplications and triplications. There is a clinic-genetic link where point mutation E46K and triplications are associated with dementia, diffuse Lewy body disease and earlier disease onset, while the point mutation A30P and gene duplication are associated with a much milder PD related phenotype and do not often result in dementia (Chartier-Harlin et al., 2004; Farrer et al., 2004; Fuchs et al., 2008; Mizuno et al., 2008; Singleton et al., 2003).

The *SNCA* gene encodes a 140 amino acid protein α -Synuclein that belongs to the Synuclein family and localises to presynaptic nerve terminals and plays a role in synaptic transmission (Polymeropoulos et al., 1997; Stefanis, 2012). Furthermore, α -Synuclein is found in Lewy bodies, a major pathological feature of sporadic PD. This can potentially highlight protein aggregation as a mechanism for PD.

1.2.1.1.2 *LRRK2* – Leucine-Rich-Repeat kinase 2 (*PARK8*)

The *PARK8* locus which contains the *LRRK2* gene, was linked to autosomal dominant forms of PD (Paisán-Ruiz et al., 2004; Zimprich et al., 2004). Mutations in *LRRK2* are the most common genetic cause of PD making up 4% of the total familial forms of PD and 1-2% of the total sporadic forms of PD across all populations (Bae and Lee, 2015). Currently there are over 80 known mutations in *LRRK2*, but only 8 that convey pathogenesis (Li et al., 2014a). *LRRK2* encodes for a 2527 amino acid protein. It consists of a series of leucine rich repeats in the N-terminus, a ROC (Ras of Complex) GTPase domain, a COR (C-terminus of ROC) domain which links to a regulatory domain, and a kinase domain (Li et al., 2014b). The disease causing mutations cluster within the ROC-COR-kinase domain of *LRRK2*. Three different pathogenic mutations occur at the same amino acid (R1441C/G/H) within the GTPase domain and the most common variant (G2019S) occurring in the kinase domain, suggesting the importance of the kinase and GTPase activity of *LRRK2* in PD. The phenotypes of *LRRK2* mutation variants can range from pure nigral degeneration with and without Lewy body aggregates to neurofibrillary tau positive tangles. These varied phenotypes all form from mutations in a single protein, suggesting multiple functions of *LRRK2* protein (Bae and Lee, 2015; Li et al., 2014b).

1.2.1.2 Autosomal Recessive Familial Parkinson's disease (AR-JP)

Since the discovery of *SNCA*, many autosomal recessive loss of function mutations have also been found in various gene loci including *PARK2* (*Parkin*), *PARK6* (*PINK1*) and more recently *PARK20* (*Synптоjanin*).

1.2.1.2.1 *Parkin* (*PARK2*)

Mutations in the *PARK2* locus were first discovered in a Japanese family who presented with early onset autosomal recessive PD (typically < 40 years). This was found to be due to mutations in the *Parkin* gene present in the *PARK2* locus (Kitada et al., 1998a). Mutations in *Parkin* are the major genetic cause of AR-JP, contributing to 50% of autosomal recessive PD patients under the age of 45 and 1-2% of the total PD cases (Kalinderi et al., 2016). There are more than 100 known mutations in *Parkin* that span throughout the gene including point mutations, insertions, deletions, duplications and triplications as either homozygous or compound heterozygous mutations (Farrer et al., 2001). Clinically these mutations present as typical motor dysfunction with a good response to L-DOPA. However the symptoms appear much earlier, progression is much slower and no Lewy bodies are present (Farrer et al., 2001).

1.2.1.2.2 *PINK1* (*PARK6*)

After *PARK2*, *PARK6* locus is the next most common genetic cause of recessive familial PD, contributing to 1%-8% of all familial PD cases. The *PARK6* locus was initially linked to AR-JP within studies of a large Sicilian family which identified mutations in *PINK1* (Valente et al., 2004). *PARK6* encodes for PTEN-Induced Kinase 1 (*PINK1*), a 581 amino acid protein that is ubiquitously expressed. *PINK1*'s structure consists of a N-terminal mitochondrial targeting sequence (MTS), a transmembrane domain (TMD), which contains a translocase stop signal, and an enzymatic kinase domain which regulates the addition of a phosphate onto either serine or threonine residues (Kawajiri et al., 2011; Valente, 2004). The mutations in *PINK1* are numerous, with approximately 50 leading to pathogenesis of PD. These mutations are found throughout *PINK1* with a clustering within the kinase domain (K219A, G309D, L347P, D362A, D384A, G386A, G409V and E417G) resulting in a decrease in kinase activity (Pridgeon et al., 2007; Silvestri et al., 2005; Sim et al., 2006). Mutations in the C-terminus, which can regulate the kinase activity, can also result in AR-JP thus suggesting a role of *PINK1*'s kinase activity in PD (Rohé et al., 2004). Furthermore single heterozygous mutations in *PINK1* may contribute to

sporadic PD, thus strengthening the overlap between familial and sporadic PD (Kumazawa et al., 2008; Li et al., 2005). Like mutations in Parkin, PINK1 mutations present with parkinsonism, including motor dysfunction and a good response to L-DOPA. However, unlike sporadic PD, PINK1-like PD has early onset (30 years) with slower disease progression (Hatano et al., 2004). Of note, the differences in PINK1-linked PD compared to Parkin-linked PD is the presence of Lewy bodies, psychiatric problems and dementia in patients with PINK1 mutations. This suggests that mutations in PINK1 present with clinical features that are more comparable to sporadic PD (Kawajiri et al., 2011).

1.2.1.2.3 Synaptojanin 1 (*SYNJ1*) (*PARK20*)

Recently, there has been a flutter of rare genes discovered which all present with AR-JP including *SYNJ1* which is found in the *PARK20* locus. Currently, 5 AR-JP families have been found to have mutations in *SYNJ1*. It was first linked to AR-JP by homozygosity mapping studies of Italian and Iranian consanguineous families, which found a missense mutation within exon 5, resulting in a Arg to Gln amino acid change (Arg258Gln)(Krebs et al., 2013a; Quadri et al., 2013a). In 2014 Olgiati et al found a mutation in *SYNJ1* (Arg258Gln) in a separate Italian family (Olgiati et al., 2014) and more recently two different mutations in *SYNJ1* have also been uncovered, Arg459Pro and Arg839Cys. All known mutations in *SYNJ1* are present in the two functional phosphatase domains (Kirola et al., 2016; Taghavi et al., 2017). *SYNJ1* encodes the SYNJ1 protein that has a dual inositol phosphatase domain structure (Drouet and Lesage, 2014). Towards the N-Terminus there is a suppressor of actin 1 (Sac1) domain with a central inositol-5-phosphate domain and a variable C terminal (Drouet and Lesage, 2014). AR-JP pathogenic mutations, Arg258Gln and Arg459Pro, are both within the Sac1 domain and the Arg258Gln mutation has been shown to decrease the mono-phosphate hydrolysis ability of SYNJ1. Interestingly, mutations in the ins-5-phosphatase domain have also been implicated in PD, suggesting that PD could be caused not just by loss of Sac1 function but the regulation of both phosphatase domains. Like other forms of AR-JP, mutations in *SYNJ1* present with early onset (early 30's), dyskinesia and tremor (Krebs et al., 2013b; Olgiati et al., 2014; Quadri et al., 2013b). However, mutations in *SYNJ1* also present with several atypical symptoms including seizures, cognitive impairment and ocular motor disturbances. Interestingly, unlike both *PINK1* and *Parkin* forms of AR-JP, there is an inability to respond to L-DOPA and the initial stage of disease progression is severe (Krebs et al., 2013b; Olgiati et al., 2014;

Picillo et al., 2014; Quadri et al., 2013b). It has been suggested that those who have mutations in both domains of SYNJ1 have a more severe progression of PD, however more research is needed to verify this conclusion (Taghavi et al., 2017).

1.2.1.3 Genetics of Sporadic PD

The most common form of PD is late onset sporadic PD that contributes to 90% of cases. Sporadic PD is a result of complicated interactions between genetic risks and the environment (Hill-Burns et al., 2014). Over the past 20 years over 800 genetic association studies have been conducted to understand the genetic basis of sporadic PD (Lill et al., 2012). These association studies have highlighted that mutations in *SNCA* (Maraganore et al., 2006), acid beta glycosidase (*GBA*) (Papapetropoulos, 2010), *LRRK2* (Zabetian et al., 2009) and microtubule associated protein Tau (*MAPT*) (Goris et al., 2007) significantly impacted on sporadic PD susceptibility. However, most early genetic association studies were inconclusive and some had conflicting results. This led to genome wide association studies (GWAS) becoming increasingly popular in understanding the genetic associations and risk factors of sporadic PD. GWAS examine hundreds or thousands of single nucleotide polymorphisms (SNPs) in large cohorts (100-1000's) to look for generic associations. These SNPs often occur in high frequencies but convey low risk individually (Pandey, 2010). Reassuringly for previous PD disease models generated from examination of monogenetic forms of PD, *SNCA* and *LRRK2* also have corresponding low risk high frequency alleles (Lill et al., 2012). For example, the 3' region of α -Synuclein has been a consistent hit in GWAS studies, suggesting that both sporadic and familial causes of PD share common disease mechanisms (Lill et al., 2012). Thus, a common disease mechanism may exist between monogenetic and sporadic forms of PD.

1.2.2 Environmental risk factors of PD

There are several environmental risk factors associated with PD. Results of meta-analyses have shown that age, gender, pesticide exposure, prior head injury, rural living, β -blocker use, agricultural occupation and well-water drinking are all associated with an increased risk of PD. Conversely, smoking, coffee drinking, dietary fats, non-steroidal anti-inflammatory drugs (NSAID) use and alcohol consumption have all been associated with a decreased risk of PD (Noyce et al 2012). (Bower et al 1999 Van Den Eeden 2003). Although these environmental risk

factors suggest some contributing factors to the cause of PD, none have been conclusively proven, making it hard to approach experimentally.

1.3 Mechanisms of Disease in PD

There are many mechanisms which can contribute to PD including oxidative stress, protein aggregation and mitochondrial dysfunction. They can function together to contribute to the degeneration of dopaminergic neurones and the movement disorder seen in PD patients. Here I will discuss how they impact in PD.

1.3.1 Oxidative stress

Mitochondria are the main source of reactive oxygen species (ROS). ROS are predominantly free radicals including O_2^- , ONOO⁻ or OH⁻ which are produced by the incomplete and premature reduction of oxygen by complexes I, II or III in the electron transport chain (ETC). O_2^- can react with nitric oxide to produce ONOO⁻ or undergo dismutation by anti-oxidants to produce H_2O_2 which can be partially reduced to OH. (Murphy, 2009; Shukla et al., 2011). ROS molecules can be used in cellular signalling, however if there is a shift in this balance and more ROS are produced, then oxidative stress predominates (Shukla et al., 2011). Oxidative stress as a result of ROS can cause damage to protein, DNA and lipids, decreasing exocytosis and increasing protein aggregation, ER stress and cell death. Due to their close proximity, mitochondria are highly vulnerable to ROS and this results in decreased efficiency of the ETC and increased mtDNA mutations in ETC enzymes, thus generating more ROS (Dias et al., 2013).

There are substantial links between PD and oxidative stress, as oxidation of DNA, protein and lipids can be observed in PD patients, with secondary damage from these oxidised molecules contributing to neuronal degeneration (Jenner, 2003; Perfeito et al., 2012). Neurones are particularly vulnerable to oxidative stress as they are post mitotic, have high oxygen consumption and have a reduced number of anti-oxidants (Shukla et al., 2011). Interestingly, dopamine itself is thought to contribute in oxidative stress. Mice with reduced Vesicular monoamine transporter 2 (VMAT2), the protein which incorporates dopamine into vesicles, have dopamine mediated toxicity and a progressive loss of dopaminergic neurones (Caudle et al., 2007; Hernandez et al., 2013). Furthermore, excess cytosolic dopamine can be easily oxidised to produce dopamine-quinones (DAQ) (Sulzer and Zecca, 2000). These can interact with known PD-linked proteins: α -Synuclein, Parkin and Protein deglycase (DJ-1) (Da Silva et al., 2013) (Zhou et al., 2014). The interaction with α -

Synuclein can prevent association with chaperone proteins, preventing efficient folding, leading to toxic aggregates and an increase in oxidative stress. Furthermore, DAQ can directly impede on the mitochondria, causing mitochondrial dysfunction, linking oxidative stress with protein aggregate formation as well as dopaminergic neuronal degradation in PD (Martinez-Vicente et al., 2008).

1.3.2 Protein aggregation

Ultimately protein aggregation is a result of failure of the proteostasis network leading to alterations in the balance between protein synthesis and clearance. The proteostasis network is composed of several pathways which regulate protein biosynthesis, protein folding and the detection and resolution of unfolded protein through the unfolded protein response (UPR) and clearance (Webster et al., 2017). There are two main ways in which the proteostasis network can clear proteins and maintain the balance: the proteasome and the lysosome. The proteasome is a multimeric ATP dependent protease complex that recognises ubiquitinated substrates. Larger protein aggregates and whole organelles can be transported to the lysosome and degraded through the process of autophagy. Together these maintain cellular homeostasis and promote cell survival (Webster et al., 2017).

A key pathological hallmark of PD is the presence of the proteinous inclusion, Lewy bodies. Lewy bodies are predominately formed of α -Synuclein and proteins associated with the ubiquitin proteasome system (UPS) such as ubiquitin (Wakabayashi et al., 2013). Furthermore, α -Synuclein is mutated in autosomal dominant PD. Together these suggest that protein aggregation is linked to PD. Interestingly there is much debate about whether the presence of Lewy bodies acts as a toxic aggregate causing neurodegeneration or if they are a by-product of a failed proteostasis mechanism. In favour of Lewy bodies as a toxic species, their presence correlates with PD progression. Furthermore, overexpression of α -Synuclein induces death of dopaminergic neurones in human dopamine cultures (Tabrizi et al., 2000; Wakabayashi et al., 2013; Xu et al., 2002). Additionally, the chaperone protein, Hsp70, can be protective against α -Synuclein mediated dopaminergic neuronal loss and neurodegeneration, suggesting that protein misfolding could contribute to PD (Auluck et al., 2002; Cook et al., 2012). However, some genetic forms of PD do not manifest Lewy body pathology, such as mutation in *PARK2*. In addition, Lewy bodies are found in approximately 10-15% of individuals with no clinical or pathological neurological illness, known as incidental Lewy body disease (Olanow et al., 2004). This suggests that a convincing

correlation between the two has not been shown. It has also been hypothesized that instead of being a toxic aggregate, Lewy bodies are instead the result of activation of a protective mechanism which sequesters misfolded proteins (Cook et al., 2012). In support of this Lewy bodies also contain γ -tubulin and pericentrin, which are present in aggresomes, and have high levels of Histone deacetylase 6 (HDAC6), which is essential for aggresome formation and autophagy (Kawaguchi et al., 2003). It is clear that more research is needed to investigate the true function of protein aggregates, specifically Lewy bodies in PD.

1.3.3 Mitochondrial dysfunction

The first clue linking PD with mitochondrial dysfunction came in 1983 at a Californian hospital where a suspiciously high number of heroin addicts were admitted with Parkinson's-like symptoms (Langdon 1983). It was deduced that the addicts were administering a synthetic form of heroin which contained the meperidine analogue, 1-methyl-4-phenyl-1,2,3,6-tetrahydropyridine (MPTP). MPTP is taken up by astrocytes and broken down by monamine oxidases to form the toxic metabolite MPP⁺. This is then released from the astrocytes and taken up by dopaminergic neurones, where it accumulates in the mitochondria and inhibits the activity of complex I, the first protein complex involved in oxidative phosphorylation to produce ATP (Hu and Wang, 2016). This incidental evidence suggested a link between mitochondrial dysfunction and PD. However, the conclusive evidence that mitochondrial dysfunction is involved in PD has come from examination of PD patient brain samples. Mitochondrial dysfunction was confirmed clinically by testing the function of respiratory chain complexes, the results of which found a specific decrease in complex 1 activity in the SNpc (Bindoff et al., 1989; Schapira et al., 1990).

Further evidence of mitochondrial dysfunction in PD has come from epidemiological studies looking at the use of pesticides and herbicides, rotenone and paraquat. It was found that there was increased prevalence of PD within farmers who were exposed to pesticides on a regular basis. Paraquat and rotenone are similar in structure to MPTP and inhibit mitochondrial complex I, reducing the ATP and increasing ROS (Gorell et al., 1998; Tanner et al., 2011). Since then, MPTP, paraquat and rotenone have been used to produce reliable PD animal models which produce phenotypes similar to their human counterparts (Jackson-Lewis and Przedborski, 2007).

Progressive advances in understanding the genetic forms of PD have helped

solidify the basis of mitochondrial dysfunction as a primary cause of PD. Many causative PD genes have been found to be associated with mitochondrial function and protection. *pink1* and *parkin* null mutant *Drosophila* show locomotive defects, mitochondria that are swollen with irregular cristae structures and indirect flight wing muscle degeneration (Clark et al., 2006; Greene et al., 2003; Park et al., 2006; Pesah et al., 2004; Yang et al., 2006). Further to this, dopaminergic neurone degeneration is seen in the brains of *pink1*^{B9} and *park*²⁵ mutant *Drosophila* with the remaining dopaminergic neurones containing a high number of swollen mitochondria (Greene et al., 2003; Park et al., 2006). Other *pink1* and *park* mutants, *pink1*⁹, *pink1*⁵ or *park*^{P21}, however, did not show dopaminergic neurone loss (Clark et al., 2006; Pesah et al., 2004). It was suggested that that PD is a multi-system based disease and may have degeneration of other neurones within the fly brain or that the assay was not sensitive enough. For example Pesah et al 2004 only looked at aging for 3 weeks (21 days) while Park et al 2006 examined dopaminergic neurone loss at 30 days and Clarke et al 2006 examined *pink1* mutants for up to 50 days (Clark et al., 2006; Park et al., 2006). It is prudent to consider that aging in *Drosophila* may differ between labs may not be equivalent to each other or that of ageing in patients. Along these lines it is important to consider is the effects of the environment. *Drosophila* food and laboratory culture conditions may differ between labs with labs with suboptimal conditions increasing stress in some cases leading to a more prominent neurodegenerative phenotype. The nature of the mutations are also different and the background effects that go with these are also variable which may contribute to the difference in phenotypes seen. Hence, discrepancies in the literature still remain for the requirement of *pink1* and *parkin* in the loss of dopaminergic neurones meaning more investigations are needed.

These phenotypes strongly suggest the involvement of mitochondrial dysfunction in PD (Park et al., 2006; Pesah et al., 2004). Mitochondrial dysfunction can also be seen in mammalian models, with *PINK1* and *Parkin* null mice showing mitochondrial respiratory chain defects and progressive mitochondrial dysfunction (Goldberg et al., 2003; Palacino et al., 2004). However, both *PINK1* and *Parkin* null mice do not show a strong phenotype of dopaminergic neurone loss like *Drosophila*. *Parkin* mutants do not have locomotor defects and *PINK1* mutants do not have neuronal degeneration or Lewy bodies. It is thought that there is some compensation and it is the failure of these compensatory mechanisms, with age, that results in the PD phenotype in mice (Dawson et al., 2010). The notion that mitochondrial dysfunction presents early in the *pink1* and *parkin* null *Drosophila* may suggest that it is an early

feature of disease progression in humans. This is important as one of the main challenges in PD treatment is that PD patients only present with symptoms at the time when the majority (approx.70%) of their dopaminergic neurones have degenerated. Mitochondrial dysfunction may be an early sign and could allow for early diagnosis and preventative treatment of PD.

1.4 Mitochondrial quality control

Dysfunction in mitochondria has been linked to PD and other neurodegenerative diseases. Therefore, it is of clear importance that mitochondrial function and integrity is maintained in neurones. Mitochondria have various intrinsic mechanisms by which they can protect themselves and promote cell survival. These include changes in mitochondrial dynamics, production of mitochondria derived vesicles (MDV) and the last resort, mitophagy, which protects the mitochondrial network by removing the severely damaged mitochondria. Together these mechanisms help to maintain the health of the mitochondria.

1.4.1. Fission and Fusion

One of the early mechanisms for mitochondrial quality control is the change in mitochondrial morphology through mitochondrial fission and fusion. Optic atrophy 1 (Opa1) is an inner mitochondrial membrane (IMM) dynamin-like GTPase which regulates fusion of the IMM. Outer mitochondrial membrane (OMM) fusion is mediated by the large dynamin-like GTPases *Mitofusin 1 (Mfn1)* and *Mitofusin 2 (Mfn2)*, which regulate OMM fusion through homo or heterodimeric binding via their coiled-coil domain. It is thought that the fusion is co-ordinated by a SNARE-like mechanism which requires force from both membranes undergoing fusion (Koshiba et al., 2004).

In addition to pro-fusion genes, there are pro-fission genes associated with constricting the mitochondria to allow spontaneous fission to occur. Fission of the mitochondria is mediated by the cytosolic dynamin-like GTPase dynamin like protein 1 (Drp1). In yeast, Dmn1 is recruited to mitochondria by Fis1, Mdv1 and the partially redundant Caf4 (Griffin et al., 2005; Mozdy et al., 2000; Tieu et al., 2002). In mammals, Drp1 is recruited by Fis1 and mitochondrial fusion factor (Mff) (Gandre-Babbe and van der Bliek, 2008; Otera et al., 2010). Upon GTP hydrolysis there is a conformational change, Drp1 oligomerises and allows constriction of both the IMM and the OMM producing fragmentation of the mitochondria (Mears et al., 2011). Together pro-fusion and pro-fission proteins maintain the balance of

mitochondrial morphology in order to regulate protection of the mitochondrial network and therefore cell survival (**Fig 1.2**).

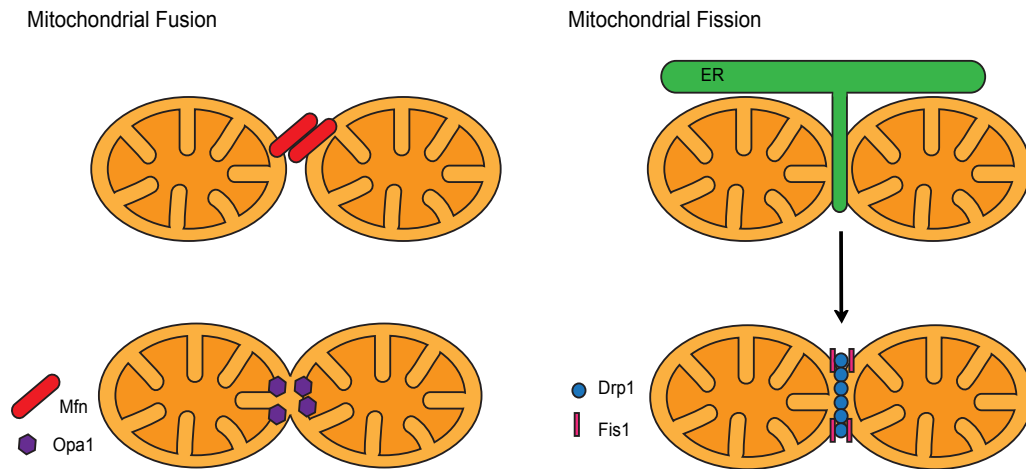


Figure 1.2: Mitochondrial fission and fusion: Schematic representation of mitochondrial fission and fusion events. During fusion Mfn1 and Mfn2, the OMM GTPases, mediate the fusion of the OMM through binding of their large coiled-coil domains. Subsequent GTP hydrolysis and IMM fusion occurs through the IMM GTPase Opa1. During mitochondrial fission the ER marks the sites of mitochondrial scission, Fis1 recruits Drp1 to the mitochondria. With GTP hydrolysis there is a conformational change and Drp1 oligomerises and constricts the mitochondria, splitting it into two parts.

Changes in mitochondrial morphology help to maintain mitochondrial health. Under insult, the mitochondria will switch to pro fusion to help ‘dilute’ the damage and maintain the overall mitochondrial membrane potential (Twig et al., 2008). When the damage becomes too pronounced, pro fission genes are used to segregate highly damaged mitochondria for efficient degradation by the autophagy process (Gomes et al., 2011; Tanaka et al., 2010). This helps to preserve the overall mitochondrial network and the health of the cell (Twig et al., 2008) (**Fig 1.3**).

The balance between fission and fusion is extremely important, as when it is not maintained it can result in various neurological diseases. Opa1 mutations, G488R and A495V, in highly conserved residues of the GTPase domain result in autosomal dominant optic atrophy which presents with optic nerve degeneration leading to a decrease in visual acuity and blindness (Alexander et al., 2000; Delettre et al., 2000). Furthermore, Mfn2 and Drp1 have been linked to neurodegenerative disease. Mutations in *Mfn2* result in Charcot-Marie-Tooth disease Type 2A, which is characterised by distal muscle weakness and wasting, whereas heterozygous mutations in Drp1 cause neonatal lethality and neurological features (Kijima et al.,

2005; Waterham et al., 2007; Züchner et al., 2004). Overall, these studies suggest that mitochondrial morphology is important in mitochondrial function and that maintaining the balance between fusion and fission is important in the maintenance of cell health and preventing neurological disease.

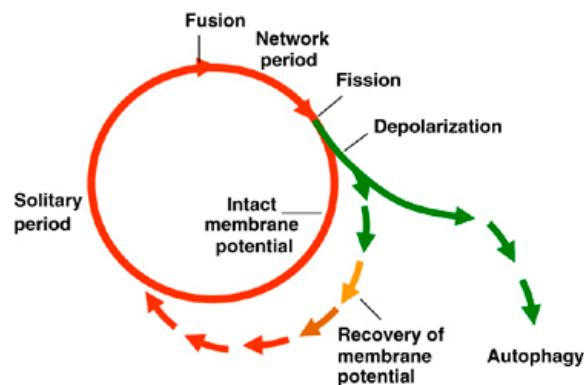


Figure 1.3: Mitochondrial fission and fusion: A model of the mitochondrion’s life cycle which is composed of various fission and fusion processes. Fusion can occur to dilute out damage and help to regain the mitochondrial membrane potential. If the damage cannot be recovered by fusion events, the mitochondria can be fragmented and separated from the overall mitochondrial network which aids efficient degradation of the damaged mitochondria by mitophagy. Together they help to maintain the health of the mitochondrial network, with mitochondrial morphology changes being the initial response to damage (Twig et al., 2008).

1.4.2 Mitophagy

Mitophagy is a specialised form of selective autophagy which regulates the bulk degradation of the mitochondria. In general, mitophagy begins with the selection of cargo to be degraded and then the production of the phagophore, a double membrane sheet, which forms a cup-like structure around the protein aggregate or organelle in question. Once sealed, the autophagosome fuses with the endolysosome, producing the autolysosomes in which the damaged organelles are degraded (Hamacher-Brady and Brady, 2016). There are 3 classified types of mitophagy which will be discussed in this section. These include PINK1/Parkin dependent mitophagy, PINK1/Parkin independent or starvation induced mitophagy and the production of mitochondrial derived vesicles .

1.4.2.1 PINK1 and Parkin Dependent Mitophagy

Genetic studies in *Drosophila* first established that PINK1 and Parkin act in a common pathway to maintain mitochondrial homeostasis (Clark et al., 2006; Park et al., 2006). A wealth of subsequent cell biology studies has indicated that a major

role of the PINK1/Parkin pathway is to target damaged or dysfunctional mitochondria for autophagic degradation, termed mitophagy.

Under basal conditions PINK1 undergoes numerous proteolytic cleavages before it is finally degraded by the N-end degradation. Like other mitochondrial targeting sequencing containing proteins, PINK1 Full length (FL) (64 kDa) is imported into the mitochondria by Translocase of the outer member complex (TOM) and Translocase of the inner membrane complex (TIM). An IMM translocation stop sequence, present in the TMD, prevents the full translocation of PINK1 into the matrix (Chin and Li, 2016; Lazarou et al., 2012). Once anchored in the IMM, the matrix localised mitochondrial processing peptidase (MPP) cleaves PINK1-FL to a 60 kDa form, removing the MTS (Greene et al., 2012). Further cleavage at A104 by presenilin-associated rhomboid-like (PARL) and intramembrane space (IMS) protease, produces the short (52 kDa) form, which is then retro-translocated and released into the cytosol. The exposed phenylalanine (F104) acts as a type 2 degron signal for N-end degradation (Deas et al., 2011; Jin and Youle, 2012; Shi et al., 2011; Whitworth et al., 2008). This means that under basal conditions, PINK1 is present in very low levels within the cell (**Fig 1.4**).

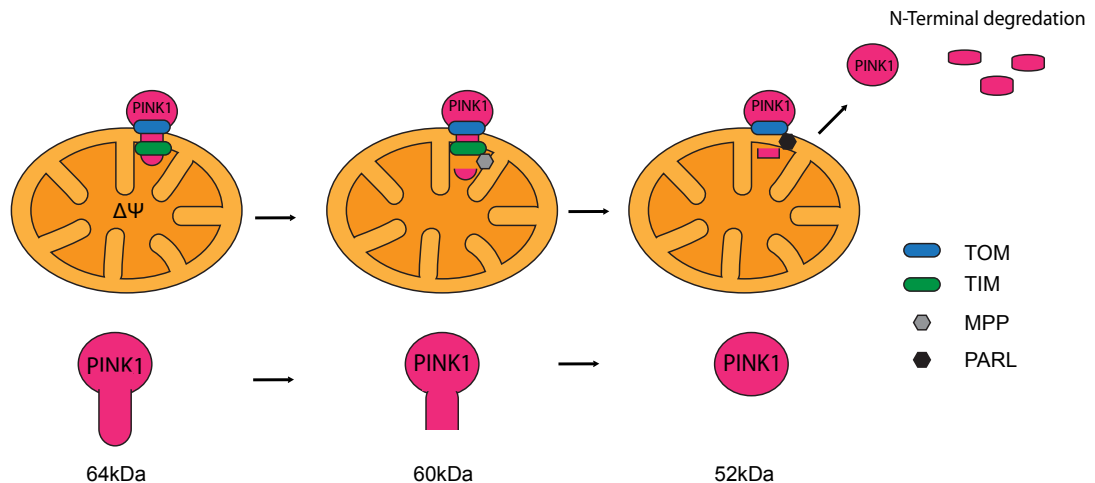


Figure 1.4: PINK1 degradation: A schematic representation of PINK1 degradation under basal conditions. When there is no mitochondrial stress or insult the mitochondrial membrane potential remains constant, this allows PINK1 to be targeted to the mitochondria and imported through the TOM/TIM complexes. Here PINK1 is cleaved by MPP in the matrix and then PARL in the IMS. This allows the release of PINK1 into the cytosol where it is degraded by N-terminal degradation.

When mitochondrial insult occurs, for example from CCCP treatment or oxidative stress, the mitochondrial membrane potential drops and prevents the import of PINK1 through the TIM complexes. This results in a stabilisation of PINK1 in the OMM, which allows the recruitment of Parkin from the cytosol to the mitochondria (Jin et al., 2010; Narendra et al., 2008a). Once PINK1 is stabilised on the OMM, its kinase activity is required for Parkin translocation to the mitochondria and mitophagy (Geisler et al., 2010a; Matsuda et al., 2010; Narendra et al., 2010a). PINK1 undergoes various phosphorylation events, including auto-phosphorylation at S228 and S402 in the kinase domain, which are necessary for Parkin recruitment (Okatsu et al., 2012). These events occur alongside the phosphorylation of S65 in Parkin's UBL domain and S65 of local ubiquitin (Kane et al., 2014; Kazlauskaitė et al., 2014; Kondapalli et al., 2012; Koyano et al., 2014; Shiba-Fukushima et al., 2012) (**Fig 1.5**). Under basal conditions, Parkin is in a closed inhibitory conformation. However, when PINK1 is stabilised it phosphorylates the UBL domain (S65), resulting in a conformation change in Parkin. This produces a 'Primed' Parkin, allowing for efficient binding of phosphorylated ubiquitin (Phos-Ub). Once bound, Parkin can be released from its auto-inhibited state, where it ubiquitinates numerous mitochondrial proteins including voltage dependent anion channel (VDAC) (Geisler et al., 2010a) Mfn2 (Ziviani et al., 2010) and Miro (Wang et al., 2011), in order to promote efficient mitophagy. In addition, there are studies that suggest that it is not which mitochondrial proteins are ubiquitinated, but instead the pattern of Phos-Ub created by phosphorylation of these proteins which allows efficient recruitment of the autophagosome and promotes mitophagy (Sarraf et al., 2013) (**Fig 1.5**).

The Phos-Ub landscape acts to recruit mitophagy adaptor proteins, which bind the phagophore membrane through LC3 via their LC3-interacting region (LIR) domain (**Fig 1.5**). There are 8 mitophagy receptors which can be placed into two groups based on their mechanistic function: Ubiquitin binding or OMM anchored receptors. Ubiquitin binding receptors predominate in PINK1/Parkin mediated mitophagy. These include P62, Optineurin and NBR1 (Kirkin et al., 2009; Narendra et al., 2010b; Wong and Holzbaur, 2014). Interestingly, a feed forward mechanism can be generated by Optineurin. Optineurin can recruit TBK1 (TANK binding kinase 1), a serine/threonine kinase, to P62 on the mitochondria. TBK1 can phosphorylate P62 at S403, enhancing its ability to bind ubiquitin, thus promoting the binding of the mitochondria to the phagophore and encouraging mitophagy (Matsumoto et al., 2011). PINK1 and Parkin are shown to precede and promote mitophagy by priming the mitochondria for engulfment by the autophagosome and degradation by the

lysosome, leaving a healthy mitochondrial network (Sarraf et al., 2013; Ziviani et al., 2010)

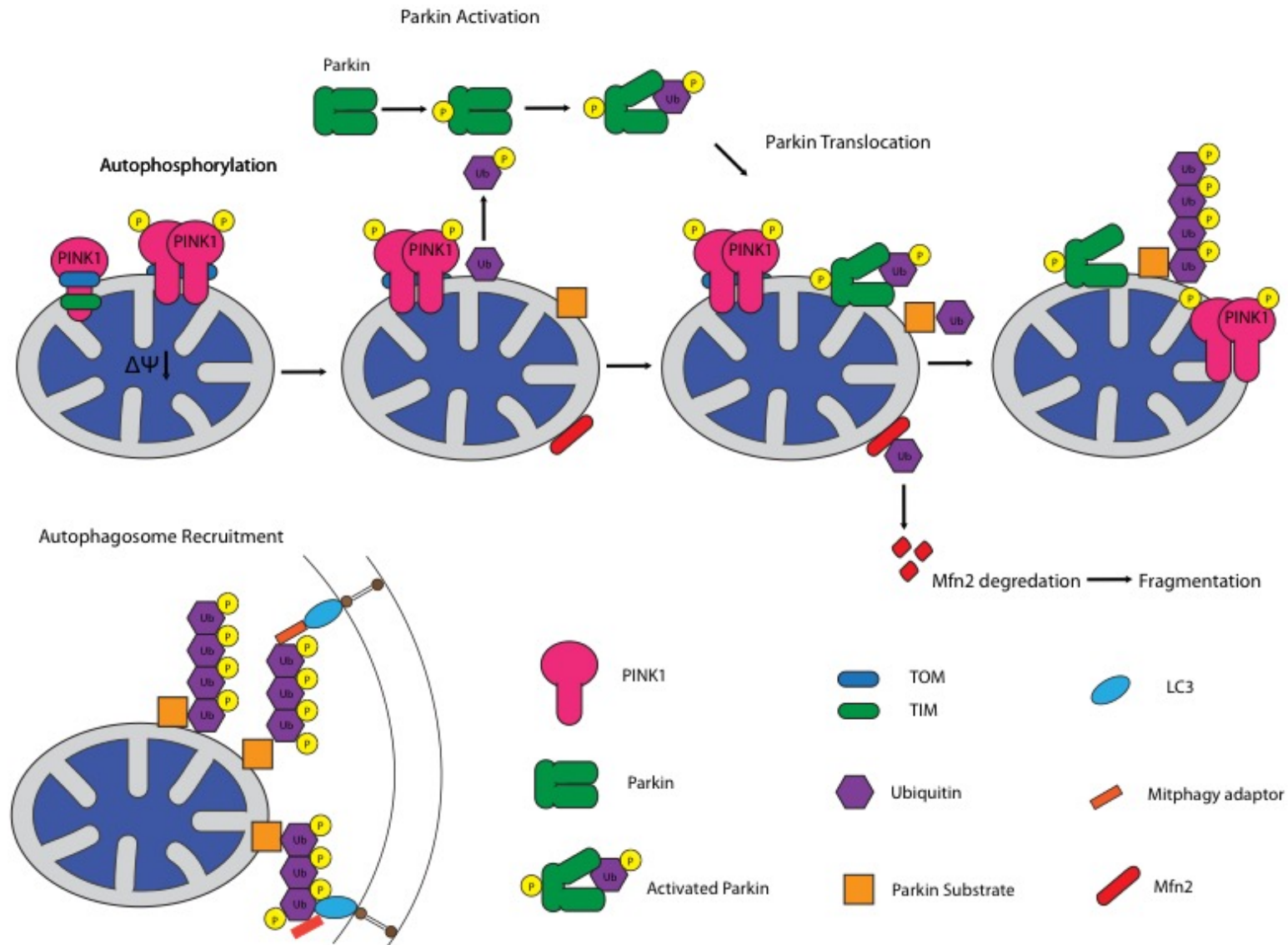


Figure 1.5: PINK1 and Parkin dependent mitophagy: Mitochondrial insult causes a reduction in the mitochondrial membrane potential and PINK1 is prevented from being imported through the TOM/TIM23 complex. This prevents its degradation and so PINK1 is stabilized on the OMM. PINK1 undergoes auto-phosphorylation, increasing its activity and helping aid the recruitment of Parkin. PINK1 helps to activate and recruit Parkin in a 2-step activation process. PINK1 phosphorylation of the ULD of Parkin primes Parkin for full activation, while PINK1 phosphorylation of local ubiquitin fully activates Parkin, changing it into an open confirmation. Once fully active, Parkin poly-ubiquitinates various mitochondrial proteins while PINK1 phosphorylates the ubiquitin. The poly phos-ubiquitin chains bind to mitophagy adaptors through their LIR domains and to LC3 which is attached to phosphatidylethanolamine (PE) on the autophagosome membrane. The autophagosome engulfs the mitochondria, promoting its degradation through the autophagy pathway

1.4.3.2 PINK1 and Parkin independent Mitophagy

PINK1/Parkin mediated mitophagy often gets a lot of attention because both PINK1 and Parkin are mutated in AR-JP (Kitada et al., 1998b; Valente, 2004). However, other forms of mitophagy can also contribute to the health of the mitochondrial network and cell survival. OMM anchored receptors, which act as mitophagy adaptors and lipids, often mediate PINK1/Parkin independent mitophagy. To allow the process of mitophagy to occur, mitophagy adaptors which contain LIR sequences must be recruited to the mitochondria. Bcl2-L-13, the mammalian homologue of atg32, can promote the removal of depolarised mitochondria in response to CCCP treatment, independent of Parkin (Murakawa et al., 2015). However it is still unknown how Bcl2-L-13 is recruited to the mitochondria to promote mitophagy. Another LIR containing protein is AMBRA1. This has been previously shown to interact with Parkin and promote mitophagy (Van Humbeeck et al., 2011). However recent evidence has suggested that AMBRA1 also promotes mitophagy and activates mitochondrial ubiquitination, independent of Parkin (Strappazzon et al., 2015).

A main stimulus of PINK1/Parkin independent mitophagy is hypoxia. During hypoxic conditions, cells switch to glycolytic metabolism in order to produce ATP and their mitochondria are removed (Roberts et al., 2016). The basal functions of Bnip3 (BCL2/adenovirus E1B 19 kDa interacting protein 3) and Nix (Nip3 like protein X) are to mediate apoptosis, but they are also upregulated in response to hypoxia (Dorn, 2010; Zhang et al., 2008). They homodimerise, insert into the OMM and from here act as a mitophagy receptor for LC3, promoting mitophagy through their LIR domains (Hanna et al., 2012; Schwarten et al., 2009). This leads to turnover of mitochondria via mitophagy. Another recently described mitochondrial adaptor for mitophagy is FUN14 domain-containing protein 1 (FUNDC1). FUNDC1 contains an LIR domain and so can recruit the phagophore membrane and in response to hypoxia. Mitophagy cannot occur when FUNDC1 is silenced (Liu et al., 2014). In order for FUNDC1 to promote mitophagy it is phosphorylated by ULK1 at S17 in order to promote the interaction between the LIR and LC3 protein. (Wu et al., 2014)

Interestingly, Nix has been suggested to be a substrate of Parkin (Gao et al., 2015) and AMBRA1, which can bind mitochondrial localised Parkin and LC3 (Van Humbeeck et al., 2011). This may suggest that there is overlap between the two forms of mitophagy, which may lead to an increase in compensatory mitochondrial

quality control mechanisms. This may explain the lack of phenotype seen in Parkinson's disease mouse models.

Finally, lipids can also act as signals for mitophagy. Cardiolipin, an IMM phospholipid, is extruded from the IMM to the OMM by PLS3, when under stress and a reduction in mitochondrial membrane potential. Here it can bind LC3B and promotes mitophagy, thus acting as a PINK1/Parkin independent adaptor (Chu et al., 2013).

1.4.3.3 Mitochondrial derived vesicles

Much of our understanding of PINK1/Parkin-mediated mitophagy arose from experiments conducted in cancer based cell lines, with the use of unspecific mitochondrial chemical un-couplers. These are highly artificial systems and do not reflect the physiological conditions of neurones (Grenier et al., 2013; Mouton-Liger et al., 2017). Neurones predominantly produce ATP by oxidative phosphorylation rather than by glycolysis, unlike cell lines (Rossignol et al., 2004). Therefore, neurones have adapted to retain their mitochondria and remove them under a greater, prolonged stress. Furthermore, many experiments investigating mitophagy use generalised mitochondrial damaging agents such as CCCP. These agents will depolarise the entire mitochondrial network, but physiologically this is unlikely to happen. It is more likely that localised segregated damage would result in small fragments of mitochondria undergoing mitophagy rather than complete removal of the mitochondrial network (Grenier et al., 2013; Mouton-Liger et al., 2017). One way this could be occurring is through the segregation of small portions of a damaged mitochondria, such as via MDV.

MDV's were first described in 2008 where MAPL, a SUMO E3 ligase, whose overexpression resulted in fragmentation of the mitochondrial network, and TOM20 positive fragments (vesicles) were identified outside the mitochondrial network. Electron microscopy revealed distinct uniform structures of 70-100nm composed of both the IMM and OMM which appeared in concentric circles, without cristae. These were termed mitochondrial derived vesicles and were found to carry a range of different cargo (Neuspiel et al., 2008). Upon addition of oxidative stressors, glucose oxidase (GO), Antimycin A (Complex III inhibitor) or Xanthine oxidase, there was an increase in TOM20 positive MDV's before global damage to the mitochondria was observed. This suggested that under stress MDV's can transport oxidised cargo to

the lysosome for degradation in order to circumvent global damage to the mitochondria (Soubannier et al., 2012).

Interestingly, there is evidence that both PINK1 and Parkin are required for MDV production. The expression of Parkin in Hela cells with Antimycin A treatment shows that Parkin is recruited to distinct puncta on the mitochondria. These puncta represent a subset of budding MDV and when PINK1 is silenced, the number of these MDV's is reduced. It is hypothesized that local stress, as opposed to a global mitochondrial insult, can result in PINK1 mediated Parkin recruitment to the mitochondria in subdomains. Import channels on the mitochondrial surface are localised to specific regions, often where the IMM and OMM are in close proximity. It is thought that the oxidation of proteins or IMM phospholipids can prevent the import of PINK1 through these channels, pinning the OMM and IMM together and thus allowing the recruitment of Parkin and the formation of MDV's (McLelland et al., 2014; Sugiura et al., 2014). Moreover, this mechanism may be more representative of the process which actually occurs in neurones.

1.5 ER-mitochondrial contact sites

1.5.1 Functions of ER-mitochondrial Contact sites

ER-mitochondria contact sites have many functions, including lipid transfer and synthesis, calcium (Ca^{2+}) homeostasis, altering mitochondrial morphology, autophagosome production and autophagy, as well as roles in ER-stress and the UPR. Here I will discuss these functions and the molecular basis of ER-mitochondria contact sites.

1.5.1.1 Lipid transfer and synthesis

ER-mitochondria contact sites are a key site of lipid metabolism. The main lipid metabolism pathway starts with phosphatidic acid (PA) being converted by phosphatidylserine synthase (Pss1/2) to phosphatidylserine (PS) in the ER. To form other phospholipids such as phosphatidylethanolamine (PE), a major component of the mitochondrial membrane, PS is shuttled from the ER to the IMS via the ER-mitochondrial contact site, where it is decarboxylated by PS decarboxylase (Psd) to PE (Rowland and Voeltz, 2012). This in turn can be further modified in the ER by PE-*N*-methyltransferase (PEMT) to phosphatidylcholine (PC) (**Fig 1.6**). As Psd is only found in the mitochondria, ER-mitochondria contact sites are extremely

important in the production of these PE, which constitute a large proportion of the membranes within the cell (Rowland and Voeltz, 2012). The transfer of lipids between the ER and mitochondria at ER-mitochondria contact sites is the rate limiting step in this lipid biogenesis pathway, therefore suggesting its importance in the maintenance of the cellular and mitochondrial phospholipid balance (Kornmann et al., 2009).

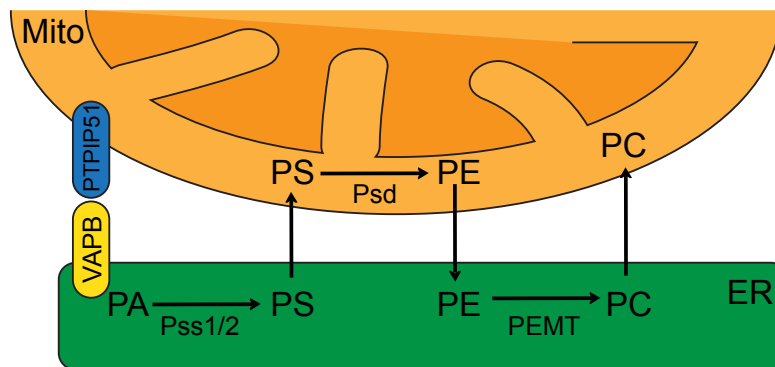


Figure 1.6: Lipid metabolism at ER mitochondrial contact sites: Schematic representation of ER-mitochondria contact sites, the process of PS, PE and PC metabolism and their transfer from the ER to the mitochondria.

1.5.1.2 Ca²⁺ Homeostasis

A predominant function of ER-mitochondrial contact sites is the ability to maintain Ca²⁺ homeostasis within the cell. It is well established that Ca²⁺ is an important second messenger in many pathways, including synaptic vesicle release in neurones and myocytes. In addition to the ER, mitochondria can also buffer cytosolic Ca²⁺ via entry through mitochondrial calcium uniporter (MCU) into the mitochondrial matrix (Baughman et al., 2011; De Stefani et al., 2011). It was discovered that MCUs are grouped into Ca²⁺ hotspots where the Ca²⁺ concentration ([Ca²⁺]) is at least one order of magnitude higher than the cytosolic [Ca²⁺], allowing the threshold for fast Ca²⁺ transport into the mitochondria to be reached (Giacomello et al., 2010). These hotspots are a result of fast opening Ca²⁺ channels such as IP₃R at the ER membrane which contacts VDAC, via Grp75, at the mitochondria (Szabadkai et al., 2006). These ER-mitochondrial tethers in conjunction with MCU allow Ca²⁺ influx into the mitochondrial matrix from the ER via ER-mitochondrial contact sites (Filadi et al., 2017). Ca²⁺ transfer to the mitochondrial matrix is extremely important in mitochondrial function, as enzymes (isocitrate dehydrogenase, oxoglutarate dehydrogenase) within the Krebs cycle and glycolysis

(pyruvate dehydrogenase (PDH)) are Ca^{2+} dependent. Hence, $[\text{Ca}^{2+}]$ is linked to the production of ATP (Denton, 2009). Perturbing Ca^{2+} shuttling through ER-mitochondria contact sites decreases ATP production and the oxygen consumption rate (Cárdenas et al., 2010; Mallilankaraman et al., 2012). Together these data suggest the importance of Ca^{2+} shuttling in ER-mitochondria contact sites on mitochondrial function.

1.5.1.3 Mitochondrial morphology

ER-mitochondria contact sites have been linked to changes in mitochondrial morphology. Mfn2, an OMM GTPase which regulates mitochondrial fusion, is also found in the ER (de Brito and Scorrano, 2008). Changes in Mfn2 have been shown to alter ER-mitochondrial contact sites, suggesting a link between the two (de Brito and Scorrano, 2008). (Cosson et al., 2012; Filadi et al., 2015). Furthermore, the ER has been shown to wrap around the mitochondria, thereby constricting them (Friedman et al., 2011). This constriction allows the oligomerised Drp1 to envelope the mitochondria, in order to propagate further constriction and fission of the mitochondrial network (Friedman et al., 2011). In further agreement, the ER-mitochondrial tethering protein complex in yeast, ER-mitochondrial encounter structure (ERMES), was found to spatially associate with sites of ER-mitochondrial squeezing and subsequent mitochondrial division (Murley et al., 2013). This opens an interesting avenue for investigation into mitochondrial quality control with respect to ER-mitochondrial contact sites, as changes in mitochondrial morphology are prominent in PD animal models

1.5.1.4 Autophagy

Pre-autophagosome marker ATG14L and ATG5, a key autophagy component, were found to localise on ER-mitochondria contact sites upon starvation (Hamasaki et al., 2013). Phosphofurin acidic cluster sorting protein 2 (PACS-2) knockdown uncouples the ER from the mitochondria, disrupting ER-mitochondria contact sites. PACS-2 deficient cells have reduced numbers of ATG14L puncta, suggesting that ER-mitochondria contact sites are involved with autophagosome formation (Hamasaki et al., 2013; Simmen et al., 2005). Furthermore, it has been suggested that Vacuole membrane protein 1 (VMP1), a transmembrane protein situated in the ER, is a negative regulator of ER-mitochondria contact sites but can also result in autophagy defects when silenced. It is hypothesized that VMP1 regulates the size of the contacts during autophagy, producing preferable domains for autophagosome

formation and recruitment of ATG14L (Tabara and Escalante, 2016). Mitophagy has also been linked to ER-mitochondria contact sites. The flux of Ca^{2+} from the ER to the mitochondria through ER-mitochondria contact sites is required for both starvation induced mitophagy as well as PINK1/Parkin induced mitophagy (Macvicar et al., 2015). In accordance with this, studies in yeast also found that efficient mitophagy depends on ER-mitochondria contact site tethers and that ERMES proteins co-localise with the sites of autophagosome biogenesis (Böckler and Westermann, 2014). Together these data suggest a function of ER-mitochondrial contact sites in regulating autophagy.

1.5.1.5 Unfolded Protein Response (UPR)

ER-mitochondria contact sites have also been implicated in UPR, an intracellular signalling pathway that is activated by the accumulation of unfolded proteins in the ER (Chakrabarti et al., 2011). Under basal conditions ER residing chaperone proteins, including BIP, hold proteins in the ER to allow them to fold correctly. An accumulation of un-folded proteins can result in ER stress which is detected by BIP and initiates the UPR (Bertolotti et al., 2000). UPR is predominantly composed of 3 major pathways: PERK, IRE1 and ATF6. Once activated, they allow the upregulation of chaperone proteins and prevent translation (Schröder and Kaufman, 2005). ER stress has been shown to increase Ca^{2+} uptake into the mitochondria, increase ATP production and increase oxygen consumption (Bravo et al., 2011). The increase in ATP production will provide energy for the chaperone machinery to aid in folding of protein in the ER, thereby preventing ER stress and apoptosis (Bravo et al., 2011). These initial responses to ER stress have been reported to be accompanied by an increase in ER mitochondrial contact sites (Bravo et al., 2011). However, when the ER stress becomes too severe, apoptosis can be induced through ER-mitochondrial contact sites (Chakrabarti et al., 2011). The protein GM1-ganglioside can accumulate at ER-mitochondria contact sites, inducing ER stress responses and promoting Ca^{2+} transfer from the ER into the mitochondria. This overloads the mitochondria and produces mitochondria determined apoptosis (Sano et al., 2009). Furthermore SIT, a truncated version of the sarco/endoplasmic reticulum Ca^{2+} -ATPase, localises to the ER and promotes Ca^{2+} overload in the mitochondria. This leads to apoptosis during ER stress and therefore suggests dual roles of ER-mitochondria contact sites in the UPR response (Chami et al., 2008). Interestingly, PERK silencing weakens ER-mitochondrial contact sites and is protective against ROS damage (Verfaillie et al., 2012). Furthermore, PERK has

been shown to directly interact with Mfn2, with this interaction being required for the progression into UPR (Muñoz et al., 2014). Together these studies suggest that ER-mitochondria contacts are vital in the regulation of ER health. They can contribute to both ER survival and cell apoptosis, however their exact role is still under much deliberation.

1.5.2 The Molecular Basis of ER-Mitochondria contact sites

1.5.2.1 ERMES

In yeast, there are two main protein complexes which act as molecular tethers between the ER and mitochondria. First, ERMES which is composed of: Mitochondrial morphology maintenance 1 (Mmm1), an ER protein, mitochondrial distribution morphology 34 and 10 (Mdm34 and Mdm10), two OMM residing proteins and the cytosolic mdm12 (Kornmann et al., 2009). In addition, Gem1, the yeast homologue of EF hand containing GTPase Miro, has been found to be a key regulatory subunit of ERMES in yeast. The ERMES complex has various functions including involvement in lipid metabolism, mitochondrial dynamics and protein sorting, as well as in mitophagy. It is shown that ERMES components co-localise with Atg8, a key protein in autophagy. In addition, defects in ERMES result in an increase in the production of immature autophagosomes (Böckler and Westermann, 2014). Many functions of ER-mitochondria contacts are conserved, highlighting their importance in cell health and function. Interestingly, despite many of its functions being well conserved, there are no current mammalian homologues of ERMES. However, many proteins have been investigated for their ability to tether the ER and the mitochondria and research has been undertaken to determine their roles at these sites.

1.5.2.2 IP₃R, Grp75 and VDAC

The first complex identified in mammals was the chaperone mediated interaction between inositol 1,4,5 triphosphate receptor (IP₃R) and VDAC through Grp75. VDAC was previously shown to accumulate at ER-mitochondria contact sites and regulates the transfer of Ca²⁺ from high [Ca²⁺] micro-domains created by IP₃R to the inner membrane space (Gincel et al., 2001; Rapizzi et al., 2002). A yeast 2-hybrid screen and follow up co-immunoprecipitation experiment found that Grp75, a chaperone protein, interacts with both IP₃R and VDAC (Szabadkai et al., 2006).

Complete loss of IP₃R did not show a physical alteration in ER-mitochondrial contact sites, however, the loss of Grp75 abolishes the Ca²⁺ influx into the mitochondria through ER-mitochondria contact sites (Szabadkai et al., 2006). This leads to the hypothesis that VDAC, IP₃R and Grp75 act as a functional tether rather than a physical one (Csordás et al., 2006).

1.5.2.3 Mfn2

The role of Mfn2 as a molecular tether is not clear. De Brito et al first described Mfn2 as a physical tether between the ER and mitochondria, as knockout of Mfn2 resulted in a decrease in ER-mitochondrial contact sites. (de Brito and Scorrano, 2008). Functional studies supported this, as depletion of Mfn2 decreases autophagosome formation and reduces calcium import (de Brito and Scorrano, 2008; Hamasaki et al., 2013). Since the original publication however, there have been disputes suggesting that Mfn2 is not a true physical tether. Mfn2^{-/-} mouse embryonic fibroblasts (MEF's), the same cell line used in the original study, showed a robust increase in ER-mitochondria contact when examined by electron microscopy (EM), contradicting the previously published data (Cosson et al., 2012). The difference was reasoned to be due to method of analysis. De Brito et al used confocal microscopy with co-localisation coefficient Menders, which is affected by changes in organelle morphology. This is extremely important when investigating Mfn2 as its removal results in highly fragmented mitochondria (Filadi et al., 2015; Ziviani et al., 2010). Overall it is thought that Mfn2 is involved with regulation of ER-mitochondria contact sites, but it is not a physical tether.

1.5.2.4 VAPB and PTPIP51

VAPB is an ER-residing protein comprised of 7 β strand globule domains. It has 22% homology to the major sperm protein (MSP), a central coiled coil domain and a C-terminus ER targeted transmembrane domain. PTPIP51 is a 470 amino acid protein with a molecular weight of 52 kDa. PTPIP51 has 2 conserved domains, conserved regions 1 and 2 (CR1 and CR2), with a transmembrane domain located in the N terminus (Brobeil et al., 2011; Ota et al., 2004). PTPIP51 mRNA is expressed in a range of tissues including cerebellum, cerebrum, kidney, liver, lung and skeletal muscles, as well as in most cell lines (Lv et al., 2006). An interaction between VAPB and PTPIP51 was established and has defined them as present in ER-mitochondria contact sites (De Vos et al., 2012). EM and confocal microscopy later confirmed that alterations in PTPIP51 or VAPB are accompanied by a changes

in proportion of ER in contact with the mitochondria, thus showing that changing these proteins can alter in ER-mitochondria contact sites (Stoica et al., 2014). These interactions between VAPB and PTPIP51 dramatically affect the function of ER-mitochondrial contact sites. Depletion of VAPB or PTPIP51 can disturb Ca^{2+} handling between the ER and mitochondria, resulting in a delay in Ca^{2+} uptake by the mitochondria. Furthermore, a VAPB mutant which decreases calcium handling also shows aggregation of the mitochondria (De Vos et al., 2012). Together these data suggest that ER-mitochondria contacts may impact on the health of the mitochondria.

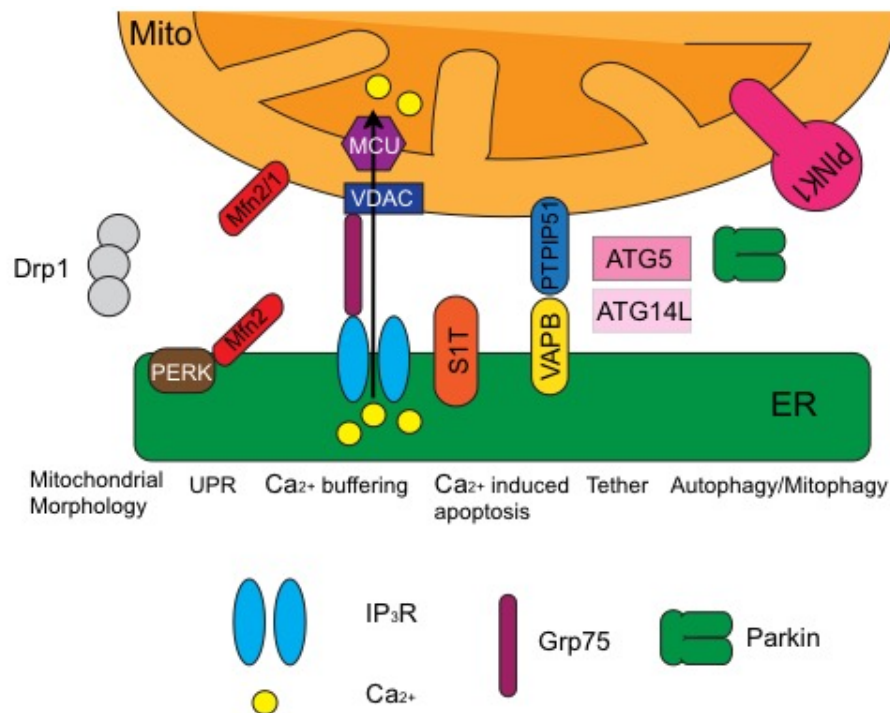


Figure 1.7: Molecular component functions of ER-mitochondrial contact sites: Schematic representation of the proteins found in ER-mitochondria contact sites grouped in relation to function.

1.6 Phosphatidylinositol (PI) metabolism

PI is synthesized by PI synthase (PIS) from cytidine diphosphate diacylglycerol (CDP-DAG) and inositol, which produces a DAG backbone with an inositol ring (Antonsson, 1997)(**Fig.1.8A**). PI is predominately produced in the ER and is the precursor to important signalling molecules, such as phosphatidylinositol 4-phosphate (PI4P) and phosphatidylinositol 4, 5 bisphosphate (PI(4,5)P₂) that are phosphorylation derivatives of PI. Phosphorylation or de-phosphorylation occurs predominantly at the D3, D4, and D5 position of the inositol ring and has a multitude of kinases and phosphatases mediating this process (**Fig 1.8**). This regulation has

to be closely monitored as phosphatidylinositols are involved in many important cellular functions including vesicle trafficking, actin rearrangement and Ca^{2+} regulation (Mejia and Hatch, 2016). Two enzymes involved in the regulation of PI have been linked to PD and mitochondrial quality control: Synaptojanin (Synj) and phosphatidylinositol 4 kinase III β (PI4KB) (**Fig 1.8**).

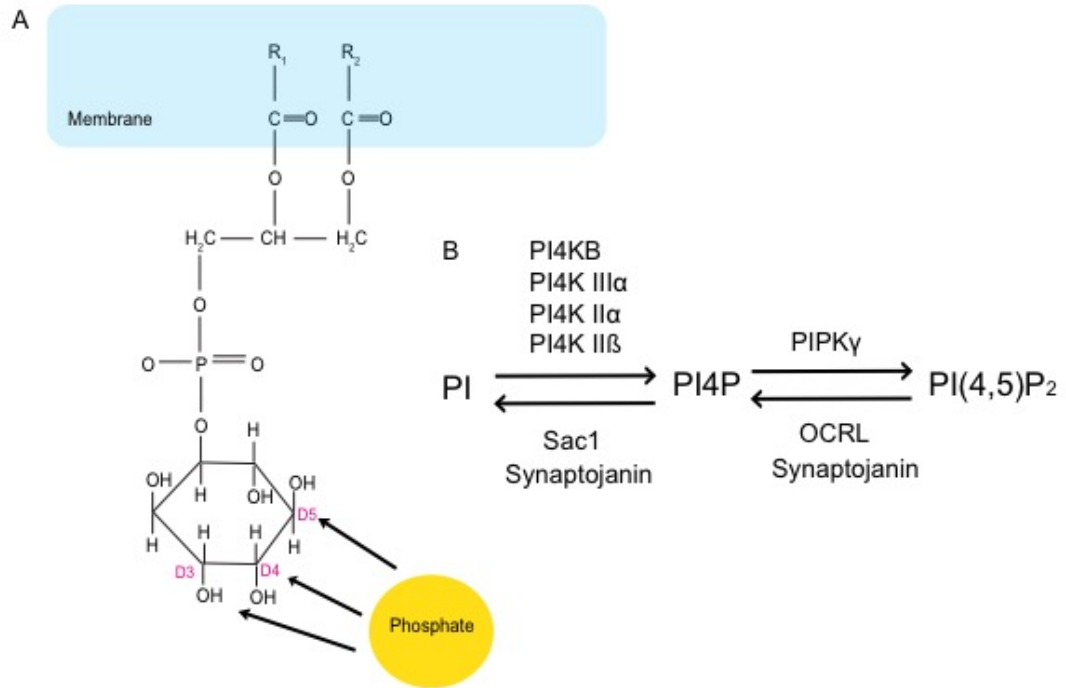


Figure 1.8: Phosphatidylinositol metabolism: (A) A schematic representation of the chemical structure of PI showing the inositol ring structure. The D3, D4 and D5 positions are highlighted (pink) and show the most common positions for phosphorylation. R1 and R2 represent the acetyl chains which are present in the phospholipid bilayer (B) Schematic representation of the phosphorylation derivatives of PI including PI4P and PI(4,5)P₂. A group of PI4 kinases including PI4KB regulate the addition of phosphate at the D4 position to produce PI4P. PI5 kinase, PIPK γ regulates the addition of phosphate onto the D5 position of the inositol ring of PI4P to produce PI(4,5)P₂. The de-phosphorylation is mediated by a group of phosphatases which include Lowe oculocerebrorenal syndrome protein (OCRL) and Sac1. Synaptojanin complements their function with its dual phosphatase domain and can de-phosphorylate both PI4P and PI(4,5)P₂.

1.6.1 Phosphatidylinositol 4 kinase III β (PI4KB)

PI4KB belongs to a family of phosphatidylinositol kinases which mediates the phosphorylation at the D4 position of the inositol ring of PI to produce phosphatidylinositol 4-phosphate (PI4P). There are four PI4K's, that produce PI4P and each isoform has a distinct subcellular localisation which suggests its product,

PI4P, may also be compartmentalised (**Fig 1.9**) (Boura and Nencka, 2015). The four PI4K's are divided into two subtypes, PI4K II and PI4K III, which each contain an α and β sub-isoform. PI4K II α and PI4K II β are highly homologous 55 kDa proteins, which are regulated by palmitoylation via a CCPC motif within their kinase domain (Jung et al., 2008). Once palmitoylated, PI4K II's can stably associate with intracellular membranes and become active (Jung et al., 2008). PI4K II α is the most active PI4K, producing 50% of the PI4P in the cell and is predominately localised to the Golgi (Wang et al., 2007). PI4K II β however is predominantly found in cytoplasmic pools and is stabilised by Hsp90. Its predominant function is in early T cell activation (**Fig 1.9**) (Jung et al., 2011; Wei et al., 2002). The PI4K III's are known as typical PI4Ks and can be split into PI4K III α and PI4KB. PI4K III α is localised in pools at the plasma membrane where it produces PI4P to be used by PI5K to generate PI(4,5)P₂, which is required for clathrin mediated endocytosis (Chung et al., 2015). PI4KB is localised predominantly at the Golgi and in the nucleus, however there are reports that PI4KB has also been identified at the OMM (Balla et al., 2002; Guo et al., 2003)(Balla et al., 2000) (**Fig 1.9**).

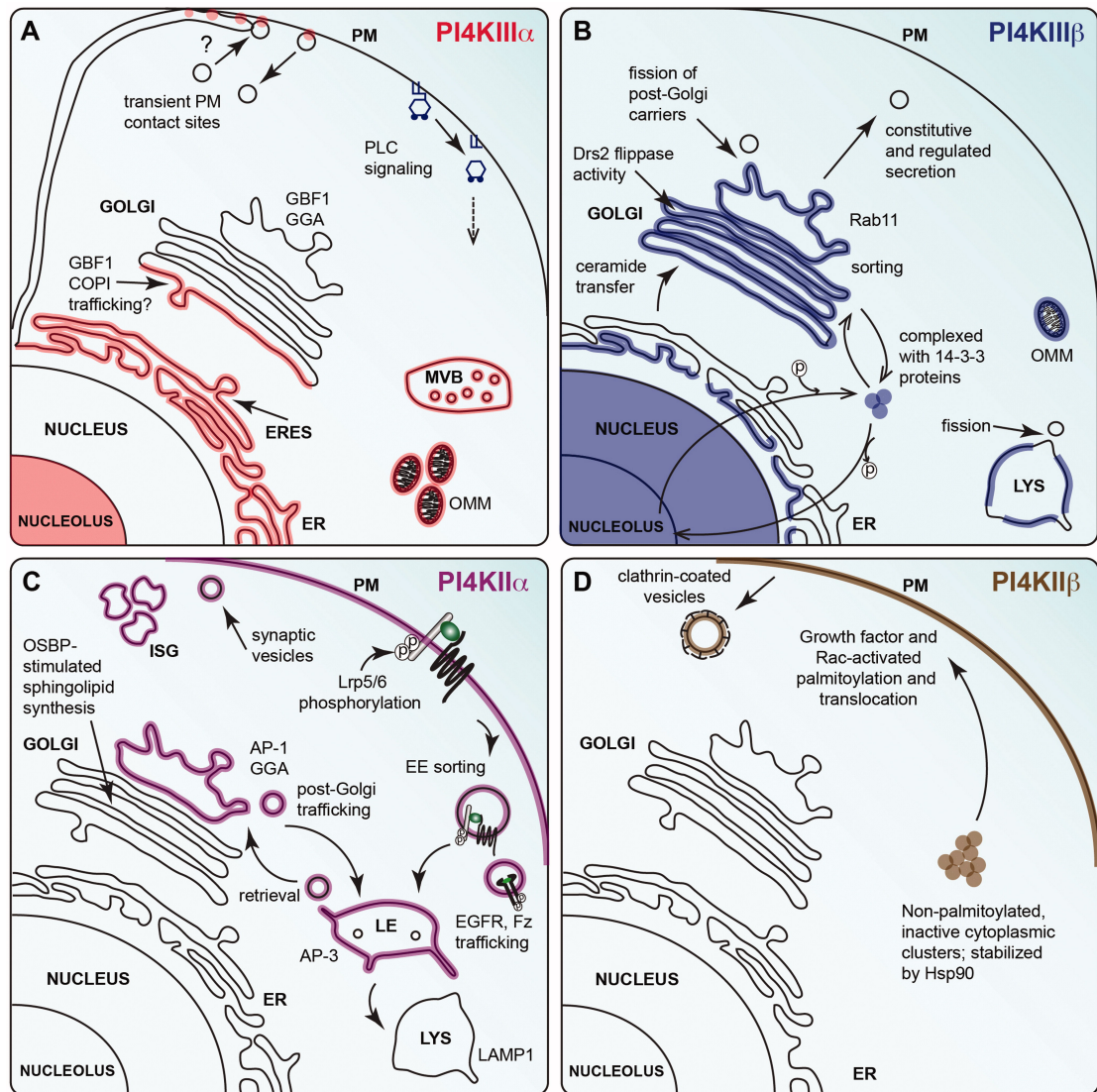


Figure 1.9: The localisation of PI4K isoforms and the processes they regulate: The data for each panel is from mammalian cells, yeast and animal model systems. Localization of endogenous and expressed kinases, as determined using immunofluorescence, immunoelectron microscopy, immunoblotting, kinase assays using fractionated membranes and live imaging of fluorescent fusions to PI4Ks. Abbreviations: EE, early endosome; ISG, immature secretory granules; LE, late endosome; LYS, lysosome; MVB, multivesicular bodies; OMM, outer mitochondrial membrane. (Tan and Brill, 2014).

1.6.1.1 PI4KB Functions

The most well established functions for PI4KB are mediated through the production of PI4P at the Golgi. PI4KB works with PI4K II α to regulate a gradient of PI4P across the Golgi (Tan and Brill, 2014). PI4P mediates various functions at the Golgi. The recruitment of Rab proteins by PI4P enhances binding to myo2, allowing the transport of vesicles along actin cables to the plasma membrane, thereby mediating vesicle transport (Demmel et al., 2008; Santiago-Tirado et al., 2011). In addition,

loss of PI4KB or PI4P results in Golgi fragmentation, suggesting a role for PI4KB in Golgi morphology in a number of systems (Daboussi et al., 2012; Godi et al., 1999; Polevoy et al., 2009; Strahl et al., 2003). In mammals, both Golgi phosphoprotein 3 like (GOLPH3L) and Golgi phosphoprotein 3 (GOLPH3) are PI4P effectors and bind PI4P (Bell et al., 2001; Snyder et al., 2006; Wu et al., 2000). GOLPH3 interacts with the actin cytoskeleton via the binding of Myosin18A, which engages tensile forces on the TGN that initiate Golgi extension and vesicle budding (Dippold et al., 2009). Interestingly, this can be antagonised by GOLPH3L which is unable to bind Myosin18A and acts as competitor for PI4P resulting in Golgi contraction (Dippold et al., 2009; Ng et al., 2013). Together these suggest a function for PI4KB in regulation of the Golgi architecture through production of PI4P and its effector proteins. Finally, other PI4P effector proteins such as CERT, FAPP2, OSBP and ORP9L are all involved with lipid metabolism, suggesting PI4KB is important in regulating the lipids within the Golgi (Brice et al., 2009). Full review of PI4P functions is reviewed in (Tan and Brill, 2014).

In addition to the production of PI4P, which can mediate different effects on the Golgi, there have also been non-enzymatic functions suggested. In *Drosophila* four wheel drive (*fwd*), the homologue of PI4KB, binds Rab11 and is required for the correct localisation of Rab11 and its downstream effector Nuf to mediate cytokinesis of spermatocytes (Polevoy et al., 2009). In mammals, PI4K can simultaneously recruit Rab11 and the downstream effector FIP3 through its helical domain, suggesting an alternative function of PI4KB at the Golgi (Burke et al., 2014). The non-catalytic functions of PI4KB have been suggested to regulate membrane changes or to be involved with endocytic pathways (Boura and Nencka, 2015). Interestingly, PI4KB is essential for some forms of viral replication including enteroviruses, for which there is currently no treatment (Hsu et al., 2010). Furthermore, mutations in PI4KB and Rab11 confer resistance to anti-malaria treatments and suggest that the non-enzymatic functions may be key to preventing viral replication (McNamara et al., 2013).

Of interest, is the localisation of PI4KB at the OMM (**Fig .1.9**) (Balla et al., 2000). Its presence on the mitochondria suggests it can be involved with mitochondrial function. Exactly what role PI4KB is conducting at the mitochondria is still under much study, however an RNAi screen based on mitochondrial morphology in S2R+ *Drosophila* cells found that knockdown of the *Drosophila* homologue of PI4KB, *fwd*, resulted in a fused mitochondrial network. Thus, implicating PI4KB in changes in

mitochondrial morphology and mitochondrial quality control (Pogson et al., 2014). However, much work needs to be conducted to reveal the mechanisms behind this result and any further PI4P function at the mitochondria.

1.6.2 Synaptojanin (Synj)

Synaptojanins are a family of phosphatidylinositol phosphatases which regulate the dephosphorylation of PI(4,5)P₂ to PI4P and the further phosphorylation of PI4P to PI through their unique dual phosphatase domain structure. There are two synaptojanins in the human genome, *SYNJ1* and *SYNJ2* (Drouet and Lesage, 2014). These genes encode for a variety of synaptojanin isoforms (**Fig 1.10A**). *SYNJ1* can be alternatively spliced to produce SYNJ1-145 (145 kDa) and SYNJ1-170 (170 kDa). Both isoforms are ubiquitously expressed, however SYNJ1-145 is found in high concentrations within the brain while SYNJ1-170 is the predominant isoform in the kidneys, making SYNJ1-145 the main neuronal phosphatase (Drouet and Lesage, 2014; Perera et al., 2006; Ramjaun and McPherson, 1996). The two isoforms differ at the C-terminus, which contains a proline rich region (PRR) that comprises at least 5 Src Homology 3 (SH3) domains. These are principally involved with protein-protein interactions (**Fig 1.10B**). Synaptojanin 2 (*SYNJ2*) can be alternatively spliced to form SYNJ2A, SYNJ2B1 and SYNJ2B2. The main difference between SYNJ2A and SYNJ2B is the addition of a 248 amino acid sequence which is rich in SH3 protein binding domains and the absence of PDZ binding domain in SYNJ2B. SYNJ2B is more similar in structure to SYNJ1, whose main function is in clathrin mediated endocytosis (Rusk et al., 2003). Reports have suggested that SYNJ2B is prominent in the early stages of clathrin coated pit formation rather than later stages like SYNJ1 (Rusk et al., 2003). SYNJ1 can bind endophilin and PI(4,5)P₂, allowing it to be recruited to clathrin coated vesicles in order to promote the dephosphorylation of PI(4,5)P₂ and clathrin un-coating later in clathrin mediated endocytosis (Itoh et al., 2005).

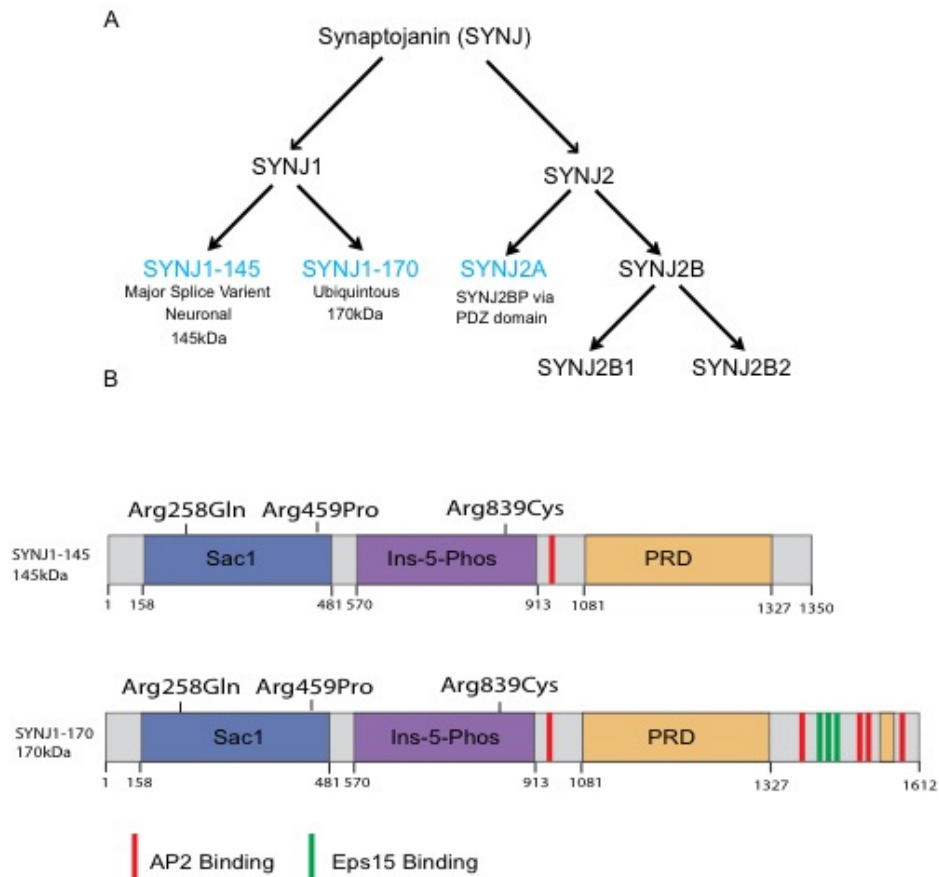


Figure 1.10: Synaptojanin isoforms and functions: There are two SYNJ's which are present in the human genome (SYNJ1 and SYNJ2). These have their own splice variants and isoforms depicted in (A). Those highlighted in blue are the ones considered important in PD. (B) Depicts the domain structure of the two alternative splice variants of SYNJ1. These include the Sac1 phosphatase domain (blue), inositol-5-phosphatase domain (purple) and proline rich domain (orange) of SYNJ1-145 and SYNJ1-170. The AP2 and Eps15 binding domains are shown in red and green, respectively. The known PD mutations are depicted with two being shown in the Sac1 domain and one situated in the Ins-5-Phos domain.

The functions of SYNJs are predominantly based at the plasma membrane and are involved with clathrin mediated endocytosis (CME) (Geng et al., 2016). CME starts with recruitment of AP2, the 2nd most common protein complex in vesicle endocytosis at the plasma membrane, to the plasma membrane by binding to PI(4,5)P₂. AP2 can recruit clathrin and bind a multitude of different cargos to be endocytosed. Three clathrin molecules can form triskelia and incorporate with curvature effector proteins to produce the force required for membrane curvature and the formation of an early vesicle. Dynamin is recruited to budding vesicles via binding to PI(4,5)P₂, oligomerises and aids the fission of the vesicle neck . Once

released, Auxillin and Synaptojanin act in the final step of clathrin mediated endocytosis to dephosphorylate PI(4,5)P₂, which aids the dissociation of AP2, clathrin and other coat proteins. This allows for un-coating of the vesicle and enables it to fuse with intracellular membranes (McMahon and Boucrot, 2011). As SYNJ1-170 contains many SH3 domains and multiple AP2 binding sites, it is thought that this isoform is the core isoform in clathrin mediated endocytosis.

The necessity of SYNJ1's role in endocytosis can be seen in SYNJ1 null mice who have muscle weakness, ataxia, poor motor control seizures and die shortly after birth. Further studies in these mice, as well as in yeast, have shown that a deficiency in SYNJ1 results in a rise in PI(4,5)P₂, an enlargement of the actin rich zones where vesicles form and an increase in clathrin coated vesicles (Cremona et al., 1999a). Mutations within the conserved regions of either domain decrease synaptic recycling, suggesting SYNJ1's dual domains are required for synaptic vesicle transmission (Mani et al., 2007).

There is mounting evidence that synaptic transmission may play a role in PD. Many PD related genes have been linked to endocytosis and vesicle recycling. SYNJ1 has been shown to be mutated in AR-JP, suggesting a function of SYNJ1 in PD. In addition there are reports that more PD related genes are now being linked to endocytosis and vesicle recycling. Auxilin-1 (*DNAJC6*) has recently been identified in atypical AR-JP and is a binding partner of SYNJ1 (Edvardson et al., 2012). Mutations in SYNJ1 and Auxilin-1 present with very similar clinical phenotypes in patients. Furthermore, SYNJ1 and Auxilin knock out mice give identical phenotypes, therefore suggesting a common pathway of synaptic transmission may be involved with PD (Yim et al., 2010). However, mitochondrial dysfunction is at the forefront of PD research and it is attractive to hypothesise that SYNJs may impact on mitochondria. SYNJ2A, which regulates the dual dephosphorylation of PI(4,5)P₂ to PI4P and PI, is recruited to the OMM by the mitochondrial targeted SYNJ2 binding proteins (SYNJ2BP). The expression of SYNJ2BP and SYNJ2 resulted in perinuclear clustering of mitochondria, thus suggesting a role of PI(4,5)P₂ metabolism at the mitochondrial membrane and in mitochondrial function (Nemoto and De Camilli, 1999a). Further investigations into PI(4,5)P₂ found that reducing or masking PI(4,5)P₂ on the OMM resulted in fragmentation of the mitochondrial network and caused a defect in starvation induced autophagy (Rosivatz and Woscholski, 2011). Together these data may implicate PI(4,5)P₂ has a role in mitochondrial quality control and that it may impact upon mitophagy.

1.7 Hypothesis and Aims

Several studies have suggested that phosphatidylinositides and ER-mitochondria contact sites could potentially contribute to mitochondrial quality control and impact on the development of PD. Following on from these studies, I hypothesised that phosphatidylinositides contribute to mitochondrial quality control by regulating the PINK1/Parkin pathway.

The aim of this project was first to take advantage of the robust *Drosophila* based PD model and numerous genetic tools available, in order to investigate genetic interactions between *fwd*, *synj* and *pink1* or *parkin* *in vivo*. The effect of altering *fwd* and *synj* on locomotor ability will be analysed via the use of climbing and flight assays to test co-ordination, strength and reflex action. A further aim was to use a dsRNA based approach to investigate the effect of *fwd* and *synj* on mitochondrial morphology in S2R+ *Drosophila* cells, in order to verify previous findings.

In parallel, I aimed to investigate the effects of manipulating the mammalian homologues, *PI4KB*, *SYNJ1* and *SYNJ2*, on aspects of the PINK1 and Parkin pathway. To do this, YFP-Parkin HeLa cells, which robustly undergo Parkin translocation and mitophagy with CCCP treatment, were employed in conjunction with siRNA knockdown to investigate the effect of depleting these homologues.

While ER-mitochondrial contacts are known to play a role in mitochondrial fission and autophagy, they are difficult to study in a dynamic context. For this reason, better imaging tools are needed in order to investigate the roles of ER-mitochondria contacts in the cell. Therefore, a secondary aim of the project was to investigate a new fluorescence protein based system to easily visualise ER-mitochondria contact sites and dynamic processes associated with them, such as mitochondrial quality control, to be assessed in real time. Two different systems, dimerising dependent GFP (ddGFP) and biomolecular fluorescence complementation (BiFC) probes were analysed for their utility as a reporter system for ER-mitochondria contacts.

2: MATERIALS AND METHODS

2.1 Drosophila Genetics

2.1.1 Drosophila Husbandry

Drosophila stocks were maintained in wool stopped plastic vials which contained cornmeal agar and bakers yeast. These stocks were kept at 18°C and flipped into new vials every 3 weeks. Experimental crosses were kept at 25°C and contained approximately 5-10 virgin females and 3-4 males. These were flipped every 2-3 days to ensure maximum progeny collection. Larvae start to be produced 3 days post cross set up and pupa start to enclose after 10 days. To collect progeny each vial were placed on a CO₂ anesthetise pad and phenotypes scored.

2.1.2 Drosophila lines

Below are a list of *Drosophila* lines that were used in this project. They include overexpression lines and knockdown lines, which used the GAL4-UAS system. The GAL4 driver was used to regulate the spatial and temporal expression of a UAS cassette. In addition, *Drosophila* strains, which harboured various mutations, of a range of different genes of interest, were also used.

Fly stocks used in this project are listed below

Stock Name	Genotype	Source
<i>park</i>²⁵	w; <i>park</i> [25]/TM6B	Whitworth lab
<i>pink</i>^{B9}	w <i>pink</i> 1[B9]/FM7.GFP	J Chung
<i>fwd</i>³	w; <i>fwd</i> [3] e/TM6B	Julie Brill
<i>fwd</i>¹	l(3)AS69 <i>fwd</i> [neo1] e/TM3	Bloomington
<i>Df</i>	Df(3L)7C/ TM6B	Bloomington
<i>UAS-fwd</i>	w; P{UAS-GFP- <i>fwd</i> }attP40	In this study
Control RNAi	w; P{UAS-LacZ-RNAi}GD51446 II	VDRRC
<i>fwd</i> RNAi KK	w; p{UAS- <i>fwd</i> -RNAi}GD12100	VDRRC
<i>fwd</i> RNAi GD	w; p{UAS- <i>fwd</i> -RNAi}KK102095}	VDRRC
<i>synj</i>^{LY}	w; FRT42D <i>synj</i> [Ly]/CyO.GFP	Patrik Verstreken
<i>synj</i>¹	y w <i>eyFLP</i> ; FRT42D <i>synj</i> [1]/CyO Kr>GFP	Patrik Verstreken
<i>UAS-synj</i>	w; P{UAS-EGFP-HA- <i>synj</i> }/TM6B	Patrik Verstreken
<i>synj</i> RNAi 2	w; p{UAS- <i>synj</i> -RNAi}TRIP27489}	Bloomington
<i>synj</i> RNAi 3	w; p{UAS- <i>synj</i> -RNAi}TRIP34378}	Bloomington
<i>da-GAL4</i>	w; P{ <i>da-GAL4</i> }	Bloomington
<i>Act-GAL4</i>	w; P{ <i>Act5C-GAL4</i> }/CyO	Whitworth lab
<i>Marf</i>^B	y w <i>marf</i> [B]/FM7c, Kr>GFP;	Hector Sandoval, Hugo Bellen
<i>Opa</i>^{1s3475}	w; <i>Opa</i> 1[s3475]/CyO.GFP	Bloomington
<i>UAS-drp1</i>	w; P{UAS- <i>drp1</i> [WT]}/TM6B	J Chung

2.1.3 Climbing Assay

Aged matched 0-3/4 days old *Drosophila* of the correct genotype were collected the night before the climbing assay. This allows for any residual effects of the CO₂ to resolve. *Drosophila* were collected in groups of 20 and each tube was blinded. On the morning of the climbing assay the *Drosophila* were left for 90 minutes, at 23°C in full light to acclimatise to the new environment. The climbing apparatus (Figure 2.1) consists of 5 upper and 6 lower tubes with *Drosophila* being inserted in position 1. Each set of 20 *Drosophila* were tapped down to the bottom of the tube, using the same force and number of taps. They were then given 10 seconds to climb. Those *Drosophila* which made it up past the junction (Position 2) were then moved into the next adjacent tube set and the process repeated 5 times. This gives the *Drosophila* 5 chances to climb for 10 seconds, testing strength and co-ordination. Those that were good at climbing made it to the last set of tubes (Positions 3) and were given a score of 5 (Maximum) those that remained at position 1 were given a score of 0 (minimum). This was then converted into a climbing index. A minimum of 50 *Drosophila* was tested in each genotype.

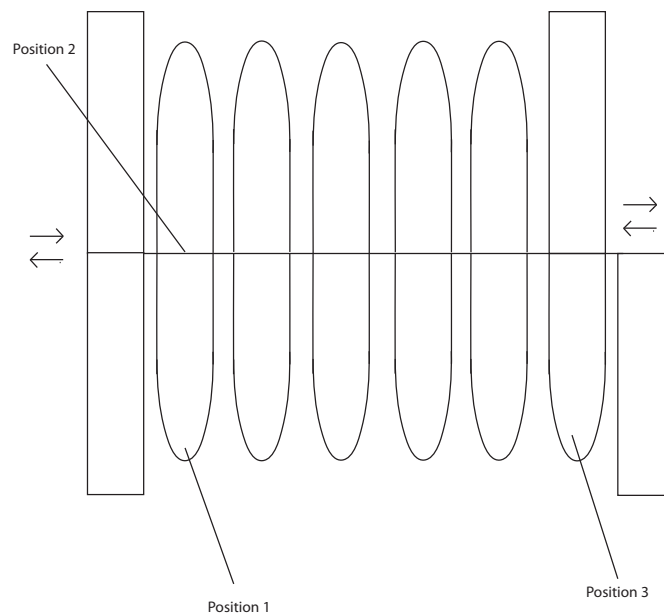


Figure 2.1: Climbing apparatus: Approximately 20 *Drosophila* are inserted in at position 1 and allowed to climb up for 10 seconds. Those that are efficient at climbing are able to move past position 2 within the time limit and are moved over into the next tube alone and the process repeated.

2.1.4 Flight Assay

The flight assay was conducted the afternoon of the climbing assay after having left the *Drosophila* in food-lined vials for 1 hour to habituate to their surroundings. Once acclimatised, the flight ability of the *Drosophila* was tested using a 1 L cylinder which had an A4 acetate sheet, coated in silicon grease, surrounding the inside. This sheet had 4 sections each of 7cm tall to allow for scoring. A funnel attached to a cork and a piece of plastic tubing was inserted in the top. The *Drosophila* were dropped down the tube from the same height. This gave them the chance to fly. Those *Drosophila*, that were able to initiate flight would fly out and get stuck to the silicon grease. This was then swiftly removed from the 1L cylinder and another clear acetate sheet was then placed on top, sandwiching the *Drosophila* and preventing any escaping therefore, leading to more accurate scoring. Those *Drosophila* which fell straight to the bottom of the cylinder were given a score of 0 (assay Minimum) while those that were in the top quarter of the acetate sheet were given a score of 4 (assay Maximum). Any *Drosophila* that managed to fly away from the sticky acetate sheet or stuck to the inside the plastic tubeing were also given a score of 4, as it suggested that they were strong flyers and had good motor ability. An average flight index was given to each genotype.

2.2 Cell Culture Techniques

2.2.1 Drosophila Cell Lines

For the purpose of examining mitochondrial morphology Schneider 2 receptor positive fly cells (S2R+) chosen based on their increased adhesive ability and relatively large size (15 μm). This made it easier for them adhere to the bottom of the culture dish, making them easier to image. The S2R+ cells were derived from a late stage embryonic tissue primary culture and are thought to be macrophage in lineage.

2.2.2 Drosophila Cell Culture

Drosophila S2R+ cells were grown at 25°C in the absence of CO₂. They have a doubling time of 39 hours and so were passaged in T75 flasks every 3-4 days in a 1:3 ratio. They were grown in Schneider *Drosophila* Media 1X liquid with L-Glutamine (Gibco, 21720-024) which was enriched with 10% Foetal bovine serum (FBS) (Sigma F4135) and 1% penicillin-Streptomycin (Sigma, P4333). To ensure sterility the media was filtered (Millipore, SCGPU05RE) and stored at 4°. Once a passage number of 30 was reached, a new aliquot was defrosted and grown until they reached a passage number of P2-3 before experiments were conducted with them.

2.2.3 Human Cell lines

HeLa cells and YFP-Parkin HeLa were used to analyse Parkin translocation, and preliminary investigation into the split GFP and ddGFP constructs. Their ease of use and transfection, made them ideal for preliminary investigation. HeLa lines stably expressing pLVX-Puro-YFP-Parkin were kindly gifted by Dr Jon Lane (University of Bristol). CV1, a monkey kidney cell line were used to image mitochondria and ER as they have a large, flat morphology making them easy to image. HEK 293 cells were used to examine the initial expression of different constructs by western blot when optimizing the ER-mitochondria screen as they are easy to transfect and lyse.

2.2.4 Cell Culture

HeLa cells were grown at 37°C with 5% CO₂. HeLa and HEK 293 cells have a doubling time of 24 hours and so were passaged in T75 flasks every 3-4 days in a ratio 1:10. Complete media consisted of MEM with HEPES and GlutaMAX™ (Gibco, 42360-032), with 10% FBS (Foetal Bovine serum) and 1% Penicillin Streptomycin

which was filtered and stored at 4°C. Before passaging the media was heated to 37°C to prevent cell shock. The old media was poured off and 10 ml of phosphate buffered saline (PBS) (Thermo scientific, OXBR0014G) was added to remove any remaining serum that may inhibit the Trypsin enzyme. 3-5 ml of 1x Trypsin (Gibco, 15090-046) is added to each flask and left at 37°C until the adherent cells had detached. 5 ml of complete culture media was then added to inhibit the trypsin and the cell re-suspended. 1-2 ml of this Trypsin media mix is added to 13 ml of complete media depending on the confluency.

2.2.5 Freezing down cells

HeLa, HEK 293, CV1 and *Drosophila* cells were grown until 100% confluent in T75 flasks. Trypsin was used to detach the cells from the bottom of the plate, they were then spun down in 15 ml Falcons (Starlab E1415-0800) at 1000g for 4 minutes. Cells were re-suspended in 1 ml of freeze down media: 20% FBS, 10% dimethyl sulfoxide (DMSO) (Sigma D2650) in complete media or just in FBS with 10% DMSO. Cells were transferred to cryovials (Nalgene, V4757) incubated at -80°C for 24 hours in propan-2-ol before being transferred to liquid nitrogen or kept at -80°C indefinitely.

2.3 Transfecting *Drosophila* cells lines

S2R+ *Drosophila* cells were plated at 50,000 cells per well in an 8 well culture slide (Ibidi, 80826) and 48 hours before imaging, they were transfected with plasmids shown in the table below.

Transgene	Vector	Source
Mitofusin-FLAG	pAct-PPA	Elena Ziviani
GFP- <i> fwd</i>	pAc5.1	This Study
GFP- <i>synj</i>	pAc5.1	This study

The plasmids were transfected with Effectene transfection reagent (Qiagen, 301425) using the standard protocol, altered for the smaller surface area of the 8 well culture slides. 500 ng of DNA was added to 30 µl of EC buffer and 0.8 µl of enhancer. This was shaken for 5 seconds, spun down and incubated at RT for 5 minutes. After 5 minutes 2.5 µl of Effectene was added. The solution was again mixed for 10 seconds, then spun down and incubated at room temperature for 8 minutes before being added straight to the already plated *Drosophila* cells. These were left for 48 hours until imaging was conducted.

2.4 Transfecting Human Cell lines

2.4.1 Effectene transfection

YFP-Parkin HeLa cells were transfected with 300-500 ng of DNA, in 8 well culture slides using the protocol as outlines in the section 2.3 *Drosophila* cell transfection. These were left for 24-48 hours with no changes to the media.

2.4.2 Polyethylenimine, linear (PEI) Transfection

HeLa, YFP-Parkin HeLa or HEK 293 cells were plated in 12 well plate, at a density which meant that they would be 70% confluent at the time of transfection. For immunofluorescence the cells were plated on 18mm sterile coverslips (VNR 631-1580) and without 18 mm cover slips for western blotting. Once the cells were 70% confluent the cells were transfected. For a 12 well plate the total DNA transfected for each well is 1000 ng in 100 µl of Opti-MEM[®] (Life Technologies, 11058-021) with 3 µl of PEI (Polysciences Inc, 23966). This can be scaled for the use of different sizes of plates. The PEI, DNA and Opti-MEM[®] mixture is vortexed immediately after the addition of the PEI, and then left for 20 minutes before being added to the cells. After 5-6 hours the media is changed to reduce cell death caused by the transfection reagent. The cells are incubated for 24 hours to allow transcription and translation to occur before being fixed or harvested.

2.4.3 Transfecting CV1 Cells

CV1 cells are unable to be transfected with PEI and therefore Turbofect (Thermo Scientific, R0531) is used as a transfection reagent using the same protocol as above (2.4.2 PEI Transfection).

2.4.4 Plasmids

The following plasmids were used in this study:

Transgene	Vector	Source
SYNJ1-145 R219Q	pcDNA2 FLAG	Pietro De Camilli
SYNJ1-145	pcDNA3 FLAG	Addgene 22291
SYNJ1-170	pCI-neo Myc	Addgene 22292
dsRED2-Mito	pDsRed2	Clontech
Empty Vector	pCI-neo	Promega
HA-PTPIP51	pCI-neo	Chris Miller
Myc-VAPB	pCI-neo	Chris Miller
GFP1-Mito	pAcGFP1	Clontech
mAKAP1 [34–63]-mRFP-yUBC6	-	György Hajnóczky
CFP-FRB-9x-ER(Sac1)	-	György Hajnóczky
mAKAP1-9x-FKBP-mRFP	-	György Hajnóczky
pBifc Constructs		
pBIFC VN155	pBIFC VN155	Addgene 22011
pBIFC VC155 (i152L)	pBIFC VC155	Addgene 27097
pBIFC VC155-VAPBTM	pBIFC VC155	This Study
pBIFC VN155(i152L)-PTPIP51TM	pBIFC VN155	This Study
ddGFP Constructs		
HA-ddGFPA	HA-pCI-neo	This Study
HA-ddGFPB	HA-pCI-neo	This Study
Myc-ddGFPA	Myc-pCI-neo	This Study
Myc-ddGFPB	Myc-pCI-neo	This Study
N-CEP10TM-HA-Linker-C	pCI-neo	This Study
N-CEP10TM-HA-Linker-C	pCI-neo	This Study
N- ddGFPA- Linker-Myc-VAPBTM-C	pCI-neo	This Study
N- ddGFPA- Linker-Myc-VAPBTM-C	pCI-neo	This Study

2.5 Western Blotting

2.5.1 Cell Lysis

Cells were cultured in a 12 well plate and seeded at 100,000 cells per well, transfected the following day then 24 hours later, harvested. The cells were placed on ice and washed with ice cold PBS before 80 μ l-200 μ l of lysis buffer was added. The monolayer of cells were dislodged via vigorous movement of a pipette tip (scraping) and repeated pipetting before transfer to a 1.5 ml tube. These were spun down for 30 minutes at 17000g (full speed).

Lysis buffer – 7ml

- NaCl Tris-HCL Buffer– 6188µl
- 1% Triton (Sigma-Aldrich)
- 10% glycerol (Fisher Scientific)
- 2 mM ethylene glycol-bis(β-aminoethyl ether)-N,N,N',N'-tetraacetic acid (EGTA) (Sigma-Aldrich)
- 1 mM magnesium chloride (BDH Laboratory supplies)
- 1x Protease inhibitor cocktail (Roche 118361700001 or Thermo Scientific 1861278)

NaCl Tris-HCL Buffer

- 50 mM Tris-HCL (Melford , B2005)
- 150 mM sodium chloride (Fisher Scientific)

2.5.2 Protein quantification

A Bradford assay was used to quantify the amount of protein in each sample. Bradford reagent was used in a 1:5 ration with double distilled water (ddH₂O). The sample was diluted 1/1000 in Bradford reagent (BioRad, 500-0006) and left 10 minutes. 1 ml of this mixture was added cuvettes (Sarstedt) and analysed by spectrophotometry at 595 nm (Eppendorf BioPhotometer). Alternatively the lysate was diluted 1/100 and plated into a 96 well plate along with a Bovine Serum Albumin (BSA, Sigma-Aldrich, 1001760904) protein standard and analysed by a PHERAstar plate reader (PHERAstar FS BMG Labtech).

2.5.3 SDS PAGE

The samples are mixed with 4x sodium dodecyl sulphate (SDS) loading buffer and heated for 10 minutes at 95°C or 5x Laemmli buffer and heated at 100°C for 5 minutes to denature the proteins producing a linear peptide.

4x SDS Loading Buffer

- 240 mM Tris-HCL pH 6.8
- 8% SDS
- 40% glycerol
- 1% beta mercaptoethanol
- 0.008% Bromophenol Blue

5x Laemmli Buffer

- 300 mM Tris pH6.8
- 10% SDS (Fisher Scientific, S/5200/53)
- 0.01% propanol (Fisher Scientific, p/7500/17)
- 25% beta mercaptoethanol
- 25% glycerol (Fisher Scientific)
- Bromophenol Blue

The samples were then centrifuged briefly and could be kept on ice or frozen for later use. Polyacrylamide gels were made using the Bio-Rad mini-PROTEAN Tetra Handcast System to manufacture instructions. Gels were loaded into electrophoresis chamber and 1x TGS (Tris/Glycine/SDS) running buffer was added.

1x TGS Tris/Glycine/SDS Buffer

- 25 mM Tris (Melford B2005)
- 190 mM Glycine (Melford, G07009)
- 1% SDS (Fisher Scientific, S/5200/53)

Varying amount of protein were added to each well depending on the concentration of the cell lysate sample and the size of the wells. In addition, a protein standard (3-5 μ l) for monitoring protein molecular weight (Bio Rad, 161-0373) was added to at least 1 well. The gels were run at 70 mV through the stacking and then at 100-200mV through the resolving gel. The protein samples were run until the protein ladder suggested high resolution of the protein band of interests. This should resolve approx. half way down the gel.

2.5.4 Transfer

Once complete the Gel was removed from the electrophoresis kit and placed in transfer buffer 1x Tris/Glycine (TG) buffer containing 20% methanol.

1x Tris Glycine buffer

- 25 mM Tris (Melford B2005)
- 190 mM Glycine (Melford, G07009)
- 20% Methanol (Fisher Scientific, M/4000/17)

In parallel filter papers, sponges and either PDVF (Millipore, IPVH00010) or Nitocellulose (Amersham 10600002) membrane were placed in transfer buffer. In addition, PDVF membranes were also placed in 100% methanol for 5 minutes to allow for membrane activation. To transfer the proteins from the polyacrylamide gel to the membrane of choice, a transfer 'sandwich' was produced. This is composed and ordered like so: Sponge, 2x filter papers, acrylamide gel, membrane, 2x filter paper, sponge. This is held together by a transfer cassette. The construction of this transfer 'sandwich' allows for the close contact between the polyacrylamide gel and the membrane of choice. This transfer sandwich is placed in a transfer chamber with plenty of 1x TG transfer buffer and an ice block. This is ran at 100 mV for 1 hour, 300 mA for 2 hours or overnight at 30 V depending on the size of the protein of interest.

2.5.5 Blocking, Antibodies and Detection

Once the protein transfer is complete the membrane is removed from the cassette and cut down to size. Ponceau red allows visualisation of the protein on the membrane to check the loading of the gel is correct.

Ponceau solution

- 0.1% Ponceau S (Sigma-aldrich, P3504)
- 5% Acetic acid (Sigma – Aldrich, 27225-2-5L-R)

It is then blocked for 1-24 hours at either room temperature or at 4°C overnight in 5% milk (Marvel) in Tris Buffered Saline with 0.1% Tween20 (TBS-T) to prevent any non-specific protein binding. The membranes were then incubated in polythene bags or 30 ml falcon tubes along with the primary antibody for 1 hour at room temperature or 16 hours at 4°C on an orbital shaker or roller. The membranes were then removed from the bag or tube and washed 3x for 10 minutes before the addition of the secondary antibody. The secondary antibody was incubated for 1 hour at room temperature on a roller. The membrane was again washed 3x with TBS-T for 10 minutes before being ready for band detection. ECL (Thermo Scientific SuperSignal West Pico Chemi-luminescent substrate, 34080) was incubated with the membrane for 5 minutes before exposure to the light sensitive photographic film (Amersham, 1151579389). A range of exposure times were used, depending on the intensity of the band. The films were developed on an automatic film developer, G-box (GBOX iChemi-XT SYNGENE) or by manually dipping the film into the developer

and fix solutions. The bands were analysed and normalised to loading controls using software on FIJI.

Tris Buffered Saline – Tween20

- 20 mM Tris
- 150 mM NaCl.
- 0.1% Tween 20

2.6 Immunofluorescence

Once transfected the cell were left for 24 hours before being washed once with 1X PBS. 3.7% formaldehyde solution (Fisher, F/1451/PB17) was then added and left to incubate for 20 minutes. The formaldehyde solution was then removed and the cells washed twice with 1x PBS and once with 50 mM ammonium chloride (NH_4Cl_2 , BDH Laboratory supplies, 100173D). The ammonium chloride solution is then left on the cells for 10 minutes to quench the formaldehyde. This is removed and the cells washed 3x in 1x PBS. To permeabilise the cells they were incubated for 3 minutes in 0.2% triton x100 (Sigma- Aldrich) which allowed for efficient incorporation of the antibodies or dyes into the cell. Once again the cells were washed with PBS and left for 1 hour in 1% BSA (Sigma-Aldrich, 1001760904) before incubation with primary and secondary antibodies in BSA, each for 1 hour. Once antibody incubations were complete the cells were washed with 2 $\mu\text{g}/\text{ml}$ Hoechst (if needed) and then washed 3x with PBS before being mounted on glass slides using anti fade mounting media (Dako, S3023)

2.7 Antibodies and Dyes

Primary antibodies

Antibody Type	Name	Source	Product code	Dilution	Species	Uses
Primary	FAM82A2	ATLAS antibodies	HPA009975	1/1000 1/500	Rabbit	WB IF
Primary	HA7	Sigma – Aldrich	H9658	1/2000 1/1000	Mouse	WB IF
Primary	Myc 9B11	Cell signalling	2276	1/2000 1/500	Mouse	WB IF
Primary	HA	Sigma – Aldrich	H6908	1/1000 1/1000	Rabbit	WB IP
Primary	Actin	MILLIPORE	MAB1501	1/5000	Mouse	WB
Primary	ATP5A	Abcam	15H4C4	1/5000	Mouse	WB IF
Primary	JL8 (GFP)	Clontech	632380	1/5000	Mouse	WB
Primary	Calreticulin	Abcam	Ab2908	1/1000	Chicken	IF
Primary	Myc – 71D10	Cell signalling	2278	1/1000	Rabbit	WB IP
Primary	Synaptojanin	Abcam	Ab84309	1/500	Rabbit	WB IF

Secondary antibodies and Fluorescent dyes

Antibody/Dye	Name	Source	Product code	Dilution	Species
Dye	MitoTracker® Red CMXRos	Molecular Probes	M7512	50-150nM	-
Dye	Hoechst 33342	Molecular Probes	H3570	2 µg/ml	-
Secondary	Alexa Fluor® 594	Molecular Probes	A11005	1/500	Donkey anti Mouse
Secondary	Alexa Fluor® 568	Life Sciences	A11011	1/500	Goat anti Rabbit
Secondary	Alexa Fluor® 568	Life Sciences	A10037	1/500	Donkey anti Mouse
Secondary	Alexa Fluor® 488	Life Sciences	A21206	1/500	Donkey anti Rabbit
Secondary	Alexa Fluor® 488	Life Sciences	A21202	1/500	Donkey anti Mouse
Secondary	Alexa Fluor® 633	Life Sciences	A21071	1/500	Goat anti Rabbit
Secondary	Alexa Fluor® 488	Life Sciences	A11039	1/500	Goat anti Chicken
Secondary	DyLight™ 405	Thermo Scientific	35500	1/500	Mouse

2.8 Gene Knockdown

2.8.1 Production of dsRNA

PCR constructs, flanked by T7 promoter sites, were bought from the Sheffield RNAi facility. These were then amplified using the primers state below and protocol outlined in PCR section (2.12.2). These PCR products were then used in the vitro transcription T7 MEGAscript kit (Ambion, AM1334) following standard protocol. TURBO DNase was then added for 30 minutes at 37°C to purify dsRNA. 2.1 µl of ammonium acetate 'stop solution' was added followed by 52.5 µl ethanol and a 2

hour incubation at -80°C to precipitate the DNA. The mix was centrifuged at full speed for 1 hour at 4°C and the resultant pellet retrained and air-dried. This was re-suspended in 100 µl of PCR-grade water (Sigma – Aldrich, W4502). The resultant dsRNAs were run on a 3% agarose gel to check their size and spectrophotometry used to calculate the concentration.

Name	Sequence
TU	TAATACGACTCACTATAGGGtggcgcccctagatg
T1	TAATACGACTCACTATAGGGcgacgcccgcctgata
T2	TAATACGACTCACTATAGGGtaggtctagccccgc
T3	TAATACGACTCACTATAGGGcgcatgtagcctgcc
T4	TAATACGACTCACTATAGGGtagcctccctagcgc

2.8.2 dsRNA mediated knockdown

S2R+ *Drosophila* cells were re-suspended in serum free media and counted using a haemocytometer. 60,000 *Drosophila* cells in 150 µl were added to each well in an 8 well culture slide (Ibidi). 1.5 µg of dsRNA was added to each well and incubated for 1 hour at 25°C. Following this 150 µl of 2x serum media was added and the cells incubated at 25°C for 4 days.

2.8.3 siRNA acquisition

All siRNA constructs used in this study were bought from Dharmacon (Thermo Scientific) or Sigma-Aldrich. Control, PINK1, PI4KCB, SYNJ1 and SYNJ2 were bought as a smart pool so has multiple targeting siRNA's for their respective mRNA. Individual siRNA's were bought for SYNJ1. Each siRNA was re-suspended to make a 20 uM stock solution and then to make a 2 uM working solution.

Product Code	Gene Symbol	Company	Sequence
D-001206-13-20	Non Targeting	Dharmacon	proprietary information
M-004030-02	PINK1	Dharmacon	GAAAUCCGACAACAUCUU GAGAUCCGCCUGCAGUUG GGAGCCAUCGCCUAUGAAA GCAAUUGUGCUUCAUCUAA
M-006777-03	PI4KB	Dharmacon	GGAUGACCUUCGGCAAGA GAGAUCCGUUGCCUAGAUG GCACCGAGAGUAUUGAUAA GCUGAUUGCCGCUCGGAAA
M-019486-01	SYNJ1	Dharmacon	GAAAUACUCUGAAUAGUGA

			GAGAUCAACUUAUCAAUCA
			GAAGAGCCCGUUACUAUCA
			GAAUCGAUCUCCCUAACGA
M-012624-01	SYNJ2	Dharmacon	GCAUUGAUCUUAUUAUGA
			GAAGAAACAUCCCUUUGAU
			AGACAGAGCAGAUGAUUUA
			GGACAGCACUGCAGGUGUU
D-019486-01	SYNJ1_01	Thermo Scientific	GAAAUACUCUGAAUAGUGA
D-019486-04	SYNJ1_04	Thermo Scientific	GAGAUCAACUUAUCAAUCA
D-019486-05	SYNJ1_05	Thermo Scientific	GAAGAGCCCGUUACUAUCA
D-019486-06	SYNJ1_06	Thermo Scientific	GAAUCGAUCUCCCUAACGA
NA	PTPIP51	Sigma-Aldrich	GAAGCUAGAUGGUGGAUGA
NA	VAPB	Sigma-Aldrich	GCUCUUGGCUCUGGUGGUU

2.8.4 siRNA mediated knockdown

Dharmafect1 (Dharmacon, T2001-02) was used for transfection of siRNAs. For an 8 well culture slide (Falcon, 354118) 0.36µl of Dharmafect1 and 55.89 µl of serum and antibody free media was added to 25 nM of siRNA and left for 30 minutes to produce a siRNA and Dharmafect1 complex. Following this 20-50,000 cells were then added per well. The cell density was determined depending on the assay conducted. 20,000 cells were plated for 0 hour, 2 hours, 4 hours CCCP treatment for parkin translocation and 40-50,00 for 24 hours CCCP treatment for mitophagy and analysis of mitochondrial morphology. Fresh media was added the next day (16-24 hours) and this was left for a following 3 days to allow the knockdown to occur.

2.9 Methods of Analysis

2.9.1 Analysis of Parkin translocation and mitophagy

2 hours, 4 hours, and 24 hours before fixation the YFP HeLa cells were treated with 10 μ M CCCP to promote parkin translocation and mitophagy respectively. The cells were fixed with 100% ice cold methanol for 10 minutes and left in 1% BSA blocking agent for 1 hour – 24 hours. The cells were then stained with ATP5A primary antibody at (1/5000) and then Alexa 594 (1/400) antibody's for a minimum of 1 hour. Samples were mounted using moviol (Sigma-Aldrich 81381) and left to dry overnight before imaging. Imaging was conducted on the FV1000 Olympus Confocal microscope. The images were then analysed by eye, on a cell by cell basis. Each cell was given a score (1= no Parkin translocation, 2= partial Parkin translocation or 3= full Parkin translocation). Mitophagy was analysed using a similar scoring system (1= Full mitochondria, 2= reduced mitochondria or 3= highly reduced mitochondria or 4= No mitochondria). Cells which appeared apoptotic or did not contain YFP-Parkin were not analysed. Each score was averaged per condition and 3 biological replicates were conducted.

2.9.2 Analysis of mitochondrial morphology in *Drosophila* cells

S2R+ cells were incubated with MitoTracker Red and 2 μ g/ml Hoechst (See secondary antibody and dye table) for 15 minutes at 25°C respectively allowing the visualisation of the mitochondria and nucleus in live cells. Images were taken on the Deltavision RT Deconvolution widefield microscope. A minimum of 3 biological replicates were conducted each with a minimum of 50 cells per condition in each replicate.

2.9.3 Analysis of Mitochondrial Morphology in Human cells

YFP-Parkin HeLa cells were transfected with DsRed2-Mito and fixed and using the method in 2.7. This allowed the visualisation of mitochondria. Images were taken on the Olympus FV1000 Fluoview confocal microscope. 3 biological replicates were conducted with a minimum of 50 cells per condition in each replicate. The mitochondria were analysed using the method outlines in (De Vos and Sheetz, 2007). The aspect ratio and branching of the mitochondria were examined. A larger the aspect ratio and increase in branching suggest a longer mitochondria with a more fused network.

2.9.4 Analysis of fluorescent intensity.

HeLa cells were transfected with either combination of BiFC probes: HA-VC155,

Myc – VN155, HA-VC155-VAPBTM and Myc-PTPIP51TM-VN155. These were fixed with 3.7% formaldehyde and the mVenus fluorescence measured using the mean gray value on image J. This is the total mVenus fluoresce per area of the cells determined by the ROI. These were taken per cell and normalised to the average mean gray value obtained from the co-expression of HA-VC155-VAPBTM + Myc-PTPIP51-VN155. This meant that replicates could be pooled. A minimum of 10-20 cells per control conditions and 20-30 cells per experimental condition.

2.10 Fluorescence microscopy

2.10.1 Deltavision RT Deconvolution widefield Microscope

The Deltavision deconvolution widefield microscope was used to image S2R+ *Drosophila* cells to evaluate the mitochondrial morphology. A 60x Plan Apo NA 1.42 (Nikon) objective was used along with various filter block to visualize fluorescence 360/457 (DAPI) and 555/617 (Alexa Fluor 594).

2.10.2 Olympus FV1000 Fluoview confocal Microscope

Olympus FV1000 Fluoview confocal Microscope (Olympus corporation) was used to image of fixed samples for the parkin translocation and mitophagy assays. The objective used was the 60x oil Plan Apo NA 1.42 (Nikon) with 1x digital zoom. Laser 405 488 and 534 were used to visualise DAPI, GFP and Alexa Fluor 594.

2.10.3 Olympus IX73 Microscope

Olympus IX73 (Olympus corporation) was used to image live samples which were expressing ddGFP probes. The objective used was a Universal Plan Super Apochromat oil immersion objective 60x 1.35NA (Olympus). DAPI/FITC/TRITC/Cy5 filters (Chroma Technology Corp) was used to visualise GFP signal.

2.11 Quantitative Real-Time PCR (qRT-PCR)

2.11.1 RNA extraction

Drosophila S2R+ and YFP HeLa cells were cultured in a 12 well plate at a cell density of 800,000 and 100,000 respectively. dsRNA and siRNA were used to knockdown genes of interest as referred to previously. After 4 days the cells were washed with ice cold PBS and RNA extracted using RNeasy RNA purification kit, (Qiagen, 74104). This protocol was performed as stated by the manufactures instructions.

2.11.2 Reverse transcription of cDNA synthesis

After RNA extraction cDNA was synthesised from total RNA using ProtoScript® II first strand cDNA Synthesis Kit (New England BioLabs, E6560S). Total RNA concentration was attained using Nano drop (Model) and typically 1 µg of totally RNA underwent Reverse transcription for each sample. It is assumed that from 1 µg of RNA the equivalent amount of cDNA, in each sample, is made and ready to be used in qRT-PCR

2.11.3 Quantitative real time polymerase chain reaction

qRT-PCR is used to measure the relative mRNA levels with cells. The qRT-PCR assay was preformed in a 96-well PCR plate (Bio-Rad) with a optimized reaction volume of 10 µl. The reaction mixture contained 1 µl of cDNA, 5 µl IQTM SYBR green supermized (Bio Rad, 170-8880), 0.6µl of forward and reverse primers and 2.4 µl of PCR grade water. For each condition the samples were assayed in triplicate. The plates were plates were sealed with Bio Rad sealant (Bio Rad, MSB1001) and centrifuged before loading into qPCR machine (Bio-Rad CFX96 Reat Time System C1000 Touch). This table outlines the primers uses during the qPCR protocol

Gene	Species	Forward	Reverse
<i>RPL32</i>	<i>Drosophila</i>	GCCGCTTCAAGGGACAGTATCTG	AAACGCGTTCTGCATGAG
<i>pink1</i>	<i>Drosophila</i>	CAACATCCTCAATCCCAACC	TCTTAGTGGTCAGCGAAAGG
<i> fwd</i>	<i>Drosophila</i>	GGCCGACCAAATCTCAGTT0	GGAAGAAGTATGCCCATGGAT
<i>synj</i>	<i>Drosophila</i>	AAAAATTCCTCCGCTTTTCG	TCTCCGTGTGTCTTCTTTTGA
<i>ACTB</i>	Human	GACGACATGGAGAAAATCTG	ATGATCTGGGTCATCTTCTC
<i>PINK1</i>	Human	GCCGGACGCTGTTCCCTCGTT	TGGACACCTCTGGGGCCATC
<i>PI4KB</i>	Human	TCCTTCTGCAGTTGCTCTCA	GGGAGCCCTCTCTGATCC
<i>SYNJ1</i>	Human	CTGCTTGGTGAGATGCAGA	GAAGTTCCTCCACTTCAGCACTA
<i>SYNJ2</i>	Human	CAAGTCACCTCTCTCACCA	CAGGTCCGCGTATCTTT

The quantification of the gene expression is proportional to the amount of SYBR® green incorporated into the DNA. When SYBR® green is incorporated into the double stranded DNA it emits fluorescence. As each cycle of the qRT-PCR passes, more and more SYBR green is incorporated into the dsDNA and more fluorescence emitted. In the exponential phase the amount of cDNA should double for each cycle. Once enough SYBR green has been incorporated into the cDNA the amount of cycle is recorded and this is referred to as the threshold level. This gives the C_T or threshold cycle value. The relative fold change of each condition can then be calculated from the C_T value.

To record this C_T value the qRT-PCR machine runs a standard qPCR program:

Step	Name	Temperature	Seconds
1	Initialisation	95°C	180
2	Denaturation	95°C	30
3	Annealing	60°C	30
4	Extension	72°C	30
5	Repeat steps 2-4 (40x)		
6	Melt Curve analysis	95°C	30
7		60°C	30
8		55°C	10
9	Increase step 8 by 1°C until 95°C is reached		

2.11.4 Melt Curve Analysis

When using dyes such as SYBR® green a melt curve analysis has to be conducted, as SYBR® green will detect any dsDNA including primer dimers and contaminating gDNA PCR product due to non specific primer binding. Therefore, performing a melt curve analysis allows the specificity of the amplicon to be calculated. For a specific primer set the melt curve should have one peak. The appearance of more than one peak suggests that there were primer dimers or contaminating gDNA. This would mean that the primers being used are not specific and therefore a re-design would be necessary.

2.11.5 Relative fold change analysis

There are two methods of qRT-PCR analysis: absolute quantification which compares the C_T values to a standard curve, or relative quantification where the C_T of the gene of interest (GOI) is normalised to a reference gene, which stays constant throughout the siRNA or any treatment of the cells. Here *Drosophila* Ribosomal gene *RPL32* and a human *ACTB* gene were used because of their reproducibility and efficiency of the primers sets. The relative fold change of the

expression of cDNA is calculated using the Livak method (Livak and Schmittgen, 2001). This assumes that the GOI and the reference gene are being amplified at the same rate. For this assumption to be true the amplification efficiencies have to be between 90-110%.

Equations to calculate the amplification efficiencies:

$$E = 10^{-1/\text{slope}}$$

$$\text{Efficiency} = (E - 1) \times 100\%$$

Ideally the amplification efficiency should be 100% so with each cycle, the PCR product would double. If this is true, then the Livak method can be applied. If this is not true then the Pfaffl method should be used. Livak method is an adaption of the Pfaffl method where the amplification efficiency is approx. 100%. An increase in amplification efficiency >100% suggests there is a pipetting error and there is increase cDNA or that they is amplification of a non specific product. A amplification efficiency of <100% is suggestive of poor primer design of sub optimal reaction conditions.

How to calculate the relative fold change is outlined below.

The normalised C_T value is known as the ΔC_T .

$$\Delta C_T = C_T (\text{GOI}) - C_T (\text{reference genes})$$

Once each sample is normalised to the reference gene the experimental samples must be normalised to the control sample (Control siRNA) which give the $\Delta \Delta C_T$ for experimental sample and the control sample.

$$\Delta \Delta C_T = \Delta C_T (\text{Experiential Sample}) - \Delta C_T (\text{Control Sample})$$

Finally this can be put in the formula from the Livak method $2^{-\Delta \Delta C_T}$. This produces the normalised expression ratio between the experimental and control samples. Here the control sample is normalized to 1 with experimental samples representing relative expression levels.

2.12 Molecular DNA Techniques

A Variety of molecular cloning techniques were used in the production of the construct used in this project.

2.12.1 Polymerase Chain Reaction (PCR)

PCR reactions were set up as stated by the manufacturers instruction using either Phusion High Fidelity (NEB, E0553L) or Bio TAQ (Bioline) DNA polymerase depending on the requirement for proof reading activity and secondary assay required. The PCR products were then checked by and quantified by gel electrophoresis. Cloning Schemes in the Appendix and throughout results chapter 3,4,and 5)

2.12.2 Ethidium bromide (EtBr) agarose gels

To allow visualisation of PCR product or plasmid DNA an agarose gel is run. Larger constructs should be run on lower percentage agarose gels (1%) while smaller (200 bp) should be run on higher percentage gels (3%). 50ml -150ml of 1X TAE buffer (diluted from 50x TAE) is combined with appropriate amounts of agarose (Bioline BIO-41025). This is then heated until the agarose has dissolved into the TAE buffer. For each 50ml 2.5µl of EtBr is added. The EtBr intercalates into the DNA, and when intercalated in to DNA and exposed to UV light EtBr has a 20 fold increase in fluoresce which allows visualisation of DNA constructs. The gels were imaged and extracted on a Genie G-Box (Syngene).

50x TAE

- 242g Tris Base
- 100ml EDTA pH8
- 57.1ml Acetic acid

2.12.3 PCR clean up and agarose Gel extraction

PCR products were either run on an agarose gel and gel extracted or cleaned up using PCR clean up kit. The bands of interest are cut from the gel and placed into eppendorf tubes and weight. The manufacturer instructions were then followed to elute the DNA from the gel (Sigma, 1002247302).

2.12.4 Digestion

Digestions were conducted from 10 minutes to overnight at 25-37°C depending on the restriction enzyme type and its efficiency. A list of restriction enzymes used and the basic conditions appears below.

Restriction Enzyme	Company	Product code	Digestion Temperature	Fast Digest
XbaI	NEB	R0145S	37°C (1 hour)	No
SacII	NEB	R0157S	37°C (1 hour)	No
NotI-HF ^(R)	NEB	R3189L	37°C (1 hour)	No
XhoI	NEB	R0146S	37°C (1 hour)	No
KpnI HF ^(R)	NEB	R3142S	37°C (1 hour)	No
ApaI	NEB	R0114S	25°C (1 hour)	No
BstXI	Thermo Scientific	FD1024	37°C (5-15 Minutes)	Yes
XhoI	Thermo Scientific	FD0694	37°C (5-15 Minutes)	Yes
NotI	Thermo Scientific	FD0593	37°C (5-15 Minutes)	Yes

2.12.5 Ligation

Once digested, the vector and insert were combined using T4 DNA ligase (NEB) or quick ligase (NEB M2200S) in a 1:3 molar ratio. This was calculated using the nebuligation calculator. The amount of DNA did not exceed 100ng in total 10µl volume. This was left for 10 minutes at room temperature for Quickligase and overnight at room temperature for the T4 DNA ligase

2.12.6 Transformation

The ligations were amplified using bacterial transformation into High efficiently NEB10 competent cells (NEB) or XL10-Gold® Ultra-competent Cells (Agilent 200314). For an amplification of an already made plasmid DH5alpha cells (Invitrogen) were used. 2 µl of ligation mixture was added directly to 20-50 µl of competent cells and incubated on ice for 30 minutes before being transferred to 42°C for 30 seconds. This heat shocks the cells and allows closure of the competent cells membrane. The heat shocked mixture was returned to the ice for 5 minutes after which 200-950 µl of pre warmed SOC media (NEB) was added. The cells were then transferred to 37°C and shaken (Max Q 3000, Thermo Scientific) for 60 minutes at 225rpm before being spread out onto warmed antibiotic plates. These were grown over night at 37°C and a single colony was picked to be grown in a suspension culture or to be analysed using Colony PCR.

2.12.7 Colony PCR

To analyse if the insert of choice had ligated into the vector, a colony PCR was performed using primers that span the both the vector and the insert. Colonies were picked, transferred to a new plate and then placed in the PCR tubes containing water. The PCR reaction was conducted via manufacturer instructions for both BioTaq and FIREpol. This main difference of colony PCR to a regular PCR reaction is that this protocol included an extra step in the beginning to break down the bacteria, freeing of the DNA (5 minutes at 95°C). This was run on an agarose gel and examined for appearance of the correct size band.

2.12.8 Extraction of Plasmids

Mini preps were performed to extra DNA from the bacteria (Macherey-Nagel 740588). To do this a bacterial colony was picked and placed in 2 ml of media and shaken (Max Q 3000, Thermo Scientific) for approx. 8 hours at 37°C 225rpm. 50-100 µl of this was then transferred to 5 ml of LB media + antibiotic and left to culture at 37°C and shaken (Max Q 3000, Thermo Scientific) at 225rpm overnight. Once the bacteria had grown and the solution became cloudy, 500 µl was combined with 500 µl of 50% Glycerol to make a stock. This was kept at -80°C until it was required. The remaining solution was centrifuged at 6000g for 10 minutes at 4°C. The pellet was extracted using the manufactures instructions. In each case the plasmids were eluted by using PCR grade water (Sigma- Aldrich, W4502) which was pH8 and heated to 72°C to help the release of DNA from the membrane. The produce was analysed using the NanoDrop spectrophotometry (LabTech ND-1000) to determine the concentration.

2.12.9 Sequencing

All constructs were sequenced at the Core genomic Facilities within University of Sheffield. They required 10 µl of 1 µM primers and 10 µl of 100 ng/µl plasmid construct for each reaction.

3. ANALYSIS OF *SYNJ* AND *FWD* IN *DROSOPHILA*

3.1 Background

Drosophila have been widely used as an animal model for PD, with many disease-relevant phenotypes being able to be reproduced in *Drosophila*. Mutations in *Drosophila pink1* and *parkin* show loss of dopaminergic neurones, defects in locomotion and mitochondrial dysfunction, including changes in the gross morphology of the mitochondria (Clark et al. 2006; Pesah et al. 2004). One of the strongest indications of the functions of *pink1* and *parkin* has come from genetic interaction studies where the overexpression of *parkin* can rescue the *pink1*^{B9} mutant phenotypes while overexpression of *pink1* is unable to rescue *park*²⁵ mutants implicating them in the same pathway (Park et al. 2006). Furthermore, genetic interaction studies with mitochondrial morphology genes also implicated *pink1* and *parkin* in mitochondria fission and fusion. When genetically combined, loss of function mutations in *Drp1* resulted in a further deterioration of the *pink1*^{B9} and *park*²⁵ climbing phenotype, while overexpression of *Drp1* or mutations in *Marf* or *Opa1* rescue the *pink1* locomotion defect. This highlights a role for *pink1* and *parkin* in mitochondrial morphology (Poole et al, Deng et al, Yang et al). Further studies in cells have also implicated *pink1* and *parkin* in regulation of mitochondrial morphology with the overexpression of *pink1* or *parkin* resulting in a highly fragmented mitochondria network, while dsRNA mediated knockdown resulted in tubular and fused mitochondrial network (Ziviani et al. 2010). Taken together, these data suggest that *pink1* and *parkin* promote mitochondrial fission and play a key role in mitochondrial quality control in *Drosophila*.

To understand how *pink1* and *parkin* may modulate mitochondrial morphology, a RNAi screen was conducted in S2R+ cells. Knockdown of *fwd* phenocopied *pink1* silencing producing a highly fused mitochondrial network suggesting a role in the regulation of mitochondrial morphology (Pogson et al. 2014). *Fwd* is the sole *Drosophila* homologue of *PI4KB*, a mammalian phosphatidylinositol kinase which mediates the addition of a phosphate group on to the D4 position of the inositol ring to produce PI4P (Brill et al. 2000). The yeast homologue of *fwd*, *pik4*, is essential (Flanagan et al. 1993; Park et al. 2009) nevertheless, *fwd* mutants in *Drosophila* progress to adulthood, are viable and female fertile, suggesting more complexity in *Drosophila*. The males however, are sterile due defects in cytokinesis of spermatocytes (Brill et al. 2000; Polevoy et al. 2009). Interestingly, the phosphatase that regulates de-phosphorylation of PI(4,5)P₂ and PI4P to PI, SYNJ1, is a causative gene for AR-JP with mutations in both phosphatase domains being linked

to PD. In *Drosophila*, *synj* homozygous mutants are fatal. Like in mammals, the main function is to regulate clathrin mediated endocytosis, and *synj* mutants have defects in synaptic vesicle recycling (Verstreken et al. 2003; Dickman et al. 2005; Geng et al. 2016). Together, these enzymes have been linked to mitochondrial morphology and PD, respectively. Their function is to regulate the metabolism of PI, which suggests that PI metabolism may be implicated in PD.

3.2 Hypothesis and Aims

It had been previously shown that the knockdown of *fwd*, the *Drosophila* homologue of PI4KB, in S2R+ *Drosophila* cells, results in a hyperfused mitochondrial network, similar to *pink1* knockdown and was therefore proposed to affect mitochondrial morphology (Pogson et al. 2014). SYNJ1, a phosphatidylinositol phosphatase which regulates the de-phosphorylation of PI(4,5)P₂ to PI4P and then to PI, has been found to be mutated, in the phosphatase domains, in AR-JP. In combination, these data lead us to the hypothesis that phosphatidylinositol levels may impact on mitochondrial quality control, and more specifically in the regulation of the PINK1 and Parkin mediated mitophagy.

The aim of this chapter was to investigate the effect of knocking down, overexpressing and mutating *fwd* and *synj*, the enzymes involved in PI metabolism, to uncover a potential genetic interaction between phospholipid metabolism and *pink1* and/or *parkin* using adult *Drosophila* as a model. A further aim was to establish the effects of *fwd* and *synj* manipulation on different aspects of mitochondrial quality control, such as mitochondrial morphology.

3.3 Genetic interactions of *synj* and *fwd* with *pink1* and *parkin*

The main aim of these experiments was to further determine and understand any potential genetic interactions between *fwd*, *synj* and the two main components of the PINK1/Parkin pathway: *pink1* and *park*. To do this, *Drosophila* were used as a model for PD as they have been robustly tested for phenotypes which correlate with that of PD patients: mitochondrial dysfunction, loss of DA neurones and defects in their locomotion. *Drosophila* locomotion can be tested using two main assays. The climbing assay, which determines the co-ordination and strength of the fly; and a flight assay, which reports on the reflex action of the indirect flight muscles of the wing. It has been repeatedly shown that *pink1*^{B9} and *park*²⁵ mutant *Drosophila* have a decreased climbing and flight ability. These phenotypes are robust and reproducible, and therefore are suitable to test for genetic interactions.

3.3.1: The knockdown of *fwd* results in an expression dependent decrease in motor ability

It has previously been suggested from behavioural experiments conducted in our lab that the knockdown of *fwd* results in a decreased climbing and flight ability of young adult *Drosophila* (Pogson thesis) similar to that of the *pink1*^{B9} mutant, leading to the hypothesis that *fwd* may phenocopy *pink1* and act in the same pathway to regulate mitochondrial quality control. To verify and further characterise these preliminary results, *fwd* was knocked down using *fwd*^{KK} RNAi line under two different temperature conditions: 25°C and 29°C. The increase in temperature from 25°C to 29°C increases the expression of the RNAi construct, as GAL4 activity is increased at higher temperature and typically generates a greater knockdown.

The knockdown of *fwd* resulted in a strong climbing defect when raised at 29°C but not at 25°C (**Fig3.1A and C**). As an increase in temperature correlates with a decrease in climbing ability, it is suggestive that there is a dosage dependent decrease in locomotor ability, strengthening the theory that the defect in climbing ability is due to the knockdown of *fwd*. These climbing defects are not likely due to expression of the RNAi construct, as the *LacZ*-RNAi control which was reared under the same conditions did not show an effect on climbing ability. In contrast, there was no significant decrease in flight ability at either 25°C or 29°C compared to the *LacZ*-RNAi control (**Fig3.1B and C**). Together these data indicate that reduction of *fwd* has a climbing phenotype but not a flight one.

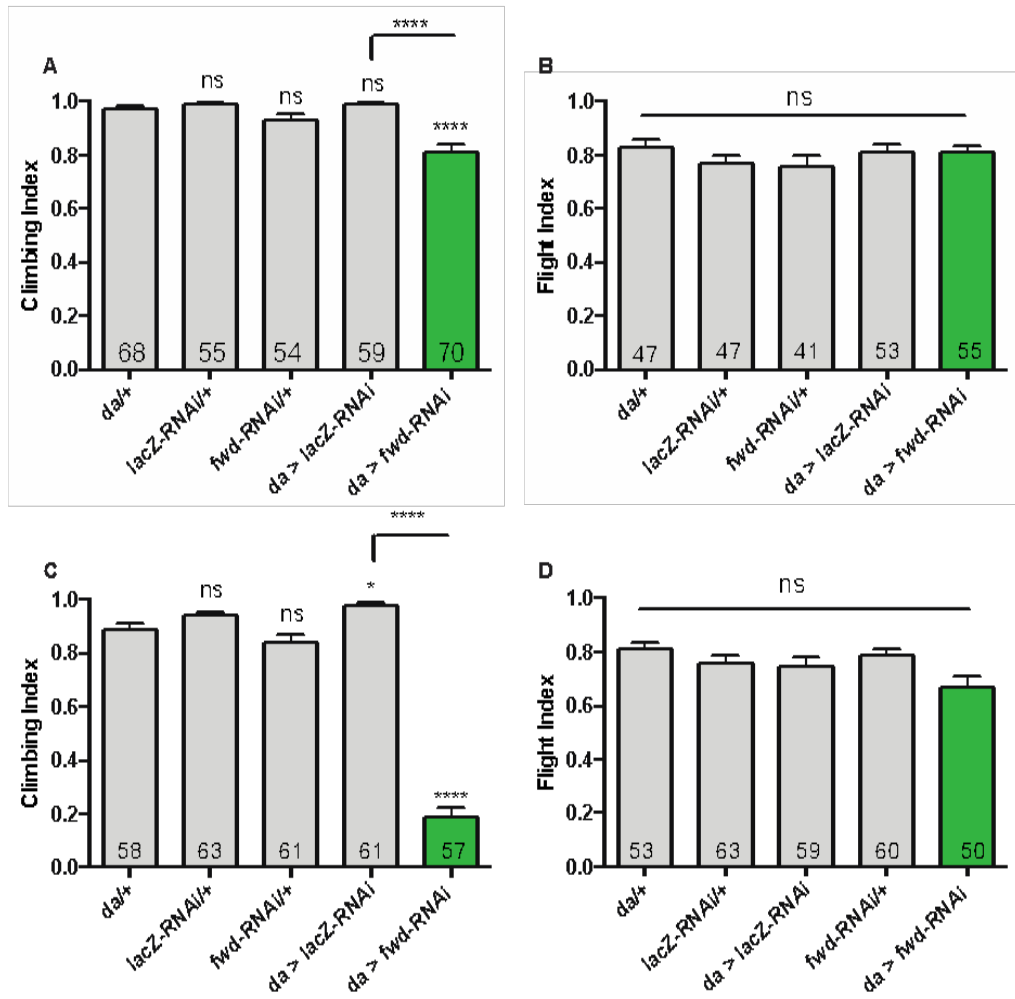


Figure 3.1: The knockdown of *fwd* results in an expression dependent decrease in motor ability. *Drosophila* expressing UAS-RNAi construct for *fwd* via the GAL4-UAS system, were assessed for their ability to climb under a strong ubiquitous driver *daughterless* (*da*) raised at 25°C (A) and 29°C (C). These *Drosophila* were then tested for their ability to fly at 25°C (B) and 29°C (D). The numbers in the bars represent the number of animals tested (n). Data was analysed using Kruskal-Wallis test with Dunn's correction. Error bars represent the standard error of the mean. ns P>0.05 *P<0.05 ****P<0.0001 with those above each bar being compared to *da*/+ outcrossed control.

3.3.2: The overexpression of *fwd* results in minimal effects of climbing ability

We also sought to assess the effect of *fwd* overexpression on climbing and flight, thus a *GFP-fwd* transgenic line was generated. Climbing and flight were then assessed using ubiquitous, neuronal and muscle specific drivers to understand the overall function, but also the cell specific functions of *fwd*. The results show that overexpressing *GFP-fwd* using a ubiquitous driver (*da-GAL4* or *Act-GAL4*) has limited effect on the climbing or flight behaviour with no significant difference seen compared to the outcrossed driver controls (**Fig 3.2A and B**). The overexpression of *GFP-fwd* using cell specific drivers, *elav-GAL4* (pan neuronal) and *Dmef-GAL4* (muscle), causes no significant effects suggesting limited importance in these cell types (**Fig 3.2A and B**). The expression of *GFP-fwd* using *D42-GAL4*, however, shows a significant decrease in climbing ability compared to the *D42/+* outcrossed control (**Fig 3.2A**). *D42-GAL4* is a motor neurone specific driver, therefore suggesting that overexpression of *fwd* in these cells has an impact on climbing ability and suggesting importance of *fwd* in motor neurones. Overall however, the data from overexpression of *GFP-fwd* suggests that *fwd* has limited effect on locomotion.

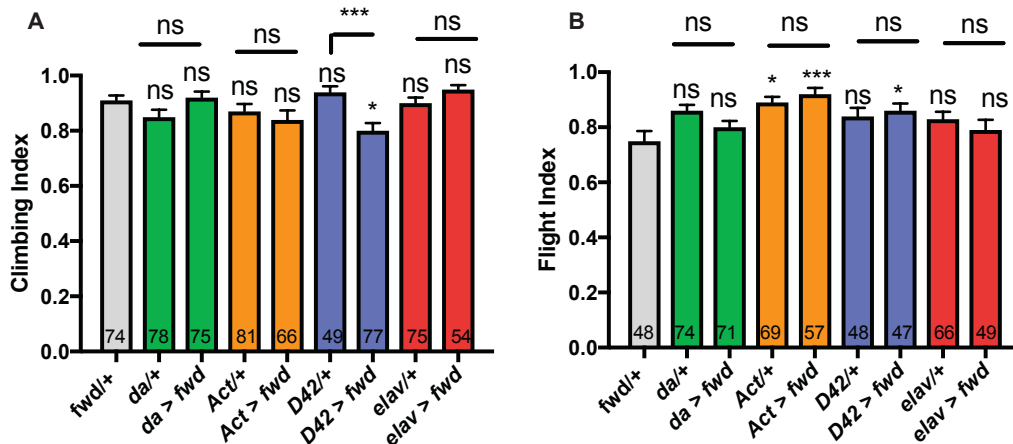


Figure 3.2: The overexpression of *fwd* has minimal effects on climbing and flight ability. *Drosophila* expressing UAS construct for *GFP-fwd* via the GAL4-UAS system, were assessed for their ability to climb under a variety of drivers including *da-GAL4*, a strong ubiquitous driver, *Act5c-GAL4*, a weak ubiquitous driver, *D42-GAL4* which expresses in motor neurones and *elav-GAL4* a pan neuronal driver (A). These *Drosophila* were also tested for flight ability under the same drivers (B). The numbers in the bars represents the number of animals tested (n). Data was analysed using Kruskal-Wallis test with Dunn's correction. Error bar represent the standard error of the mean. Statistical significance is represented by stars (ns $P > 0.05$ *** $P < 0.001$ with those above each bar being compared to *fwd/+* outcrossed control).

3.3.3 Mutations in *fwd* result in severe climbing but not flight defects.

Previous data showed that knockdown of *fwd* caused a defect in climbing but not flight. To confirm the climbing phenotype, two independently derived *fwd* mutant alleles were obtained (*fwd*¹ and *fwd*³). *fwd*¹ is a null allele, which results from a chromosomal rearrangement of chromosome 3, while *fwd*³ harbours a Q310 to stop codon mutation, prematurely terminating the translation of *fwd*, resulting a functionally null protein. Both *fwd*¹ and *fwd*³ are homozygous lethal but viable in combination with *Df(3L)7C*, a large deletion which spans across the *fwd* gene but does not have the same genetic background as either *fwd*¹ and *fwd*³, thus allowing investigation of *fwd* null adult mutants.

The results show that both *fwd*¹ and *fwd*³ cause a significant decrease in climbing ability compared to the outcrossed control genotype as well as the *fwd*³/+, *fwd*¹/+ and *Df(3L)7C*/+ heterozygotes (**Fig 3.3A**). With regards to flight however, no significant decrease in the flight ability is seen with *fwd*¹ or *fwd*³ compared to *da*/+ outcross control (**Fig 3.3B**). This climbing phenotype is more severe than the phenotype seen when *fwd* is knocked down (**Fig 3.1C**), but supports the premise that mutation in *fwd* reduce climbing ability while having a limited effect on flight. To further confirm the specificity of this result, *GFP-fwd* was expressed in both *fwd*³ and *fwd*¹ mutants which rescued the climbing defect as expected (**Fig 3.3C**). These data from *fwd*³ and *fwd*¹ supports the data from the *fwd* RNAi lines, and shows that loss of *fwd* affects climbing ability of *Drosophila*.

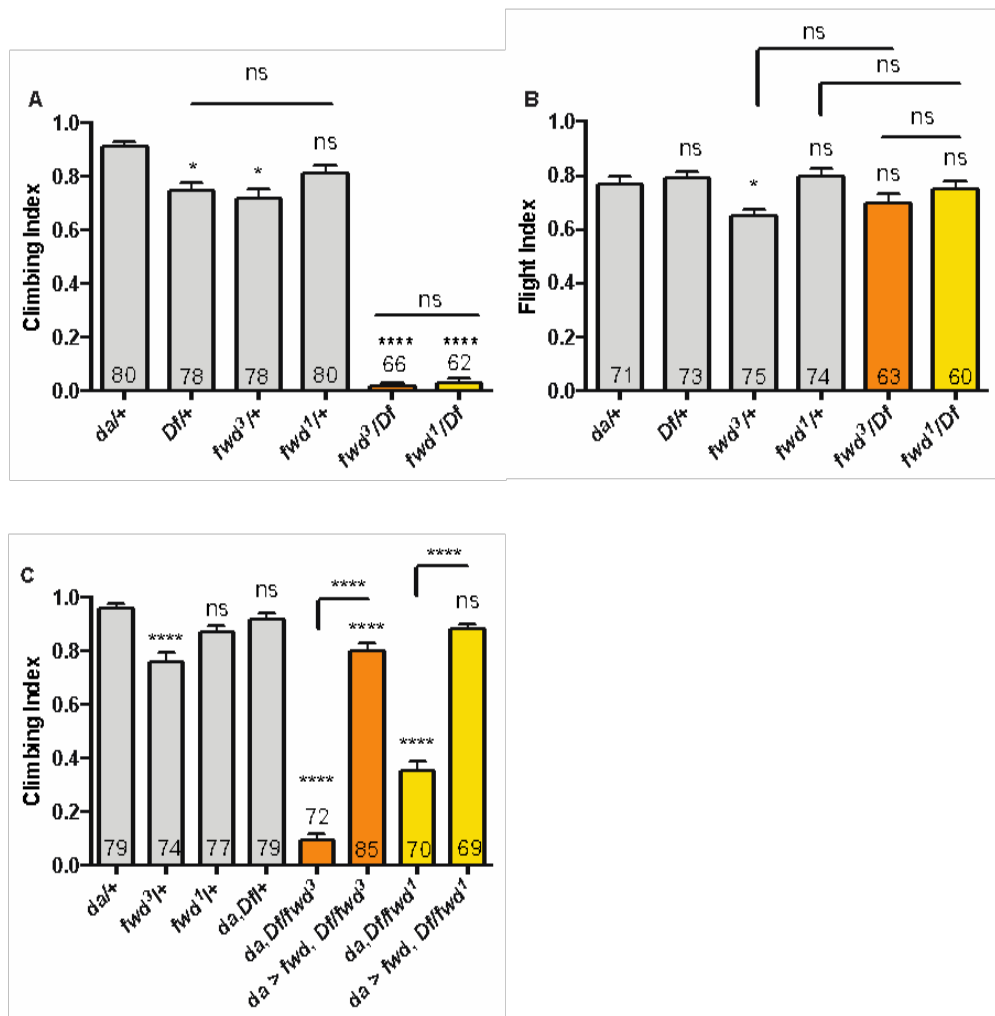


Figure 3.3: Mutations in the *fwd* gene result in sever climbing defects that can be rescued by the overexpression of *fwd*. *Drosophila* containing a null mutation (*fwd³*) or a complex genomic rearrangement (*fwd¹*) were assessed for their ability to climb (A) and fly (B). (C) shows the same mutants but in combination with a GFP-*fwd* overexpression construct which is expressed using a *da*-GAL4 driver. The numbers in the bars represents the number of animals tested (n). Data was analysed using Kruskal-Wallis test with Dunns correction. Error bar represent the standard error of the mean. Statistical significance is represented by ns P>0.05 ****P<0.0001 with those above each bar being compared to *da/+* outcrossed control

3.3.4: *fwd* does not genetically interact with mitochondrial fission/fusion genes

In Section 3.3.3 I have shown that knockdown or mutation of *fwd* results in a strong climbing defect, however, the mechanisms causing this climbing phenotype are not clear. Previous investigations suggested that knockdown of *fwd* in S2R+ *Drosophila* cells results in fusion of the mitochondrial network, phenocopying the knockdown of *pink1* in the same cell line. This led to the hypothesis that the climbing defect in *fwd*¹ and *fwd*³ mutants may be due to changes in mitochondrial fission/fusion dynamics, namely an increase in fusion. Notably, it has been shown in that genetic combination of *Opa1*^{S4579} with *pink1*^{B9} rescues the climbing defect of *pink1*^{B9} mutants (**Fig 3.4**), therefore suggesting that genetic regulation of mitochondrial morphology gene can alter climbing phenotypes *in vivo*. Thus, genetically shifting the mitochondrial dynamics balance towards fission, like with combination of *pink1*^{B9} and *Opa1*^{S4579}, may rescue the climbing defect seen with *fwd* mutants.

To test this hypothesis and shift the balance of mitochondrial dynamics towards fission *in vivo*, *fwd*¹ and *fwd*³ were genetically combined with mutants of mitochondrial fusion: *Opa1*^{S4579}, *Drosophila* homologue of *OPA1*, and *Marf*^B, *Drosophila* homologue of *Mitofusin*. In addition the GAL4/UAS system was used to over express the cytosolic dynamin like protein (*Drp1*) that mediates mitochondrial fission. Both *Marf*^B and *Opa1*^{S4579} are lethal in homozygosis, but in heterozygosis these mutants can be used to alter the mitochondrial morphology and push the system towards mitochondrial fission.

The results show that when *fwd*¹ or *fwd*³ were genetically combined with *Opa1*^{S4579} or *Marf*^B no rescue of the climbing defect in either *fwd* mutant was seen (**Fig 3.5A, B and C**). As the mitochondrial fusion proteins were in heterozygosis, it was hypothesized that there might not be enough fission occurring to reverse the strong *fwd* climbing defect. Therefore, the GAL4/UAS system was adopted to overexpress *Drp1* via *da-GAL4*. Overexpression of *Drp1* in *fwd*³ mutant also showed no significant difference in climbing ability from the *fwd*³ mutant alone (**Fig 3.5 D**), thus suggesting that *fwd* climbing defect is not caused by changes in mitochondrial morphology. It is important to note that the effect of these mutants on mitochondrial morphology were not checked *in vivo* and the level of fission occurring was not examined. Therefore, the amount of fission may not be enough to rescue the *fwd* mutants if they had such a fused mitochondrial network. It may also be possible that loss of *fwd* does not cause changes in the mitochondrial network *in vivo*, as was previously reported in cells.

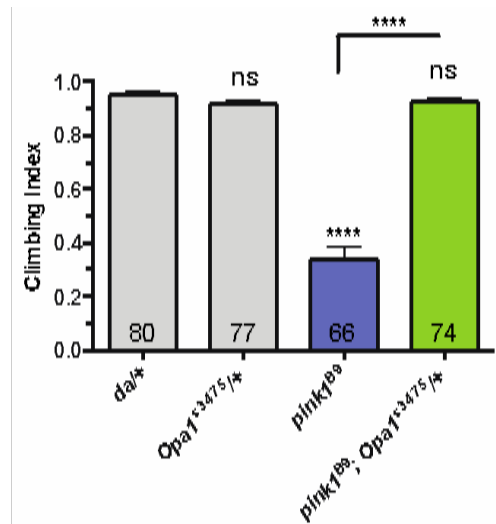


Figure 3.4: Loss of *Opa1*^{s3475} rescues the climbing defect of *pink1*^{B9} mutants: *Drosophila* harbouring mutations in *Opa1* (*Opa1*^{s3475}) an inner mitochondrial membrane fusion protein were genetically combined with *Drosophila* containing *pink1*^{B9} mutations. These *Drosophila* were tested for their ability to climb. The numbers in the bars represents the number of animals tested (n). Data was analysed using Kruskal-Wallis test with Dunns correction. Error bar represent the standard error of the mean. **** P < 0.0001

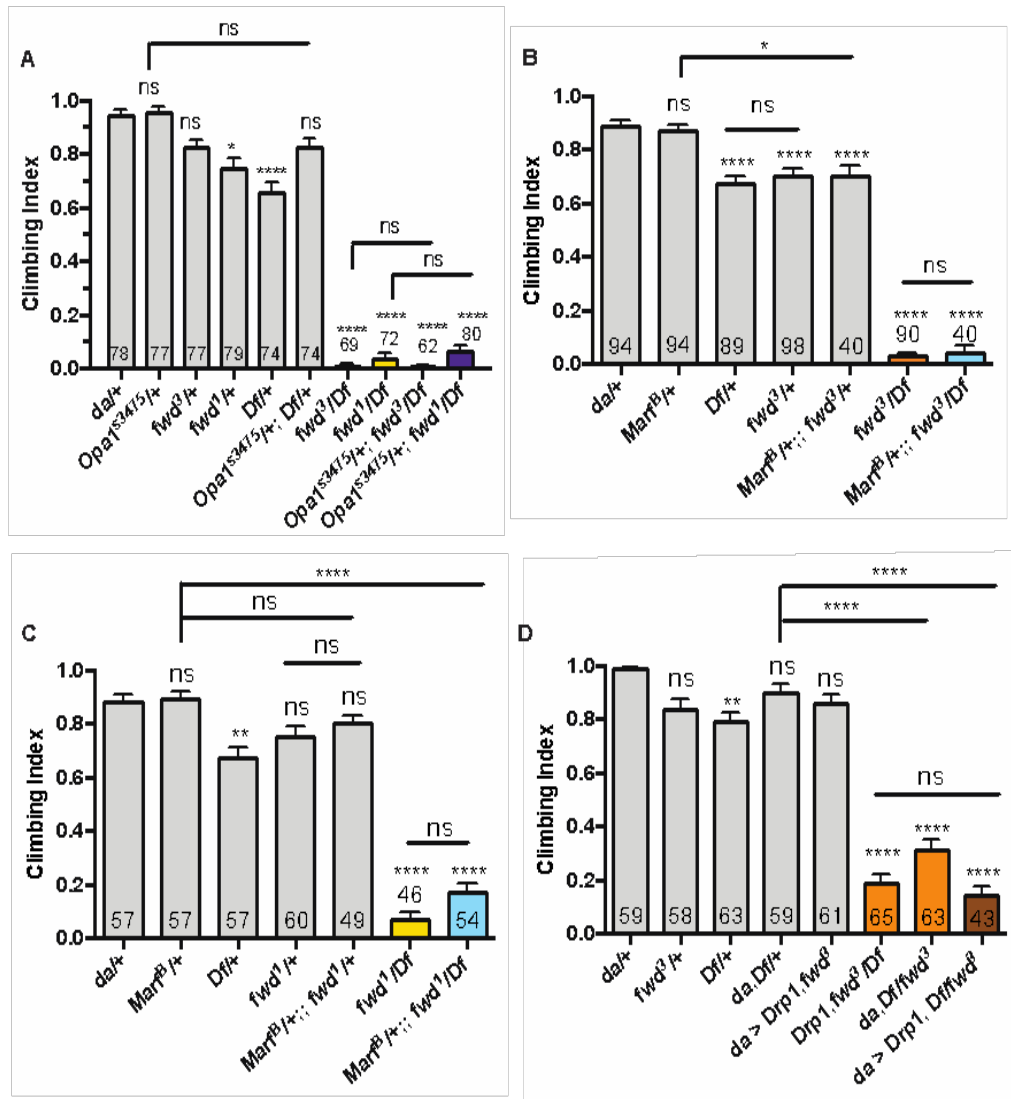


Figure 3.5: The genetic manipulations to increase mitochondrial fission has no effect on the *fwd* phenotype: *Drosophila* containing a null mutation (*fwd³*) or a complex genomic rearrangement (*fwd¹*) were genetically combined with *Opa1^{S3475}* mutant (A) *Marf^B* mutant (B) and their climbing ability tested (B). *Drosophila* containing *fwd¹* mutation were also genetically combined with *Marf^B* and their ability to climb tested (C). *Drosophila* with *fwd³* or *fwd¹* overexpressing *Drp1*, a pro-fission gene, using GAL4-UAS system and a strong ubiquitous driver *daughterless*. Their ability to climb was then assessed (D). The numbers in the bars represents the number of animals tested (n). Data was analysed using Kruskal-Wallis test with Dunns correction. Error bar represent the standard error of the mean. ns P>0.05 **P<0.01 ****P<0.0001.

3.3.5: The knockdown of *fwd* and *synj* does not alter Mitochondrial morphology in S2R+ *Drosophila* cells.

The previous data indicates no genetic interaction between mitochondrial morphology genes and *fwd*, therefore suggesting the organismal phenotypes of *fwd* does not result from mitochondrial morphology defects *in vivo*. However, *fwd* knockdown in S2R+ *Drosophila* cells results in a fused mitochondrial network (Pogson et al. 2014). We next decided to reassess whether *fwd* affects mitochondrial morphology. Thus, dsRNA targeting *fwd*, *synj* (the opposing phosphatase), *pink1*, *Marf*, *Drp1* were analysed alongside a non-targeting control dsRNA in S2R+ *Drosophila* cells for effects on mitochondrial morphology as outlined in **Fig 3.6**. It was hypothesized that knockdown of *fwd* would produce a fused mitochondrial network and *synj*, the opposing phosphatase, would produce a fragmented mitochondrial network.

As expected, *Marf* knockdown results in a highly fragmented mitochondrial network while *Drp1* knockdown produced a highly fused or clumped mitochondrial network. In addition, knockdown of *pink1* produced a fused mitochondrial network as previously reported (**Fig 3.7A**). The knockdown of *fwd* however does not result in a significant difference in mitochondrial morphology score compared to the non-targeting control (**Fig 3.7B**). Thus suggesting that *fwd* does not affect mitochondrial morphology in *Drosophila* S2R+ cells. Similarly, the knockdown of *synj* does not show a significant difference in mitochondrial morphology (**Fig 3.7B**). One reason for the lack of effect on mitochondrial morphology would be that *synj* or *fwd* were not efficiently knocked down. To test this, RT-qPCR was used to examine the mRNA transcript level of *pink1*, *fwd* and *synj* upon knockdown. The results showed that there is a significant decrease in the mRNA expression level of *fwd*, *synj* and *pink1* with expression levels being 30% of the control (**Fig 3.7C**). Overall, these data suggest that knockdown of *fwd* and *synj* does not grossly affect mitochondrial morphology in these cells.

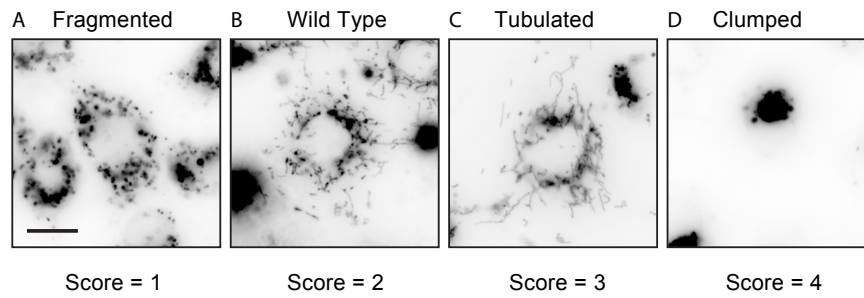


Figure 3.6: Mitochondrial Morphology scoring scale: S2R+ *Drosophila* cells were stained with MitoTracker Red (1/20000) to allow visualisation of the mitochondrial network. The scale is based on a 4 point scale which selectively looked at the gross structure of the mitochondrial network in one cell. A score of 1 is given to a cell, which has many highly rounded and fragmented mitochondria (A). A score of 2 is given to a cell, which has WT mitochondria (B). A score of three is given when A cell has high connected and fused mitochondria (C). Finally, a score of 4 is given to a cell which has a highly connected network that the mitochondria form a clump (D). Scale bar 10 μ m.

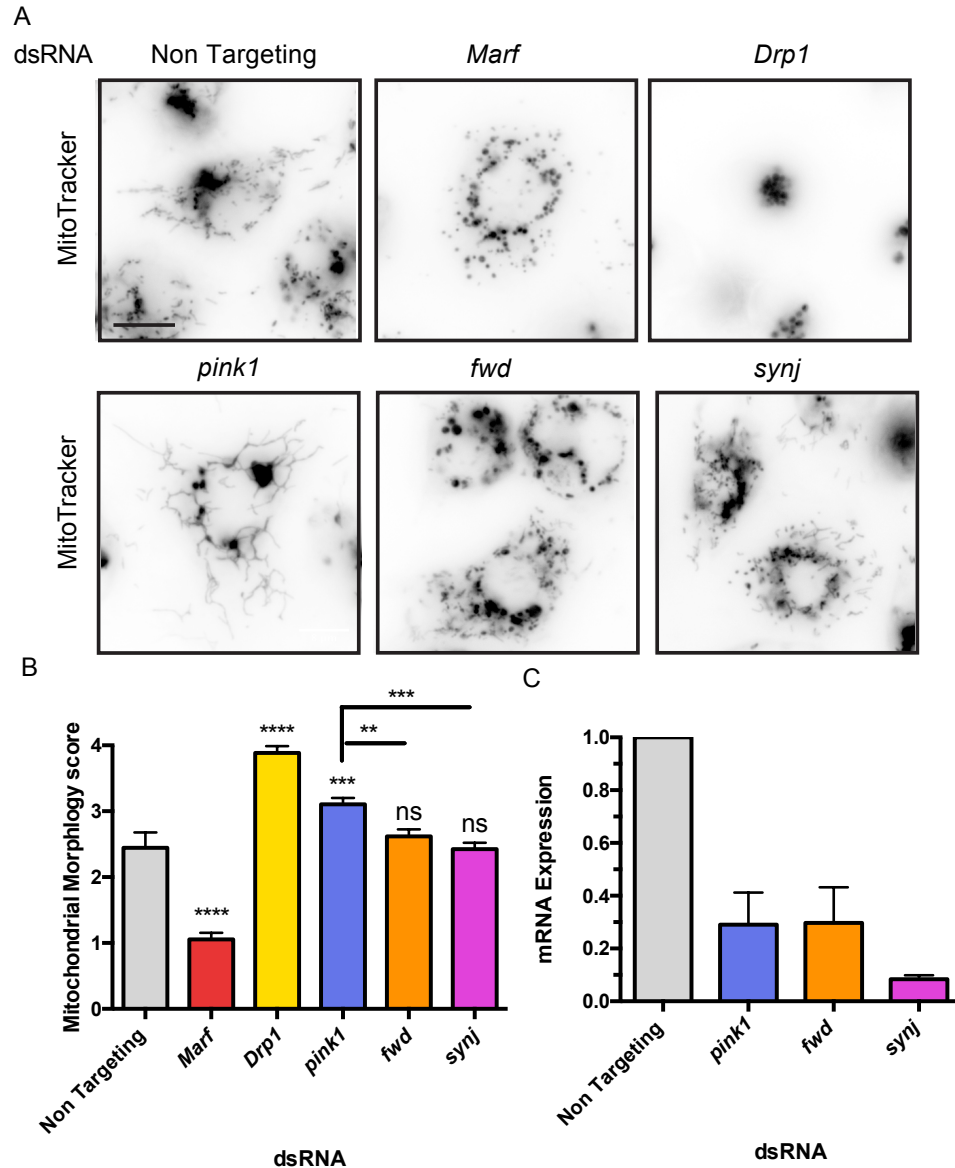


Figure 3.7: The knockdown of *fwd* or *synj* does not alter mitochondrial morphology in S2R+ *Drosophila* cells. S2R+ *Drosophila* cells were stained with MitoTracker Red to allow visualisation of the mitochondrial network. (A) shows the mitochondrial network when *Marf*, *Drp1*, *pink1*, *fwd*, *synj* and a nonspecific *C. elegans* gene is targeted for RNAi knockdown. (B) A graphical representation of these mitochondrial morphologies based on the 4-point mitochondrial morphology scoring scale. (C) RT-qPCR analysis quantifying the RNAi knockdown of *pink1*, *fwd* and *synj* dsRNA constructs. Results were analysed using one-way ANOVA with Bonferroni post hoc test. ns $P > 0.05$ ** $P < 0.01$ *** $P < 0.001$ **** $P < 0.0001$. Scale bar 10 μm .

3.3.6: The overexpression of *GFP-fwd* and *GFP-synj* does not alter Mitochondrial morphology in S2R+ *Drosophila* cells.

Contrary to what was published in Pogson et al 2014, I found that knockdown of *fwd* in S2R+ *Drosophila* cells does not cause fusion of the mitochondrial network. As discussed, this could be due to differences in the levels of knockdown or the subjective nature of the scoring system. To help understand this, *GFP-fwd* and *GFP-synj* were cloned and overexpressed in S2R+ *Drosophila* cells and effects on mitochondrial morphology assessed using methods outlined in **Fig 3.6**. The rationale being that, only the cells expressing *GFP-fwd* or *synj* would be quantified, unlike with the dsRNA knockdown where it was assumed that the majority of cells had, *fwd* or *synj* knockdown. In addition, the fragmented phenotype is easier to define than fusion, therefore reducing the subjective nature of this method of analysis. It was predicted that overexpression of *GFP-fwd*, like overexpression of *pink1*, will produce increased fission and a fragmented mitochondrial network (Ziviani et al. 2010)

As expected, the overexpression of Mitofusin-FLAG resulted in a highly fused mitochondrial network that appears clumped (**Fig 3.8A**). However, the overexpression of *GFP-fwd* or *GFP-synj* did not cause any changes in mitochondrial morphology or any significant difference in mitochondrial morphology score (**Fig 3.8A and B**). The images show a mitochondrial network similar to the GFP control (**Fig 3.8 A**). These data suggest that overexpression of *GFP-fwd* and *GFP-synj* does not affect mitochondrial morphology, thus implying that regulation of PIs by *fwd* and *synj* does not grossly affect mitochondrial morphology.

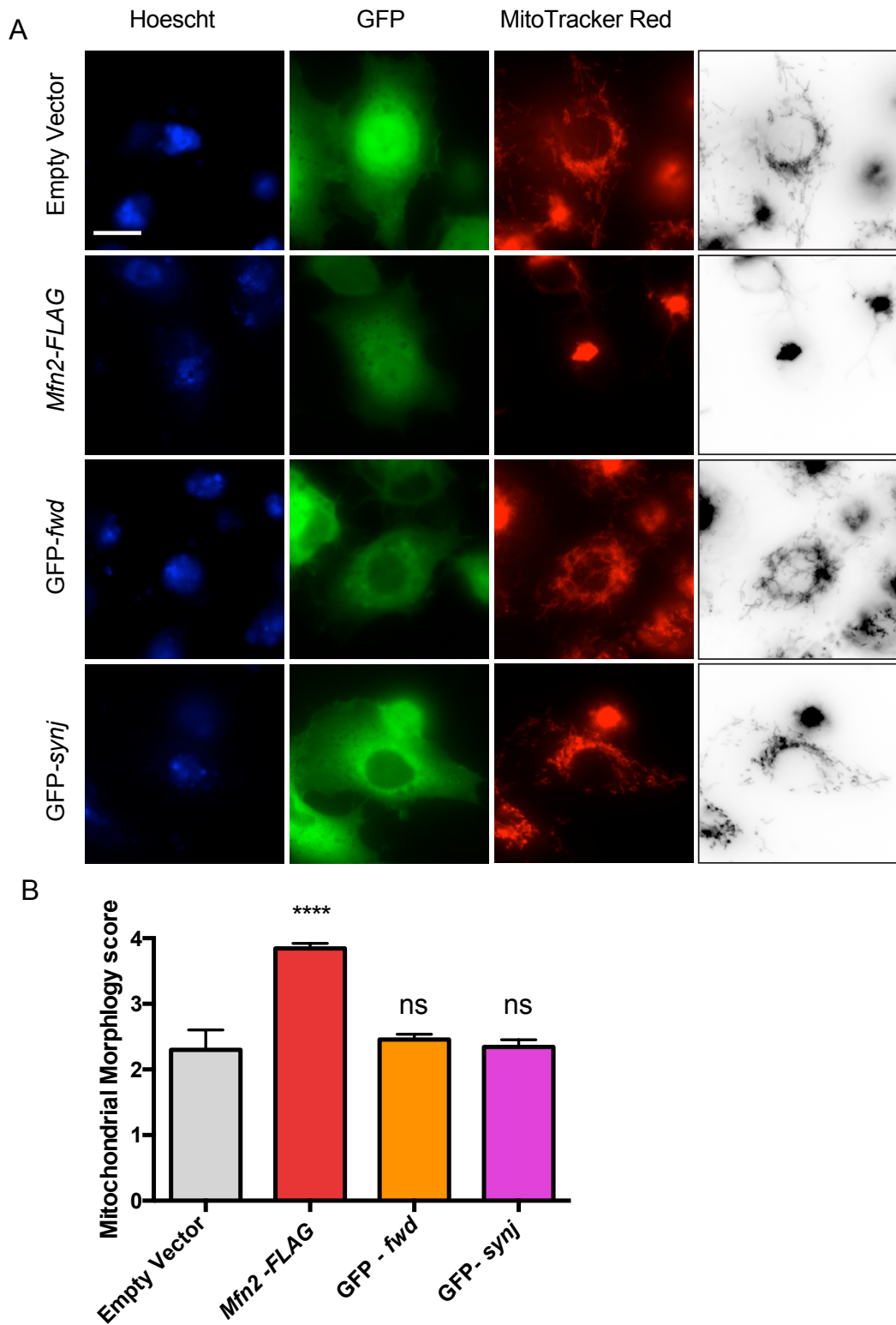


Figure 3.8: The overexpression of *fwd* or *synj* does not alter mitochondrial morphology in S2R+ *Drosophila* cells: S2R+ *Drosophila* cells were stained with MitoTracker (Red) to allow visualisation of the mitochondrial network and 2 $\mu\text{g/ml}$ Hoechst to visualise the nuclei. (A) Shows the mitochondrial network when an empty vector, *Marf*,

GFP-fwd and *GFP-synj* are expressed in S2R+ *Drosophila* cells. In the empty vector and *Marf* experimental conditions GFP was also expressed in a 1:3 ratio. (B) A graphical representation of these mitochondrial morphologies based on the 4-point mitochondrial morphology scoring scale. Results were analysed using one-way ANOVA with Bonferroni post hoc test. ns $P>0.05$ **** $P<0.0001$ Scale bar 10 μm .

3.3.7: The overexpression of *synj* results in a minimal effect on climbing ability.

Drosophila synaptojanin (synj) is the sole homologue of SYNJ1 and 2 which acts to de-phosphorylate PI4P and PI(4,5)P₂ to PI thus, *fwd* and *synj* determine the balance of PI, PI4P and PI(4,5)P₂ within the cell. Since knockdown or mutation of *fwd* can cause climbing defect in adult *Drosophila*, we wondered whether manipulating *synj* expression may also affect neuronal function. To examine this, a *GFP-synj* transgenic line was expressed using an ubiquitous drivers *da-GAL4* climbing ability was then examined.

The results show when *UAS-synj* is driven by *da-GAL4*, there is no significant difference between *da/+* or when *synj* is overexpressed (**Fig 3.9A**). Overall these data indicate that overexpression of *synj* does not substantially alter climbing in adult *Drosophila*.

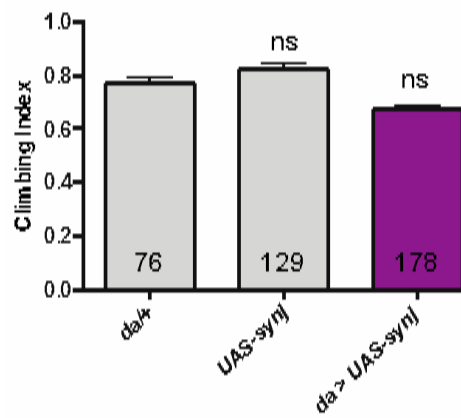


Figure 3.9: The overexpression of *synj* results in minimal effects of climbing ability: *Drosophila* expressing UAS construct for *synj* via the GAL4-UAS system, were assessed for their ability to climb under a strong ubiquitous driver *daughterless*. The numbers in the bars represents the number of animals tested (n). Data was analysed using Kruskal-Wallis test with Dunn's correction. Error bar represent the standard error of the mean. ns P>0.05 *P<0.05

3.3.8: The knockdown of *synj* results in an expression dependent decrease in motor ability.

To further investigate the impact of PI's in climbing ability, two *synj* knockdown lines were obtained, *synj*-RNAi (34378) and *synj*-RNAi (27489), and expressed via *da*-GAL4 (strong) and *Act*-GAL4 (weak) ubiquitous drivers. With strong ubiquitous knockdown of *synj*, both RNAi lines showed a strong climbing defect which was significantly different from the *da* > *lacZ*-RNAi control (**Fig 3.10A**). In addition, the knockdown of *UAS-synj* with *Act*-GAL4 showed a less severe climbing defect than with *da*-GAL4 (**Fig 3.10B**). Thus, *synj* impacts on the climbing ability of *Drosophila* in a dose dependent manner. While these results may suggest a common mechanism with *fwd* to impact mitochondrial function, alternative mechanisms are also likely. For example, *synj* has been shown to be involved in un-coating of clathrin coated vesicles to affect synaptic vesicle recycling (Verstreken et al., 2003).

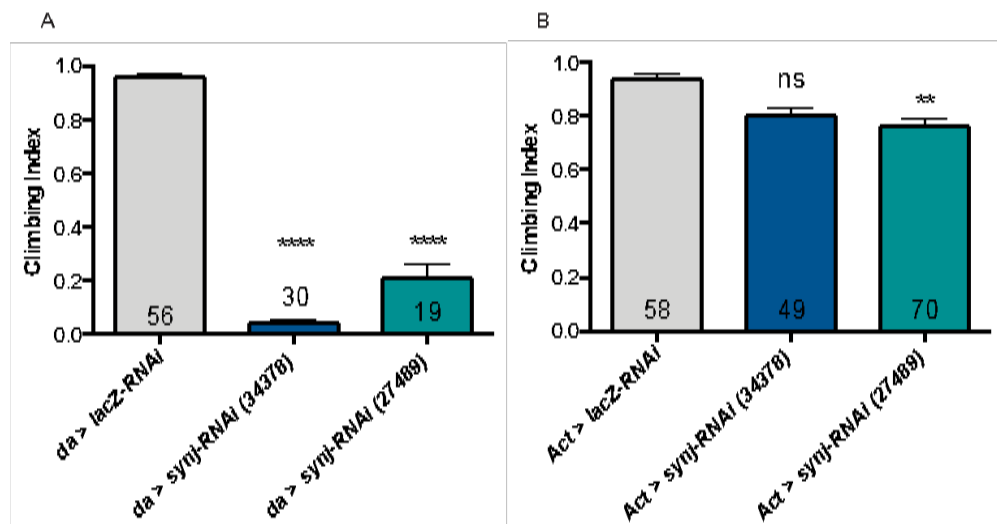


Figure 3.10: The knockdown of *synj* results in an expression dependent decrease in motor ability: *Drosophila* expressing UAS-RNAi construct for *synj* via the GAL4-UAS system, were assessed for their ability to climb under a strong ubiquitous driver *daughterless* (A) and a weak ubiquitous driver *Act5c* (B) The numbers in the bars represents the number of animals tested (n). Data was analysed using Kruskal-Wallis test with Dunns correction. Error bar represent the standard error of the mean. ns P>0.05 **P<0.01 ****P<0.0001

The overexpression, knockdown and mutation of both *fwd* and *synj* were analysed to understand the importance of PI's in *Drosophila* locomotion, with possible implications on mitochondrial homeostasis. Although *fwd* or *synj* loss has shown a strong climbing defect, it does not necessarily mean that regulation of PI's is involved with the PINK1-Parkin pathway. Therefore, the next half of this chapter I will focus on genetic interactions with *pink1^{B9}* and *park²⁵* with the aim of trying to determine a possible genetic interaction between *fwd*, *synj* and *pink1* and *parkin*.

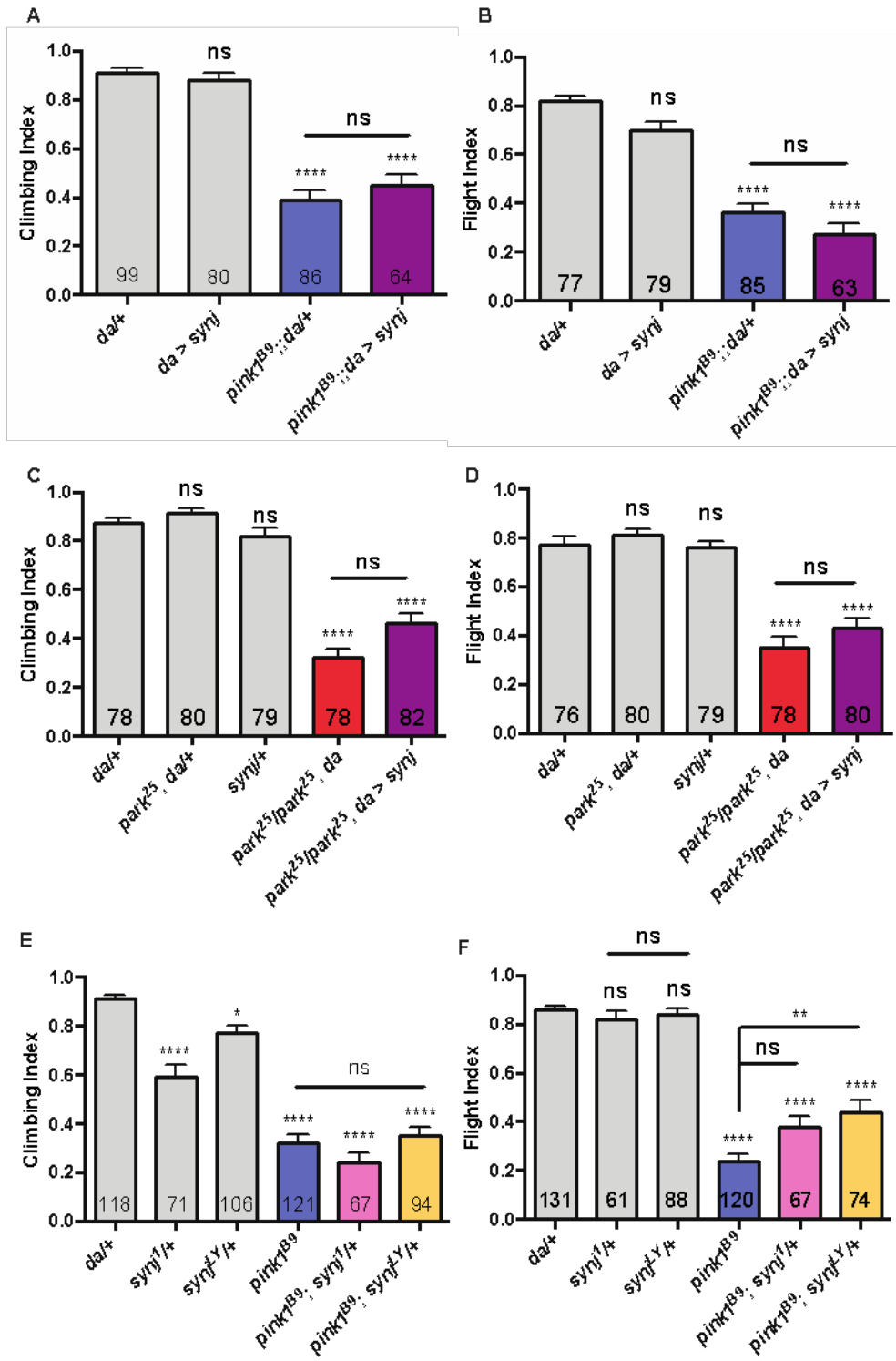
3.3.9: *synj* does not genetically interact with *pink1^{B9}* or *park²⁵*

We first tested whether *synj* genetically interacts with *pink1^{B9}* or *park²⁵*. First, *GFP-synj* was overexpressed using the strong ubiquitous driver *da-GAL4* in either *pink1^{B9}* mutant background and climbing and flight assessed. However, there was no significant modification in climbing or flight ability of *pink1^{B9}* mutants (**Fig 3.11A and B**). Similarly, the overexpression of *GFP-synj* in a *park²⁵* mutant background does not alter climbing or flight ability of *park²⁵* mutants (**Fig 3.11C and D**).

To further explore a possible genetic interaction, we tested two *synj* loss of function mutations; *synj¹* harbours a point mutation after the Sac1 domain while *synj^{L^Y}* harbours an early nonsense mutation. It has been suggested that if there were no non-sense mediated decay of *synj¹*, the Sac1 domain would still persist. This would allow investigation into the importance of the different domains of *synj* and their involvement with *pink1^{B9}* and *park²⁵* as well. As both mutants are lethal in homozygous, *park²⁵* and *pink1^{B9}* were genetically combined with *synj¹* and *synj^{L^Y}* in heterozygosis.

The results show that when both *synj¹* and *synj^{L^Y}* were genetically combined with either *pink1^{B9}* or *park²⁵* there is no significant difference in the climbing ability compared to *pink1^{B9}* or *park²⁵* mutants alone (**Fig 3.11E and G**). This, like the overexpression data indicates that *synj* does not genetically interact with to *pink1* or *parkin*. Similarly, the data from flight shows that the genetic combination of *synj¹* mutant with *pink1^{B9}* or *park²⁵* again does not result in a significant difference in locomotion (**Fig 3.11F and H**). However, the genetic combination of *synj^{L^Y}* mutant with *pink1^{B9}* results in a statistically significant increase in flight ability (**Fig 3.11F**).

Overall these data suggest there is no genetic interaction between *synj* and *pink1^{B9}* or *park²⁵*.



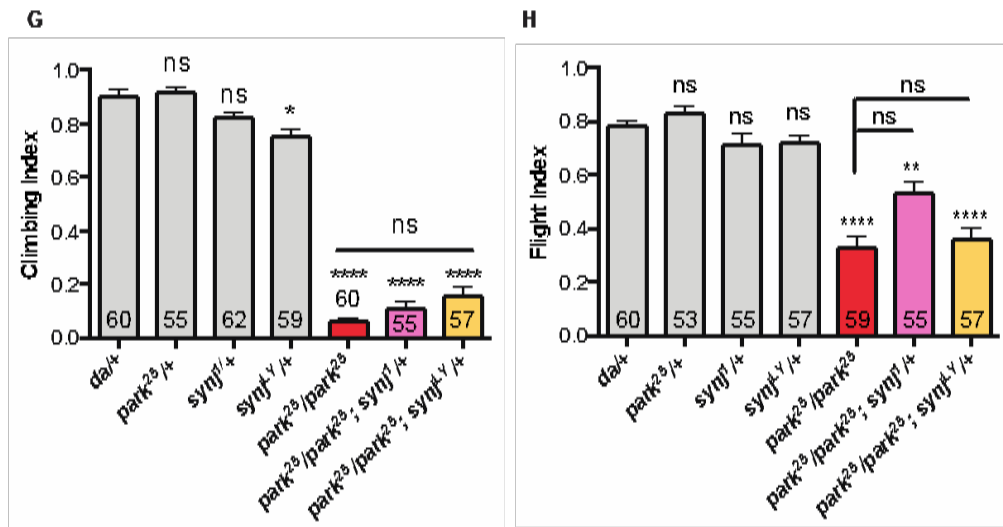


Figure 3.11: The depletion of *synj* in a *pink1^{B9}* or *park²⁵* mutant background has no effect on climbing but does show a minimal rescue of flight: *Drosophila* harbouring mutations for *synj* were genetically combined with *pink1^{B9}* mutant and tested for their ability to climb (A) and fly (B). *Drosophila* harbouring mutations for *synj* were genetically combined with *park²⁵* mutants and tested for their ability to climb (C) and fly (D). The numbers in the bars represents the number of animals tested (n). Data was analysed using Kruskal-Wallis test with Dunns correction. Error bar represent the standard error of the mean. ns P>0.05 *P<0.05 **P<0.01 **P<0.0001**

3.3.10: The reduction or loss of *fwd* does not result in any change to the motor phenotype of a *pink1^{B9}* or *park²⁵* mutant *Drosophila*

To look for a synergistic effect of losing of *fwd* on *pink1^{B9}* or *park²⁵* locomotion, we first tested a weak *fwd* knockdown condition and genetically combined this with *pink1^{B9}* or *park²⁵* mutants and tested climbing ability. The combination of *fwd* knockdown with *pink1^{B9}* mutant resulted in no significant changes in the climbing or flight ability compared to the *pink1^{B9}* mutants alone (**Fig 3.12 A and B**). Similarly, the knockdown of *fwd* in *park²⁵* mutant also showed no change to the climbing and flight ability compared to *park²⁵* mutant alone (**Fig 3.12C and D**).

To further investigate and confirm these results, *fwd¹* and *fwd³* mutants were genetically combined with *pink1^{B9}* and *park²⁵*. The results show that when *fwd³/+* and *pink1^{B9}* are genetically combined there is a significant decrease in climbing ability compared to *pink1^{B9}* mutant alone (**Fig 3.13A**). However, this is not observed when *fwd¹/+* is genetically combined with *pink1^{B9}* (**Fig 3.13C**). In addition, *fwd* mutations do not significantly affect flight ability of *pink1^{B9}* mutants (**Fig3.13B and D**). Similarly, the hemizygous combination of *fwd³* did not significantly affect the *park²⁵* mutants in either climbing or flight (**Fig 3.13E and F**). Notably, the outcross control of *fwd³/+* showed a significant decrease in climbing ability compared to the *da/+* control (**Fig 3.13A**). Thus, it is likely that the decreased climbing seen with the *pink1^{B9}; fwd³/+* combination results from the combined effects of *pink1^{B9}* and *fwd³/+* rather than a synergistic effect. Overall these results suggest that reduction or loss of *fwd* does not have any effect on the motor ability of *pink1* or *parkin* mutants.

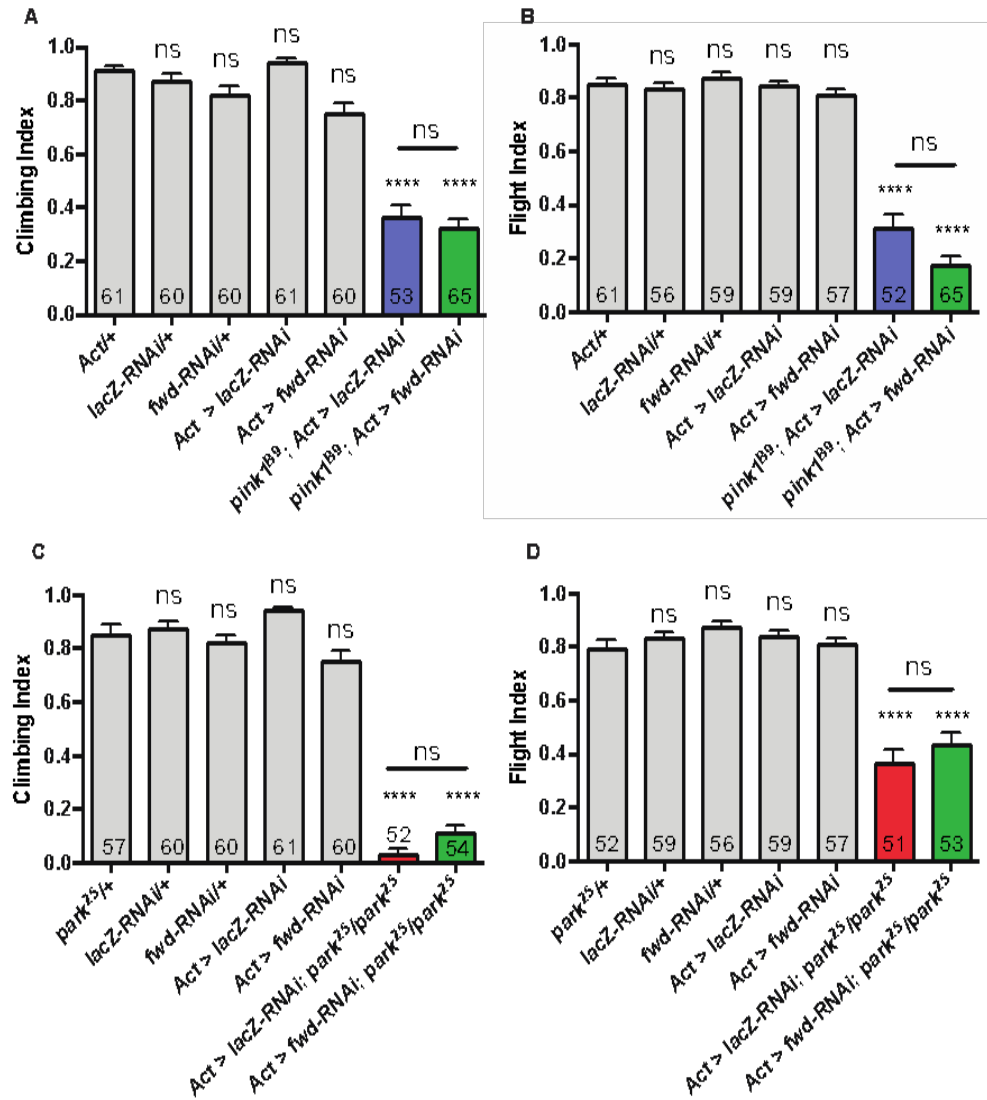


Figure 3.12: The depletion of *fwd* in a *pink1^{B9}* or *park²⁵* mutant background has no effect on climbing or flight: *Drosophila* expressing UAS-RNAi construct for *fwd* via the GAL4-UAS system, were expressed in *pink1^{B9}* and *park²⁵* mutants and assessed for their ability to climb (A and C) and fly (B and D) under a strong ubiquitous driver *daughterless* (*da*). The numbers in the bars represents the number of animals tested (n). Data was analysed using Kruskal-Wallis test with Dunn's correction. Error bar represent the standard error of the mean. ns P>0.05 *P<0.05 ****P<0.0001 with those above each bar being compared to *da*/+ outcrossed control.

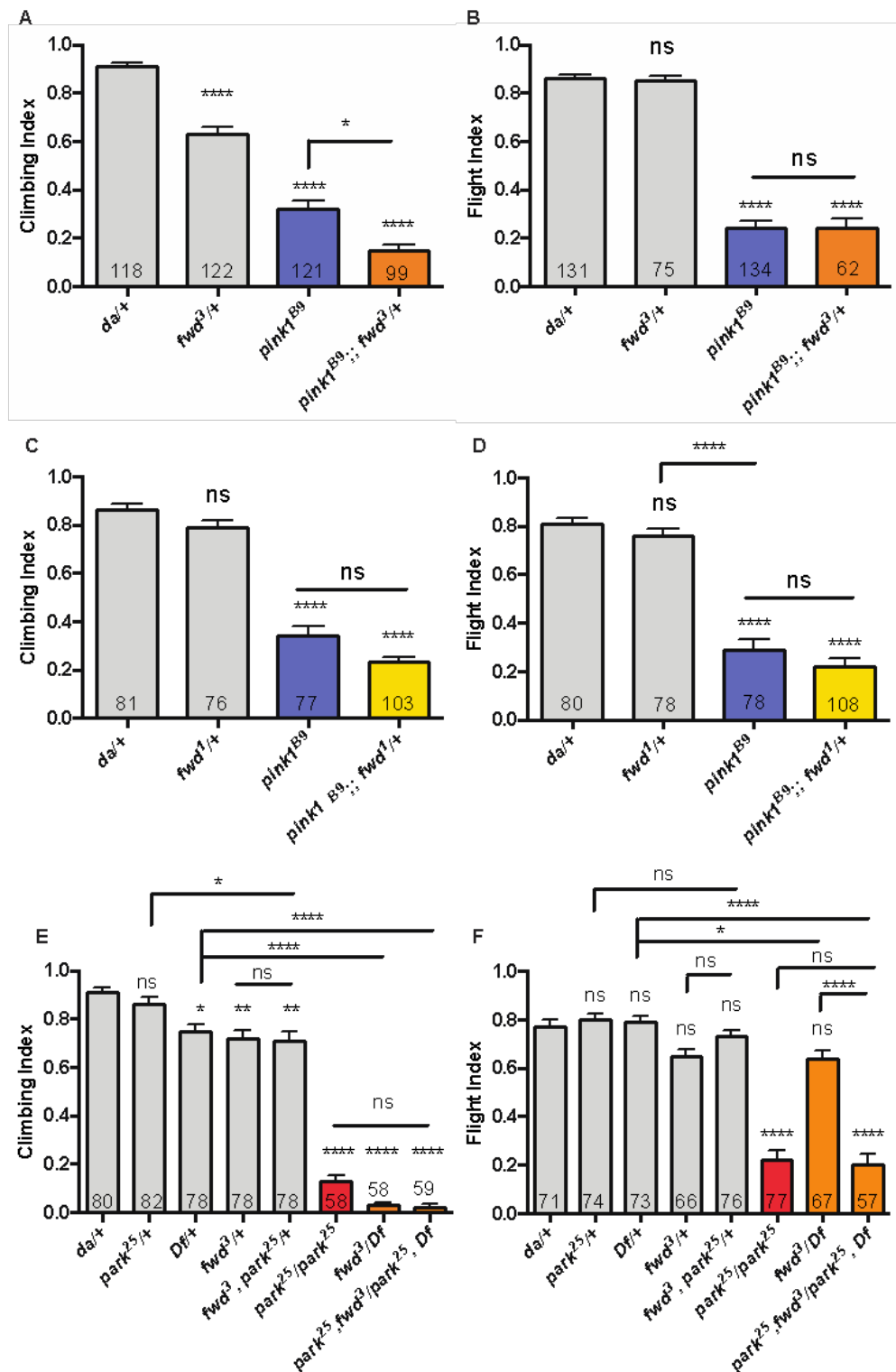


Figure 3.13: The depletion of *fwd* in a *pink1^{B9}* or *park²⁵* mutant background has no effect on climbing or flight: *Drosophila* harbouring mutations for *fwd* (*fwd³*) were genetically combined with *pink1^{B9}* mutant and tested for their ability to climb (A) and fly (B). *Drosophila* harbouring mutations for *fwd* (*fwd¹*) were genetically combined with *pink1^{B9}* mutant and tested for their ability to climb (C) and fly (D). *Drosophila* harbouring mutations for *fwd* were genetically combined with *park²⁵* mutants and tested for their ability to climb (E)

and fly (F). The numbers in the bars represents the number of animals tested (n). Data was analysed using Kruskal-Wallis test with Dunns correction. Error bar represent the standard error of the mean. ns $P>0.05$ * $P<0.05$ ** $P<0.01$ **** $P<0.000$.

3.3.11: The overexpression of *fwd* partially suppresses climbing defects in *pink1^{B9}* and *park²⁵* mutants.

As a final approach, we tested whether overexpression of *fwd* in either *pink1^{B9}* or *park²⁵* mutant background modified their climbing and flight ability. Interestingly, when *fwd* is overexpressed in the *pink1^{B9}* mutant background by the strong ubiquitous driver *da-GAL4* there is a significant increase in the climbing ability compared to the *pink1^{B9}* mutant alone (**Fig 3.14A**). However, the overexpression of *GFP-fwd* did not rescue the flight ability of the *pink1^{B9}* mutant (**Fig 3.14B**). Similarly, the overexpression of *fwd* in *park²⁵* mutant background also shows a significant increase in the climbing ability compared to the *park²⁵* mutant alone, but and again no rescue was seen for flight (**Fig 3.14C and D**). For both genetic combinations, overexpression of *fwd* is unable to fully rescue the climbing defect of *pink1^{B9}* or *park²⁵* as there is significant decrease in climbing ability compared to the outcrossed control *da/+* (**Fig 3.14A and C**).

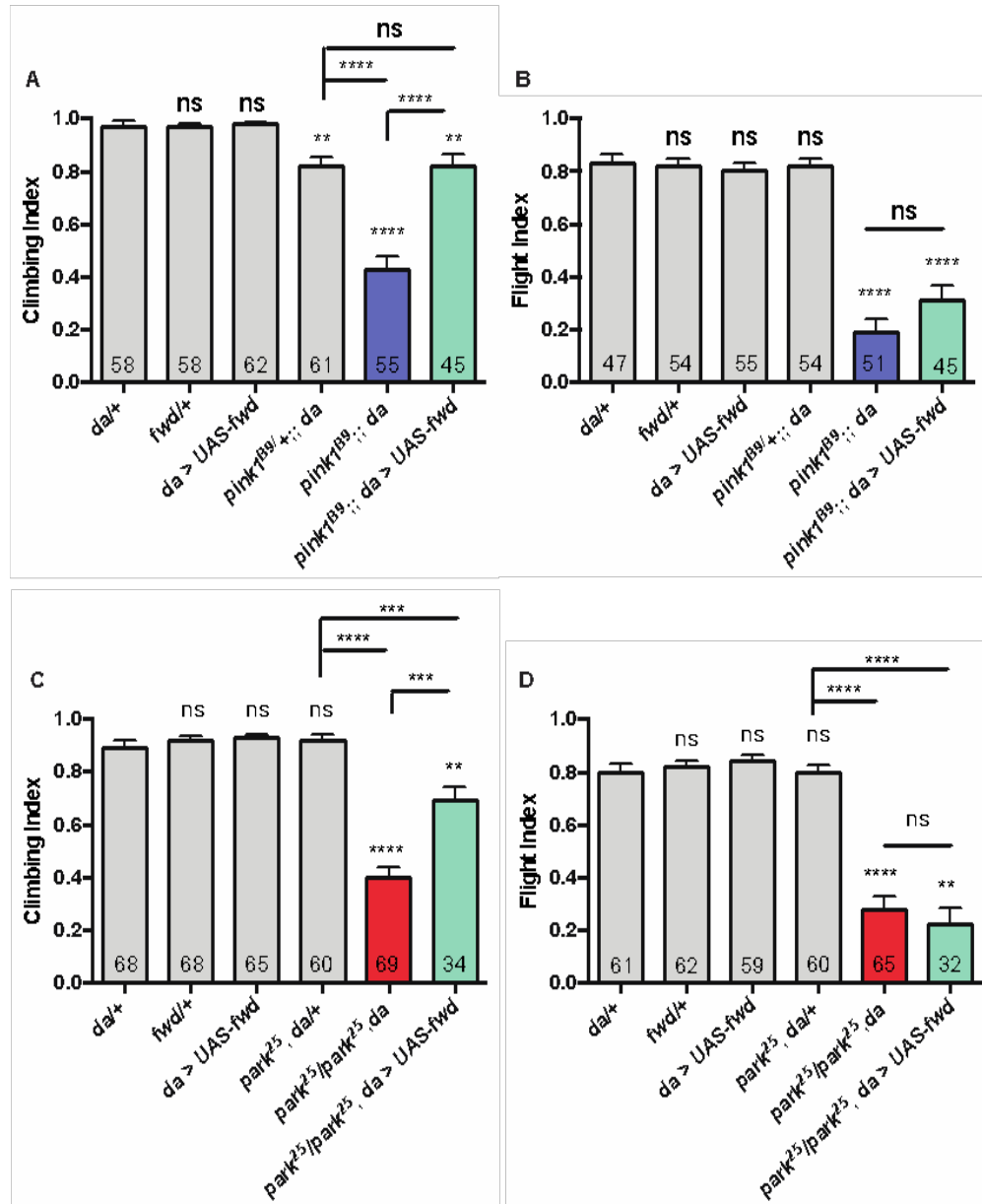


Figure 3.14 The overexpression of *fwd* results in a rescue of both *pink1^{B9}* and *park²⁵* mutant climbing ability: *Drosophila* overexpressing *GFP-fwd* via the GAL4-UAS system, were genetically combined with *pink1^{B9}* mutants and tested for their ability to climb (A) and fly (B). *Drosophila* overexpressing *GFP-fwd* through the GAL4-UAS system, were genetically combined with *pink1^{B9}* mutants and tested for their ability to climb (C) and fly (D). The numbers in the bars represents the number of animals tested (n). Data was analysed using Kruskal-Wallis test with Dunns correction. Error bar represent the standard error of the mean. ns P>0.05 **P<0.01 ***P<0.001 ****P<0.0001

3.4 Discussion

The aim of this chapter was to investigate *in vivo* the impact of *fwd* and *synj* on phenotypes known to be affected by mitochondrial quality control pathways, such as those observed in *pink1/parkin* mutants, e.g. climbing and flight.

fwd has previously been investigated in the context of cytokinesis, predominantly in spermatogenesis. It was found that *fwd* is required for intracellular bridge formation and localisation of Rab11 to the mid-zone during cytokinesis (Polevoy et al. 2009; Brill et al. 2000). However, there are no studies that have examined *fwd* with regards to defects in mitochondrial morphology. This is the first study to investigate the locomotor ability of *fwd* mutant *Drosophila*. Depleting *fwd* causes a severe climbing defects which can be rescued by reintroducing *fwd* into the system. This implicates *fwd* in adult *Drosophila* locomotion and suggests loss of *fwd* can result in neurological defects. The phenotype seen is like the climbing defect seen in *pink1^{B9}* or *park²⁵* mutants (Pesah et al. 2004; Clark et al. 2006; Park et al. 2006; Yang et al. 2006), suggesting that they may be converging on the same pathway. However, no formal evidence for a genetic interaction has been found between *fwd* or either *pink1* or *parkin*. Nevertheless, it was interesting to observe the rescue of *pink1^{B9}* and *park²⁵* mutant climbing ability, but not flight, with the overexpression of *fwd*. This is only a partial rescue and therefore suggests that other factors may also be at play. The PINK1/Parkin pathway is highly complex and it is expected that there could be many regulatory proteins contributing to its efficient function in maintaining mitochondrial health.

The predominant function of *fwd* is to produce PI4P though the phosphorylation of PI at the D4 position and hence, the rescue of the *pink1^{B9}* or *park²⁵* climbing defect by the overexpression of *fwd* may suggests that PI4P is impacting on downstream branches of the PINK1/Parkin pathway. These may include mitochondrial transport, mitochondrial morphology, mitophagy and MDV formation which all act to promote the health of the mitochondria and survival of the dopaminergic neurones. Although exact mechanisms are not known it can be speculated that changes in mitochondrial morphology are at play due to previously reported mitochondrial hyperfusion observed upon *fwd* knockdown (Pogson et al 2014). Further characterisation of *fwd* mutants should be conducted to look for other phenotypes that are present in *pink1^{B9}* and *park²⁵* mutants, such as dopaminergic neurone loss or gross mitochondrial defects.

Interestingly, *Drosophila* which had a depletion of *fwd* have a strong climbing defect with no effect seen in flight. The climbing and flight assays measure different aspects of locomotion: climbing assay tests coordination and strength while the flight assays test the reflex action of the indirect flight wing muscles. Therefore, the ability to climb can be indicative of *fwd* having prominent roles in different cell types. It was hypothesized that a decrease in climbing but not flight ability suggests that *fwd* has a greater requirement in neuronal populations. Coordination in *Drosophila* is predominantly regulated by the central complex and mushroom bodies with many dopaminergic neurones, including those which degenerate in aging, projecting to the mushroom body (Serway et al. 2009; Poeck et al. 2008; White et al. 2010). As dopaminergic neurones regulate locomotion and impact on coordination, it may suggest that *fwd* has a greater impact in dopaminergic neurones, hence the defect in climbing but not flight. However, *fwd* is expressed ubiquitously with enrichments in the adult brain and testis, therefore the enrichment in the brain may also contribute to the decrease in co-ordination (Robinson et al. 2013). To further examine this, climbing and flight could be tested with the knockdown of *fwd* with neuronal and muscle specific drivers. If *fwd* is having a greater effect in neurones, then a climbing defect would be seen with neuronal drivers but not muscles specific drivers.

Since previous data had shown that in S2R+ cells the loss of *fwd* affects mitochondrial morphology, causing hyper-fusion (Pogson et al. 2014), it was hypothesised that the climbing defect seen in *fwd* mutants may be due to hyper-fusion of the mitochondrial network. However, surprisingly, this phenotype was not affected by manipulation of mitochondrial morphology genes *Opa1*, *Marf* and *Drp1*. The inability to rescue the climbing defect seen in *fwd* mutants led us to re-examine the effect of loss of *fwd* on mitochondrial morphology in *Drosophila* S2R+ cells. Surprisingly, despite extensive analysis, the knockdown or overexpression of *fwd* or *synj* did not yield any changes in mitochondrial morphology. It is unclear why different results were obtained but there could be many contributing factors. First, we use a 4-point scoring system which is defined by eye, making it subjective. However, while this can readily distinguish between highly distinct phenotypes, such as knockdown of *Marf* or *pink1*, more subtle phenotypes may not be easily differentiated. Alternative methods are available, such as analysis of aspect ratio and overall network using Image J (De Vos & Sheetz 2007) but these are difficult to apply to *Drosophila* cells due to their small size making them hard to image. Alternatively, there are multiple technical factors that may influence this assay.

These could include aspects such as the relative vitality or passage number of the cells, batch-to-batch variation in growth media or other consumables, or subtle changes in environmental conditions from when the original screen was conducted. Similarly, the degree of knockdown could have been different in my tests from those achieved in the original screen. Unfortunately, the knockdown efficiency was not routinely assayed during the screening process which makes it hard to compare, but may have been more effective leading to a more pronounced effect. Thus, taken together these data are not conclusive but suggest that the *fwd* climbing defect is not likely to be due to mitochondrial morphology changes.

The mammalian homologue of *synj*, *SYNJ1*, has been found to be mutated in both the Sac1 and ins-5-phosphatase domain in AR-JP. This led to the hypothesis that *synj* and the regulation of PI's may impact the PINK1/Parkin pathway. *synj* was investigated for phenotypes related to *pink1* and *parkin*. The knockdown of *synj* produced a clear climbing defect and the *synj* mutants were homozygous lethal, suggesting a necessity for the *synj* in adult *Drosophila*. While *synj* depletion results in a climbing defect similar to *pink1^{B9}* and *park²⁵* mutants the genetic interaction studies between the *synj* mutants and *pink1^{B9}* and *park²⁵* mutants show no genetic interaction. Thus, the climbing defect in *synj* knockdown is unlikely due to the same mechanisms as *pink1^{B9}* and *park²⁵* mutants. *Synj* has a predominant role in the presynaptic terminal of the neuromuscular junction (NMJ) in *Drosophila*. *synj¹* mutants have impaired endocytosis and synaptic vesicle recycling at the NMJ (Verstreken et al. 2003). Without efficient vesicle recycling, neurotransmitter cannot be released and the impulses cannot be propagated across the NMJ. Thus, the muscle is getting a reduction in impulses stimulating it, preventing movement. These data suggest that the climbing defect is not specific to alterations in the PINK1/Parkin pathway components but is due to reduced synaptic vesicle recycling.

Interestingly, when *synj^{LY}* is genetically combined with *pink1^{B9}* mutant climbing is not affected but there is a small but significant rescue in flight ability of *pink1^{B9}* mutant which is not seen when *synj¹* is combined with *pink1^{B9}*. The *synj^{LY}* harbours a point mutation early in the protein and therefore results in a functionally null protein. *synj¹* contains a point mutation after the Sac1 domain and if there is no non-sense mediated decay, the Sac1 domain would persist (Verstreken et al. 2003; Dickman et al. 2005). This would suggest that a non-functional protein, unable to de-phosphorylate PI(4,5)P₂, can rescue the *pink1^{B9}* phenotype while the Sac1 domain, which can de-phosphorylate PI4P to PI prevents this rescue so a decrease in PI4P

is detrimental. However, the rescue is small and maybe acting in a separate mechanism not linked to *pink1* or *parkin* and it maybe more likely that the differences between the two isoforms are due to differences in their genetic background. Interestingly, mice carrying the pathological mutation found in PD patients, have neurological defects similar to those in PD patients including a decrease in locomotor ability but also delayed endocytosis in presynaptic nerve terminal of cortical neurones and dystrophic dopaminergic neurones (Cao et al. 2017). With no clear genetic interaction between *synj* and *pink1* or *parkin*, this may suggest that the PD phenotypes in patients are through synaptic vesicle recycling dysfunction rather than links to mitochondrial quality control.

In this chapter, I have determined that *fwd* loss can result in a previously un-seen defect in locomotor ability and that this is unlikely to be due to alterations in mitochondrial morphology. The rescue of the *pink1*^{B9} and *park*²⁵ climbing defect with overexpression of *fwd* may suggest that *fwd* may act to help regulate parallel pathways which converge and promote mitochondrial quality control. However, the exact mechanism of this is not known. Key aspects of the PINK1/Parkin pathway, mitophagy and Parkin translocation, can be evoked robustly in YFP-Parkin cells and hence can be utilised to understand the molecular mechanism further in a mammalian model.

4. THE ANALYSIS OF *PI4KB* AND *SYNJ* IN YFP-PARKIN HELA CELLS

4.1 Background

The PINK1/Parkin pathway is a key mitochondrial quality control pathway that regulates various mechanisms to protect the mitochondria from insults including oxidative stress. The main mechanisms by which the PINK1/Parkin pathway protects the mitochondria are: changes in mitochondrial morphology, axonal transport and the bulk degradation of mitochondria known as mitophagy (Liu et al., 2012; Narendra et al., 2008a; Ziviani et al., 2010). Under mitochondrial insult, such as CCCP treatment an mitochondrial uncoupling agent, the mitochondrial membrane potential is depolarised and PINK1 becomes stabilised on the OMM (Narendra et al., 2008a). Upon this stabilisation, PINK1 phosphorylates local ubiquitin, Parkin translocates from the cytosol to the OMM. Here, both phospho-Ub and PINK1 activate Parkin in a two-step process (Kane et al., 2014; Kazlauskaitė et al., 2014; Kondapalli et al., 2012; Koyano et al., 2014; Shiba-Fukushima et al., 2012). Once active, Parkin poly-ubiquitinates a variety of OMM proteins including Mfn2 and VDAC. The poly-ubiquitination of Mfn2 results in its degradation and changes in mitochondrial morphology which help to isolate damaged mitochondria, thereby aiding mitophagy (Ziviani et al., 2010). Poly-ubiquitinated OMM proteins are recognised by P62, Optineurin and NBR1 which are LIR containing adaptors which bind LC3 on the phagophore membrane allowing engulfment into autophagosome, thus starting the process of mitophagy (Kirkin et al., 2009; Narendra et al., 2010b; Wong and Holzbaur, 2014).

Much of the analysis of the PINK1/Parkin pathway has been conducted in mammalian cell lines with HeLa cells often being the model of choice (Geisler et al., 2010b; Matsuda et al., 2010; Narendra et al., 2008a). There are many advantages of using HeLa cells: they are large and flat, allowing for easy image acquisition and analysis, they are readily transfected with plasmids and siRNA, and they are extremely easy to grow in culture (Denison et al., 2003). Despite these advantages, HeLa cells lack endogenous Parkin but, it has been shown that exogenous tagged Parkin, such as YFP-Parkin, shows robust recruitment of Parkin to the mitochondrial following mitochondrial toxification equivalent to that seen with endogenous Parkin in HEK293 cells or SH-SY5Y cells (Geisler et al., 2010b; Narendra et al., 2008a). With the advantages outweighing the disadvantages, YFP-Parkin HeLa cells are an attractive model to study PINK1/Parkin pathway which we adopted here to assess three main steps: Parkin translocation, changes in mitochondrial morphology and the reduction in the mitochondrial content indicating that mitophagy has occurred.

4.2 Hypothesis and Aims

Following work conducted in chapter 3 it was shown that *fwd* can rescue the climbing defect of both *pink1* and *parkin* mutants, therefore suggesting that manipulation of PI's maybe involved with the PINK1/Parkin pathway. However, these genetic interaction studies are unable to reveal details of the function of *fwd* in the PINK1/Parkin pathway. In addition, *SYNJ1* is mutated in AR-JP disease while *SYNJ2* has been shown to be recruited to mitochondria via the *SYNJ2BP* (Krebs et al., 2013b; Nemoto and De Camilli, 1999b; Quadri et al., 2013b). Thus, suggesting that PI manipulation by *SYNJ1/2* may also have an impact on PINK1/Parkin pathway. To understand role of *PI4KB*, *SYNJ* and to investigate the effect of PI manipulation in PINK1/Parkin pathway, a robust mammalian cell model was used and the mammalian homologue of *fwd* and *synj*, *PI4KB*, *SYNJ1* and *SYNJ2* were manipulated in YFP-Parkin HeLa cells.

The aim of this chapter is to investigate the manipulation of *PI4KB* and *SYNJ* on Parkin translocation, changes in mitochondrial morphology and mitophagy, using YFP-Parkin HeLa cells. If *SYNJ* or *PI4KB* are impacting early in the PINK1/Parkin pathway then a delay in Parkin translocation or changes in mitochondrial morphology maybe seen. Alternatively, if *SYNJ* or *PI4KB* impact downstream of PINK1 or Parkin then changes to mitophagy, maybe perceived without changes to parkin translocation. A further aim is to determine which *SYNJ* isoform has the greatest impact on mitochondrial quality control and Parkin translocation.

4.3 Investigation of *PI4KB*, *SYNJ* loss in the PINK1/Parkin pathway

4.3.1: The transfection of *PI4KB*, *SYNJ1* or *SYNJ2* siRNA in YFP-Parkin HeLa cells results in an efficient knockdown in mRNA levels.

To begin investigating the impact of *PI4KB* and *SYNJ1/2* in a mammalian cell model, the efficiency of knockdown of each *PI4KB*, *SYNJ1* and *SYNJ2* siRNA was examined by quantitative real-time-PCR. HeLa cells stably expression YFP-Parkin (herein, YFP-Parkin HeLa cells) were transfected with either control, *PINK1*, *PI4KB*, *SYNJ1*, *SYNJ2* or both *SYNJ1* and *SYNJ2* SMARTpool siRNA and incubated for 4 days and the expression levels of *PINK1*, *PI4KB*, *SYNJ1* or *SYNJ2* were analysed relative to a house keeping gene, *β -Actin*. All primers had efficiency provided between 90-110% allowing for the Livakk method of analysis to be used. Compared to samples treated with control siRNA, those transfected with *PINK1*, *PI4KB*, *SYNJ1* and *SYNJ2* siRNAs had a significant decrease in their corresponding mRNA levels.

With all siRNA showing a minimum of 70% decrease in *PINK1*, *PI4KB*, *SYNJ1* and *SYNJ2* (Fig 4.1A and B). In addition, when both *SYNJ1* and *SYNJ2* (*SYNJ1/2*) siRNA were co-transfected there was still a significant decrease in expression of both *SYN1* and *SYNJ2* suggesting that the method of conducting dual knockdown is efficient. Overall, these data indicate that the siRNAs used create efficient and reliable knockdown in YFP-Parkin HeLa cells and therefore can be used in the following experiments.

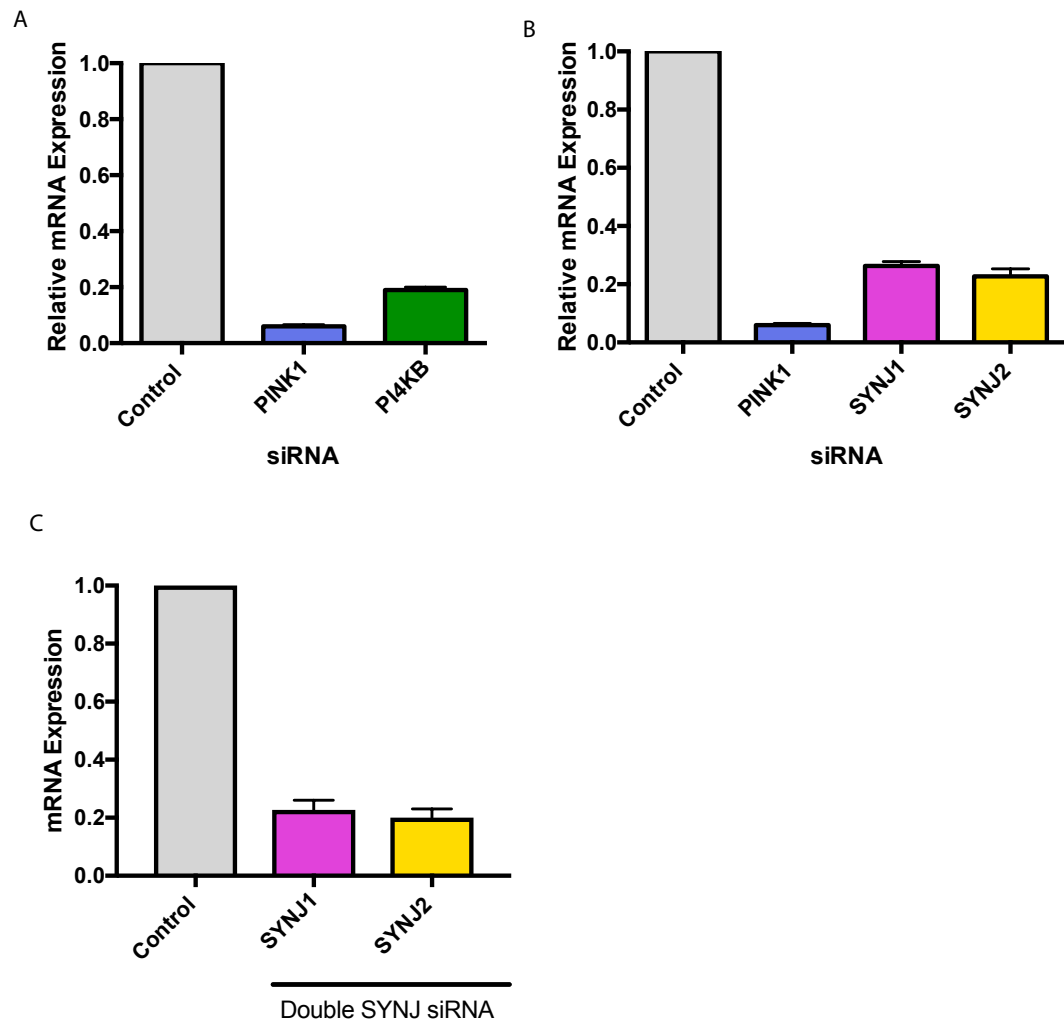
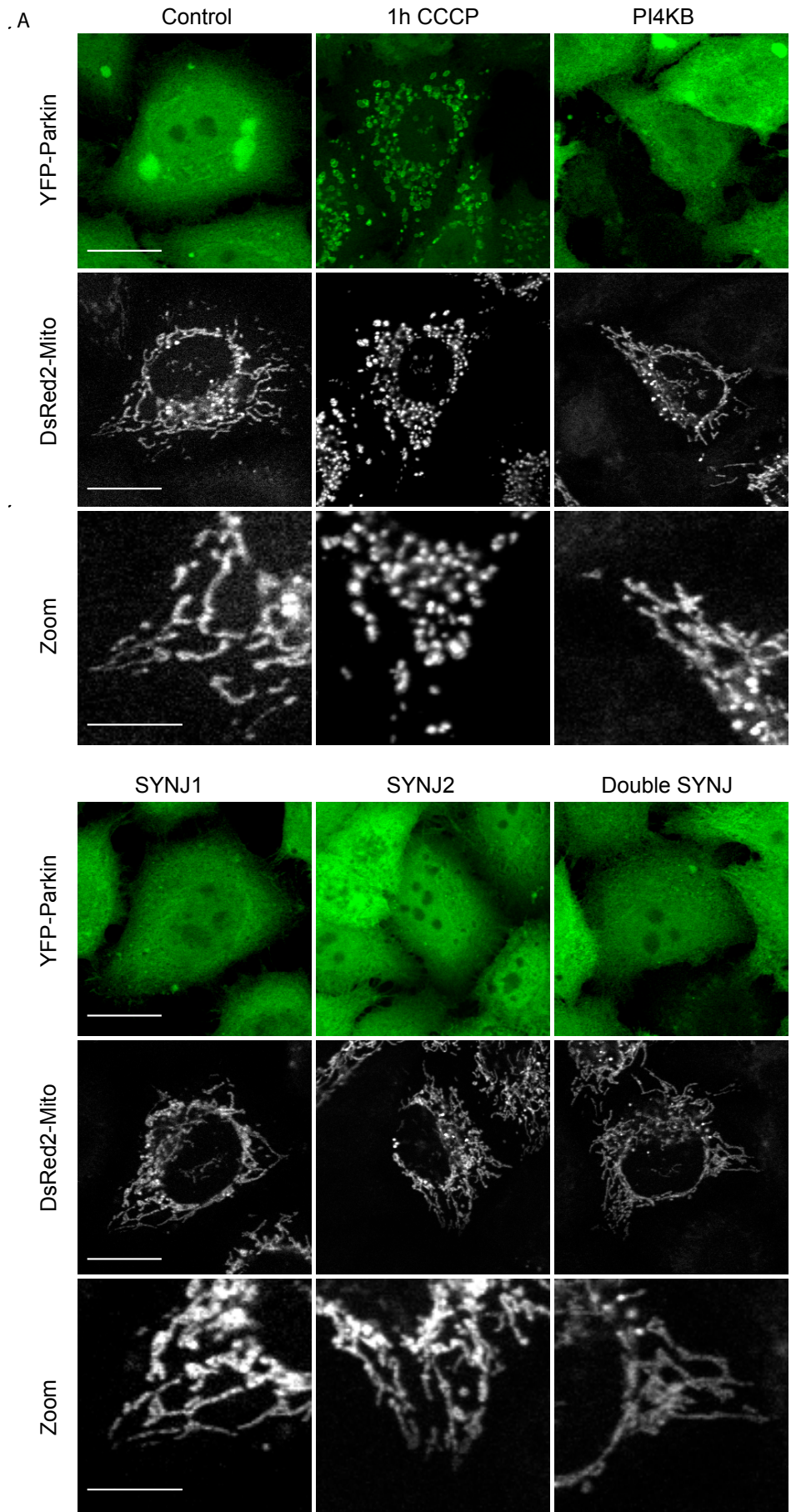


Figure 4.1: The qPCR analysis *PINK1*, *PI4KB*, *SYNJ1* and *SYNJ2*: YFP-Parkin HeLa cells were treated with either control, *PINK1*, *PI4KB* (A), *SYNJ1* (B), *SYNJ2* (B) or *SYNJ1* and *SYNJ2* (c) siRNA for 4 days before harvesting for RNA. Data represents 3 biological replicates. *β-Actin* was used as a housekeeping gene and all qPCR primers tested for amplification efficiency (80-110%). Livvack method was used to analyse the knockdown. Error bars represent standard error of the mean.

4.3.2: The silencing of *PI4KB* or *SYNJ* in YFP-Parkin HeLa cells does not alter mitochondrial morphology

Previously it was shown that knockdown of *fwd* in S2R+ *Drosophila* cells produced a hyper-fused mitochondrial network which phenocopied the knockdown of *pink1* (Pogson et al., 2014). We therefore decided to analyse any possible changes of mitochondrial morphology in a mammalian model. To examine this YFP-Parkin HeLa cells were transfected with *PI4KB*, *SYNJ1*, *SYNJ2* or both *SYNJ1* and *SYNJ2* siRNA and incubated for 4 days. DsRed2-Mito was transfected into cells to allow visualisation of the mitochondrial network. Images were taken of cells which were co-expressing YFP-Parkin and DsRed2-Mito and analysed using Image J to look at both aspect ratio (width: height) and the overall network (branch points/end points) of the cells (De Vos and Sheetz, 2007). A fused mitochondrial network would have an aspect ratio (width: height) greater than 1 and that the mitochondrial network would have more branch points resulting in a greater network score. 1 h CCCP treatment was used as a control to show that these methods of analysis can quantify changes in the mitochondrial network. As expected the 1 h CCCP treatment resulted in a highly fragmented mitochondrial network which had a significantly decrease in aspect ratio and network score. When YFP-Parkin cells were treated with *PI4KB* siRNA, no change in the mitochondrial network was observed. The cells appeared healthy with tubular mitochondria similar to that seen in control siRNA treated cells. Once quantified the mitochondrial network and aspect ratio showed no significant difference between the *PI4KB* and control siRNA (**Fig 4.2A, B and C**). The same is observed with *SYNJ1*, *SYNJ2* and the double knockdown of both *SYN1/2*. There is no difference in the appearance of the mitochondrial network between the control condition and the any of the knockdown conditions, mitochondria remain tubular and within a larger network (**Fig 4.2A**). There is no significant difference in the aspect ratio or network of the control and the *SYNJ* knockdown conditions (**Fig 4.2B and C**). Overall, these data show that there is no significant different in the branching or aspect ratio of the mitochondrial network with knockdown of *PI4KB*, *SYNJ1* or *SYNJ2*. These data, together with results from *Drosophila* cells and adult *Drosophila* genetic interaction studies, suggest that the alteration of *PI4KB* and *SYNJ* does not impact on mitochondrial morphology.



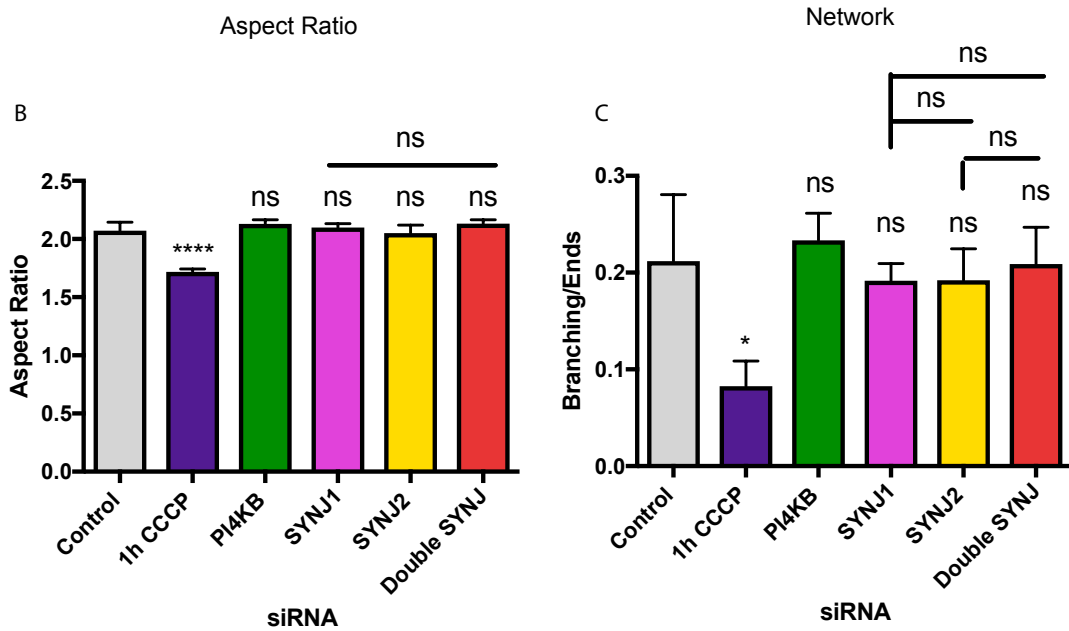


Figure 4.2: The knockdown of PI4KB or SYNJ in YFP-Parkin HeLa cells does not result in changes to mitochondrial morphology: (A) YFP-Parkin HeLa cells (YFP-Parkin (Green) Mitochondria (DsRed2-Mito (gray))) were treated with either control, *PI4KB*, *SYNJ1*, *SYNJ2* or *SYNJ1/2* siRNA for 4 days before the analysis of the mitochondrial network by fluorescence confocal microscopy (60X objective, 1x Zoom, scale bar 20 μm or 10 μm) using the mitochondrial morphology analysis published in (De Vos and Sheetz, 2007). (B) Graphical representation of aspect ratio of the mitochondrial network. (C) The graphical representation of the ratio between the end points and branch points of the mitochondrial network. Data represents 3 biological replicates with >100 cells analysed per condition, per assay. Error bars represent standard error of the mean. ns $P > 0.05$ * $P < 0.05$ **** $P < 0.0001$ (one-way ANOVA with Bonferroni's post hoc test).

4.3.3: The knockdown of *PI4KB* in YFP-Parkin HeLa cells slows Parkin translocation

To further understand the effects of *PI4KB* on the PINK1/Parkin pathway Parkin translocation, a key aspect of the PINK1/Parkin pathway, was examined. This was examined by treating YFP-Parkin HeLa cells with 10 μ M CCCP, a mitochondrial uncoupling agent which depolarizes the mitochondrial membrane, for 2 or 4 h. Under control conditions by 4 h CCCP treatment YFP-Parkin robustly translocates from the cytosol to the mitochondria, where it can be activated and begin to signal for degradation of that mitochondria (Narendra et al., 2008a). Parkin translocation was examined under control, *PINK1* and *PI4KB* knockdown conditions. To quantify YFP-Parkin translocation, each condition was imaged and given a Parkin translocation score. 1 = No Parkin translocation where the YFP-Parkin remains in the cytosol, 2 = Partial Parkin translocation where some YFP-Parkin is co-localized to the mitochondria but a significant amount still remains in the cytosol and 3 = full Parkin translocation where the majority of YFP-Parkin is present on the mitochondria and co-localises with mitochondria marker ATP5A (Fig 4.3).

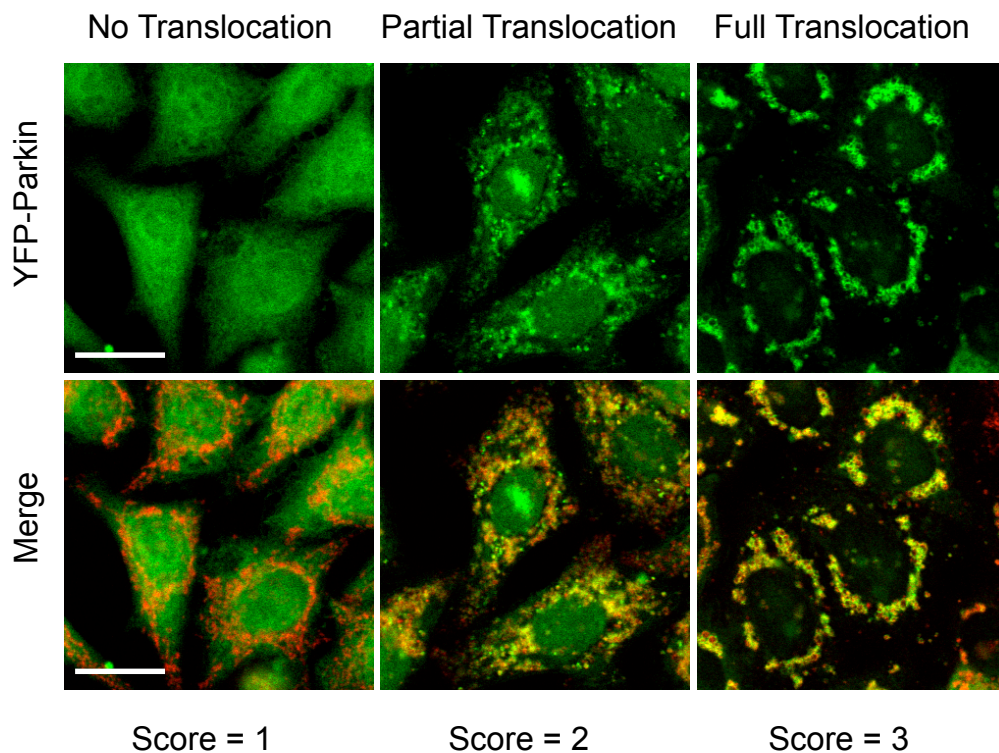
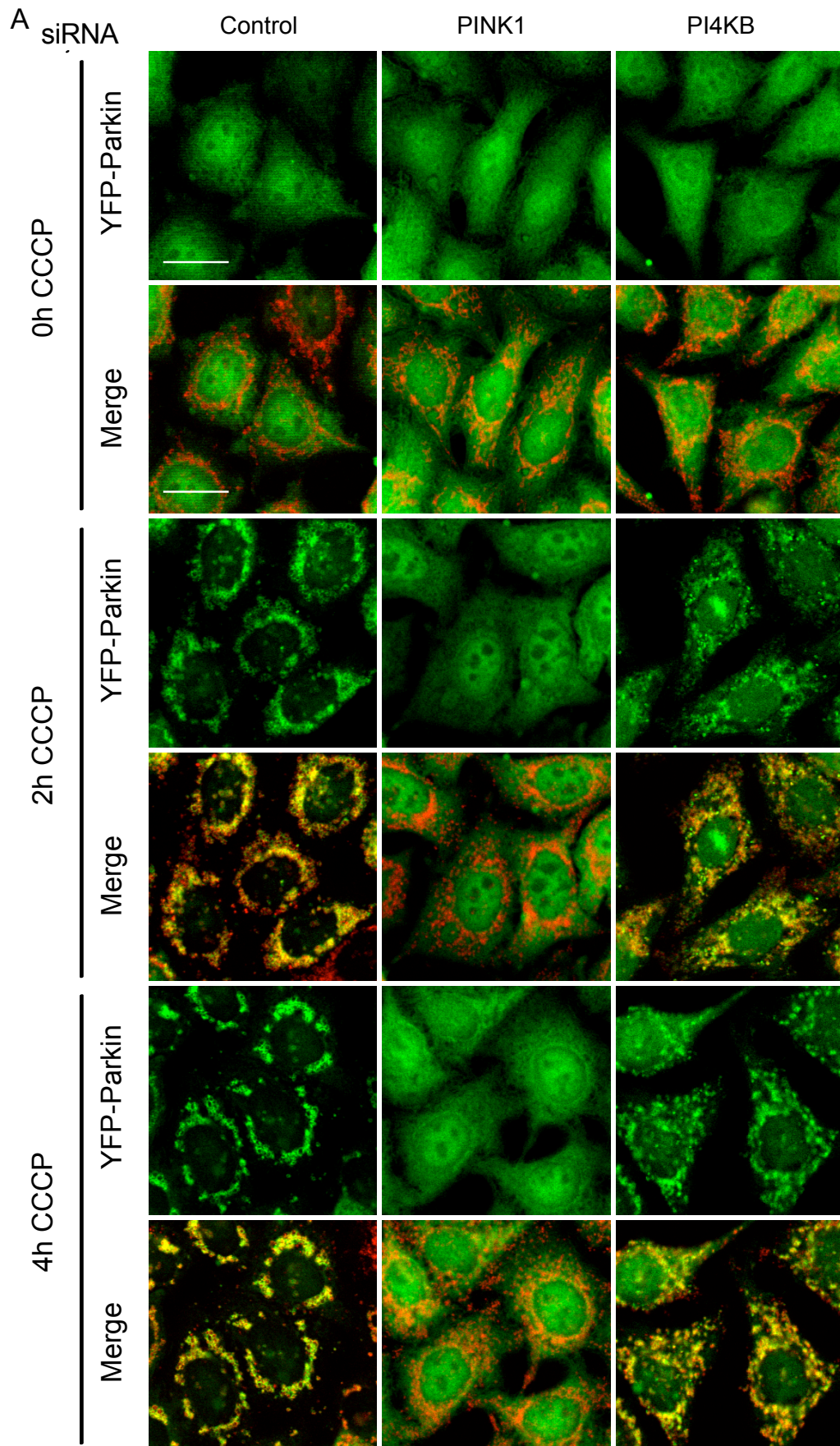


Figure 4.3: Parkin translocation scoring system: Examples of the 3 'parkin translocation' phenotypes in YFP-Parkin HeLa cells (YFP-Parkin (Green) Mitochondria (ATP5A;Red)). A score of 1 refers to no Parkin translocation where all Parkin is cytosolic and non-is co-localised with the mitochondria (A). A score of 2 refers to partial Parkin translocation, where some Parkin is co-localised with the mitochondria but some remains in

the cytosol (B) and a score of 3 refers to full parkin translocation where most, if not all Parkin is co-localised with mitochondria (ATP5A). Scale bar = 10 μ m

The results show that with control siRNA and then 2 and 4 h CCCP treatment there is robust Parkin translocation from the cytosol to the mitochondria. Parkin appears predominately to localise with the mitochondrial marker while the cytosol is severely depleted of YFP-Parkin. The Parkin translocation score is statically significant compared to 0 h CCCP treatment where the YFP-Parkin is diffuse throughout the cytosol and does not localise to the mitochondria (**Fig 4.4**). As expected, under *PINK1* siRNA knockdown conditions, with either 2 or 4 h CCCP treatment, the YFP-Parkin remains cytosolic and does not translocate to the mitochondria, thus showing the knockdown of *PINK1* results is a severe Parkin translocation defect, which significantly differs from control siRNA (**Fig 4.4A and B**). When *PI4KB* is silenced and left un-toxified, no change in Parkin translocation is seen, suggesting that knockdown of *PI4KB* alone, does induce Parkin translocation (**Fig 4.4A**). However, under 2 h and 4 h CCCP treatment more YFP-Parkin is diffusely localized in the cytosol compared to the control where the majority of YFP-Parkin is co-localizing with the mitochondria (**Fig 4.4A and B**). Overall these data suggest that knockdown of *PI4KB* results in a slowing of Parkin translocation, thus *PI4KB* loss is impacting on the PINK1 and Parkin pathway.



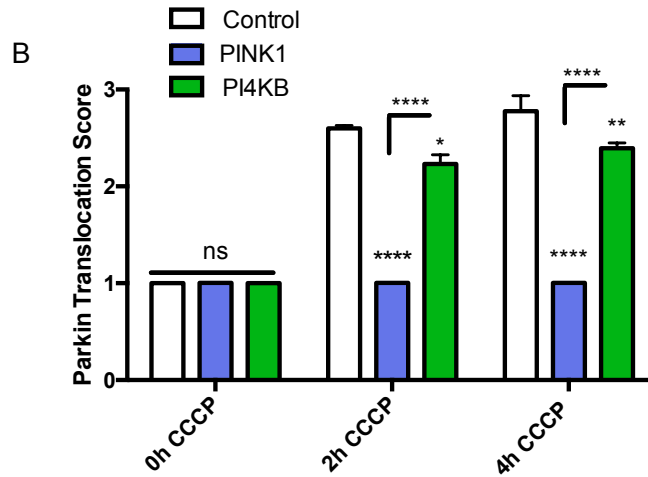
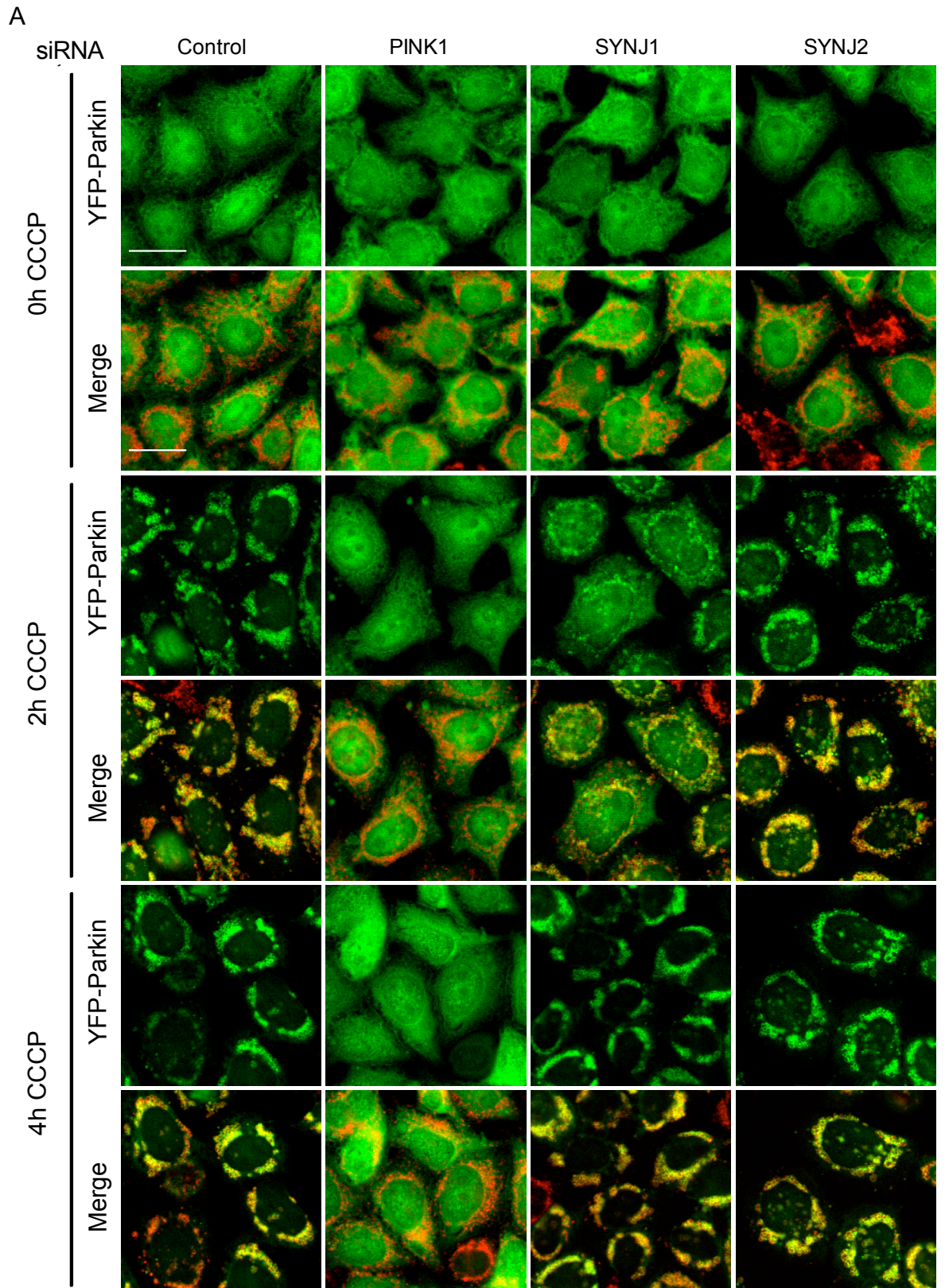


Figure 4.4: The knockdown of *PI4KB* in YFP-Parkin HeLa cells results in a Parkin translocation defect. (A) YFP-Parkin HeLa cells (YFP-Parkin (Green), mitochondria (ATP5A; Red) were treated with either *control*, *PINK1* or *PI4KB* siRNA for 4 days before the addition of either CCCP (10 μ M) for 0h, 2h or 4h. Parkin translocation was assessed by fluorescence confocal microscopy (60X objective, 1x Zoom, scale bar 10 μ m) using the scoring system outlined in Fig 4.1 (B) Graphical representation of Parkin translocation quantification following the application of CCCP. Data represents 3 biological replicates with >100 cells analysed per condition, per assay. Error bars represent standard error of the mean. ns $P > 0.05$ * $P < 0.05$ ** $P < 0.01$ **** $P < 0.0001$ (one-way ANOVA with Bonferroni post hoc test).

4.3.4: The knockdown of *SYNJ* in YFP-Parkin HeLa cells results in reduced Parkin translocation.

To examine what effect *SYNJ* is having in PINK1/Parkin pathway and which family member, *SYNJ1* or *SYNJ2*, may be more important, YFP-Parkin HeLa cells were transfected with control, *PINK1*, *SYNJ1* and *SYNJ2* siRNA for 4 days and then treated with 0 h, 2 h or 4 h CCCP. Images were taken then scored based on the scoring system outlined in (Fig 4.3). As expected with control siRNA transfections there was full robust Parkin translocation from the cytosol to mitochondria under 2h and 4h CCCP treatment, while *PINK1* knockdown prevented Parkin translocation (Fig 4.5A and B). When *SYNJ1* or *SYNJ2* are knocked down but un-toxified, no change in YFP-Parkin localization is seen with it remaining diffuse in the cytosol (Fig 4.5). After 2 h CCCP treatment however, compared to control siRNA knockdown, the knockdown of *SYNJ1*, results in a Parkin translocation defect, with more YFP-Parkin appearing diffuse throughout the cytosol and less localising on the mitochondria. By 4 h CCCP treatment the YFP-Parkin defect seen with knockdown of *SYNJ1* had been resolved with the majority of YFP-Parkin co-localizing with the mitochondria (Fig 4.5A and B). With the knockdown of *SYNJ2* there is no defect seen at either 2 h or 4 h CCCP treatment with the YFP-Parkin remaining co-localised on the mitochondria similar to control siRNA treatment.

Since there is no effect seen on Parkin translocation with *SYNJ2* knockdown, we hypothesized that this may be due to compensation by *SYNJ1*. To address this, both *SYNJ1* and *SYNJ2* were knocked down simultaneously. Parkin translocation was analysed under control, *PINK1* or *SYNJ1* and *SYNJ2* double knockdown. While the controls behaved as expected, when both *SYNJ1* and *SYNJ2* were knocked down a Parkin translocation defect was seen at 2 h CCCP treatment (Fig 4.6A and B). In addition, there was a Parkin translocation defect at 4 h CCCP treatment with YFP-Parkin remaining the cytosol more than with control siRNA treatment (Fig 4.6). These data suggest that *SYNJ* may indeed play a role in Parkin translocation and that *SYNJ1* can compensate for *SYNJ2*. *SYNJ1* may regulate early aspects of Parkin translocation while *SYNJ2* may act slightly later.



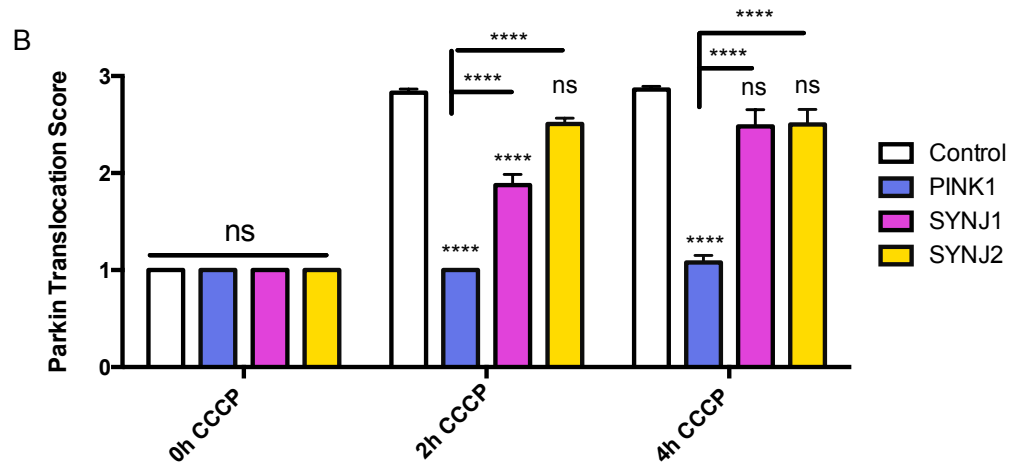
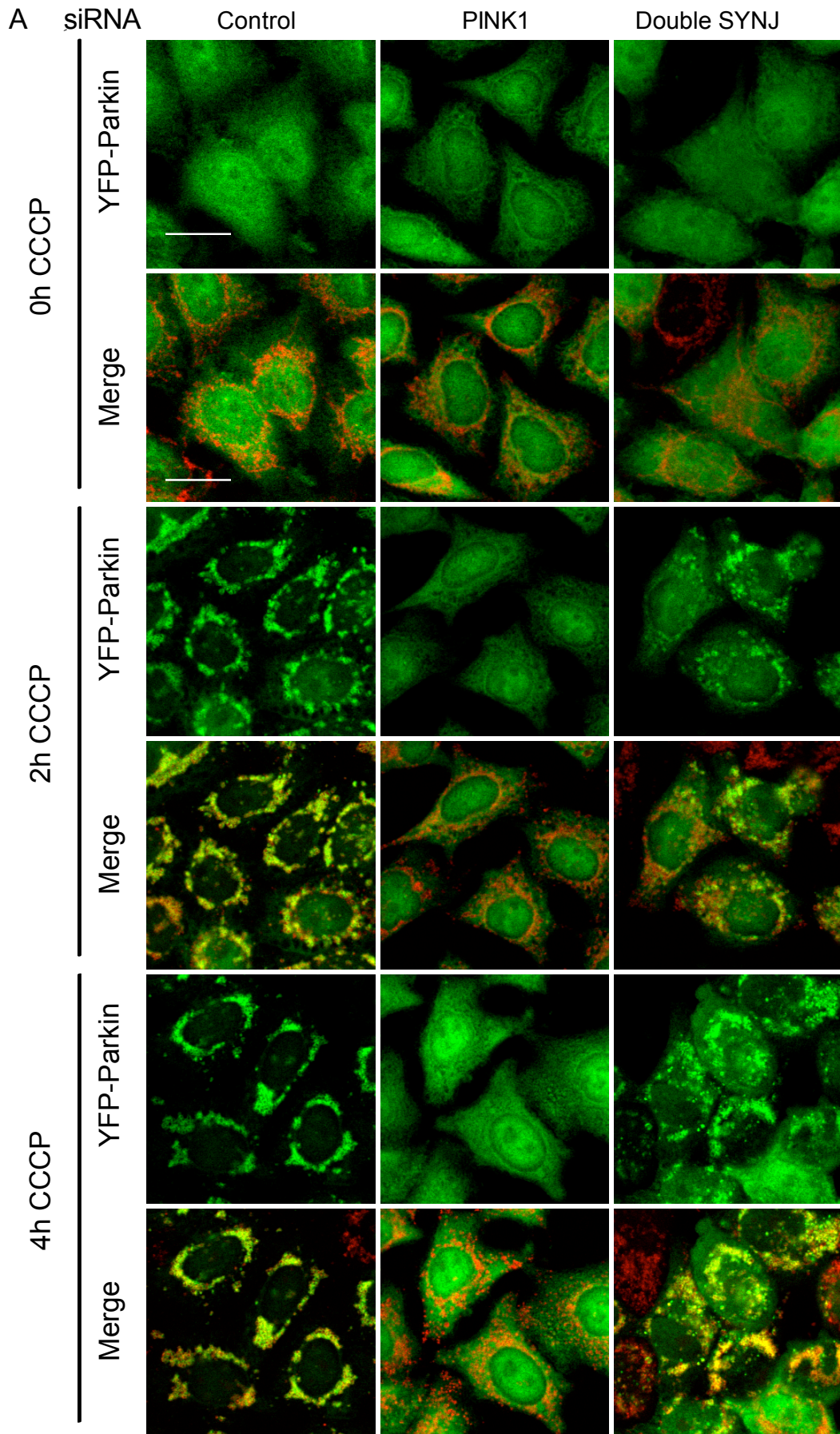


Figure 4.5: The knockdown of *SYNJ1* in YFP-Parkin HeLa cells results in a slowing of Parkin translocation: (A) YFP-Parkin HeLa cells (YFP-Parkin (Green) Mitochondria (ATP5A; Red) were treated with either control, *PINK1*, *SYNJ1* or *SYNJ2* siRNA for 4 days before the addition of either 0 h 2 h or 4 h CCCP (10 μ M). Parkin translocation was assessed qualitatively by fluorescence confocal microscopy (60X objective, 1x Zoom, scale bar 10 μ m). (B) Graphical representation of Parkin translocation quantification following the application of 0h 2h and 4h CCCP. Data represents 3 biological replicates with >100 cells analysed per condition, per replicate. Error bars represent standard error of the mean. ns $P > 0.05$ **** $P < 0.0001$ (one-way ANOVA with Bonferroni's Post Hoc Test).



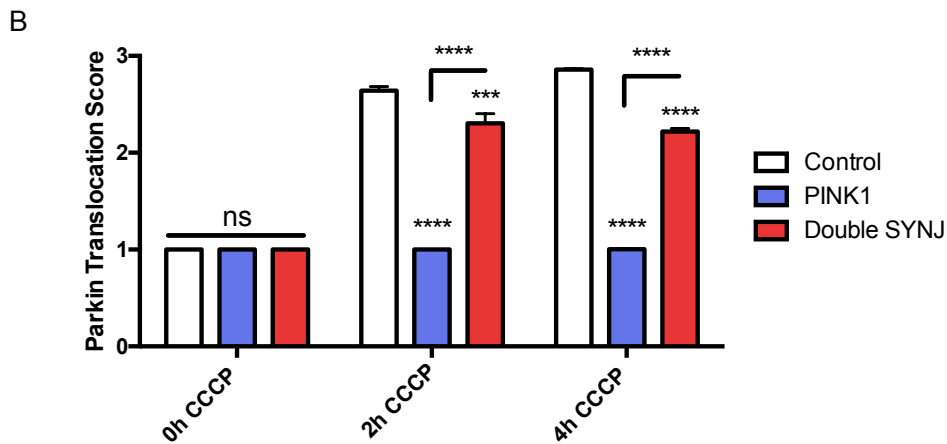


Figure 4.6: The double knockdown of *SYNJ1* and *SYNJ2* in YFP-Parkin HeLa cells result in a Parkin translocation defect: (A) YFP-Parkin HeLa cells (YFP-Parkin (Green) Mitochondria (ATP5A; Red) were treated with either control, *PINK1* or both *SYNJ1* and *SYNJ2* siRNA for 4 days before the addition of either 0 h 2 h or 4 h CCCP (10 μ M). Parkin translocation was assessed qualitatively by fluorescence confocal microscopy (60X objective, 1x Zoom, scale bar 10 μ m) using the scoring system outlined in Figure 4.3. (B) Graphical representation of Parkin translocation quantification following the application of 0 h 2 h and 4 h CCCP. Data represents 3 biological replicates with >100 cells analysed per condition, per replicate. Error bars represent standard error of the mean. ns $P > 0.05$ *** $P < 0.001$ **** $P < 0.0001$ (one-way ANOVA with Bonferroni post hoc test).

4.3.5: The *SYNJ1* constructs are readily expressed in HeLa, YFP-HeLa and HEK cells.

To further understand the effect of *SYNJ1* on the PINK1/Parkin pathway, plasmids containing Flag tagged versions of two splice variants of *SYNJ1* (*SYNJ1*-145 and *SYNJ1*-170, along with *SYNJ1*-145 R219Q which harbours a mutation in the Sac1 domain similar to that of PD patients, were obtained. To check that these construct express efficiently they were transfected in HEK293 and YFP-Parkin HeLa cells, with expression being tested by both immunofluorescence and western blotting.

The results from the western blot show that all three constructs express and run at the predicted molecular weight (145 and 170 kDa) in both YFP-Parkin HeLa and HEK293 cells (**Fig 4.7A**). However, large amounts of protein were loaded suggesting the transfection efficiency is inefficient. The western blot shows *SYNJ1*-145 R219Q has the highest expression (**Fig 4.7A**). The constructs can also be visualised using immunofluorescence (**Fig 4.7B**). Overall the *SYNJ1* constructs express and can be detected via western blotting or immunofluorescence in YFP-Parkin cells therefore allowing further investigation into its function in the PINK1/Parkin pathway.

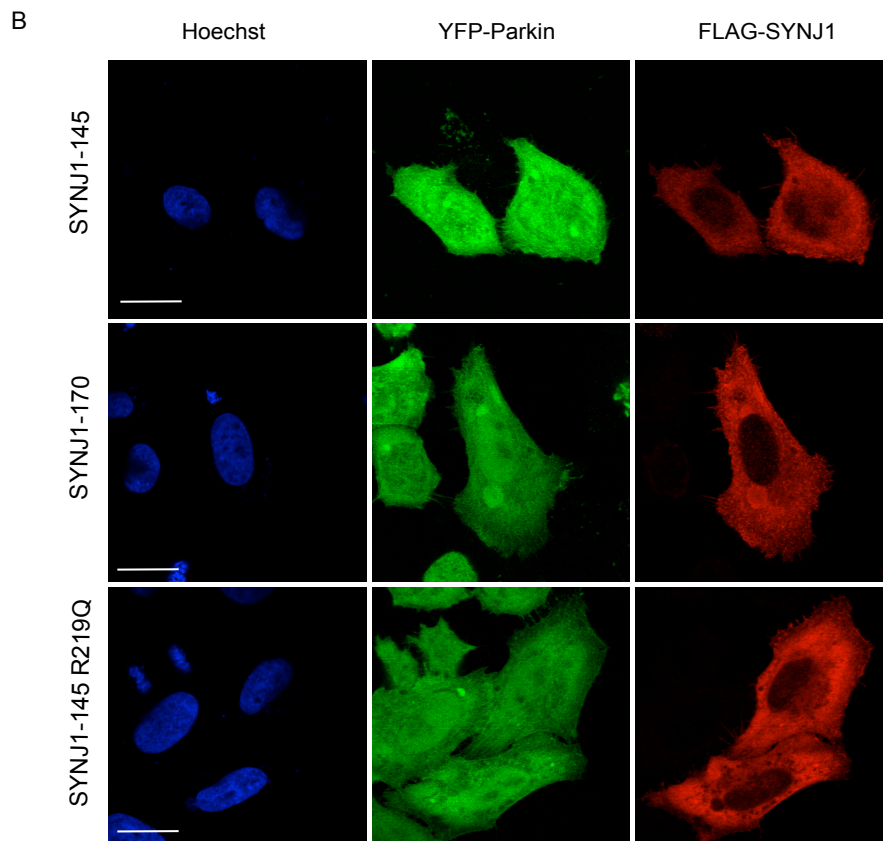
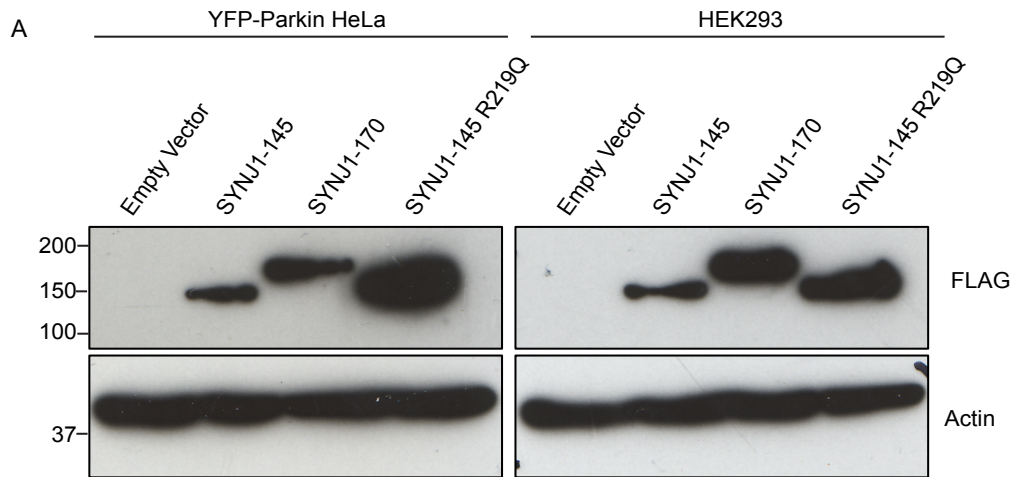
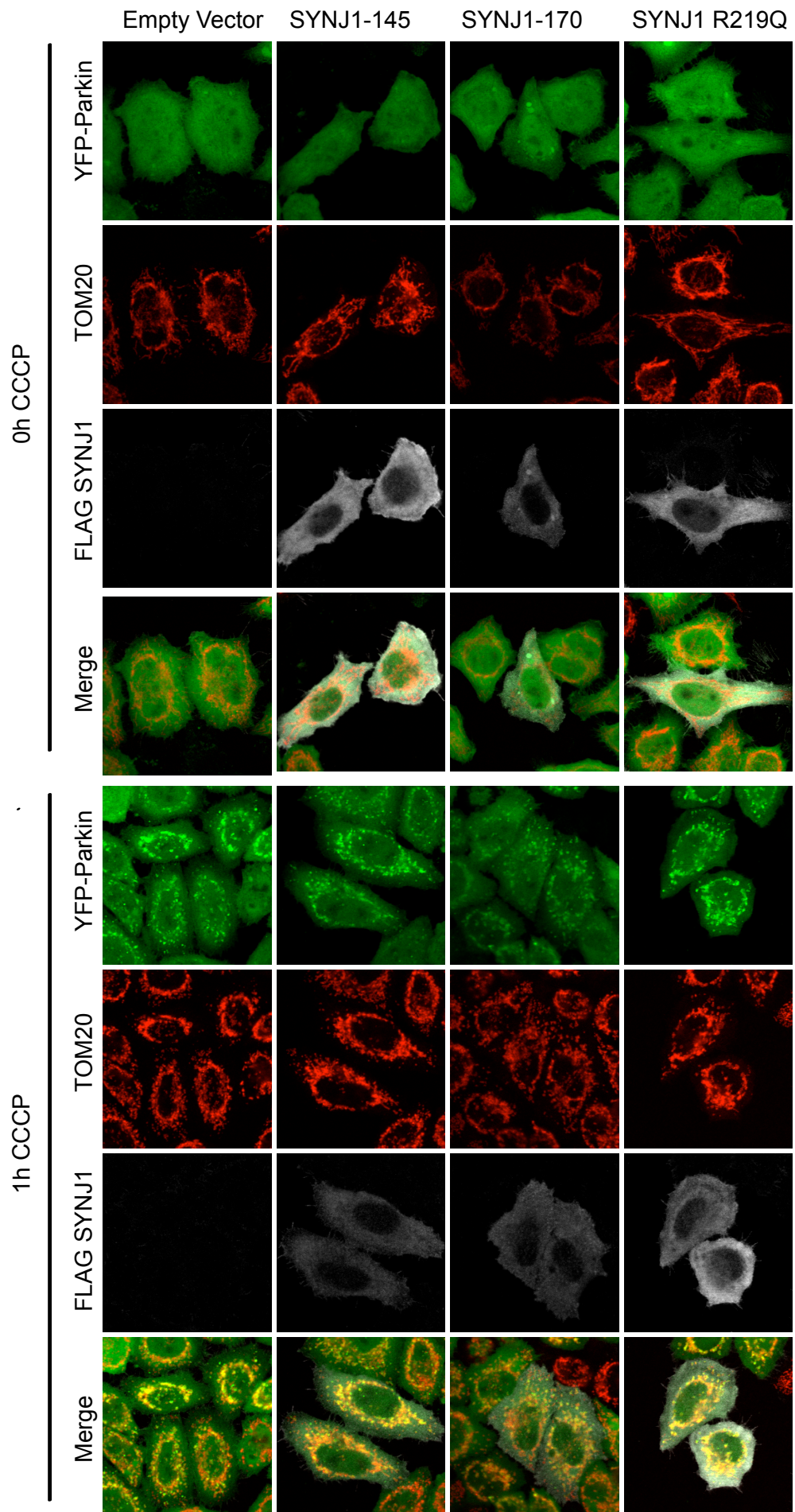


Figure 4.7: SYNJ1-145, SYNJ1-170 and SYNJ1-145 R219Q FLAG tagged constructs express in YFP-Parkin HeLa and HEK293 cells: YFP-Parkin HeLa were transfected with either control SYNJ1-145, SYNJ1-170 or SYNJ1-145 R219Q to test expression of these constructs. After transfection lysates were collected for western blot (A) or coverslips fixed for immunofluorescence (B). Images were assessed qualitatively by fluorescence confocal microscopy (60X objective, 1x Zoom, scale bar 20 μ m).

4.3.6 The overexpression of SYNJ1 in YFP-Parkin HeLa cells causes no change in Parkin translocation

As knockdown of *SYNJ1* results in a Parkin translocation defect it would be plausible that the PD causing variant may also perturb Parkin translocation. To test this hypothesis, SYNJ1-145 (brain specific), SYNJ1-170 (ubiquitous) and SYNJ1-145 R219Q were overexpressed in YFP-Parkin HeLa cells. These three constructs were transfected alongside empty vector, and the cells treated with 10 μ M CCCP for 0 h, 1 h and 2 h. Parkin translocation was examined and scored using the scoring system in **Fig 4.3**. Compared to control (empty vector), the overexpression of both SYNJ1-145 and SYNJ1-R219Q had no influence on Parkin translocation under any of the condition tested (**Fig 4.8**). However, for SYNJ1-170 at both 1h and 2h CCCP treatment the YFP-Parkin appears more cytosolic and less mitochondrial (**Fig 4.8**) suggestive of a delay in Parkin translocation. This effect is greater at 1 h CCCP treatment than at 2 h CCCP treatment suggesting it may cause an early delay. Overall these data suggest that with the brain predominant isoform and the PD mutated form of SYNJ1 there is a limited effect on Parkin translocation when SYNJ1 is overexpressed.



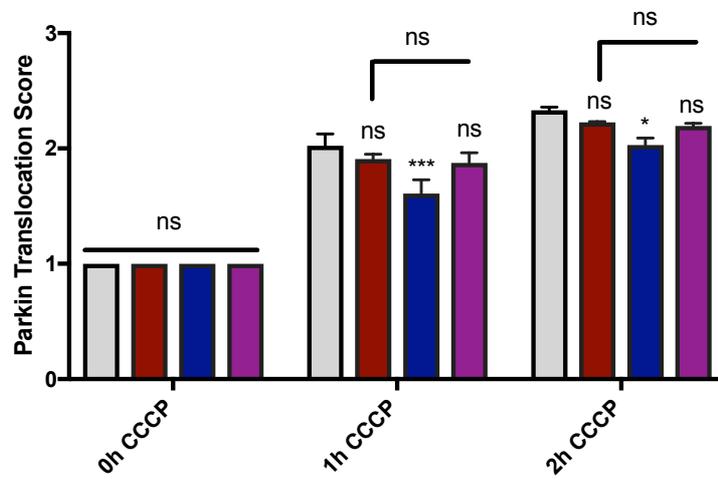
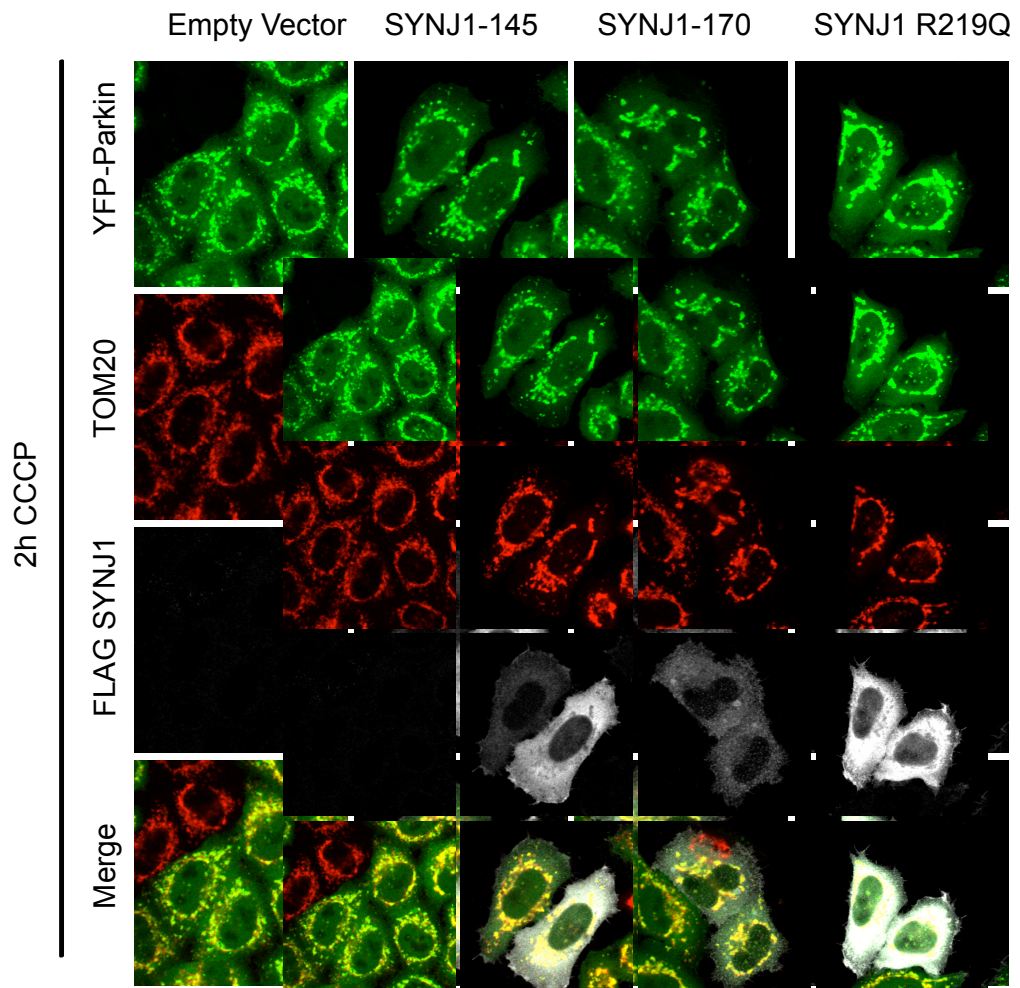


Figure 4.8: The overexpression of SYNJ1 in YFP-Parkin HeLa cells results in no Parkin translocation defect: (A) YFP-Parkin HeLa cells (YFP-Parkin (Green) Mitochondria (TOM20; Red)) were transfected with either Empty Vector, SYNJ1-145, SYNJ1-170 or SYNJ1-145 R219Q before the addition of either 0 h, 1 h or 2 h CCCP (10 μ M). Parkin translocation was assessed qualitatively by fluorescence confocal microscopy (60X objective, 1x Zoom, scale bar 10 μ m) using the scoring system outlined in Figure 4.3. (B) Graphical representation of Parkin translocation quantification following the application of 0 h 1 h and 2 h CCCP. Data represents 3 biological replicates with >20 cells analysed per condition, per replicate. Error bars represent standard error of the mean. ns $P > 0.05$ **** $P < 0.0001$ (one-way ANOVA with Bonferroni post hoc test).

4.3.7 The knockdown of *PI4KB* in YFP-Parkin HeLa cells results in a mitophagy defect.

One of the main functions of the PINK1 and Parkin pathway is to begin the process of mitophagy by signalling to the autophagosome that mitochondria are damaged and need to be degraded. With *SYNJ1* and *PI4KB* silencing, slowing Parkin translocation we next wanted to examine how this defect would translate downstream of PINK1 and Parkin. To do this we examined mitophagy which occurs robustly with 24 h CCCP treatment (Ivatt et al., 2014; Narendra et al., 2008b). We developed a 4-point system, outlined in **Fig 4.9**, to give each cell a mitophagy score, which is averaged for each treatment. A score closer to 1 suggests no mitophagy is happening and a score closer to 4 suggesting a high amount of mitophagy or full mitophagy is occurring (**Fig 4.9**). With no treatment cells had a score of 1 as the mitochondrial network is broad and appears full, with tubular process being seen. Score of 2 shows the beginnings of mitophagy where mitochondria move to peri-nuclear regions. A score of 3 is where those mitochondria have noncable been reduced and only small amount are left. A score of 4 is where all the mitochondria in a cell have been removed by mitophagy and Parkin has become cytosolic. This scoring system allows for analysis of all aspects to mitophagy to see more subtle effects (**Fig 4.9**).

The knockdown of *PI4KB* results in a Parkin translocation defect. To investigate if the Parkin translocation defect translates to a defect downstream effect in the pathway, mitophagy was examined. YFP-Parkin HeLa cells were transfected with Control, PINK1 and *PI4KB* siRNA and then treated with 24 h CCCP treatment and assessed as described above. As expected, robust mitophagy was observed in control cells which was completely abolished in *PINK1* siRNA treated cells (**Fig 4.10**). Interestingly, the knockdown of *PI4KB* results in a significant defect in mitophagy, as at 24 h CCCP treatment the majority of the mitochondria network has been retained and not removed by mitophagy (**Fig 4.10**). This suggests that knocking down *PI4KB* results in a slowing of mitophagy. As *PI4KB* helps to control PI4P levels it suggests that mitophagy may be affected by PI levels.

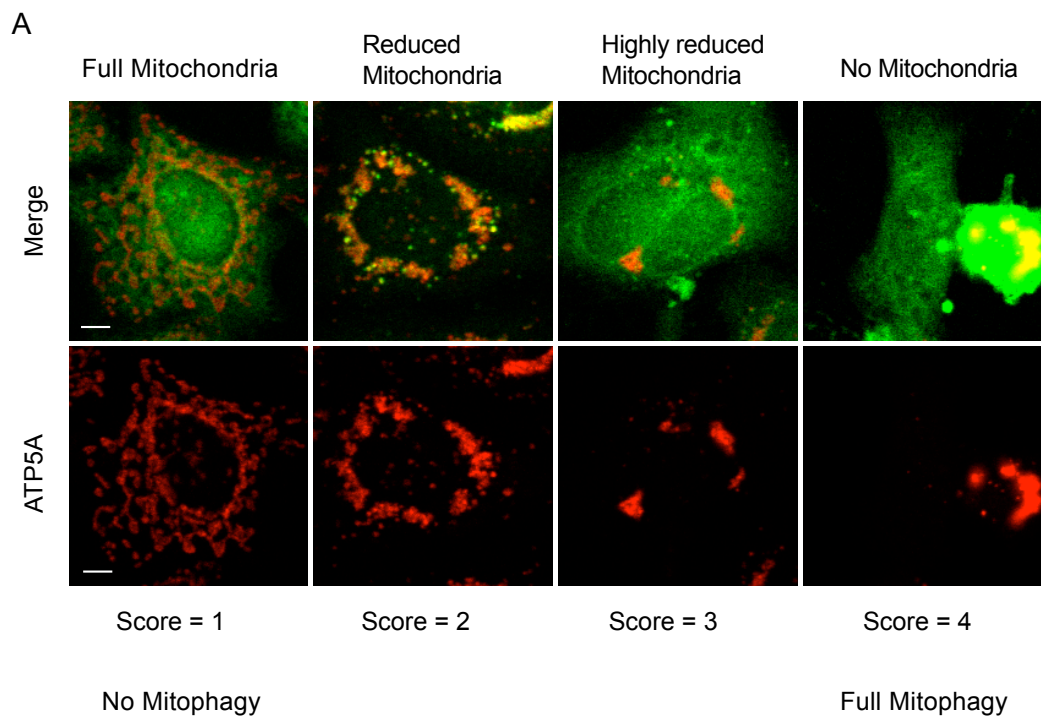


Figure 4.9: The mitophagy scoring system: (A) Examples of the 4 ‘Mitophagy’ phenotypes in YFP-Parkin HeLa cells (YFP-Parkin (Green) Mitochondria (ATP5A;Red). A score of 1 refers to no mitophagy where the mitochondrial forma full network. A score of 2 refers to reduced mitochondria where the mitochondrial network has become perinuclear suggesting mitophagy process is starting. A score of 3 refers to highly reduced mitochondria where the mitochondria which are left are peri-nuclear, but many of them have already undergone mitophagy. A score of 4 refers to no mitochondria where most if not all mitochondria have undergone mitophagy Scale bar 5 μ m

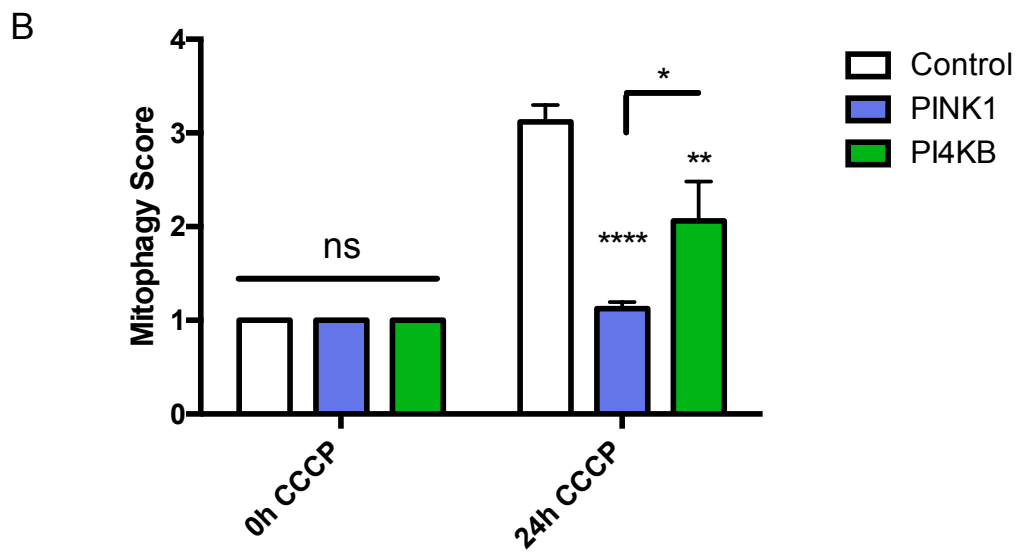
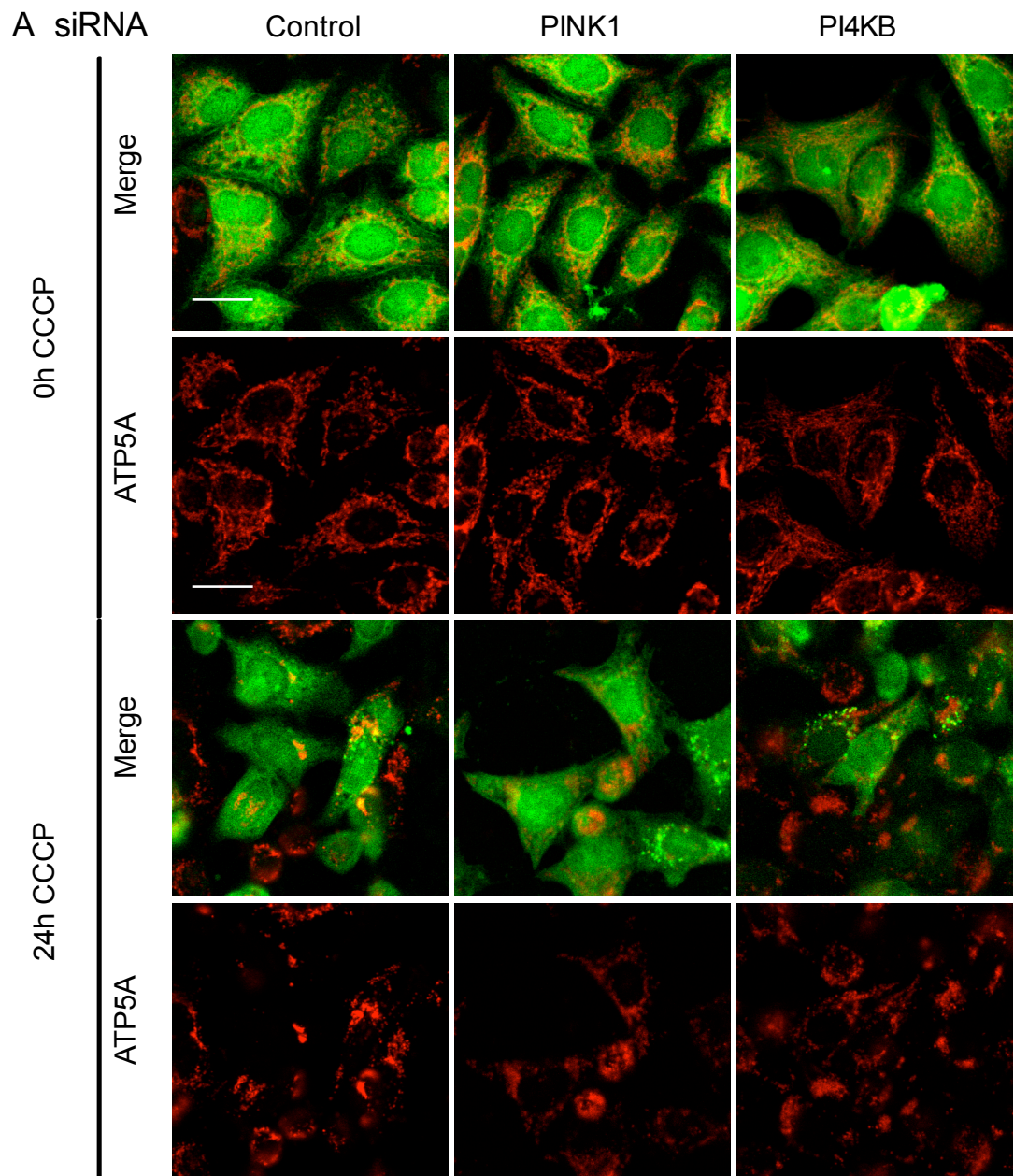


Figure 4.10: The knockdown of *PI4KB* in YFP-Parkin HeLa cells results in slowing of mitophagy: (A) YFP-Parkin HeLa (YFP-Parkin (Green) Mitochondria (ATP5A; Red) were treated with either control, *PINK1* or *PI4KB* siRNA for 4 days before the addition of either 0h CCCP or 24h CCCP (10 μ M). Mitophagy (was assessed qualitatively by fluorescence confocal microscopy (60X objective, 1x Zoom, scale bar 20 μ m) using the scoring system outlined in Figure 4.5. (B) Graphical representation of mitophagy quantification following the application of CCCP is shown in (B). Data represents 3 biological replicates with >100 cells analysed per condition, per assay. Error bars represent standard error of the mean. ns $P > 0.05$ * $P < 0.05$ ** $P < 0.01$ **** $P < 0.0001$ (one-way ANOVA with Bonferroni post hoc test).

4.3.8: The knockdown of *SYNJ* in YFP-Parkin HeLa cells results in a mitophagy defect

The knockdown of *SYNJ1* and the double knockdown of *SYNJ1/2* together results in a defect in Parkin translocation, thus, we next addressed whether these conditions also affected mitophagy. For *SYNJ1* knockdown, mitophagy is significantly decreased compared to the control siRNA (**Fig 4.11**). Interestingly, the knockdown of *SYNJ2* does not appear to have an effect on mitophagy, as most cells have a reduced or no mitochondrial network and the mitophagy score is not significantly different from that with control siRNA (**Fig4.11**). However, when both *SYNJ1* and *SYNJ2* are knocked down in combination, there is a strong mitophagy defect as many cells have retained most of their mitochondrial network. Overall these results implicate a role for *SYNJ1* in mitophagy, mirroring the results seen with Parkin translocation. *SYNJ2* knockdown alone does not result in an effect on mitophagy or Parkin translocation but when *SYNJ1* and *SYNJ2* are knocked down in combination there is a slowing of mitophagy suggesting that *SYNJ1* maybe compensating for *SYNJ2*. This would suggest that *SYNJ1* is the main isoform involved with mitophagy.

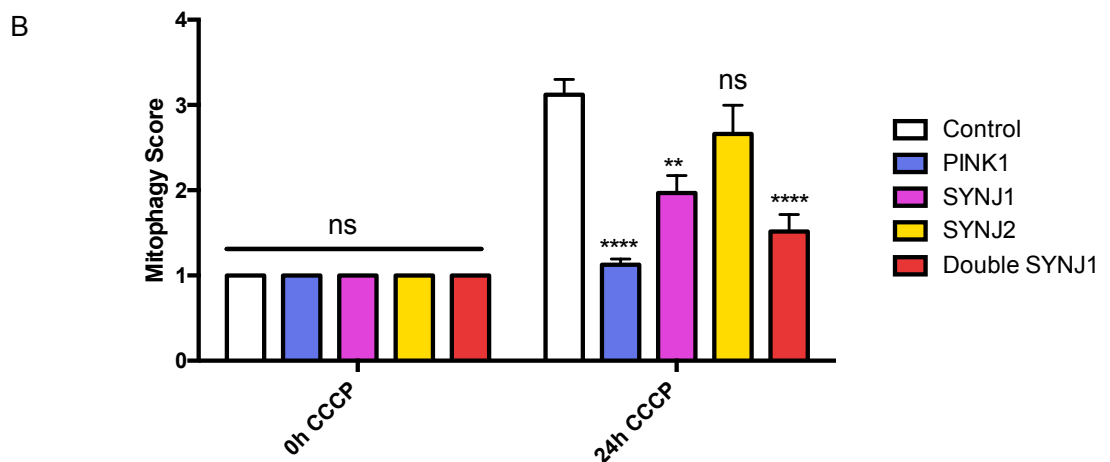
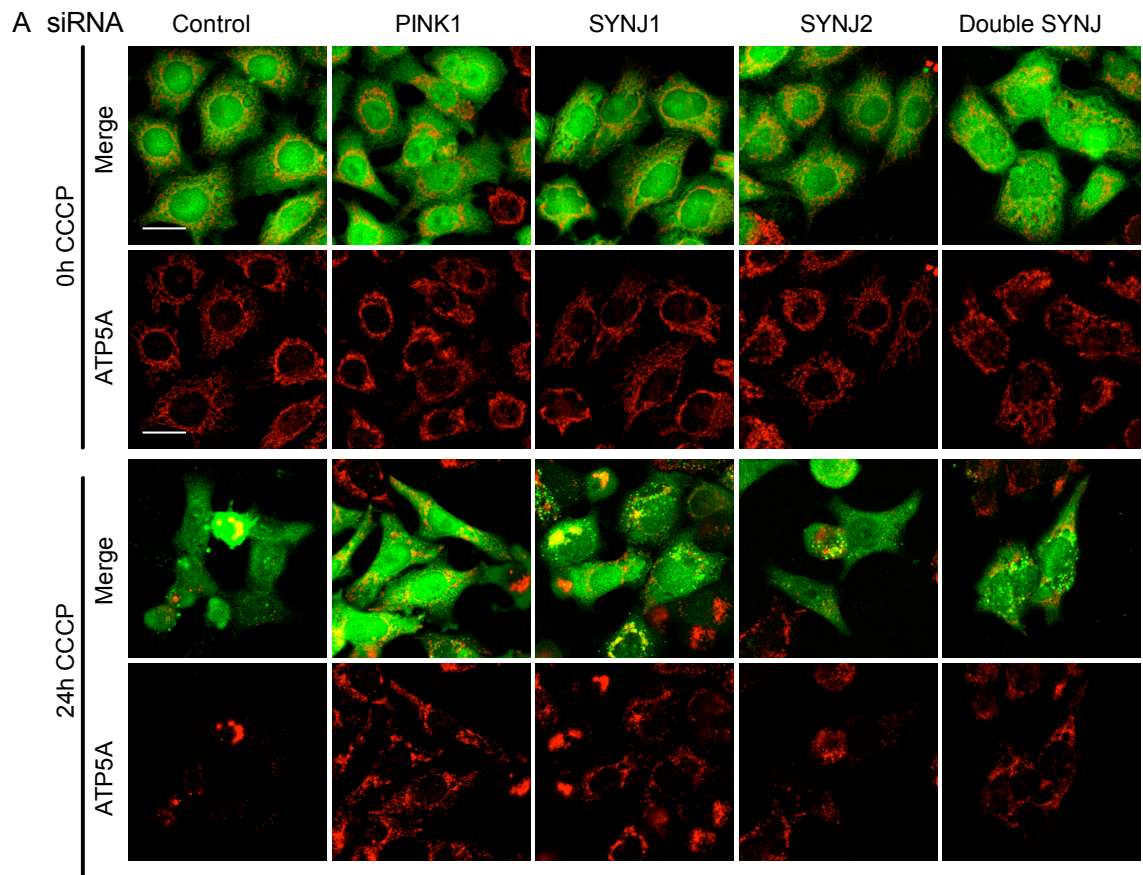


Figure 4.11: The knockdown of *SYNJ* in YFP-Parkin HeLa cells results in slowing of mitophagy: (A) YFP-Parkin HeLa (YFP-Parkin (Green) Mitochondria (ATP5A (Red))) were treated with either control, *PINK1*, *SYNJ1*, *SYNJ2* or both *SYNJ1/2* siRNA for 4 days before the addition of either 0h CCCP or 24 h CCCP (10 μ M). Mitophagy (was assessed qualitatively by fluorescence confocal microscopy (60X objective, 1x Zoom, scale bar 20 μ m) using the scoring system outlined in Figure 4.5. (B) Graphical representation of mitophagy quantification following the application of CCCP is shown in. Data represents 3 biological replicates with >100 cells analysed per condition, per assay. Error bars represent standard

error of the mean. ns $P > 0.05$ ** $P < 0.01$ **** $P < 0.0001$ (one-way ANOVA with Bonferroni's correction).

4.4 Discussion

This chapter outlines the investigation into the influence of *PI4KB* and *SYNJ* on the PINK1/Parkin pathway in a mammalian cell system. This was conducted in YFP-Parkin HeLa cells to further explore the initial findings from a *Drosophila* work, which showed the *pink1* and *parkin* null phenotype can be rescued with overexpression of *fwd*. The use of YFP-Parkin HeLa cells will allow further understanding of molecular basis of any collaboration between PIs and the PINK1/Parkin pathway.

I have assessed the requirements of *PI4KB* and *SYNJ* in different aspects of the PINK1/Parkin pathway, by examining Parkin translocation and the overall reduction in the mitochondrial network (mitophagy). The knockdown of *PI4KB* and *SYNJ1* both resulted in a slowing of Parkin translocation and mitophagy indicating that both *PI4KB* and *SYNJ* are important in regulation of these processes. Exactly how these enzymes are eliciting these effects is not known however, there is evidence that *PI4KB* is present on the OMM (Balla et al., 2000) and that *SYNJ2*, a *SYNJ1* family member, can be recruited to mitochondria (Nemoto and De Camilli, 1999a) suggesting that they may be acting at the mitochondria directly. The presence of these enzymes at the mitochondria may suggest that their substrates and derivatives are also present. There is evidence to support a role for $PI(4,5)P_2$ at the mitochondria, as masking or removing it results in changes in mitochondrial morphology and autophagy (Rosivatz and Woscholski, 2011; Watt et al., 2002). Currently however, there is no direct evidence to suggest that $PI4P$ is present at the mitochondrial membrane but the present of the *PI4KB* and $PI(4,5)P_2$, $PI4P$'s most common phosphorylation derivative, suggests that $PI4P$ may be present in the OMM. In addition, unpublished studies have suggested that $PI4P$ is present at sites of mitochondrial scission linking it to changes in mitochondrial morphology (unpublished data Pogson McBride Lab). Thus, suggesting that manipulation of PIs at the mitochondria can alter mitochondrial function and potentially mitochondria quality control mechanisms.

How $PI4P$ or $PI(4,5)P_2$ may be altering Parkin translocation is not known. Parkin translocation is modulated by a PINK1 mediated phosphorylation cascade with additional translocation factors aiding Parkin translocation, such as Phos-Ubiquitin

(Geisler et al., 2010a; Greene et al., 2012; Kondapalli et al., 2012; Matsuda et al., 2010; Narendra et al., 2010a; Rakovic et al., 2010; Ziviani et al., 2010). One hypothesis is that PI4P and PI(4,5)P₂ can act as Parkin translocation co-factors. Both PI4P and PI(4,5)P₂ can interact with effector proteins through their PH domains and recruit them to different membranes: such as the PI(4,5)P₂ which recruits AP2 to the plasma membrane for clathrin mediated endocytosis (Gaidarov et al., 1996) or the recruitment of a variety of adaptor proteins to the Golgi by PI4P (Tan and Brill, 2014). Parkin however, does not contain a PH domain, suggesting that PI4P or PI(4,5)P₂ cannot directly bind Parkin to aid its recruitment to the mitochondria. Alternatively, other effector proteins of PI4P help maintain Golgi function (Daboussi et al., 2012; Godi et al., 1999; Polevoy et al., 2009; Strahl et al., 2003). PI4P could be conducting a similar role here, recruiting PH domain containing proteins to act as a co-factor for Parkin translocation or to promote its catalytic activity (Matsuda, 2016; Ordureau et al., 2014; Zheng and Hunter, 2013). However, most of the known effector proteins of PI4P or PI(4,5)P₂ are involved with clathrin mediated vesicle sorting at the plasma membrane or lipid metabolism at the Golgi, suggesting a yet unidentified PH containing protein would have to be contributing to Parkin translocation.

Interestingly, the slowing of Parkin translocation is seen predominantly at 2 h CCCP and not at 4 h CCCP treatment, suggesting that the defect occurs earlier in the Parkin translocation pathway but can be resolved. One way in which the initial Parkin translocation reduction could be resolved is via the feed forward mechanisms between PINK1 and Parkin. It has been proposed that Parkin is continuously sampling the mitochondrial surface, and once it finds activated PINK1, it is phosphorylated on S65 leading to ubiquitin chain assembly. PINK1 then promotes phosphorylation of new ubiquitin chains which associate with Parkin and allow retention on the mitochondria. PINK1 and Parkin then work together to promote production of poly-phos-ubiquitin chains and associations with Parkin and aiding Parkin recruitment (Ordureau et al., 2014). This mechanism could be employed by the cell to increase Parkin translocation when there is inefficient recruitment of Parkin to the mitochondria initially.

In combination with the Parkin translocation data, it would suggest that the defect in mitophagy is due to a slowing of Parkin translocation with these previously being shown to be related (Narendra et al., 2010a). However, PIs maybe having effects directly on mitophagy. One of the effector proteins of PI4P is Ceramide transfer

protein (CERT) which is involved with the production of Ceramide, a sterol lipid (Brice et al., 2009; Tan and Brill, 2014). Ceramide is known to influence autophagy (Mayinger, 2009; Scarlatti et al., 2004; Sims et al., 2010) and there is evidence to suggest that ceramide is involved in mitophagy as an adaptor between LC3 and phagophore for PINK1/Parkin independent mitophagy (Sentelle et al., 2013). Together suggesting that management of ceramide can impact on autophagy and mitophagy. As ceramide production is influenced by PI4P and the ability to recruit CERT, a reduction in PI4P, through knockdown of *PI4KB* or *SYNJ*, may impact on its ability to promote ceramide production and thereby eliciting secondary effects on LC3 and phagophore binding, thus decreasing the rate of mitophagy. Interestingly, CERT and LC3B have a similar structure in their lipid binding domains, hence suggesting the potential for LC3 to bind lipids including PI4P (Sentelle et al., 2013). It could be informative to study the binding of PI4P to LC3, since evidence suggests that CERT and LC3 have similar lipid binding domains and that CERT is a well characterised PI4P effector protein.

Of considerable confusion, is the fact that knockdown of *PI4KB* and *SYNJ1* both produce a slowing of Parkin translocation and mitophagy despite their hypothesized 'opposing' function on PI phospho-status; *PI4KB* phosphorylates PI to PI4P while *SYNJ* de-phosphorylates PI4P. However, *SYNJ* as well as containing a Sac1 domain, also contains an Ins-5-phosphatase domain which also de-phosphorylates PI(4,5)P₂. Thus, with silencing of *SYNJ* both phosphatase domain function will be removed, altering the PI balance differently. This has not been assessed within this system and currently, we do not know which phosphatase domain of *SYNJ* is the most active and most likely to have an impact. This may impact on the levels of the other PIs or how the changes in PI derivatives are compensated for by the other proteins kinases or phosphatases. Therefore, I can only conclude that alterations in PI and its derivatives can slow Parkin translocation and mitophagy but how this occurs is not known. The effect on different PIs phospho status would have to be assessed to give more reliable hypothesis to this unexpected result.

At the start of this study, *SYNJ1* was known to be mutated in AR-JP, while *SYNJ2* was known to be recruited to the mitochondria through binding *SYNJ2BP* an OMM protein. This being so, an additional aim of this chapter was to investigate which *SYNJ* family member could be impacting on the PINK1/Parkin pathway. Both were examined for effects on Parkin translocation and mitophagy. The depletion of *SYNJ1* slowed Parkin translocation and mitophagy, but silencing of *SYNJ2* did not.

However, when SYNJ1 and SYNJ2 were silenced in conjunction, a greater reduction in Parkin translocation was seen than when SYNJ1 was depleted alone. This indicates that SYNJ1 is the predominant SYNJ family member affecting Parkin translocation and mitophagy but also suggests that SYNJ1 can compensate for SYNJ2. In support of this further slowing of Parkin translocation and mitophagy were seen when both SYNJ1 and SYNJ2 were silenced in conjunction. As SYNJ1 is cytosolic and not known to be targeted to the OMM, other proteins or lipids may direct its localisation. For example SYNJ2 which is directed to the mitochondria via binding of SYNJ2BP (Nemoto and De Camilli, 1999b) or PI(4,5)P₂ which can recruit SYNJ1 to vesicles during the clathrin mediated endocytosis process. PI(4,5)P₂ is present at the mitochondria and may be able to recruit SYNJ1 to the mitochondria (Watt et al., 2002). However no studies have suggested that SYNJ1 is localised at the mitochondria. Alternatively, Parkin binds endothelin-A, a common SYNJ1 binding protein which is involved with recruitment of SYN, to PI(4,5)P₂ on clathrin coated vesicles and synaptic transmission, (Song and Zinsmaier, 2003; Trempe et al., 2009b) thus linking SYNJ1 and Parkin together in the cytosol. This may suggest that SYNJ1 can affect parkin translocation without being present at the mitochondria.

Further work

To further interpret these results, it would be valuable to verify that expression of PI4KB or SYNJ1 construct that are insensitive to siRNA can rescue the Parkin translocation and mitophagy defect, thus determining that the effects are due to the reduction in those specific mRNA's rather than any off-target effects of the siRNA. In addition to this, while I have shown that dominant expression of SYNJ1 R219Q does not adversely affect Parkin translocation, it would be interesting to examine whether re-expression of the pathogenic SYNJ1 mutations rescue these defects upon loss of *SYNJ1*. This would help understand if the Parkin translocation defect maybe contributing to the progression of PD.

Currently, these results have shown that PI metabolism is important in Parkin translocation and mitophagy. However, it is not known which PI derivative, PI4P or PI(4,5)P₂, is required. To understand this further, a combination of the two methods may be employed. First, other phosphatases such as Sac1 or OCRL can be knocked down and Parkin translocation or mitophagy examined. These enzymes only act to dephosphorylate PI4P to PI to PI(4,5)P₂ to PI4P, respectively meaning a clearer result can be gained without the added complication of a dual phosphatase domain like in synaptojanin. Second, the PH domain of FFAT, a PI4P interacting

protein, and PH domain of PLC δ 1, a PI(4,5)P₂ specific binding protein can be targeted to the mitochondria to mask PI4P and PI(4,5)P₂ individually or in combination. Parkin translocation, mitochondrial morphology and mitophagy can then be examined.

With regards to the impact of PI4P in the recruitment of the phagophore, it would be interestingly to look to see if there is a direct interaction between PI4P and LC3, and whether disruption of this interaction has effects on mitophagy or phagophore recruitment directly. Phagophore recruitment can be visualised or assed using EM.

In this chapter I have determined that the regulation of PI phosphorylation derivatives can impact on Parkin translocation and mitophagy, therefore suggesting a link to mitochondrial quality control. Furthermore, these data suggest that SYNJ1 is the more predominant isoform to be involved with Parkin translocation and mitophagy which links to mutation in SYNJ1 causing PD. The mechanisms behind this has not been investigated fully but it does highlight a different avenue to investigate with regards to the mechanisms of which SYNJ1 can result in PD.

5.VISUALISATION OF ER-MITOCHONDRIA CONTACT SITES

5.1 Background

ER-mitochondria contact sites have emerged as important signalling hubs that link a number of processes including lipid metabolism, Ca^{2+} handling, autophagosome formation, and mitochondrial morphology. Furthermore, evidence, including from our group, implicates ER-mitochondria contacts in mitochondrial quality control pathways (Friedman et al., 2011; Lee and Voeltz, 2015; Stoica et al., 2014; De Vos et al., 2012). Moreover, both PINK1 and Parkin were shown to localise to ER-mitochondrial contact sites. The levels of PINK1 in at ER-mitochondria contacts increased after induction of mitophagy using the mitochondrial uncoupler CCCP (Gelmetti et al., 2017) while overexpression of Parkin caused enhanced calcium signalling and ATP production which correlated with an increase in ER-Mitochondria contact sites (Cali et al., 2013). The ER has also been shown to wrap around the mitochondria, constrict it and facilitate Drp1 mediated fission causing changes in mitochondrial morphology.(Friedman et al., 2011; Lee and Voeltz, 2015). Together with my data showing that *PI4KB* loss can result in slowing of Parking translocation and mitophagy, and that overexpression of *fwd*, the *Drosophila* homologue of *PI4KB*, can partially rescue the *pink1^{B9}* and *park²⁵* climbing defects suggests a possible role for PI4P at ER-mitochondria sites with possible functions in mitochondrial quality control.

As previously described ER-mitochondria contact sites range from 10 to 30 nm in size, which is beyond the refractive index of light and hence cannot be resolved by conventional and even super-resolution light microscopy. Currently, the gold standard to view ER-mitochondrial contact sites is through electron microscopy (EM). EM requires fixation and to be conducted in a vacuum, meaning that highly dynamic processes such as mitochondrial quality control cannot be investigated in real time.

5.2 Hypothesis and Aims

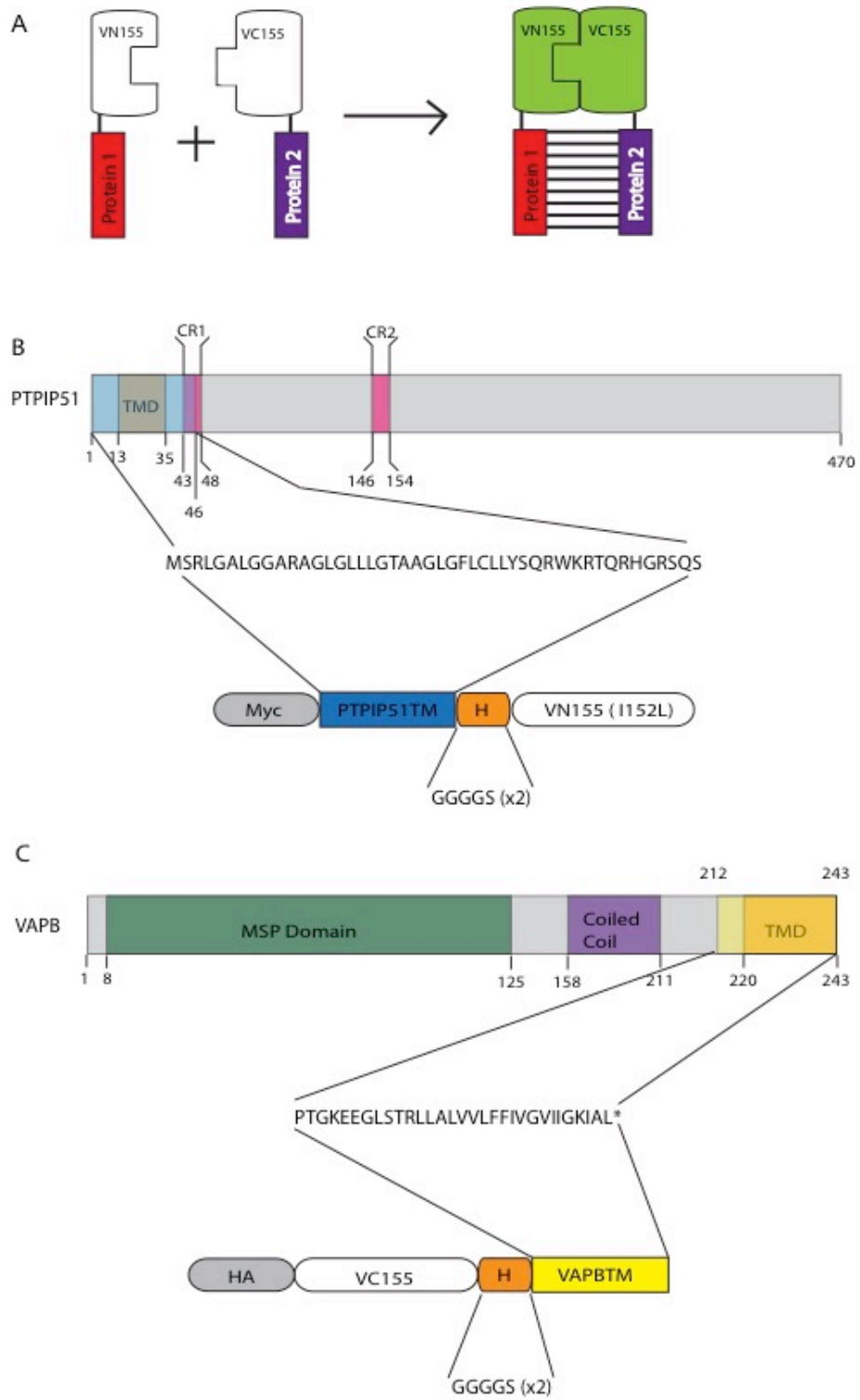
ER-Mitochondrial contact sites have been highlight to be perturbed in various neurodegenerative diseases including PD. The limitations of light microscopy and EM makes it hard to visualise these contacts during dynamic process such as mitochondrial quality control. The aim of this section of my project was to design and test novel fluorescent reporters of ER-mitochondria contact sites which can be used to visualise ER-mitochondria contacts in real time in living cells. I investigated two approaches, the first based on biomolecular fluorescence complementation (BiFC) and the second using dimerization-dependent GFP (ddGFP).

5.3 Two novel systems to visualise ER-Mitochondrial contact sites

5.3.1: A new system for looking at ER-mitochondria contact sites: Bimolecular Fluorescence Complementation (BiFC)

In a first approach to develop a real time fluorescent reporter of ER-mitochondria contact sites the BiFC system was used as basis. The BiFC assay is typically used to study protein-protein interactions and is based on the observation that N-Terminal and C-Terminal fragments of fluorescent proteins such as EGFP and mVenus, a YFP variant, can refold into a functional fluorescent protein as they come in close proximity. Separately, these fragments do not produce any fluorescence. However, when fused to two interacting proteins the fragments of fluorescent proteins can refold and produce fluorescence. This can be detected using fluorescence microscopy and is a measure of protein-protein interactions (Fig 5.1A) (Wong and O'Bryan, 2011). This method has successfully been used to investigate protein-protein interactions in both fixed and living cells (Hu et al., 2002; Shyu et al., 2006).

Here, the BiFC system was adapted to investigate ER-mitochondrial contact sites by fusing the N-Terminus (VN155) or C-terminus (VC155) of mVenus to the organelle targeting sequences of the OMM protein PTPIP51 and ER protein VAPB which we have identified as a bona-fide ER-mitochondria tether previously (Stoica et al., 2014; De Vos et al., 2012) (Fig 5.1B and C). It was hypothesised that when the ER and mitochondria are in close proximity at ER-mitochondria contact sites the VN155 and VC155 fragments would be able to refold and produce fluorescence denoting ER-mitochondria contact (Fig 5.1D). The mVenus variant was chosen as it contained a mutation (I152L) that had been shown to reduce nonspecific binding and enhance the signal to noise ratio (Kodama and Hu, 2010). A short hinge region, composed of amino acids Gly and Ser (GGGGS (2x)) was added between the organelle targeting regions of PTPIP51 (PTPIP51TM) and VAPB (VAPBTM) and the VC155 and VN155 fragments to facilitate VC155/VN155 complementation (Fig 5.1). The small size and lack of branched side chains of Gly and Ser provides flexibility and increases the dynamics protein fusions (Argos, 1990; Chen et al., 2013). The GGGGS hinge region has also been shown to increase the expression of fusion proteins (Trinh et al., 2004). Lastly, Myc and HA tags were added to the PTPIP51 and VAPB-based constructs, respectively, to allow easy verification of their expression levels and localisation (Fig 5.1).



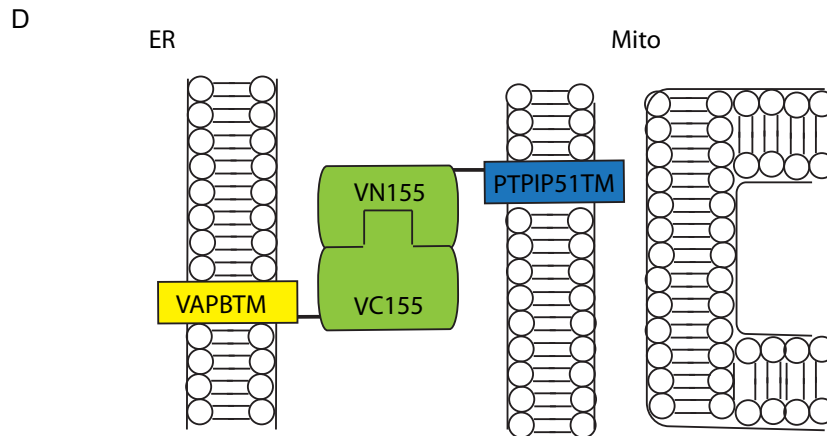


Figure 5.1: The BiFC system: (A) Schematic representation of the how the BiFC system works. (B) Schematic representation of PTPIP51 showing the conserved regions, CR1 and CR2 (pink) and the transmembrane domain (TMD). The fragment used in the BiFC ER-mitochondria reporter is indicated (blue). The amino acids sequence of both the organelle targeting PTIP51 fragment and hinge region is shown. The structure of the PTPIP51-VN155 BiFC constructs including the amino acid sequence, position of the Myc tag and hinge region is also shown. (C) Schematic representation of VAPB showing the MSP domain (green), coiled coil domain (purple) and the transmembrane domain (orange). The fragment used in the BiFC ER-mitochondria reporter is indicated (yellow). The amino acids sequence of both the organelle targeting VAPB fragment and hinge region is shown. The structure of VC155-VAPBTM BiFC constructs including the amino acid sequence and the positions of the HA tag and hinge region is also show. (D) Schematic representation of the hypothesised orientation and interaction of the PTPIP51 and VAPB BiFC constructs in ER-mitochondria contacts. When in the correct orientation, the two mVenus fragments complement and refold into full length fluorescent mVenus.

5.3.1.1: The BiFC constructs express in HeLa cells

First the expression and localisation of the VAPB and PTPIP51 BiFC constructs were examined. HeLa cells were transfected with Myc-VN155, HA-VC155, HA-VC155-VAPBTM, Myc-PTPIP51TM-VN155 or Myc-PTPIP51FL-VN155 and samples harvested for western blot analysis. The predicted molecular weights of these probes are outlined in Table 5.1. The results show that all constructs run at their predicted molecular weights (Fig 5.2).

To examine if the PTPIP51-based BiFC probes localised to mitochondria as predicted HeLa cells were transfected with Myc-VN155, Myc-PTPIP51TM-VN155 or, as positive control, HA-PTPIP51. AcGFP1-Mito was co-transfected to visualise mitochondria. The samples were fixed and stained using anti-Myc antibodies and the localisation of the transfected proteins was examined by confocal microscopy. As expected the OMM protein HA-PTPIP51 co-localised with AcGFP1-Mito (Fig 5.3). Myc-PTPIP51TM-VN155 co-localized with AcGFP1-Mito in a similar fashion to HA-PTPIP51 (Fig 5.3). This was due to the addition PTPIP51TM to VN155 because Myc-VN155 without targeting sequences (TMD) appeared cytosolic throughout the cell and did not co-localise with AcGFP1-Mito.

A similar approach was used to investigate if the TMD of VAPB was sufficient to promote localisation of VC155 to the ER. HeLa cells were transfected with HA-VC155, HA-VC155-VAPBTM or Myc-VAPB and stained with antibodies to calreticulin to visualise the ER (Michalak et al., 1999). As expected, Myc-VAPB co-localised with calreticulin in the typical web like ER network (Fig 5.4). Similarly, HA-VC155-VAPBTM co-localised with calreticulin indicating that the VAPBTM region efficiently targeted VC155 to the ER (Fig 5.4). Indeed, HA-VC155 was found in a cytosolic and diffuse localisation throughout the cell with no distinguishable localisation or co-localisation with calreticulin (Fig 5.4).

Together, these data show that the addition of the organelle targeting region of PTPIP51 efficiently targeted Myc-VN155 to the OMM whereas the organelle targeting region VAPB directed HA-VC155 to the ER, optimally situating them for their interactions in ER-mitochondria contact sites.

Table 5.1: The molecular weights of the BiFC constructs: A table to show the calculated molecule weights of the individual BiFC fragments with and without PTPIP51FL, PTPIP51TM or VAPBTM.

CONSTRUCT	Predicted molecular weight
HA – VC155	14 kDa
HA – VC155 – VAPBTM	18 kDa
Myc – VN155	21 kDa
Myc – VN155 – PTPIP51TM	26 kDa

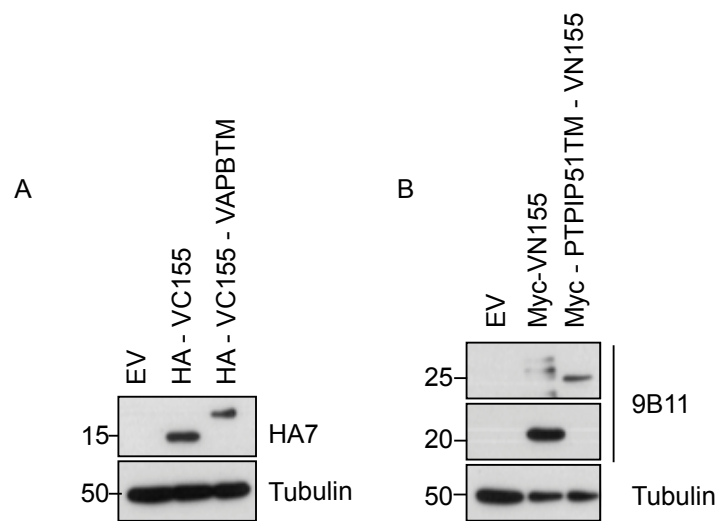


Figure 5.2: The BiFC constructs express in HeLa cells: (A) HeLa cells were transfected with HA-VC155 or HA-VC155-VAPBTM. Expression was analysed by western blot using anti-HA7 and anti-Tubulin to verify equal loading. (B) HeLa cells were transfected with Myc-VN155 or Myc-VN155-PTPIP51TM. Protein expression was analysed by western blot using anti-Myc (9B11). α -Tubulin was used as loading control.

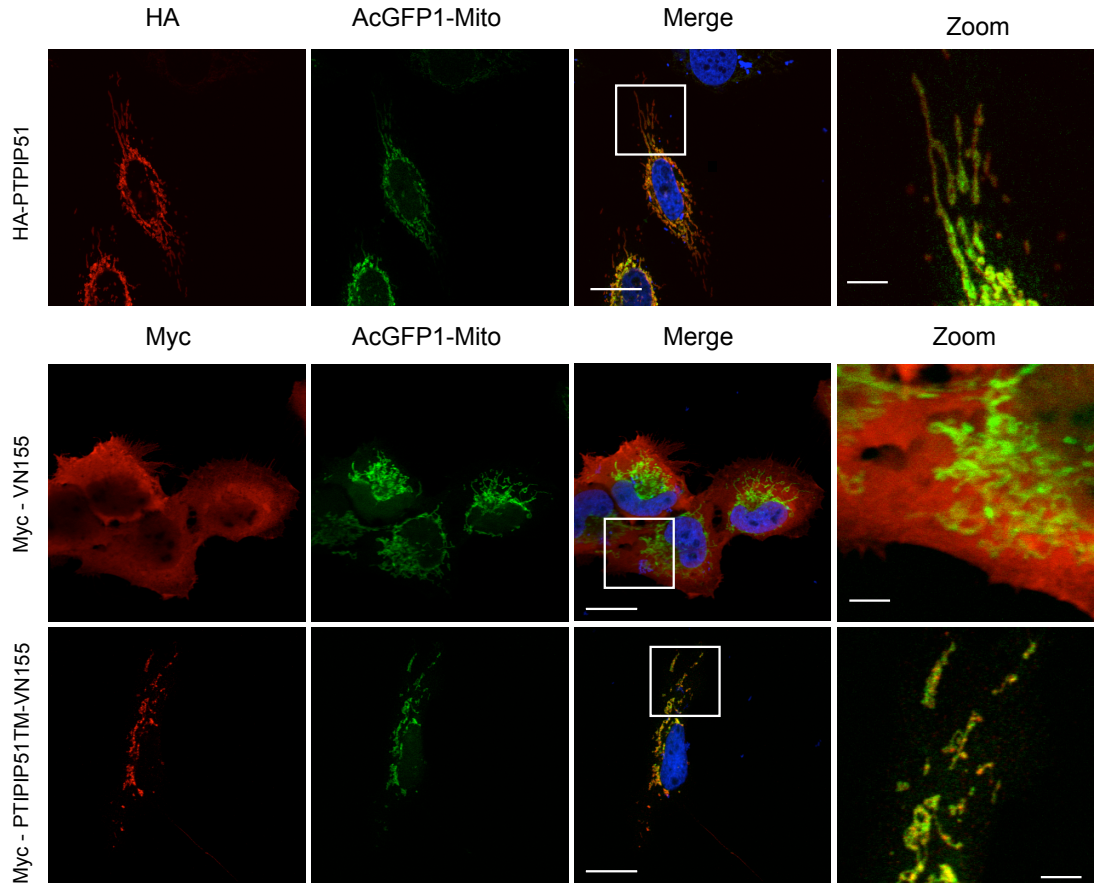


Figure 5.3: Myc-PTPIP51TM-VN155 localises to mitochondria: HeLa cells were transfected with HA-PTPIP51, Myc-VN155 or Myc-PTPIP51TM-VN155 (Red) alongside a mitochondrial marker, AcGFP1-Mito (Green) to examine localisation. Representative images show co-localisation of HA-PTPIP51, or Myc-PTPIP51TM-VN155 with AcGFP1-Mito. Myc-VN155 was localised to the cytosol. Scale Bar, 20 μ m and 5 μ m (zoom).

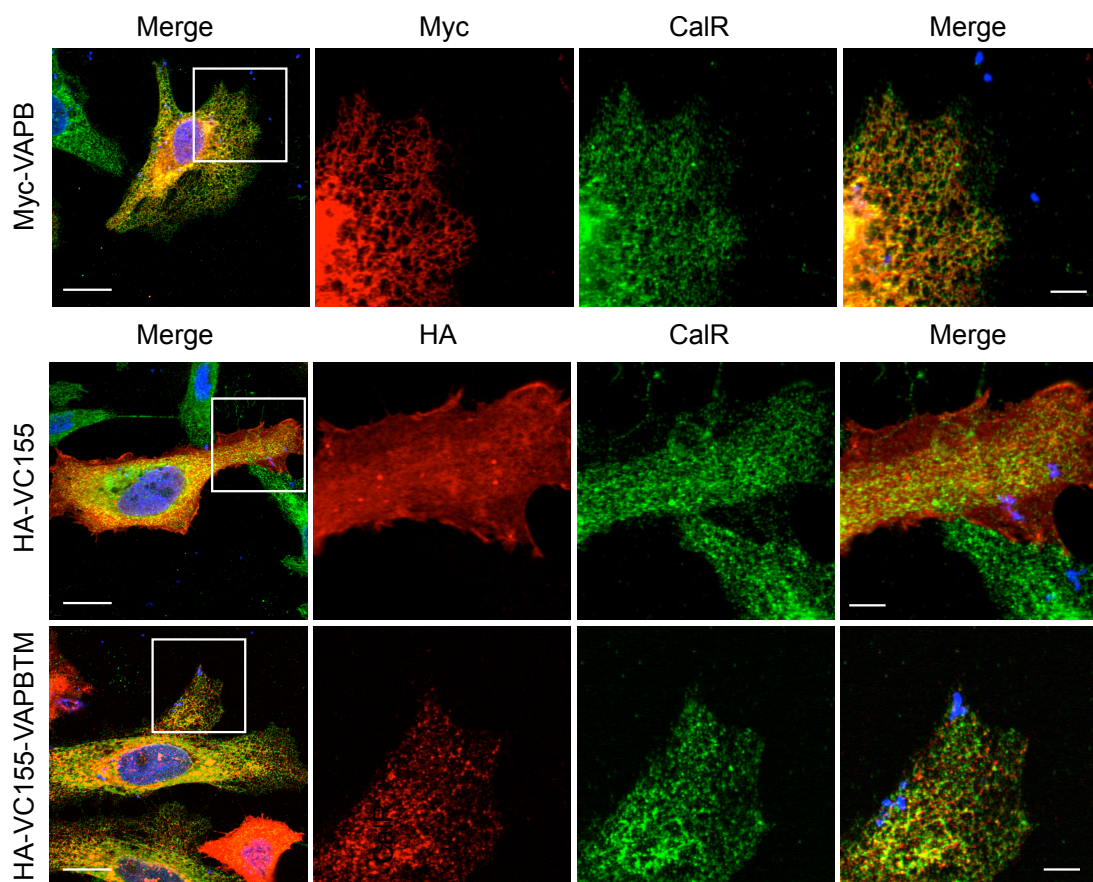
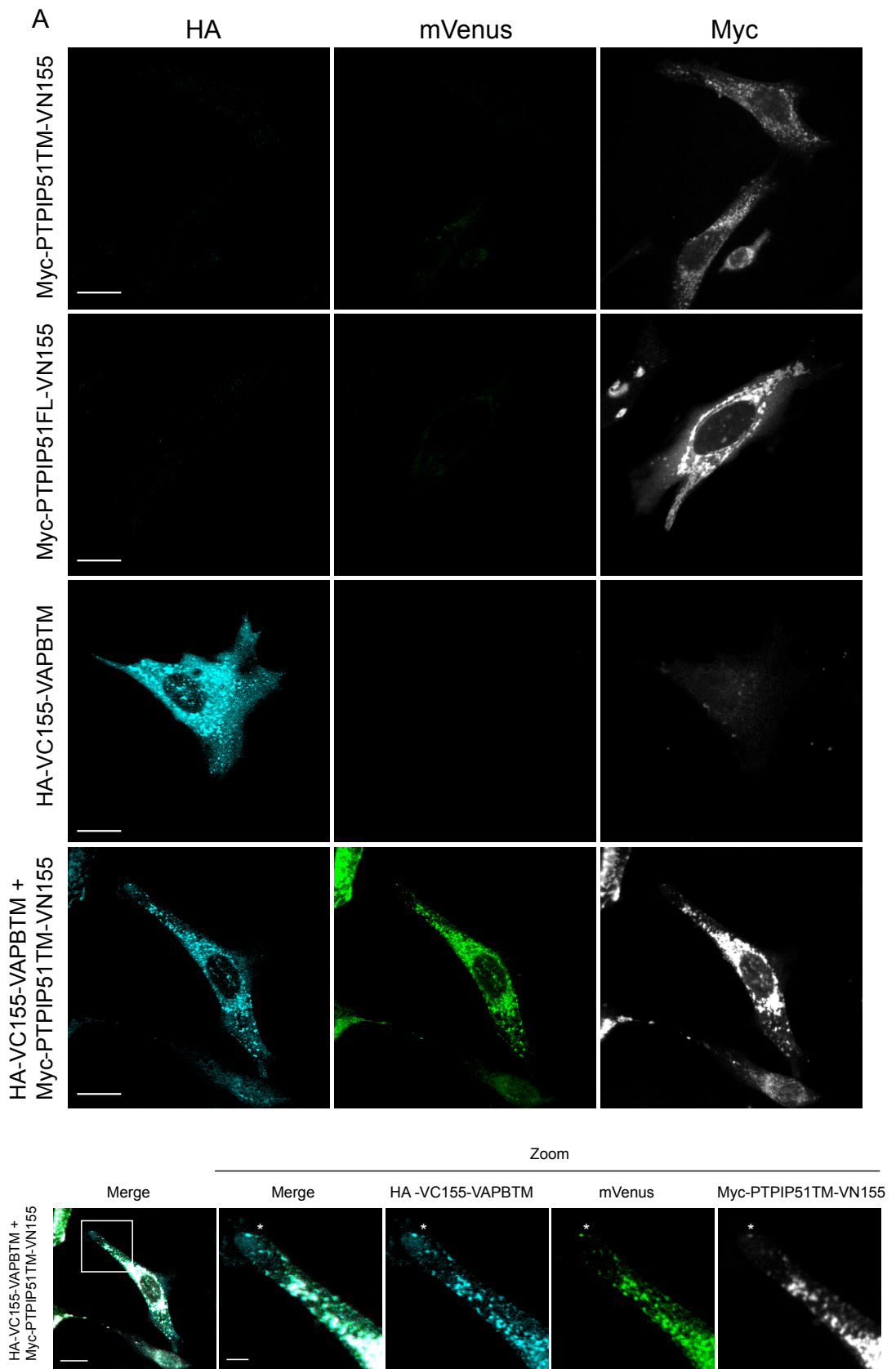


Figure 5.4: VC155-VAPBTM localises to the ER: HeLa cells transfected with Myc-VAPB, HA-VC155 or HA-VC155-VAPBTM (Red) were stained for endogenous calreticulin (CalR; Green) to visualise the ER. Representative images show co-localisation of Myc-VAPB and HA-VC155-VAPBTM (Red) with calreticulin. HA-VC155 was localised to the cytosol. Scale Bar, 20 μm and 5 μm (zoom).

5.3.1.2: Co-expression of VC155-VAPBTM with PTPIP51TM-VN155 produces mVenus fluorescence at ER-mitochondria contacts.

Having established that Myc-PTPIP51TM and HA-VC155-VAPBTM localised robustly to the mitochondria and ER, respectively, we next set out to investigate if the constructs were functional as ER-mitochondria contact reporters. HA-VC155-VAPBTM, Myc-PTPIP51TM-VN155, Myc-PTPIP51^{FL}-VN155 were expressed alone and in combination in HeLa cells and the cells analysed for mVenus fluorescence. The mVenus fluorescence was imaged using confocal microscopy of fixed samples and analysed by measuring the overall intensity of all the mVenus fluorescence in a cell and then normalising this value to the area of the cell to generate the (mean gray value). To verify expression of the transfected constructs the samples were stained using anti-HA and anti-Myc antibodies.

When expressed alone the localisation of Myc-PTPIP51TM-VN155 and Myc-PTPIP51^{FL}-VN155 appeared mitochondrial while HA-VC155-VAPBTM localised to the ER (**Fig 5.5A**). As expected, minimal mVenus fluorescence was detected in these samples (**Fig 5.5A and C**). In cells co-transfected with Myc-PTPIP51TM-VN155 and HA-VC155-VAPBTM, mVenus fluorescence was readily detected and appeared mitochondrial in localisation, consistent with localisation to ER-mitochondria contacts. In co expressing cells, the localization of the individual PTPIP51-based probes remained mitochondrial and puncta of mVenus fluorescence co-localised with HA-VC155-VAPBTM positive puncta (**Fig 5.5B**). Analysis of the mVenus fluorescence intensity confirmed a significant increase in fluorescence when HA-VC155-VAPBTM was co-expressed with Myc-PTPIP51TM-VN155 compared to the corresponding control conditions (**Fig 5.5A and C**). These data suggest that the BiFC probes are able to complement, fold and produce mVenus fluorescence at ER-mitochondria contact sites.



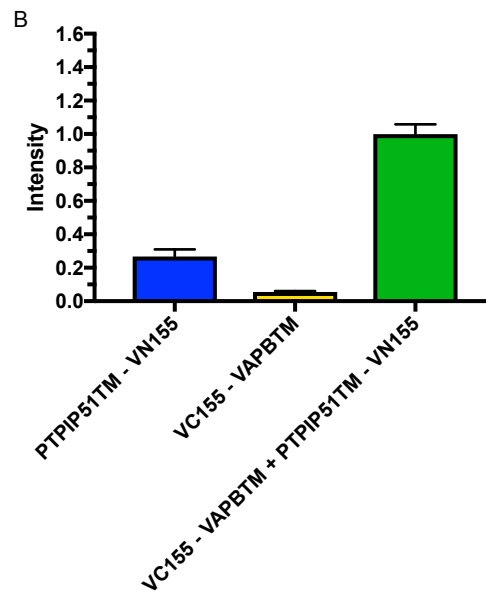


Figure 5.5: The HA-VC155-VAPBTM and Myc-VN155-PTPIP51TM probes are functional in HeLa cells: (A) HeLa cells transfected with HA-VC155-VAPBTM (Cyan) and Myc-PTPIP51TM-VN155 (Gray) were examined for mVenus fluorescence (Green, middle panel) Scale bar 20 μm , 5 μm (Zoom). (B) mVenus fluorescence was quantified per cell by taking the mean gray value, and then normalised to the VAPBTM + PTPIP51TM condition. Data represents 1 biological replicate with 30-50 cells per experimental condition and 10-20 cells per control condition. Error bars represent standard error of the mean. ns $P > 0.05$ **** $P < 0.0001$ (one-way ANOVA with Bonferroni post hoc test).

5.3.1.3: The BiFC system reports on an increase in ER-Mitochondrial contact sites.

Co-expression of PTPIP51TM-VN155 and VC155-VAPBTM results in mVenus fluorescence which appears mitochondrial, thus suggesting that under steady state conditions the BiFC probes can come together in areas of ER-mitochondrial contact. We next wanted to address the question of whether if the BiFC probes could detect changes in the level of ER-mitochondria contact. We first examined if the BiFC system could report on an increase in ER-Mitochondria contact sites using 3 different techniques that have been shown to increase ER-mitochondria contact previously. First, the mAKAP1 [34–63]-mRFP-yUBC6 synthetic ER-mitochondria tether (OMM-ER Linker) was used. In the OMM-ER Linker RFP is targeted to the OMM using the the N-terminal OMM targeting sequence of mAKAP1 an OMM residing protein, and to the ER membrane using the C-terminal ER localisation sequence of yUBC6. Accordingly the OMM-ER linker connects ER to mitochondria and causes an artificial increase in ER-Mitochondria contact sites (Csordás et al., 2006). Second, the overexpression of PTPIP51 results in an increase in ER-Mitochondrial contact sites and therefore was used as an alternative to the OMM-ER linker (Stoica et al., 2014). Finally, it has been shown that an increase in ER stress, through Thapsigargin or Tunicamycin treatment, can increase ER-mitochondria contact sites (Bravo et al., 2011).

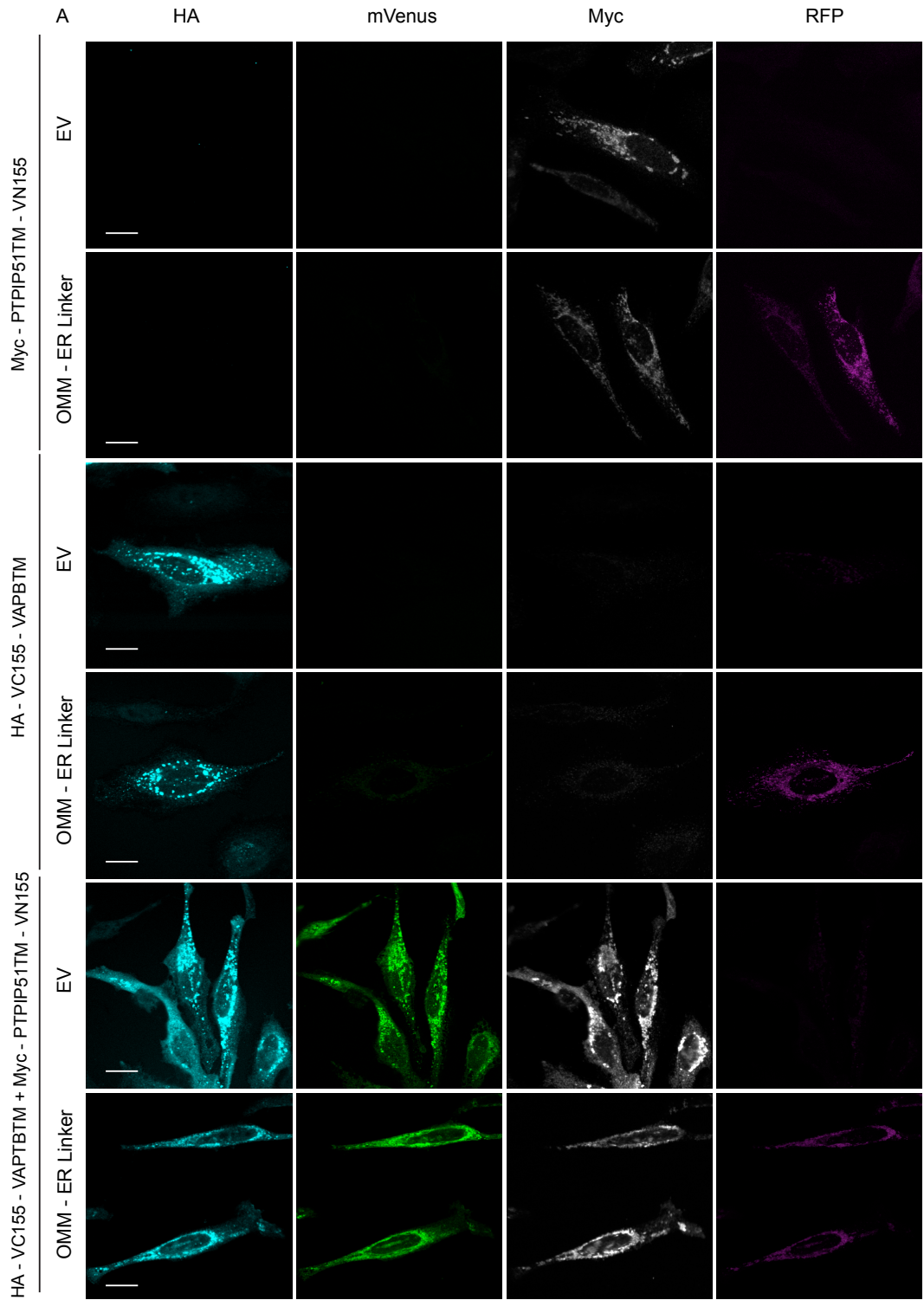
Myc-PTPIP51TM-VN155 and HA-VC155-VAPBTM were expressed alone and in combination with either the addition of the OMM-ER linker or HA-PTPIP51 and treatment of Tunicamycin (4 µg/ml) or Thapsigargin (0.5 or 1 µM). An increase in ER stress was determined using western blotting and detection of an increase in the ER stress marker BIP (Kozutsumi et al., 1988). Under both Thapsigargin treatments there was an increase in BIP expression compared to the non-treated control, suggesting an increase ER stress and contact sites (**Fig 5.8C**). The mVenus fluorescence was examined under these 3 sets of conditions using confocal microscopy and analysed by recording the mean gray value as a measure of intensity.

As expected, expression of HA-VC155-VAPBTM or Myc-PTPIP51TM-VN155 alone did not produce mVenus fluorescence, which is reflected in the numerical analysis (**Fig 5.6A and B, Fig 5.7A and B**). Co-transfection of HA-VC155-VAPBTM and Myc-PTPIP51TM-VN155 produced mVenus fluorescence which appeared to localise to the mitochondria (**Fig 5.7B and Fib 5.8B**). There appears to be minimal difference between those transfected with EV and those cells transfected with

OMM-ER linker. The mitochondrial morphology in OMM-ER transfected cells does not appear to change from the clumped phenotype, that is originally seen when the constructs are co-expressed (**Fig 5.6A**). Similarly, the expression of HA-PTPIP51 or induction of ER stress does not appear to significantly change the localisation of mVenus fluoresce or mitochondrial morphology compared to the transfected or untreated control (**Fig 5.6, 5.7 and 5.8**). Of note, is the examination of cells which are stained with endogenous PTPIP51 antibody, which show a large expanse of mitochondrial network, whole those that do show mVenus fluorescence suggesting that both constructs are present have a more clumped mitochondrial network (**Fig 5.7B**).

Unexpectedly, increasing ER-mitochondria contacts using the OMM-ER linker or HA-PTPIP51 did not increase mVenus fluorescence (**Fig5.6A and B**). To the contrary, there was a significant decrease in mVenus fluorescence in cells expressing the OMM-ER linker (**Fig5.6A and B**). In contrast, induction of ER stress caused an increase in mVenus fluorescence that correlated with the level of ER stress (**Fig 5.8A, B and C**). Possibly overexpression of OMM-ER linker of HA-PTPIP51 tightens the connections between ER and mitochondria to such an extent that the complementation of the BiFC probes is sterically hindered. Alternatively, BiFC complementation was saturated under these conditions.

Collectively, these data suggest that an increase in ER-mitochondria contact sites can be detected using the BiFC system.



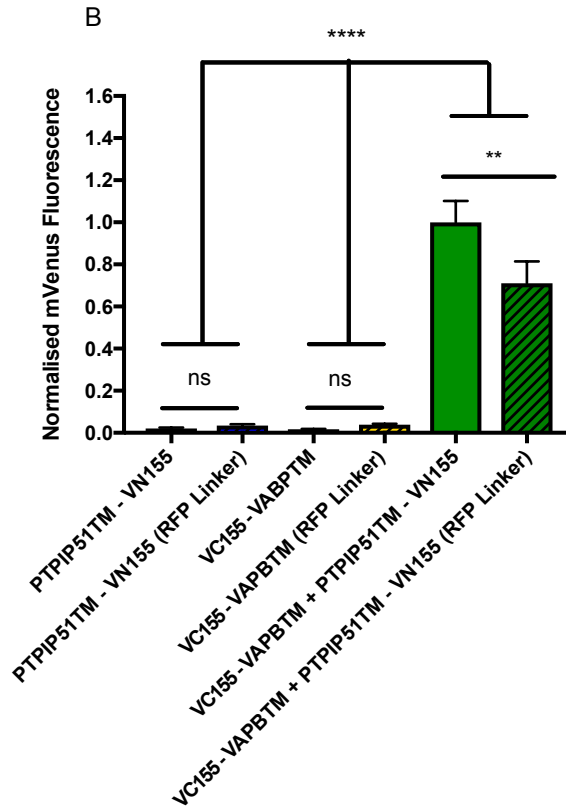
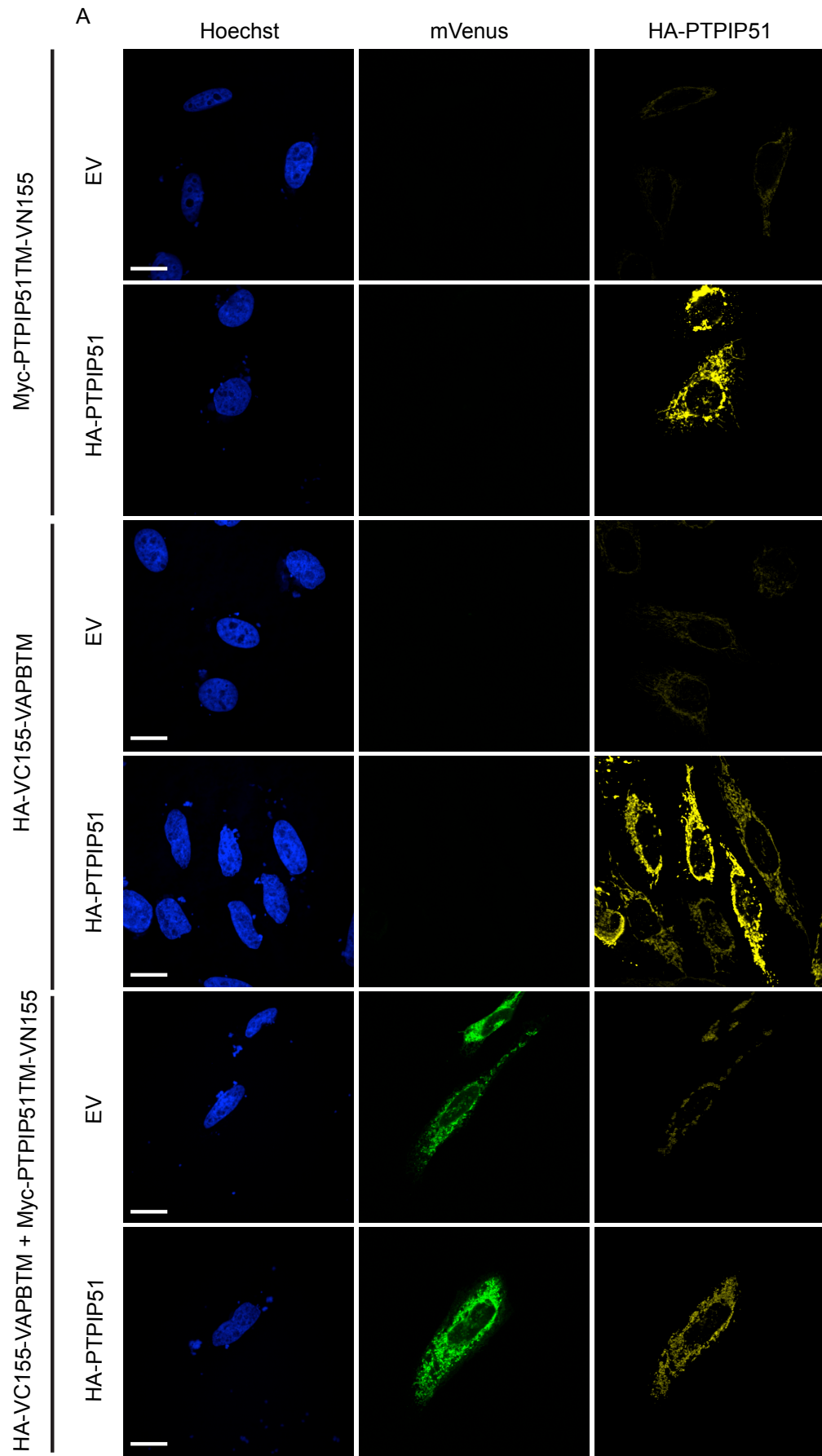


Figure 5.6: Increasing ER-mitochondria contacts using an OMM-ER linker does not increase in BiFC mVenus fluorescence: (A) HeLa cells transfected with HA-VC155-VAPBTM (Cyan), Myc-PTPIP51TM-VN155 (Gray) either alone or in combination were examined for mVenus fluorescence (Green, middle panel) with and without co-expression of the OMM-ER linker (Magenta). Scale bar, 20 μ m. (B) mVenus fluorescence was quantified per cell as the mean gray value, which was normalised to the VC155-VAPBTM + PTPIP51TM-VN155 condition to allow combination of different data sets. Data represents 2 biological replicates with 30-50 cells per experimental condition and 10-20 cells per control condition. Error bars represent standard error of the mean. ns $P > 0.05$ **** $P < 0.0001$ ** < 0.001 (one-way ANOVA with Bonferroni post hoc test),



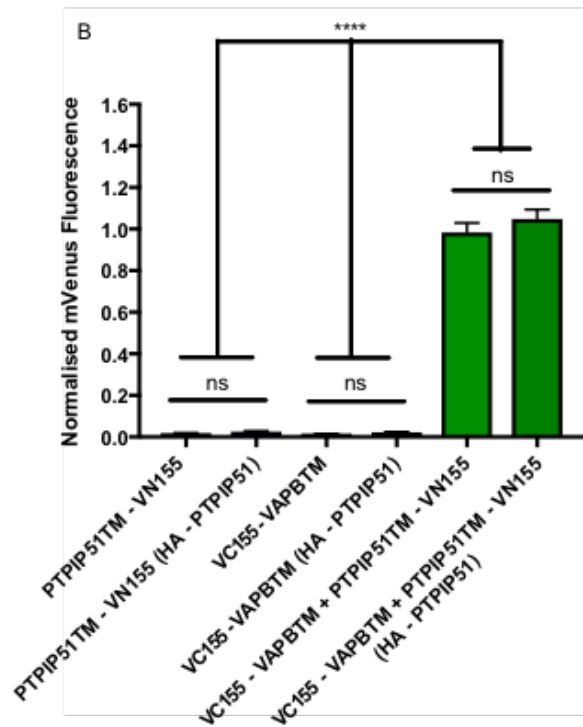
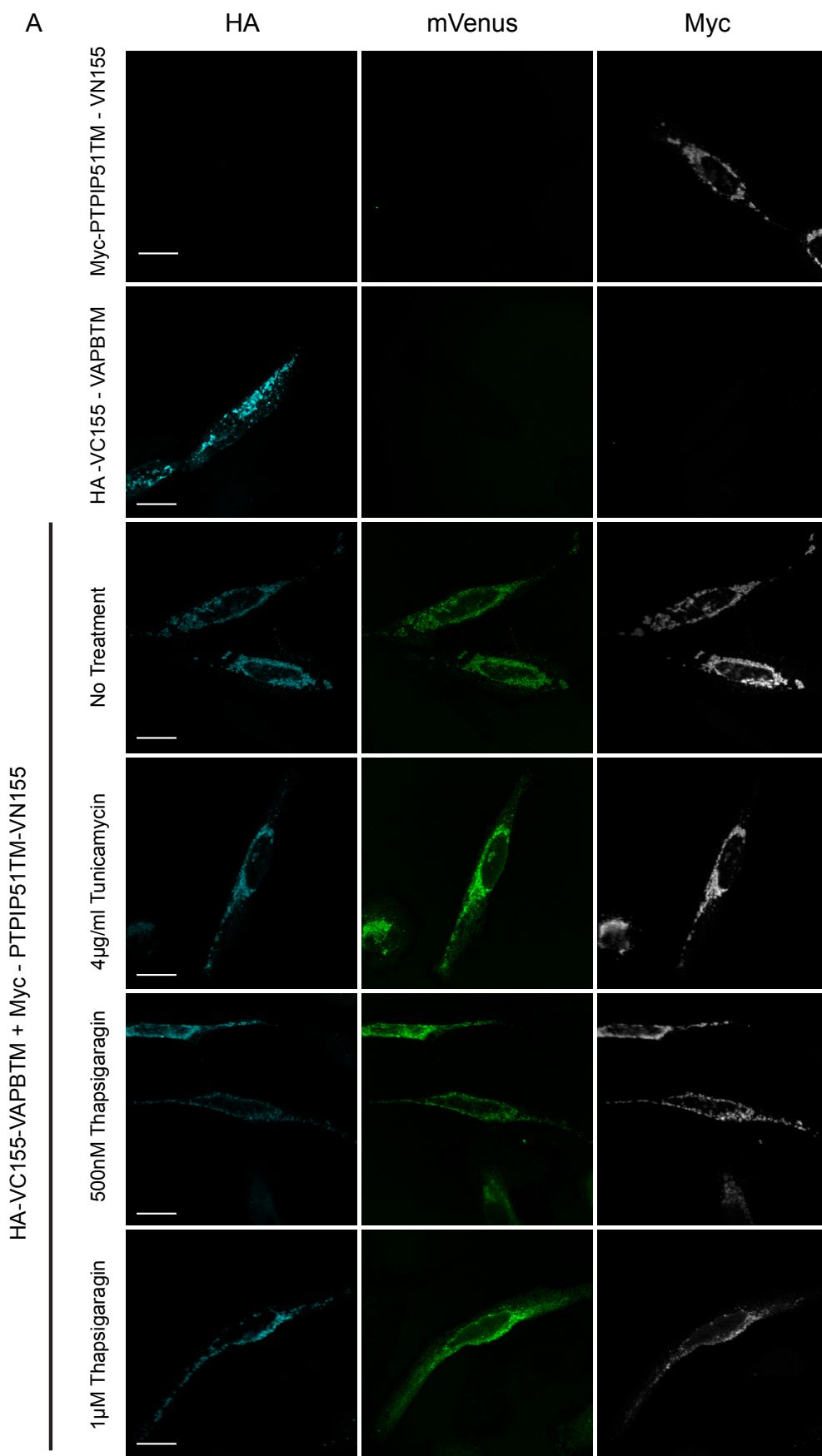


Figure 5.7: Increasing ER-mitochondria contacts using HA-PTPIP51 does not increase in BiFC mVenus fluorescence: (A) HeLa cells transfected with HA-VC155 VAPBTM (Cyan), Myc-PTPIP51TM-VN155 (Gray) either alone or in combination, were examined for mVenus fluorescence (Green, middle panel) with and without the overexpression of HA-PTPIP51 (Yellow). Scale bar, 20 μ m. (B) mVenus fluorescence was quantified per cell as the mean gray value which was normalised to the PTPIP51TM-VN155 and VC155-VAPBTM condition to allow comparisons between data sets. Data represents 4 biological replicates with 30-50 cells per experimental condition and 10-20 cells per control condition. Error bars represent standard error of the mean. ns $P > 0.05$ **** $P < 0.0001$ (one-way ANOVA with Bonferroni post hoc test).



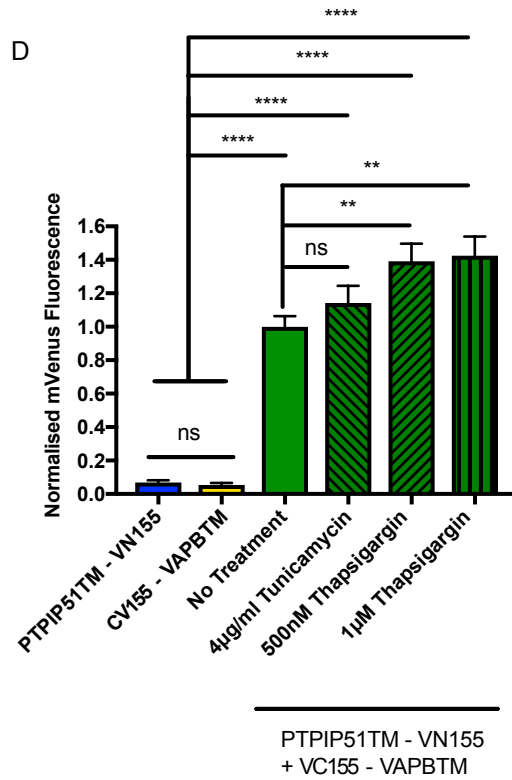
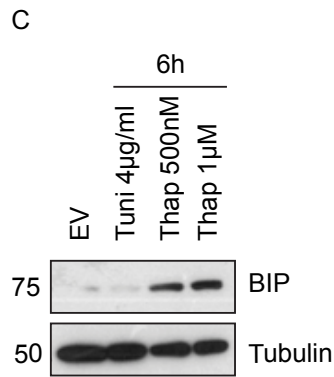
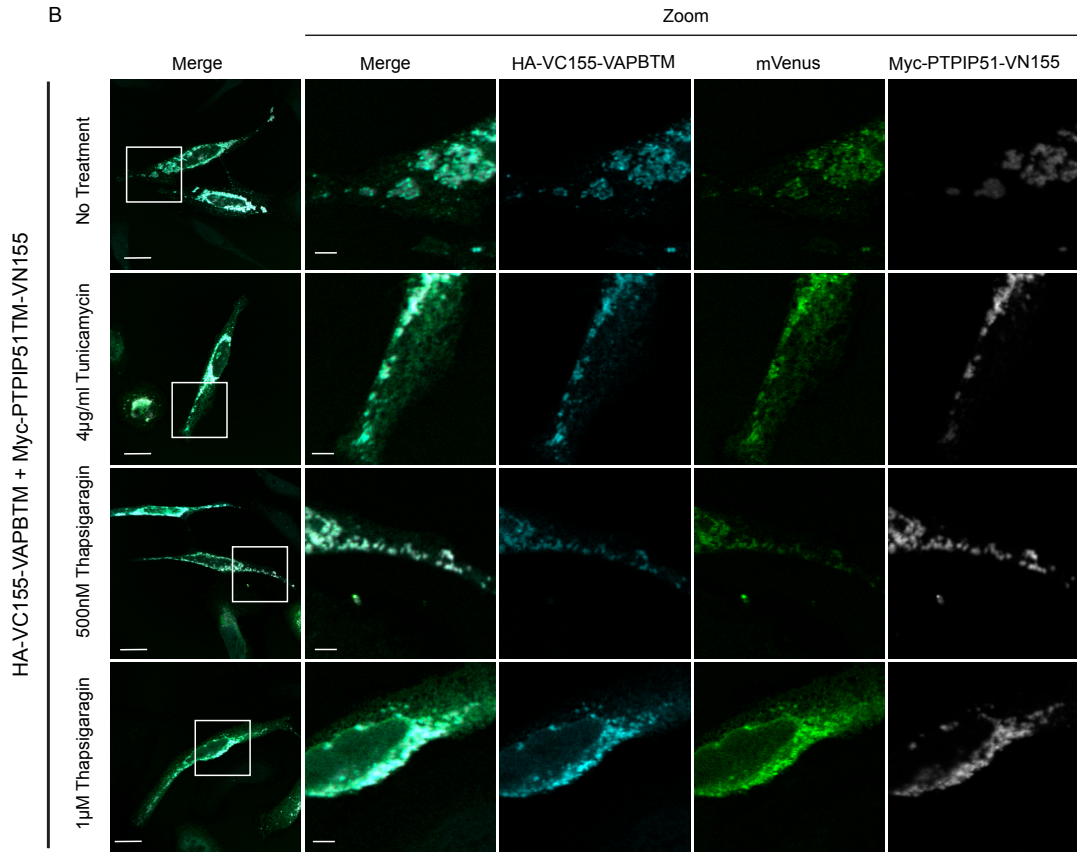


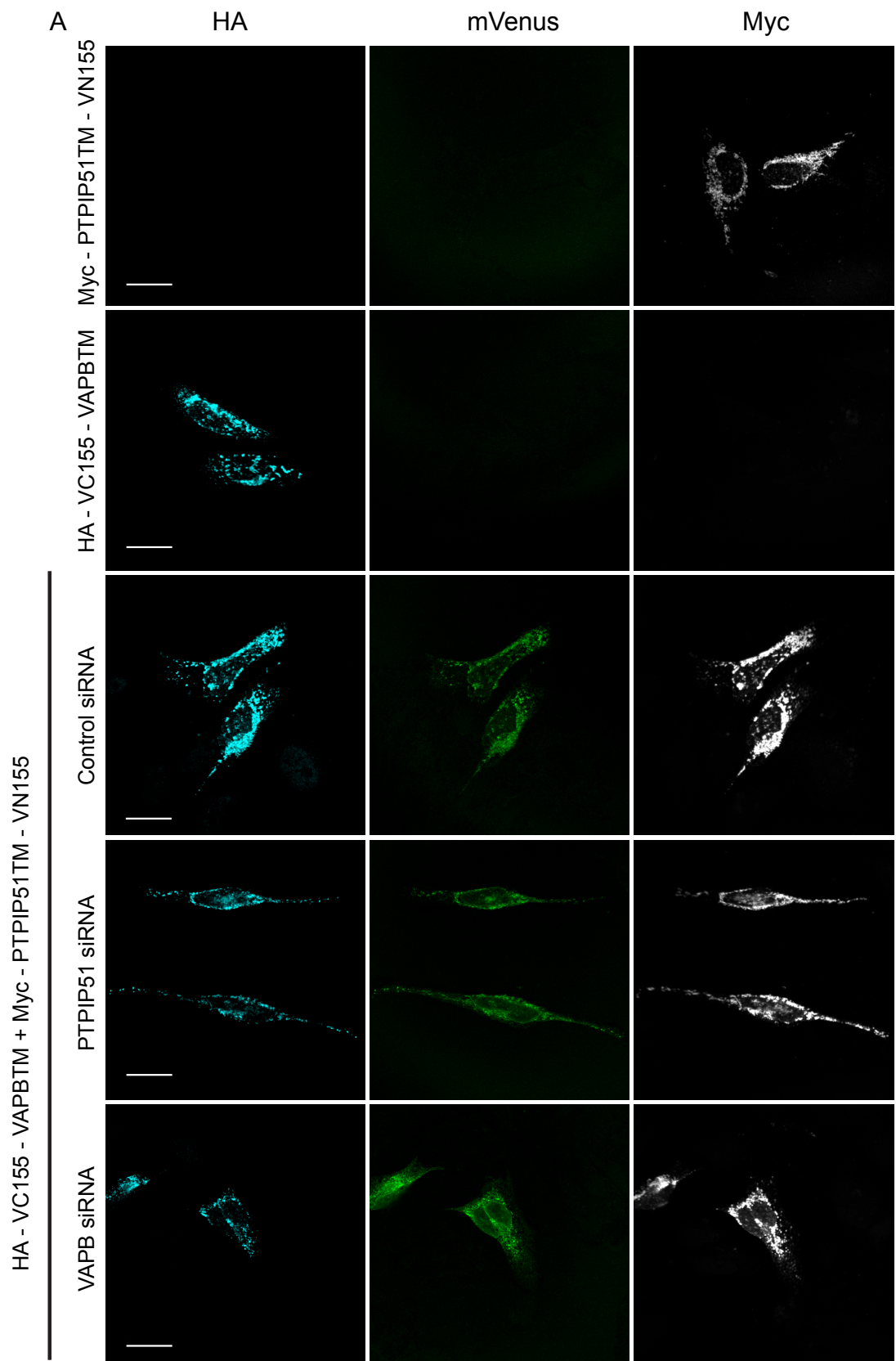
Figure 5.8: Increase ER-mitochondria contact by inducing ER stress results in an increase in BiFC mVenus fluorescence:

(A) Induction of ER stress was determined by western blot of endogenous BIP in untreated HeLa cells and cells treated for 6 h with Tunicamycin (4 μ g/ml) or Thapsigargin (1 μ M or 500 nM) and examined (anti-BIP). α -Tubulin was used as a loading control.

(B and C) HeLa cells transfected with HA-VC155-VAPBTM (Cyan), Myc-PTPIP51TM-VN155 (Gray), either alone or in combination, and treated as indicated were examined for BiFC mVenus fluorescence (Green, middle panel). Scale bar, 20 μ m and 5 μ m (Zoom). (D) BiFC mVenus fluorescence was quantified per cell as the mean gray value normalised to the PTPIP51TM-VN155 + VC155-VAPBTM condition to allow comparisons between data sets. Data represents 2 biological replicates with 30-50 cells per experimental condition and 10-20 cells per control condition. Error bars represent standard error of the mean. Ns, not significant, **** P<0.0001, ** P<0.001 (one-way ANOVA with Bonferroni post hoc test).

5.3.1.4: Loss of VAPB or PTPIP51 does not result in a decrease in BiFC mVenus fluorescence.

To further characterise the BiFC system, we next determined if the BiFC ER-mitochondria contact probes were able to detect a decrease in ER-mitochondria contact sites. It has been shown that siRNA mediated depletion of PTPIP51 or VAPB reduces ER mitochondria contact sites (Stoica et al., 2014). Hence, HeLa cells were transfected with either Control, PTPIP51 or VAPB siRNA and incubated for 5 days to allow efficient knockdown of the respective proteins after which they were transfected with HA-VC155-VAPBTM and/or Myc-PTPIP51TM-VN155 to determine ER-mitochondria contacts. Knockdown was verified by western blot, which showed that PTPIP51 and VAPB were successfully knockdown down at the protein level (**Fig 5.9C**). As expected the expression of HA-VC155-VAPBTM or Myc-PTPIP51TM-VN155 alone produced no mVenus fluorescence (**Fig 5.9A and B**). Control, PTPIP51 and VAPB siRNA treated cells co-transfected with HA-VC155-VAPBTM and Myc-PTPIP51TM-VN155 showed an increase in mVenus fluorescence compared to cells transfected with HA-VC155-VAPBTM or Myc-PTPIP51TM-VN155 alone. Both HA-VC155-VAPBTM and Myc-PTPIP51TM-VN155 appeared mitochondrial and co-localised with mVenus fluorescence (**Fig 5.9B**). Quantification of the BiFC mVenus fluorescence levels revealed that neither knockdown of PTPIP51 nor of VAPB significantly affected mVenus fluorescence (**Fig 5.9A and D**). These data suggest that the BiFC system does not report on a decrease in ER-mitochondria contact sites.



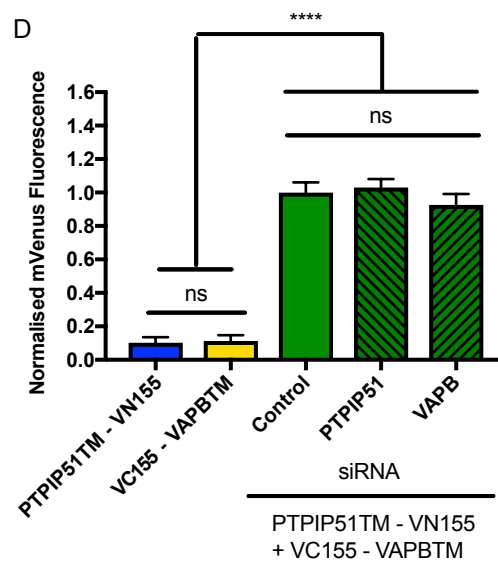
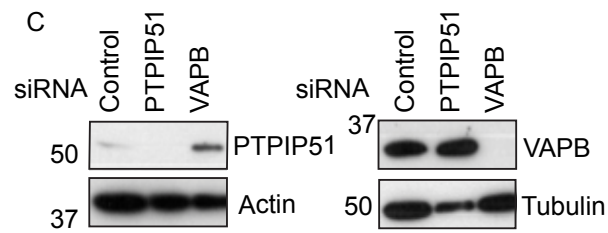
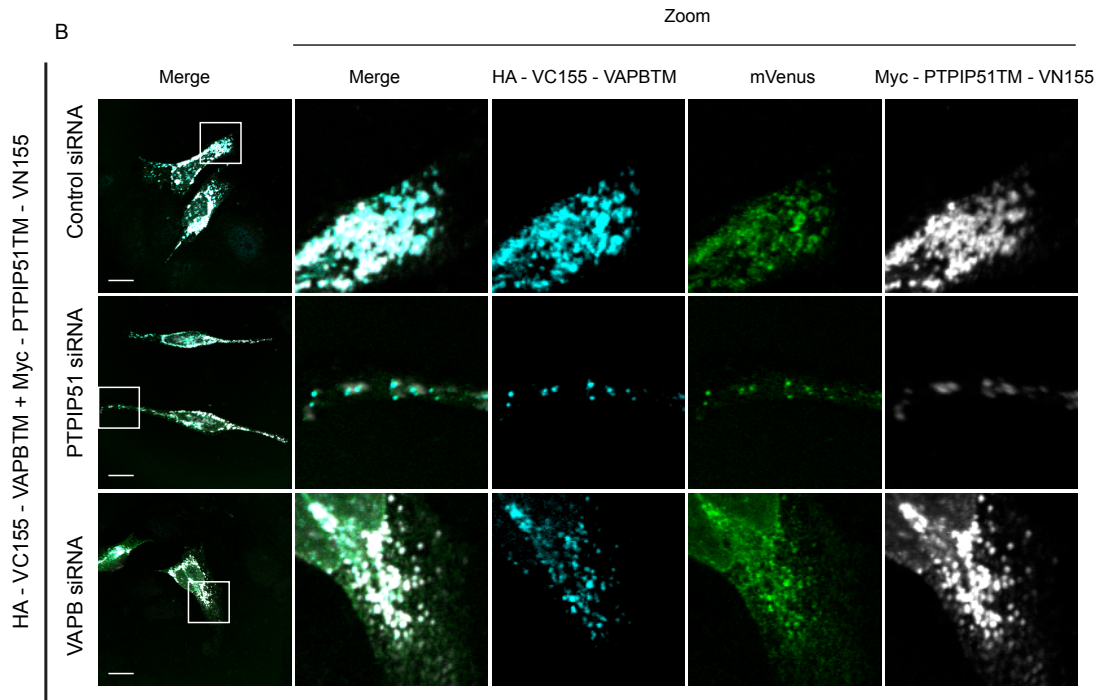


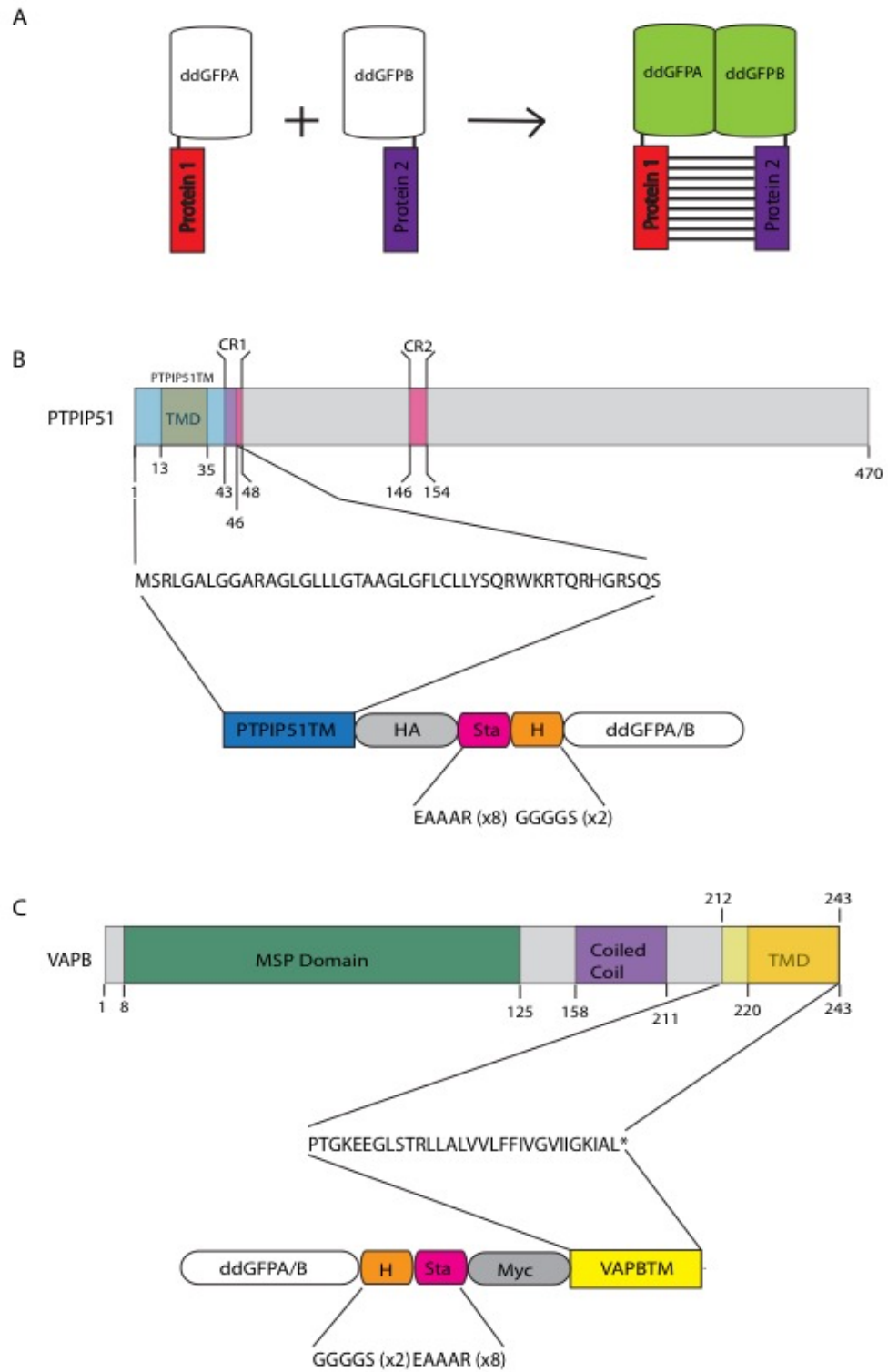
Figure 5.9: Knockdown of PTPIP51 or VAPB does not affect BiFC mVenus fluorescence: (A) Knockdown of PTPIP51 and VAPB was determined by western blot for

endogenous PTPIP51 (anti-RMD3) and VAPB (anti-VAPB) protein levels. α -Tubulin or actin levels were used as loading controls. (B) HeLa cells treated with either Control, PTPIP51 or VAPB siRNA were transfected with HA-VC155-VAPBTM (Cyan) and/or Myc-PTPIP51TM-VN155 (Gray) as indicated and examined for mVenus fluorescence (Green, middle panel). HA-VC155-VAPBTM (Cyan) and Myc-PTPIP51TM-VN155 were detected using HA-7 anti-HA and 9B11 anti-Myc antibodies, respectively. Scale bar 20 μ m and 5 μ m (Zoom). (C) BiFC mVenus fluorescence was quantified per cell as the mean grey value which was normalised to the average mean gray value of the VC155-VAPBTM + PTPIP51-VN155 condition to allow combination of data sets. Data represents 2 biological replicates with 30-50 cells per experimental condition and 10-20 cells per control condition. Error bars represent standard error of the mean. ns $P > 0.05$ **** $P < 0.0001$ (one-way ANOVA with Bonferroni post hoc test)

5.3.2: Dimerization dependent GFP (ddGFP) as a reporter of ER-mitochondria contact

There have been conflicting reports on the reversibility of BiFC with some authors suggesting that BiFC systems are reversible while others have suggested that the refolding of the fluorescence protein fragments holds the resulting full molecule in a stable conformation which is not reversible (Hu et al., 2002; Kodama and Hu, 2010; Robida and Kerppola, 2009). Our data above showing that decreasing ER-mitochondria contacts does not result in reduced BiFC mVenus fluorescence also indicates that the BiFC system is not reversible, making it unsuitable to investigate ER-mitochondria contact sites in real time. To potentially overcome this limitation of the BiFC system we turned to dimerization dependent (dd) fluorescent proteins (FP). The ddFP system involves the reversible binding of two non-fluorescent, “dark”, ddFP monomers, ddFPA and ddFPB, to produce a fluorescent heterodimer. ddFPA is mutated (I11L and S14A and K163G) such the chromophore is destabilised and quenched, while ddFPB completely lacks a chromophore. When ddFP heterodimerises with ddFPB they complement each other and form a fluorescent heterodimeric complex (**Fig 5.10A**) (Alford et al., 2012a). Originally, the dimerization dependent system was based on the inherent properties of RFP to form low affinity tetramers, however, the colour pallet now includes both YFP and GFP which have increased *in vitro* brightness and contrast compared to the ddRFP variant (Alford et al., 2012b; Campbell et al., 2002). ddFP has been used successfully to study protein-protein interactions by fusing ddFPA and ddFPB to interacting proteins (Alford et al., 2012a).

Similar to our BiFC ER-mitochondria contact probes, the organelle targeting fragment of either PTPIP51 or VAPB containing the transmembrane domains was fused to ddGFPA and ddGFPB using a flexible hinge region (**Fig 5.10 B and C**). In addition, we inserted 3 nm α -helical ‘stalk’ region (EAAAR x8) to ensure correct spacing of the space between ER and mitochondria (Csordás et al., 2010). Myc and HA tags were added to allow detection of the individual constructs (**Fig 5.10 B and C**).



D

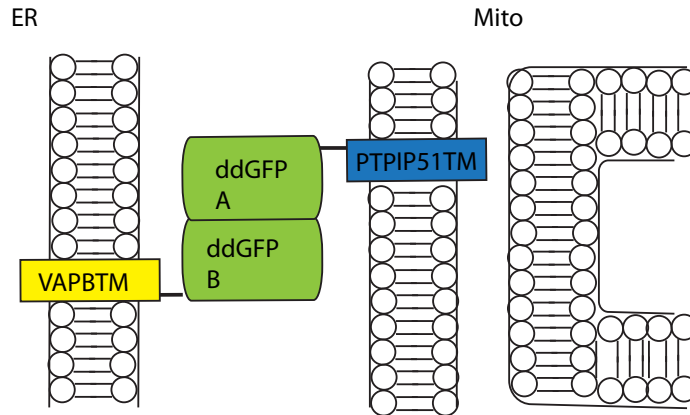


Figure 5.10: The ddGFP system: (A) Schematic representation of the how the principle of how the ddGFP system. (B) Schematic representation of PTPIP51 showing the conserved regions, CR1 and CR2 (pink) and the transmembrane domain (TMD). The fragment used in the ddGFP ER-mitochondria reporter is indicated (blue). The amino acids sequence of both the organelle targeting PTIP51 fragment and hinge region is shown. The structure of the PTPIP51-ddGFPA/B constructs including the amino acid sequence, position of the Myc tag and hinge region is also shown. (C) Schematic representation of VAPB showing the MSP domain (green), coiled coil domain (purple) and the transmembrane domain (orange). The fragment used in the ddGFP ER-mitochondria reporter is indicated (yellow). The amino acids sequence of both the organelle targeting VAPB fragment and hinge region is shown. The structure of ddGFPA/B-VAPBTM constructs including the amino acid sequence and the positions of the HA tag and hinge region is also show. (D) Schematic representation of the hypothesised orientation and interaction of the PTPIP51 and VAPB ddGFP constructs in ER-mitochondria contacts. When in the correct orientation, the two GFP complement and produce GFP fluorescence.

5.3.2.1: Expression and localisation of the ddGFP ER-mitochondria contact probes

To begin, the characterisation of our ddGFP ER-mitochondria contact probes we first determined their expression and cellular localisation. The expression of the ddGFP probes was examined by western blot analysis of HEK293 cells transiently transfected with ddGFPA, ddGFPB, ddGFPA-VAPBTM, ddGFPB-VAPBTM, PTPIP51TM-ddGFPA or PTPIP51TM-ddGFPB. ddGFPA and ddGFPB were detected using their HA or Myc tag, PTPIP51TM-ddGFPA and PTPIP51TM-ddGFPB using their Myc tag, and ddGFPA-VAPBTM and ddGFPB-VAPBTM using their Myc tag. All the ddGFP ER-mitochondria contact probes expressed and ran at their predicted molecular weight (**Fig 11A and B Table 5.2**).

To examine the localisation of PTPIP51TM-ddGFPA and PTPIP51TM-ddGFPB, HeLa cells were transfected with ddGFPA, ddGFPB, PTPIP51-ddGFPA, PTPIP51-ddGFPB or, as positive control, HA-PTPIP51 together with AcGFP1-Mito as a mitochondrial marker. PTPIP51TM-ddGFPA, PTPIP51TM-ddGFPB and HA-PTPIP51 appeared mitochondrial and co-localised with AcGFP1-Mito (**Fig 5.12**). This was due to the organelle targeting sequences of PTPIP51 because ddGFPA or ddGFPB without the PTPIP51TM sequence appeared cytosolic with no co-localisation with AcGFP1-Mito (**Fig 5.12**).

To examine the localisation of the VAPBTM ddGFP fusion proteins, CV1 cells transfected with ddGFPA, ddGFPB, ddGFPA-VAPBTM, or ddGFPB-VAPBTM were stained anti-Myc antibodies to visualise the ddGFP proteins and antibodies to endogenous calreticulin to visualise the ER (Michalak et al., 1999). CV1 cells transfected with Myc-VAPB were used as a positive control for the localisation of VAPB. ddGFPA-VAPBTM, ddGFPB-VAPBTM and Myc-VAPB appeared as a web like network, typical of ER proteins and co-localised with calreticulin (**Fig 5.13**). In contrast, staining of ddGFPA and ddGFPB not fused to VAPBTM was diffuse and localised throughout the cytosol with no co-localisation with calreticulin (**Fig 5.13**). Together, these data show that of PTPIP51TM targeted ddGFPA or ddGFPB to the OMM while VAPBTM directed ddGFPB and ddGFPA to the ER.

Table 5.2: The molecular weights of the ddGFP constructs: A table to show the calculated molecule weights of the individual ddGFP fragments with and without PTPIP51TM or VAPBTM

CONSTRUCTS	PREDICTED MOLECULAR WEIGHT
ddGFPA	29 kDa
ddGFPB	27 kDa
PTPIP51- ddGFP	40 kDa
PTPIP51 – ddGFP	38 kDa
ddGFPA – VAPBTM	39 kDa
ddGFPB – VAPBTM	37 kDa

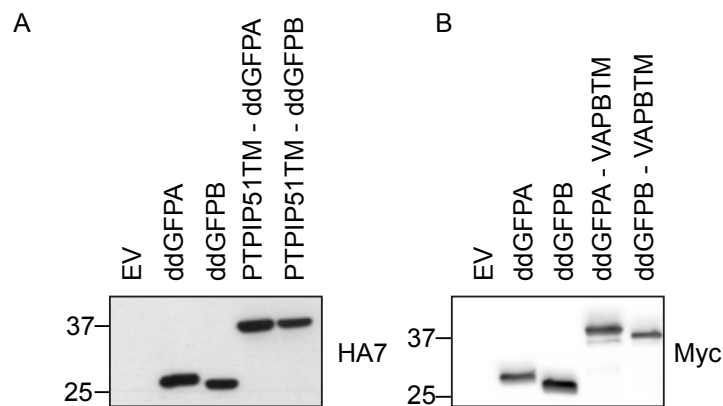


Figure 5.11: Expression of ddGFP ER-mitochondria contact probes in HEK293 cells: (A) HEK293 cells were transfected with ddGFPA, ddGFPB, PTPIP51TM-ddGFPA, PTPIP51-ddGFPB or empty pCI-neo vector (EV) and expression was analysed by western blot using anti-HA (HA7) (B) HEK293 cells were transfected with ddGFPA, ddGFPB, ddGFPB-VAPBTM, ddGFPA-VAPBTM or empty pCI-neo vector and expression was analysed by western blot using anti-Myc (9B11).

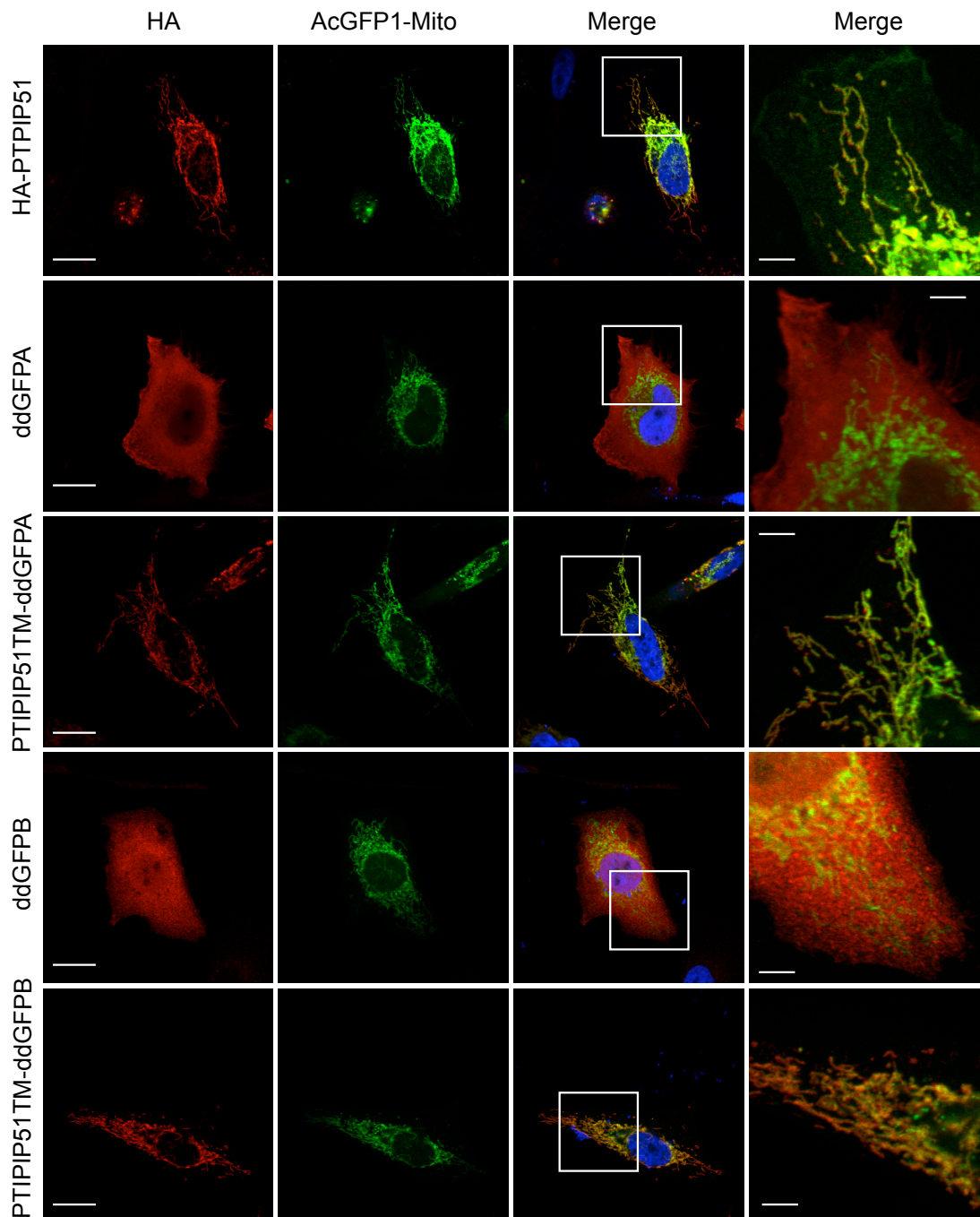


Figure 5.12: PTPIP51TM-ddGFPFA and PTPIP51TM-ddGFPB localise to the mitochondria: HeLa cells were co-transfected with HA-PTPIP51, ddGFPFA, ddGFPB, PTPIP51TM-ddGFPFA or PTPIP51TM-ddGFPB (Red, anti-HA7) and AcGFP1-Mito (Green). Scale Bar 20 μm and 5 μm (Zoom)

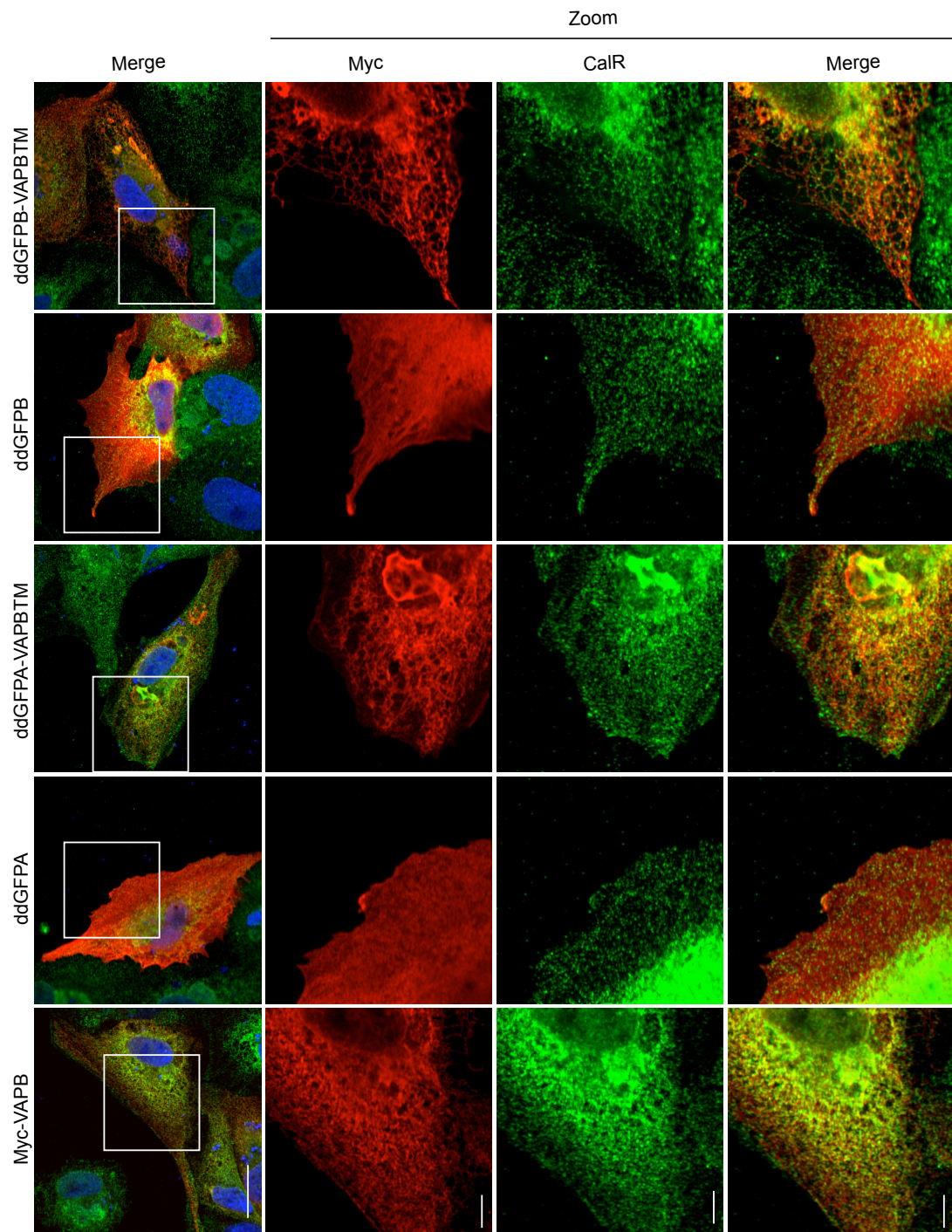


Figure 5.13: ddGFPB-VAPBTM and ddGFPA-VAPBTM localise to the ER. CV1 cells were transfected with Myc-VAPB, ddGFPA, ddGFPB, ddGFPA-VAPBTM or ddGFPB-VAPBTM (Red, anti-Myc) and the ER visualised using an endogenous calreticulin antibody (Green (anti-calreticulin)). Scale Bar 20 μm and 5 μm (zoom)

5.3.2.2: The ddGFP ER-mitochondria contact probes report on ER-mitochondria contact.

After establishing that the ddGFP ER-mitochondria contact probes express and localises correctly to the ER and mitochondria we next wanted to determine if they could report on ER-mitochondria contact. To do this HeLa cells were transfected with ddGFPA-VABPTM or ddGFPB-VAPBTM and their complementary mitochondria targeted ddGFP partner, PTPIP51TM-ddGFPA or PTPIP51TM-ddGFPB. As controls, the recently described ddGFPA-Calnexin and ddGFPB-TOM20 ER-mitochondria contact probes and ddGFPA and ddGFPB were transfected (Alford et al., 2012a). The cells were then imaged live and examined for GFP fluorescence. Co-expression of ddGFPA and ddGFPB resulted in bright diffuse GFP fluorescence throughout the cytoplasm (**Fig 5.14 Aiii, Avi and Biii and Bvi**). In contrast, in cells transfected with ddGFPA-VAPBTM and PTPIP51TM-ddGFPB, ddGFPB-VAPBTM and PTPIP51TM-ddGFPA or ddGFPA-calnexin and TOM20-ddGFPB GFP fluorescence appeared distinctly mitochondrial (**Fig 5.14 A**). In all 3 cases, multiple phenotypes are observed. Some cells appeared to have long extended mitochondrial networks (**Figure 5.14A**), while in other appeared to have fused and clumped mitochondria (**Fig 5.14B**). The latter may be due to higher expression levels of the ddGFP probes, or might indicate stabilisation of ER-mitochondria contact by ddGFP dimers.

These results suggest that ddGFP system can be used to detect ER-mitochondria contact sites. Due to time constraints, we have not yet characterised the ddGFP probes any further.

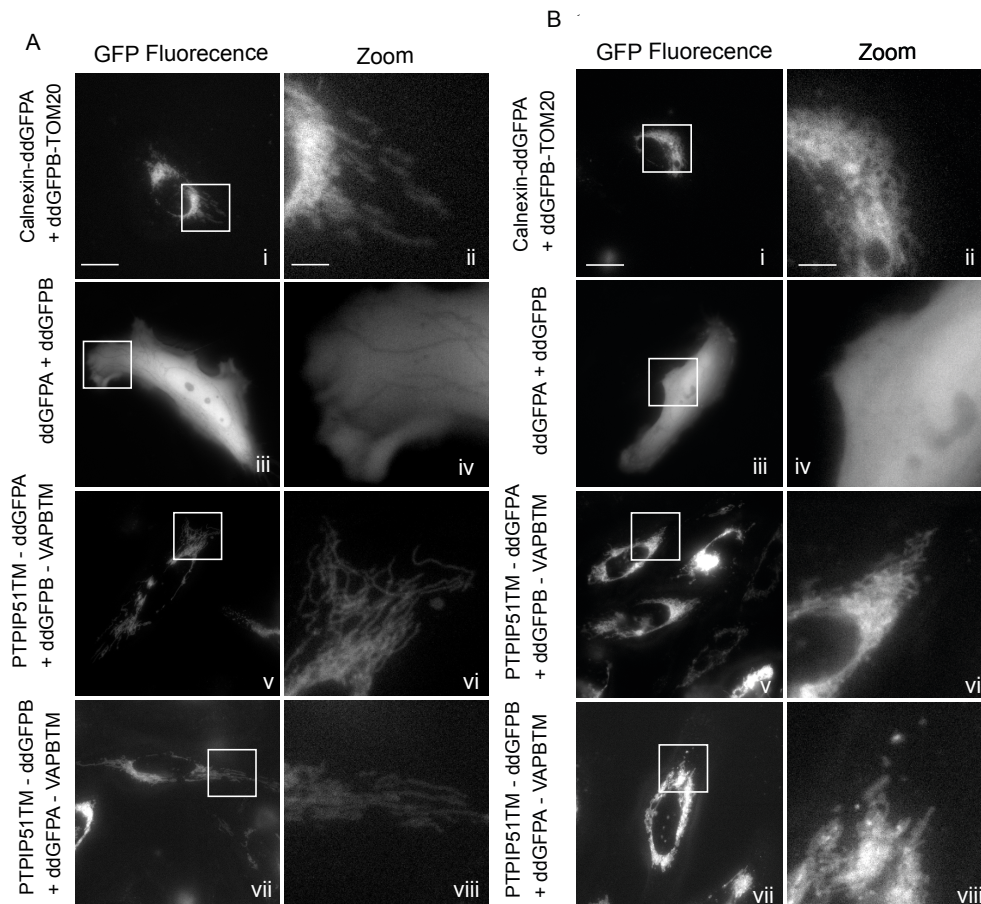


Figure 5.14. The ddGFP ER-mitochondria contact probes report on ER-mitochondria contact: HeLa cells were transfected with 4 combinations of ddGFP molecules: ddGFPA-Calnexin and TOM20-ddGFPB, ddGFPA and ddGFPB, PTPIP51TM-ddGFPA and ddGFPB-VAPBTM and finally, PTPIP51TM-ddGFPB and ddGFPA-VAPBTM. The resultant GFP fluorescence shown. (A) shows mitochondria from all the combinations which appear 'normal' while (B) shows mitochondrial with are abnormal and appear to have a clumped mitochondrial network. Images are enlarged in A ii, iv, vi and viii and B ii, iv, vi and viii for clarity of this phenotype. Scale bar 20 μm and 5 μm (Zoom)

5.4 Discussion

In this chapter I have developed and investigated new tools to visualise ER-mitochondria contacts in real time using light microscopy. The results have shown that the organelle targeting fragments of VAPB and PTPIP51 correctly target both BiFC and ddGFP probes to the ER and mitochondria, respectively. Furthermore, co-transfection of these ER and mitochondria targeted probe pairs produce fluorescent signal that are consistent with ER-mitochondria contacts.

The BiFC probes were investigated for their ability to report on changes in ER-mitochondria contact sites through use of a synthetic OMM-ER linker, overexpression of HA-PTPIP51, induction of ER-stress and knockdown of PTPIP51 or VAPB. The BiFC probes successfully detected increases in ER-mitochondria contact sites by inducing by ER-stress but not by overexpression of HA-PTPIP51 or OMM-ER linker, even though both the OMM-ER linker and HA-PTPIP51 can promote ER-mitochondria contact sites (Csordás et al., 2006; Stoica et al., 2014). Since the OMM-ER linker has been shown to decrease the ER to OMM distance from 24 nm to 6 nm (Csordás et al., 2006) it is possible that this increase in contacts prevents interaction of the BiFC probes. Indeed, the large decrease in ER-OMM distance in large areas around the mitochondria may change the positioning of the VC155 and VN155 domains so they are unable to fold efficiently, thus decreasing the BiFC mVenus fluorescent signal. A similar mechanism may be at play in cells overexpressing HA-PTPIP51. The increase in ER-mitochondria contact sites by PTPIP51 overexpression was determined to be regions of the ER and mitochondria which are less than 30nm apart and so it is conceivable that the overexpression of HA-PTPIP51 does not decrease the distance between the ER and OMM as much as the OMM-ER linker (Stoica et al., 2014). Consistent with this we found that the effect of HA-PTPIP51 was not as dramatic as that of the OMM-ER linker (**Fig 5.15**). We did however, detect an increase in mVenus fluorescence after induction of ER-stress. In this case ER-mitochondria contacts were not affected by overexpression of synthetic linker or tether proteins, thus it appears that under physiological conditions the BiFC probes can detect increases in ER-mitochondria contacts. It has to be noted that the increase in ER-mitochondrial contact sites was not determined by EM or confocal co-localisation studies and this would have to be conducted to robustly confirm the results seen here. Overall these data suggest the BiFC have the ability constructs to detect physiological increases in ER-mitochondrial contact sites.

Alternatively, however, knockdown of PTPIP51 or VAPB did not result in any change in mVenus fluorescence with the BiFC system. One possibility is that the decrease elicited by was too small to detect; indeed, it has been shown that knockdown of PTPIP51 or VAPB decreases ER-mitochondria contact by only approximately 20 % (Stoica et al., 2014). Alternatively, it has been reported that the BiFC system is not reversible, meaning that once VN155 and VC155 re-fold, into a full mVenus protein they are unable to separate (Hu et al., 2002; Kodama and Hu, 2010; Robida and Kerppola, 2009). In this case, the BiFC probes may in fact act as physical tethers between ER and mitochondria which may prevent any decreases in ER-mitochondria contact (**Fig 5.15**).

In the extreme, this property of the BiFC system may result in an increase in ER-mitochondria contact sites like the one observed using OMM-ER linkers. In support, we observed, a similar phenotype is observed in all cells transfected with the BiFC system to those transfected with OMM-ER linker (Csordás et al., 2006). Similarly, the examination of mitochondria in cells which show mVenus fluorescence and those that don't show a significant difference in their mitochondria morphology. Some cells lack a peripheral mitochondrial network and contain fused and clumped mitochondria, thus suggesting mitochondrial dysfunction, with more cells appearing apoptotic. This phenotype can help explain the lack of increase in mVenus signal with PTPIP51 overexpression. The BiFC system may link the ER to mitochondria and already has increased contacts, so the overexpression of PTPIP51 does not have as pronounced effect. Once again this suggests that use of the BiFC probes to investigate modulators of ER-mitochondria contact sites in fixed or live cells has to be approached with caution.

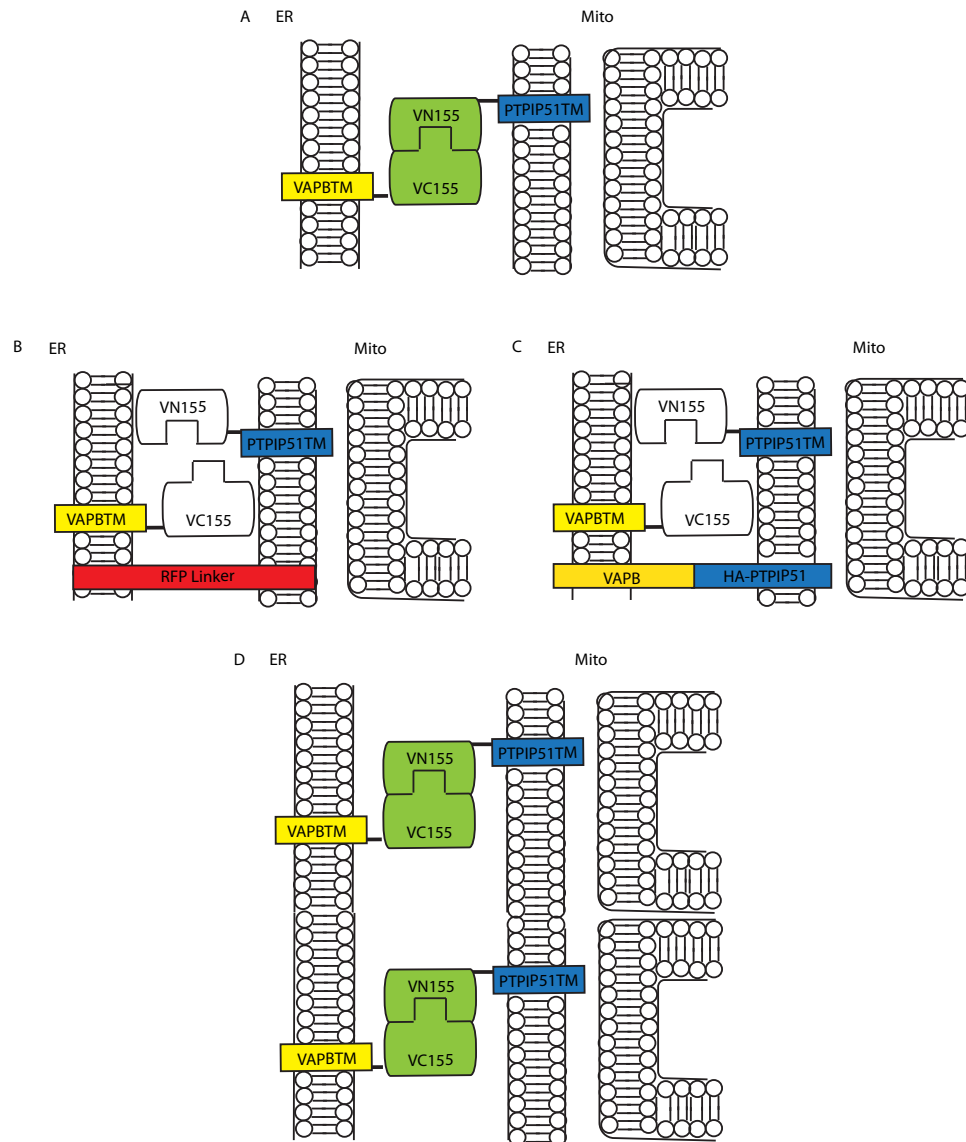


Figure 5.15: The expression of RFP-Linker or HA-PTPIP51 disrupts binding of VN155 to VC155 VAPBTM: (A) Schematic representation of the effect of co-expressing PTPIP51TM-VN155 with VC155-VAPBTM. The VN155 and VC155 can align, refold and produce mVenus fluorescence (Green). (B and C) Schematic representation of the effect of co-expressing the RFP linker or HA-PTPIP51 with VC155-VAPBTM and PTPIP51TM-VN155. Overexpression of RFP Linker or HA-PTPIP51 decreases ER to OMM distance and therefore the constructs cannot align and refold to produce mVenus fluorescence. (D) The schematic representation of the predicted increases in amount of ER-mitochondrial contact sites by increasing ER stress. There are more areas where the ER-mitochondria are in close proximity and with more opportunity for BiFC system to re fold and produce an increase in mVenus fluorescence.

As an alternative to BiFC we developed ddGFP probes. The ddGFP system has been reported to be reversible and so was investigated as an alternative option to the BiFC system which had issues with irreversibility that were thought to be causing changes to mitochondrial morphology (Alford et al., 2012a). We show that the ddGFP probes produce a clear GFP signal, however two main phenotypes are seen. The GFP signal can either appear in a branched mitochondrial network or can appear fused and clumped. This suggested that the ddGFP heterodimers may have limited ability to dissociate. Indeed, the system was originally developed from tetrameric RFP which was altered to produce ddRFP system whose natural energy state favours dimerisation (Alford et al., 2012b; Campbell et al., 2002). Preliminary data indicates that the clumped mitochondrial phenotype correlates with higher expression of the ddGFP probes. Thus, optimisation of transfections may help with this problem however, the ddGFP system appear more promising than the BiFC system. The next step is to investigating the ddGFP system further by testing if it can report on ER mitochondrial sites and changes in them.

Further work

The BiFC constructs have been reported and suggest in this study to have issues with irreversibility and so will not be investigated further. However, the ddGFP probes appear to be more promising. One of the main drawbacks of the ddGFP system is the appearance of clumped mitochondrial morphology which may signify some irreversibility in the system. This is reasoned to be due to differences in the amount of each probe being expressed. So, those with a higher transfection efficiency express more and appear more clumped as there is a greater number of ddGFP constructs to dimerize with. Therefore, to overcome this optimisation of the transfection efficiency should be conducted to examine if this is the case. Another option to preventing dimerization would be to induce point mutations which can help keep GFP as a monomer hopefully reducing the dimerization properties (Nakagawa et al., 2012).

It would also be interesting to investigate if the GFP fluorescence, which is reporting on ER-mitochondria contact sites, is correctly localised. It appears to look mitochondrial however the co-expression with an ER and mitochondria marker would easily be able to show this is the case and to see if it did represented ER-mitochondrial contact sites. Next, similar approaches of can be used to investigate the ability of ddGFP probes to report on ER-mitochondria contacts sites as were used for the BiFC, such as induction of ER stress of siRNA mediated loss of VAPB

or PTPIP51. Alternatively, the other linkers which are rapamycin inducible could be used to examine irreversibility of the ddGFP probes (Csordás et al., 2010).

6.DISCUSSION

6.1: Phosphatidylinositol metabolism

6.1.1 Phosphatidylinositol metabolism in neurodegeneration

The focus of this study was to investigate the potential role of PI and its phospho-derivatives in mitochondrial quality control, with respect to PD. The results of this study show that the silencing of PI4KB or SYNJ1, two enzymes which mediate PI metabolism, result in a slowing of both Parkin translocation and mitophagy under mitochondria depolarisation, suggesting that PI derivatives impact on PINK1/Parkin mediated mitophagy. However, the exact mechanism has not been explored fully. Our data correlates with currently published work, as PD has been suggested to have altered PI metabolism, with mutations in SYNJ1 being found in AR-JP (Kirola et al., 2016; Krebs et al., 2013a; Quadri et al., 2013c; Taghavi et al., 2017).

There is also evidence that PI metabolism is perturbed in other neurodegenerative disorders. Expression of the ALS-associated VAPB mutant (P56S) in *Drosophila* results in neurodegeneration due to an alteration in VAPB-Sac1 interaction and an increase in PI4P (Forrest et al., 2013). Furthermore, expression of wild type VAPB or ALS mutant VAPB (P56S) in *C. elegans* resulted in locomotion defects and neuronal death, with these phenotypes being improved by inhibition of PI4P production (Zhang et al., 2017). There is also evidence for perturbed PI metabolism in AD. Both PI levels and PI4K levels are reduced by 50% in AD patients and γ -secretase activity is strongly inhibited by PI *in vitro* (Holmes et al., 2012; Stokes and Hawthorne, 1987; Zubenko et al., 1999). In addition OCRL, a PI(4,5)P₂ phosphatase, is mutated in Lowe syndrome with patients presenting intellectual impairment, seizures and a neuronal phenotype in males (Hichri et al., 2011). The cellular effect of mutations in the OCRL gene is an increase in PI(4,5)P₂ in the early endosome, resulting in a trafficking defect (Vicinanza et al., 2011). Together these observations suggest that alterations in PI metabolism can result in neurodegeneration, however much work is required to understand exactly how PI metabolism is contributing to the neurodegeneration in AD, ALS and PD. How PI metabolism affects neurones is not clear, however the data from this study suggests that mitochondrial quality control may be perturbed, leading to neurodegeneration.

6.2.2 Phosphatidylinositol metabolism in mitochondrial quality control.

Studies in both adult *Drosophila* and mammalian cell lines have suggested that the metabolism of PI can impact on aspects of mitochondrial quality control. Pogson et al. identified *fwd* (PI4K) as a modulator of mitochondrial morphology (Pogson et al., 2014), and my genetic interaction studies in *Drosophila* showed that the climbing

defects observed in both *pink1* and *parkin* null *Drosophila* can be rescued by overexpression of *fwd*. In addition, data from this thesis shows that knockdown of *PI4KB* or *SYNJ1* resulted in a reduction of Parkin translocation and mitophagy in YFP-Parkin-expressing Hela cells. Together these data suggest that PI metabolism may be impacting on mitochondrial quality control. The loss of *PI4KB* and *SYNJ1* causes a slowing of mitophagy, which may suggest that overexpression of *fwd* can rescue the climbing defect in *pink1*^{B9} or *park*²⁵ null *Drosophila* by altering mitophagy and increasing the removal of damaged mitochondria. However, there is limited evidence *in vivo* to support a link between climbing defects and mitophagy. Nevertheless, Vincow et al have provided evidence that the loss of *pink1* or *parkin* *in vivo* can slow mitophagy, yet a definitive link between the climbing defect and mitophagy was not examined (Vincow et al., 2013). Alternatively, there are also PINK1/Parkin-independent forms of mitophagy that involve PI metabolism. Starvation-induced, PINK1/Parkin-independent mitophagy is Wortmannin sensitive, and was found to require phosphatidylinositol-3-kinase which modulates the production of phosphatidylinositol 3 phosphate (Lemasters, 2014). Furthermore, ceramide, a sterol lipid produced by recruitment of CERT via PI4P to the Golgi, has been shown to influence autophagy and may act as an adaptor between LC3 and the phagophore to promote mitophagy (Brice et al., 2009; Mayinger, 2009; Scarlatti et al., 2004; Sentelle et al., 2013; Sims et al., 2010; Tan and Brill, 2014). These data suggest that management of ceramide can impact on autophagy and mitophagy. As ceramide production is influenced by PI4P and its ability to recruit CERT, a reduction in PI4P, through knockdown of *PI4KB* or *SYNJ*, may influence ceramide production. This can elicit secondary effects on LC3 and phagophore binding, thus decreasing the rate of mitophagy. It may also be possible that altering PI derivatives by modulating *PI4KB* or *SYNJ1* can shift mitochondrial quality control from PINK1/Parkin-dependent mitophagy to PINK/Parkin independent mitophagy

6.2: Synaptic vesicle trafficking and PD

Dysfunctional synaptic vesicle trafficking is emerging as another disease mechanism in PD, along with mitochondrial dysfunction, protein aggregation and oxidative stress. Synaptic vesicle transmission requires a specialised pre-synaptic terminal containing pools of 'primed' synaptic vesicles, which fuse with the pre-synaptic membrane and release neurotransmitter upon stimulation of an action potential. This propagates the action potential across the synaptic cleft. Once the action potential is propagated, the neurotransmitter is recycled by endocytosis,

allowing the formation of these primed pools once again (Esposito et al 2012). Previous reports have linked, α -Synuclein, LRRK2, PINK1 and Parkin to roles in synaptic vesicle trafficking (Burre et al., 2010; Morais et al., 2009; Trempe et al., 2009a). More recently however, synaptic trafficking has been further highlighted in PD by the discovery of mutations in SYNJ1 and DNAJC6, two genes which encode proteins involved in clathrin mediated endocytosis (Edvardson et al., 2012; Krebs et al., 2013a; Quadri et al., 2013c). The *DNAJC6* gene encodes the neuronal protein auxilin, which functions with SYNJ in clathrin-mediated endocytosis to allow the uncoating of endocytic vesicles and efficient vesicle recycling (Kononenko and Haucke, 2015; Yim et al., 2010). SYNJ1 and DNAJC6 knockout mice have strikingly similar phenotypes, such as clathrin coated vesicle accumulation, ataxia and neurological abnormalities, suggesting a common disease mechanism (Cremona et al., 1999b; Yim et al., 2010). Furthermore, common variants in cyclin G dependent kinase (GAK or auxillin 2), which is highly homologous to auxillin and shares a common domain structure, was identified in a GWAS study for idiopathic PD (Nalls et al., 2014; Pankratz et al., 2009). In mice, pathogenic PD mutations in the Sac1 domain of SYNJ1 showed endocytic defects and accumulation of clathrin mediated endocytosis components, in addition to dystrophic axons in the dopaminergic neurones (Cao et al., 2017). These studies suggest that clathrin mediated endocytosis, which is key in the recycling of synaptic vesicles, may be involved in the pathogenic disease mechanisms of PD.

It is hypothesized that reductions in synaptic vesicle loading or efficient recycling reduces the amount of dopamine in synaptic vesicles. This causes an increase in cytosolic dopamine, leading to increased oxidative stress and degeneration of the dopaminergic neurones (Miyazaki and Asanuma, 2008). However, our discovery of a link between SYNJ1 and mitophagy may suggest that SYNJ1 also impacts on mitochondria and mitochondrial quality control. Mfn2 knockdown in human iPSC cortical neurones has been shown to cause both mitochondrial dysfunction and also synaptic dysfunction during development. This could potentially link mitochondrial dysfunction to synaptic dysfunction (Fang et al., 2016). It is well established that synaptic vesicle release and recovery is an energy demanding process (Harris et al., 2012). Hence it is tempting to speculate that mutations in SYNJ have a dual effect: on the one hand PD-mutant SYNJ1 affects clathrin-mediated synaptic vesicle recycling directly via its regulation of clathrin un-coating and on the other hand it affects synaptic vesicle recycling indirectly by reducing ATP availability via its role in mitochondrial quality control. These studies suggest that mishandling of synaptic

vesicle recycling or trafficking is an important mechanism in the pathogenesis of PD. However, the link between mitochondrial quality control, SYNJ1 and synaptic vesicle recycling is not clear and more work remains to be done to understand the effect further.

6.3 Mitochondrial quality control, ER-mitochondria contact sites and PD

Relatively little is known about the role of ER-mitochondria contact sites in PD, however recent studies investigating genetic forms of PD have begun to reveal a link between the two. PARK2 knockout mice and patient cells showed an increase in the proximity of the ER and mitochondria, which also altered Ca^{2+} flux (Gautier et al., 2016). In addition, α -Synuclein has been found to localise to ER-mitochondria contact sites (Guardia-Laguarta et al., 2014) and to interact with the ER-mitochondria tethering protein VAPB (Paillusson et al., 2017). Overexpression of α -Synuclein WT, A30P or A53T caused a decrease in VAPB and PTPIP51 binding, which correlates with a reduction in ER-mitochondria contact sites, Ca^{2+} flux and ATP production (Paillusson et al., 2017). In addition to α -Synuclein, both Parkin and PINK1 have been found at ER-mitochondria contact sites (Gelmetti et al., 2017). Overexpression of Parkin increases ER-mitochondria contact sites and this correlated with enhanced Ca^{2+} signalling and ATP production (Cali et al., 2013). In addition, induction of mitophagy caused increased localisation of PINK1 at ER-mitochondria contact sites and this correlated with an increase in ER-mitochondria contact sites (Gelmetti et al., 2017). Interestingly, PINK1 has also been shown to bind Grp75 (Rakovic et al., 2011). Grp75 bridges IP₃R and VDAC to form a functional ER-mitochondria connection that modulates the transfer of Ca^{2+} from ER to mitochondria (Csordás et al., 2006; Gincel et al., 2001; Rapizzi et al., 2002; Szabadkai et al., 2006). Ca^{2+} entry in mitochondria is via the low affinity MCU channel in the IMM, which requires the high local concentration of Ca^{2+} at ER-mitochondria contact sites to efficiently allow Ca^{2+} uptake (Baughman et al., 2011; Giacomello et al., 2010; Rizzuto et al., 1992; De Stefani et al., 2011). Thus, it is hypothesized that PINK1 may regulate MCU-mediated Ca^{2+} entry into the mitochondria and this may be disturbed in PD. In agreement, it has been shown that inhibition of MCU rescues dopaminergic neurone loss in PINK1 knockout zebrafish (Soman et al., 2017). In addition NSC-1, an EF hand protein which recruits PI4KB to membranes under high [Ca^{2+}], binds PINK1 in zebrafish. This could potentially allow for the production of PI4P at the mitochondria (Petko et al., 2009). This, combined with the results presented in this thesis, suggests a link between PINK1, PI

metabolism, ER-mitochondria contact sites and mitochondrial quality control (**Fig. 6.1**).

One way in which PI may regulate mitophagy is through changes to mitochondrial morphology. An increase in fission has been shown facilitate mitophagy (Twig et al., 2008). Nonetheless, this study failed to see changes in gross mitochondrial morphology with depletion of *fwd* (*PI4KB*) or *synj* (*SYNJ1* or *SYNJ2*) in *Drosophila* and HeLa cells or with the overexpression of *fwd* and *synj* in *Drosophila* cells. This is in direct contrast with previously published results which show that knockdown of *fwd* can result in a fused mitochondrial network in *Drosophila* cells (Pogson et al., 2014). As previously discussed (Chapter 3), this may be due to differences in the method of analysis used, which is highly subjective. Moreover, the changes in PI or its derivatives were not examined and therefore may not have been eliciting a great enough effect to see a gross mitochondrial morphology change. Instead the effects may have been more subtle. Nonetheless, evidence from the literature suggests a potential role for PI derivatives in regulating mitochondrial morphology. ER-mitochondria contact sites are found in sites of mitochondrial fission. At these sites, the ER wraps around the mitochondria in order to promote mitochondrial constriction and facilitate Drp1 mediated fission events (Friedman et al., 2011). Interestingly, dynamin acts in a parallel process at the plasma membrane, where it is recruited to the PM by binding to PI(4,5)P₂ to promote vesicle scission (Jost et al., 1998; Ramachandran and Schmid, 2008). Unlike dynamin however, Drp1 does not contain a PH domain but instead has a variable or insert-B domain (Otera et al., 2013). The insert-B domain shows a weak interaction with lipids, suggesting that Drp1 cannot integrate into the lipid bilayer (Mears et al., 2011; Otera et al., 2013). Furthermore, the insert-B domain has been suggested to be dispensable for the recruitment of Drp1 to the mitochondria (Gandre-Babbe and van der Blik, 2008; Strack and Cribbs, 2012). This suggests that PIs do not confer the ability to recruit Drp1. Alternatively, there have been reports that Dynamin 2 (Dyn2) can contribute to membrane fission events at multiple organelles (Ferguson and De Camilli, 2012). Notably, Dyn2 contains a PH domain, putatively capable of binding phospholipids. The removal of Dyn2 results in a hyperfused mitochondrial network, where Drp1 labelled constrictions are present but fail to divide without the presence of Dyn2 (Lee and Voeltz, 2015). Intriguingly, this phenotype could not be rescued with Dyn2 that had mutation in the PH domain (Lee and Voeltz, 2015). Interestingly, unpublished data from the McBride lab has suggested that there is accumulation of PI4P at sites of mitochondria scission (Pogson unpublished, McBride Lab).

Together, these findings imply that the presence of PI4P at ER-mitochondrial contact sites is a factor in the recruitment of Dyn2 to the mitochondria, thereby mediating mitochondrial fission. These studies have highlighted a new pathway to be explored in the regulation of mitochondrial morphology, relating to recruitment of Dyn2 to mitochondrial fission and PI4P.

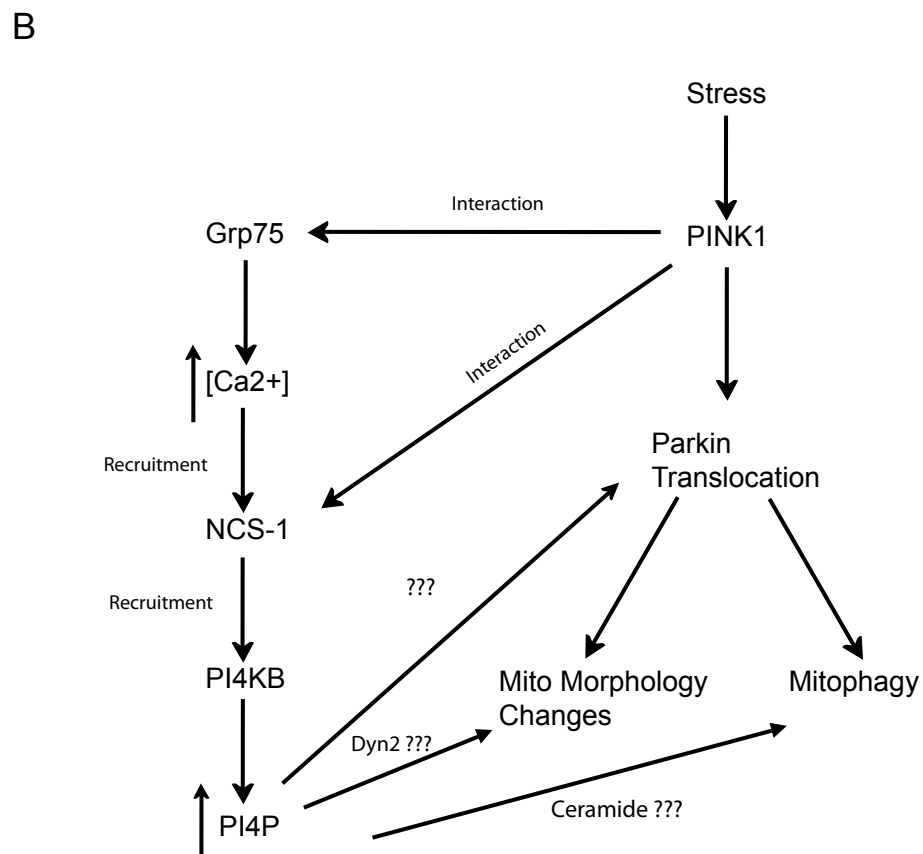
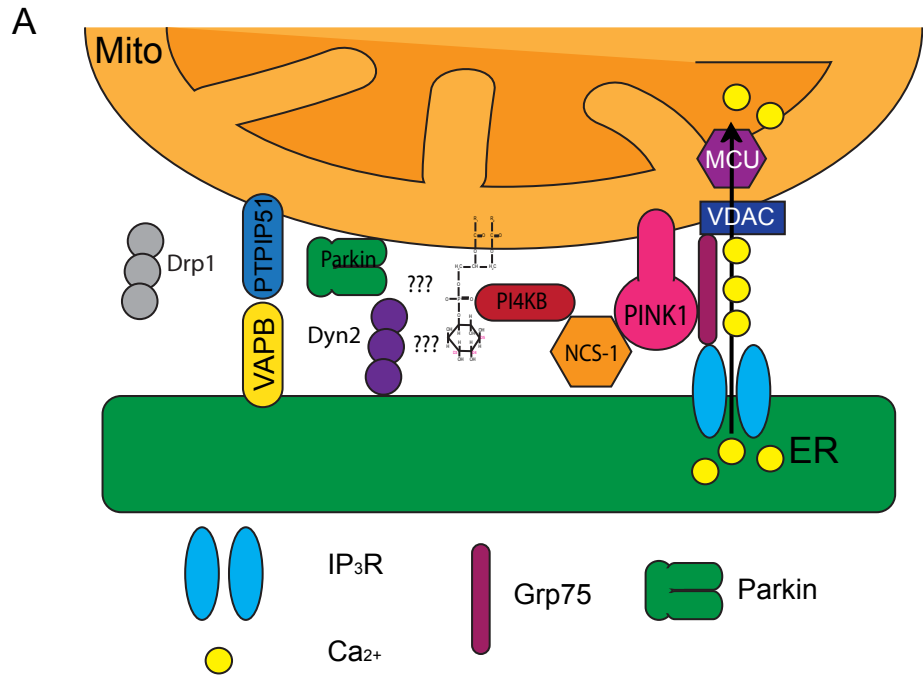


Figure 6.1: Hypothetical model for the relationship between PI metabolism and mitochondrial quality control: A schematic (A) and simplified pathway (B) of the proposed interaction between PI metabolism, PINK1/ Parkin pathways and mitochondrial quality control mechanisms. In brief, it can be hypothesized that under stress PINK1 is stabilised on the OMM in ER-mitochondria contact sites, where it can interact Grp75. Grp75 can modulate the transfer of Ca^{2+} via ER-mitochondria contact sites, potentially increasing local $[\text{Ca}^{2+}]$ at these contact sites. The local increase in Ca^{2+} and the reported interactions with PINK1 can recruit NCS-1 to the mitochondria and ER-mitochondria contact sites. NCS-1 has been known to recruit PI4KB to membranes with high $[\text{Ca}^{2+}]$. PI4KB can then mediate the addition of a phosphate group onto the mitochondrial localised PI, which increases PI4P production at ER-mitochondrial contact sites. The exact effect of the increase in PI4P is hypothesized to regulate changes in Parkin translocation, mitochondrial morphology and mitophagy.

6.4 Current methods to visualise ER-mitochondrial contact sites.

6.4.1 Electron microscopy (EM), confocal microscopy, super resolution microscopy

Currently, the gold standard in visualising ER-mitochondrial contact sites is through EM techniques. EM is currently the only technique that can resolve the close apposition of the ER and mitochondrial membranes, which is estimated to be between 10 and 30 nm at ER-mitochondria contact sites. However, due to the nature of EM where samples must be fixed, ER-mitochondria contacts cannot be viewed dynamically in real time. Currently, confocal microscopy can be used to visualise ER-mitochondrial contact sites, complementing data gained from EM. This can be done in real time using fluorescent proteins, however confocal microscopy does not have a high enough resolution to unambiguously distinguish ER-mitochondria contact sites (Yamanaka et al., 2014). What is visualised is the overlapping volumes of fluorescent proteins and the area present in 3D space (Filadi et al., 2015). Although it can be used to visualise ER-mitochondrial contact in real time, there are limitations and considerations to be made when using this system.

There have been great advances in the field of microscopy, with the development of super resolution techniques including stimulated emission depletion (STED). This system exploits the energy state of fluorescent molecules, in order to efficiently reduce the size of the excitation beam so that it is smaller than the diffraction limit of light (Yamanaka et al., 2014). The use of STED provides increased resolution (20 nm and 60 nm) for the imaging of fluorescent proteins (Han et al., 2013). However, STED is not ideal for imaging live samples, as photo bleaching is common and can result in damage to the sample (Leung and Chou, 2011). Other techniques which are more suited to live cell imaging include localization microscopy techniques such as photo-activation localization microscopy (PALM), fluorescence PALM (FPALM) and stochastic optical reconstruction microscopy (STORM). The basis of these techniques is that a greater resolution can be gained by recording the illumination of one fluorescent probe at a time, then collecting many images and collating them, reducing the overlap between the fluorescent proteins and forming a high-resolution image (10-30nm). These techniques have the resolution to visualise ER-mitochondrial contact sites and can be conducted in live cells (Biteen et al., 2008; van de Linde et al., 2011; Shroff et al., 2008). However, the requirement to collate many images means temporal resolution is low and that dynamic processes cannot

be visualised (Yamanaka et al., 2014). Other super-resolution microscopy techniques use a more optical approach, in order to improve the resolution of wide-field microscopy. These include structural illumination microscopy (SIM) and saturated SIM (SSIM). SIM treats the wide-field image as an unknown, following on from which a known grid is overlaid, thereby producing moire fringes. Subtraction of the moire fringes allows further information to be extracted. SIM however is still diffraction limited and so higher frequency harmonics are introduced into the moire pattern to increase the resolution further. In theory, SSIM can produce a resolution well below the diffraction limit, however photo bleaching is a large problem for biological samples and so a resolution of approximately 50 nm is the best that can be achieved (Rego et al., 2012). SSIM has already been used to visualise ER-Mito contact sites to date (Stoica et al., 2016) and there is potential for it to be used in live cell imaging. However, a specialised microscope is needed, the technique is highly computation heavy and like with all deconvolution microscopy, artefacts can remain. Each of these methods have their own advantages and disadvantages, however they do not appear to be well suited to imaging dynamic structures in real time.

6.4.2 Fluorescent protein based systems

One of the aims of this project was to develop and investigate a new tool which would allow easy visualisation of ER-mitochondria contact sites. Two strategies were used: the BiFC and ddGFP system. The BiFC system is able to produce GFP fluorescence under basal conditions and can detect physiological increases in ER-mitochondrial contact sites. However, decreases in ER-mitochondrial contact sites by the knockdown of PTPIP51 or VAPB were unable to be detected, suggesting that the BiFC probes are not sensitive to all modulations of ER-mitochondrial contacts. The ddGFP system was also functional, however due to time restraints was unable to be tested for its ability to report on the modulation of ER-mitochondrial contact sites. The ddGFP system has been used previously to examine ER-mitochondrial contact sites. In the previous system, ER protein calnexin and the OMM protein TOM20 were fused to ddGFPB and ddGFPA, respectively. Once expressed, GFP fluorescence was observed which appeared mitochondrial in localisation but also partially co-localised with the ER (Alford et al., 2012a). When the ddGFP calnexin/TOM20 system was compared to the ddGFP VAPBTM/PTPIP51TM system, it was observed that the ddGFP calnexin/TOM20 system had a decreased GFP fluorescence. This suggests that fewer ER-mitochondria contact sites were being detected. Potential reasons for this could be due the difference in design of

the two sets of probes. For example, Alford et al use full length calnexin and full length TOM20 while our system used only the transmembrane domains of PTPIP51 and VAPB. It could be hypothesized that as calnexin has an extended cytosolic P domain and globular domain (Leach et al., 2002) in addition to the GFP, this may limit the ability of the ddGFPA and ddGFPB domains to dimerize, reducing the GFP signal (**Fig 6.2**). It was also hypothesized that the use of only the membrane targeting sequences would produce probes of a more appropriate length. This would increase their ability to dimerise, producing more GFP fluorescence. It is also thought that use of the TMDs of PTPIP51 and VAPB confers advantages over the use of full length PTPIP51 or VAPB, as overexpression of the full length versions are known to alter ER-mitochondrial contact sites (Stoica et al., 2014). As calnexin has been reported to be present in ER-mitochondrial contact sites whereas TOM20 has not (Lynes et al., 2012; Myhill et al., 2008), there may be limited availability for these probes to bind when compared to VAPB or PTPIP51, which are known to be present in ER-mitochondrial contact sites. This discussion highlights the advantages and disadvantages of the two systems and suggests potential lessons to be learnt from both sets of ddGFP probes.

From our investigation of the ddGFP probes, it was observed that in some cells the mitochondrial morphology appeared to be clumped, while others appeared to have a normal mitochondrial network. This is thought to be related to expression of the probes themselves. With increased amount of expression there could be an increased amount of ddGFP probes binding at one time, potentially tethering the ER and mitochondria together. In support of this, the BiFC system shows a similar phenotype with changes in mitochondria morphology also being observed. The BiFC system has previously been reported to fold irreversibly when forming the mVenus fluorophore (Hu et al., 2002; Kodama and Hu, 2010; Robida and Kerppola, 2009), which may suggest that the clumped mitochondrial phenotype observed with the ddGFP probes is also due to a tendency to bind together. One way to overcome this issue would be to optimize the expression levels of the ddGFP probes. Expressing less of each probe would decrease the amount of dimerization that occurs, thereby preventing artificial changes to mitochondrial morphology which may affect the results. In addition, these probes should also be amenable to investigate ER-mitochondria contacts in real time in living cells.

Another system which could alleviate some of these difficulties could employ fluorescence resonance energy transfer (FRET). FRET is a collision free but

distance-dependent process, which involves the transfer of energy from one excited donor fluorophore to a suitable acceptor protein or fluorophore (Shrestha et al., 2015). In the FRET based system, a donor or acceptor fluorophore could be fused to the TMD of PTPIP51 or VAPB. As the ER and mitochondria come into close apposition at ER-mitochondria contact sites, more fluorophores would come into proximity, allowing the FRET process to occur. This means that when the donor fluorophore is excited, the two FRET based probes would be close enough to allow energy transfer from the donor fluorophore to the acceptor fluorophore. The fluorescence of the acceptor fluorophore could then be detected and measured. This method would hopefully be reversible as no protein folding or binding is required. As FRET is intrinsically sensitive to molecule distance, it may also be a read out not only for an increase in ER-mitochondrial contact sites, but also of how close the ER and mitochondria are to each other (Shrestha et al., 2015). However, separating these two phenomena from each other may be problematic as an increase in GFP fluorescence maybe seen in both circumstances. Nevertheless, the use of fluorescent protein based systems is promising for investigating dynamic ER-mitochondrial contact sites in real time.

6.5 Further work

Mitochondrial dysfunction contributes to PD and it has been highlighted that ER-mitochondrial contact sites are involved with quality control, playing an important role in mitochondrial fission as well as regulating Ca^{2+} entry into the mitochondria (Friedman et al., 2011; Lee and Voeltz, 2015). Furthermore, PINK1 has been shown to increase ER-mitochondria contact sites after induction of mitophagy, suggesting that ER-mitochondria contacts are involved in the PINK1/Parkin pathway (Gelmetti et al., 2017). The fluorescent protein based system can be used to understand the function of ER-mitochondrial contacts during dynamic processes such as mitophagy or mitochondrial fission. In addition, this could be conducted in a variety of cell types, including patient-derived cells, in order to investigate ER-mitochondria contact sites in PD. There is a lot of potential for using a fluorescent protein based system to investigate ER-mitochondrial contact sites in PD, as well as in other neurodegenerative diseases. Previously there have been limitations due to the inability to see ER-mitochondrial contacts in real time. With these probes, and others like them, ER-mitochondrial contact sites could be observed with a fluorescent light or confocal microscope.

With its ease of use, these probes can be used to investigate the effects of PINK1/Parkin pathway related proteins and lipids, potentially including PI4KB or SYNJ1. A predominant theme of this thesis was to investigate the impact of PI's on mitochondrial quality control in the PINK1/Parkin pathway. With new evidence that PI's are present at ER mitochondrial contact sites, the probes would allow us to easily investigate the impact of PI's, in particular PI4P, on ER-mitochondrial contact formation. We could then investigate how they may later impact the PINK1/Parkin pathway with regards to changes ER-mitochondrial contact sites. Importantly, as these investigations can all be conducted in real time, the temporal dynamics of ER-mitochondrial contact sites can be assessed.

The work in this thesis has highlighted that PI and its derivatives may help to regulate mitochondrial quality control by acting alongside the PINK1/Parkin pathway, as alteration in PI metabolism enzymes can result in a slowing of Parkin translocation and mitophagy. Furthermore, this work has provided the foundation to develop a workable ER-mitochondrial contact site reporter tool. This tool has opened up the possibility to investigate new regulatory proteins that may impact on ER-mitochondrial contact sites. Many membrane tethers have been identified, with some acting as physical tethers (VAPB and PTPIP51) or functional tethers (Mfn2, Grp75, IP3R and VDAC). However, there is still a lot which remains unknown about how ER- mitochondria sites are regulated and this can be particularly difficult to determine. The fluorescence protein based system uses confocal or light microscopy and so is amenable for high throughput analysis. An RNAi screen would be an obvious choice to find new regulators, with the screening parameter being an increase or decrease in GFP fluorescence. This could potentially uncover novel regulators that may not have been found using a biased approach.

7. REFERENCES

Alexander, C., Votruba, M., Pesch, U.E., Thiselton, D.L., Mayer, S., Moore, a, Rodriguez, M., Kellner, U., Leo-Kottler, B., Auburger, G., et al. (2000). OPA1, encoding a dynamin-related GTPase, is mutated in autosomal dominant optic atrophy linked to chromosome 3q28. *Nat. Genet.* 26, 211–215.

Alford, S.C., Ding, Y., Simmen, T., and Campbell, R.E. (2012a). Dimerization-dependent green and yellow fluorescent proteins. *ACS Synth. Biol.* 1, 569–575.

Alford, S.C., Abdelfattah, A.S., Ding, Y., and Campbell, R.E. (2012b). A fluorogenic red fluorescent protein heterodimer. *Chem. Biol.* 19, 353–360.

Antonsson, B. (1997). Phosphatidylinositol synthase from mammalian tissues. *Biochim. Biophys. Acta - Lipids Lipid Metab.* 1348, 179–186.

Appel-Cresswell, S., Vilarino-Guell, C., Encarnacion, M., Sherman, H., Yu, I., Shah, B., Weir, D., Thompson, C., Szu-Tu, C., Trinh, J., et al. (2013). Alpha-synuclein p.H50Q, a novel pathogenic mutation for Parkinson's disease. *Mov. Disord.* 28, 811–813.

Argos, P. (1990). An investigation of oligopeptides linking domains in protein tertiary structures and possible candidates for general gene fusion. *J. Mol. Biol.* 211, 943–958.

Auluck, P.K., Chan, H.Y.E., Trojanowski, J.Q., Lee, V.M.Y., and Bonini, N.M. (2002). Chaperone suppression of alpha-synuclein toxicity in a *Drosophila* model for Parkinson's disease. *Science* 295, 865–868.

Bae, J.R., and Lee, B.D. (2015). Function and dysfunction of leucine-rich repeat kinase 2 (LRRK2): Parkinson's disease and beyond. *BMB Rep.* 48, 243–248.

Balla, A., Vereb, G., Gülkan, H., Gehrman, T., Gergely, P., Heilmeyer Jr, L.M.G., and Antal, M. (2000). Immunohistochemical localisation of two phosphatidylinositol 4-kinase isoforms, PI4K230 and PI4K92, in the central nervous system of rats. *Exp. Brain Res.* 134, 279–288.

Balla, A., Tuymetova, G., Barshishat, M., Geiszt, M., and Balla, T. (2002). Characterization of type II phosphatidylinositol 4-kinase isoforms reveals association of the enzymes with endosomal vesicular compartments. *J. Biol. Chem.* 277, 20041–20050.

Baughman, J.M., Perocchi, F., Girgis, H.S., Plovanich, M., Belcher-Timme, C.A., Sancak, Y., Bao, X.R., Strittmatter, L., Goldberger, O., Bogorad, R.L., et al. (2011). Integrative genomics identifies MCU as an essential component of the mitochondrial calcium uniporter. *Nature* 476, 341–345.

Bell, A.W., Ward, M.A., Blackstock, W.P., Freeman, H.N.M., Choudhary, J.S., Lewis, A.P., Chotai, D., Fazel, A., Gushue, J.N., Paiement, J., et al. (2001). Proteomics Characterization of Abundant Golgi Membrane Proteins. *J. Biol. Chem.*

276, 5152–5165.

Bertolotti, A., Zhang, Y., Hendershot, L.M., Harding, H.P., and Ron, D. (2000). Dynamic interaction of BiP and ER stress transducers in the unfolded-protein response. *Nat. Cell Biol.* 2, 326–332.

Bindoff, L.A., Birch-Machin, M., Cartlidge, N.E., Parker, W.D., and Turnbull, D.M. (1989). Mitochondrial function in Parkinson's disease. *Lancet* 2, 49.

Biteen, J.S., Thompson, M. a, Tselentis, N.K., Bowman, G.R., Shapiro, L., and Moerner, W.E. (2008). Super-resolution imaging in live *Caulobacter crescentus* cells using photoswitchable EYFP. *Nat. Methods* 5, 947–949.

Böckler, S., and Westermann, B. (2014). Mitochondrial ER contacts are crucial for mitophagy in yeast. *Dev. Cell* 28, 450–458.

Bonifati, V., Rizzu, P., Squitieri, F., Krieger, E., Vanacore, N., van Swieten, J.C., Brice, A., van Duijn, C.M., Oostra, B., Meco, G., et al. (2003). DJ-1 (PARK7), a novel gene for autosomal recessive, early onset parkinsonism. *Neurol. Sci.* 24, 159–160.

Boura, E., and Nencka, R. (2015). Phosphatidylinositol 4-kinases: Function, structure, and inhibition. *Exp. Cell Res.* 337, 136–145.

Braak, H., Del Tredici, K., Rüb, U., De Vos, R.A.I., Jansen Steur, E.N.H., and Braak, E. (2003). Staging of brain pathology related to sporadic Parkinson's disease. *Neurobiol. Aging* 24, 197–211.

Braak, H., Ghebremedhin, E., Rüb, U., Bratzke, H., and Del Tredici, K. (2004). Stages in the development of Parkinson's disease-related pathology. *Cell Tissue Res.* 318, 121–134.

Braak, H., Bohl, J.R., Müller, C.M., Rüb, U., de Vos, R.A.I., and Del Tredici, K. (2006). Stanley Fahn lecture 2005: The staging procedure for the inclusion body pathology associated with sporadic Parkinson's disease reconsidered. *Mov. Disord.* 21, 2042–2051.

Bravo, R., Vicencio, J.M., Parra, V., Troncoso, R., Munoz, J.P., Bui, M., Quiroga, C., Rodriguez, A.E., Verdejo, H.E., Ferreira, J., et al. (2011). Increased ER-mitochondrial coupling promotes mitochondrial respiration and bioenergetics during early phases of ER stress. *J. Cell Sci.* 124, 2511–2511.

Brice, S.E., Alford, C.W., and Cowart, L.A. (2009). Modulation of sphingolipid metabolism by the phosphatidylinositol-4-phosphate phosphatase Sac1p through regulation of phosphatidylinositol in *Saccharomyces cerevisiae*. *J. Biol. Chem.* 284, 7588–7596.

de Brito, O.M., and Scorrano, L. (2008). Mitofusin 2 tethers endoplasmic reticulum to mitochondria. *Nature* 456, 605–610.

Brobeil, A., Bobrich, M., and Wimmer, M. (2011). Protein tyrosine phosphatase interacting protein 51--a jack-of-all-trades protein. *Cell Tissue Res.* 344, 189–205.

Burke, J.E., Inglis, A.J., Perisic, O., Masson, G.R., McLaughlin, S.H., Rutaganira, F., Shokat, K.M., and Williams, R.L. (2014). Structures of PI4KIII complexes show simultaneous recruitment of Rab11 and its effectors. *Science (80-.)*. 344, 1035–1038.

Burre, J., Sharma, M., Tsetsenis, T., Buchman, V., Etherton, M.R., and Sudhof, T.C. (2010). -Synuclein Promotes SNARE-Complex Assembly in Vivo and in Vitro. *Science (80-.)*. 329, 1663–1667.

Calì, T., Ottolini, D., Negro, A., and Brini, M. (2013). Enhanced parkin levels favor ER-mitochondria crosstalk and guarantee Ca²⁺ transfer to sustain cell bioenergetics. *Biochim. Biophys. Acta - Mol. Basis Dis.* 1832, 495–508.

Campbell, R.E., Campbell, R.E., Tour, O., Tour, O., Palmer, A.E., Palmer, A.E., Steinbach, P. a, Steinbach, P. a, Baird, G.S., Baird, G.S., et al. (2002). A monomeric red fluorescent protein. *Proc. Natl. Acad. Sci. U. S. A.* 99, 7877–7882.

Cao, M., Wu, Y., Ashrafi, G., McCartney, A.J., Wheeler, H., Bushong, E.A., Boassa, D., Ellisman, M.H., Ryan, T.A., and De Camilli, P. (2017). Parkinson Sac Domain Mutation in Synaptojanin 1 Impairs Clathrin Uncoating at Synapses and Triggers Dystrophic Changes in Dopaminergic Axons. *Neuron* 93, 882–896.e5.

Cárdenas, C., Miller, R.A., Smith, I., Bui, T., Molgó, J., Müller, M., Vais, H., Cheung, K.H., Yang, J., Parker, I., et al. (2010). Essential Regulation of Cell Bioenergetics by Constitutive InsP3 Receptor Ca²⁺ Transfer to Mitochondria. *Cell* 142, 270–283.

Caudle, W.M., Richardson, J.R., Wang, M.Z., Taylor, T.N., Guillot, T.S., McCormack, A.L., Colebrooke, R.E., Di Monte, D. a, Emson, P.C., and Miller, G.W. (2007). Reduced vesicular storage of dopamine causes progressive nigrostriatal neurodegeneration. *J. Neurosci.* 27, 8138–8148.

Chakrabarti, A., Chen, A.W., and Varner, J.D. (2011). A review of the mammalian unfolded protein response. *Biotechnol. Bioeng.* 108, 2777–2793.

Chami, M., Oulès, B., Szabadkai, G., Tacine, R., Rizzuto, R., and Paterlini-Bréchet, P. (2008). Role of SERCA1 Truncated Isoform in the Proapoptotic Calcium Transfer from ER to Mitochondria during ER Stress. *Mol. Cell* 32, 641–651.

Chan, C.S., Gertler, T.S., and Surmeier, D.J. (2009). Calcium homeostasis, selective vulnerability and Parkinson's disease. *Trends Neurosci.* 32, 249–256.

Chartier-Harlin, M.C., Kachergus, J., Roumier, C., Mouroux, V., Douay, X., Lincoln, S., Levecque, C., Larvor, L., Andrieux, J., Hulihan, M., et al. (2004). alpha-Synuclein locus duplication as a cause of familial Parkinson's disease. *Lancet* 364, 1167–1169.

Chartier-Harlin, M.C., Dachsel, J.C., Vilarinho-Güell, C., Lincoln, S.J., Leprêtre, F., Hulihan, M.M., Kachergus, J., Milnerwood, A.J., Tapia, L., Song, M.S., et al. (2011). Translation initiator EIF4G1 mutations in familial parkinson disease. *Am. J. Hum. Genet.* *89*, 398–406.

Chaudhuri, K.R., Healy, D.G., and Schapira, A.H. V (2006). Non-motor symptoms of Parkinson's disease: diagnosis and management. *Lancet. Neurol.* *5*, 235–245.

Chen, X., Zaro, J.L., and Shen, W.C. (2013). Fusion protein linkers: Property, design and functionality. *Adv. Drug Deliv. Rev.* *65*, 1357–1369.

Chin, L.-S., and Li, L. (2016). Ubiquitin phosphorylation in Parkinson's disease: Implications for pathogenesis and treatment. *Transl. Neurodegener.* *5*, 1.

Chu, C.T., Ji, J., Dagda, R.K., Jiang, J.F., Tyurina, Y.Y., Kapralov, A. a, Tyurin, V. a, Yanamala, N., Shrivastava, I.H., Mohammadyani, D., et al. (2013). Cardiolipin externalization to the outer mitochondrial membrane acts as an elimination signal for mitophagy in neuronal cells. *Nat. Cell Biol.* *15*, 1197–1205.

Chung, J., Nakatsu, F., Baskin, J.M., and De Camilli, P. (2015). Plasticity of PI4KIIIalpha interactions at the plasma membrane. *EMBO Rep.* *16*, 312–320.

Clark, I.E., Dodson, M.W., Jiang, C., Cao, J.H., Huh, J.R., Seol, J.H., Yoo, S.J., Hay, B. a, and Guo, M. (2006). Drosophila pink1 is required for mitochondrial function and interacts genetically with parkin. *Nature* *441*, 1162–1166.

Cook, C., Stetler, C., and Petrucelli, L. (2012). Disruption of protein quality control in Parkinson's disease. *Cold Spring Harb. Perspect. Med.* *2*.

Cosson, P., Marchetti, A., Ravazzola, M., and Orci, L. (2012). Mitofusin-2 Independent Juxtaposition of Endoplasmic Reticulum and Mitochondria: An Ultrastructural Study. *PLoS One* *7*.

Cremona, O., Di Paolo, G., Wenk, M.R., Lüthi, a, Kim, W.T., Takei, K., Daniell, L., Nemoto, Y., Shears, S.B., Flavell, R. a, et al. (1999a). Essential role of phosphoinositide metabolism in synaptic vesicle recycling. *Cell* *99*, 179–188.

Cremona, O., Di Paolo, G., Wenk, M.R., Lüthi, A., Kim, W.T., Takei, K., Daniell, L., Nemoto, Y., Shears, S.B., Flavell, R.A., et al. (1999b). Essential role of phosphoinositide metabolism in synaptic vesicle recycling. *Cell* *99*, 179–188.

Csordás, G., Renken, C., Várnai, P., Walter, L., Weaver, D., Buttle, K.F., Balla, T., Mannella, C.A., and Hajnóczky, G. (2006). Structural and functional features and significance of the physical linkage between ER and mitochondria. *J. Cell Biol.* *174*, 915–921.

Csordás, G., Várnai, P., Golenár, T., Roy, S., Purkins, G., Schneider, T.G., Balla, T., and Hajnóczky, G. (2010). Imaging Interorganelle Contacts and Local Calcium Dynamics at the ER-Mitochondrial Interface. *Mol. Cell* *39*, 121–132.

Daboussi, L., Costaguta, G., and Payne, G.S. (2012). Phosphoinositide-mediated clathrin adaptor progression at the trans-Golgi network. *Nat. Cell Biol.* 14, 239–248.

Dauer, W., and Przedborski, S. (2003). Parkinson's disease: mechanisms and models. *Neuron* 39, 889–909.

Dawson, T.M., Ko, H.S., and Dawson, V.L. (2010). Genetic animal models of Parkinson's disease. *Neuron* 66, 646–661.

Deas, E., Plun-Favreau, H., Gandhi, S., Desmond, H., Kjaer, S., Loh, S.H.Y., Renton, A.E.M., Harvey, R.J., Whitworth, A.J., Martins, L.M., et al. (2011). PINK1 cleavage at position A103 by the mitochondrial protease PARL. *Hum. Mol. Genet.* 20, 867–879.

Delettre, C., Lenaers, G., Griffoin, J.M., Gigarel, N., Lorenzo, C., and Belenger, P. (2000). Nuclear gene OPA1, encoding a mitochondrial dynamin-related protein, is mutated in dominant optic atrophy. *Nat Genet* 26.

Demmel, L., Gravert, M., Ercan, E., Habermann, B., Müller-Reichert, T., Kukhtina, V., Haucke, V., Baust, T., Sohrmann, M., Kalaidzidis, Y., et al. (2008). The clathrin adaptor Gga2p is a phosphatidylinositol 4-phosphate effector at the Golgi exit. *Mol. Biol. Cell* 19, 1991–2002.

Denison, S.R., Wang, F., Becker, N. a, Schüle, B., Kock, N., Phillips, L. a, Klein, C., and Smith, D.I. (2003). Alterations in the common fragile site gene Parkin in ovarian and other cancers. *Oncogene* 22, 8370–8378.

Denton, R.M. (2009). Regulation of mitochondrial dehydrogenases by calcium ions. *Biochim. Biophys. Acta - Bioenerg.* 1787, 1309–1316.

Dias, V., Junn, E., and Mouradian, M.M. (2013). The role of oxidative stress in Parkinson's disease. *J. Parkinsons. Dis.* 3, 461–491.

Dippold, H.C., Ng, M.M., Farber-Katz, S.E., Lee, S.K., Kerr, M.L., Peterman, M.C., Sim, R., Wiharto, P.A., Galbraith, K.A., Madhavarapu, S., et al. (2009). GOLPH3 Bridges Phosphatidylinositol-4- Phosphate and Actomyosin to Stretch and Shape the Golgi to Promote Budding. *Cell* 139, 337–351.

Dorn, G.W. (2010). Mitochondrial pruning by nix and BNip3: An essential function for cardiac-expressed death factors. *J. Cardiovasc. Transl. Res.* 3, 374–383.

Drouet, V., and Lesage, S. (2014). Synaptotagmin 1 Mutation in Parkinson's Disease Brings Further Insight into the Neuropathological Mechanisms. *Biomed Res. Int.* 2014.

Edvardson, S., Cinnamon, Y., Ta-Shma, A., Shaag, A., Yim, Y.I., Zenvirt, S., Jalas, C., Lesage, S., Brice, A., Taraboulos, A., et al. (2012). A deleterious mutation in DNAJC6 encoding the neuronal-specific clathrin-uncoating Co-chaperone auxilin, is associated with juvenile parkinsonism. *PLoS One* 7.

Fang, D., Yan, S., Yu, Q., Chen, D., and Yan, S.S. (2016). Mfn2 is Required for Mitochondrial Development and Synapse Formation in Human Induced Pluripotent Stem Cells/hiPSC Derived Cortical Neurons. *Sci. Rep.* 6, 31462.

Farrer, M., Chan, P., Chen, R., Tan, L., Lincoln, S., Hernandez, D., Forno, L., Gwinn-Hardy, K., Petrucelli, L., Hussey, J., et al. (2001). Lewy bodies and parkinsonism in families with parkin mutations. *Ann. Neurol.* 50, 293–300.

Farrer, M., Kachergus, J., Forno, L., Lincoln, S., Wang, D.S., Hulihan, M., Maraganore, D., Gwinn-Hardy, K., Wszolek, Z., Dickson, D., et al. (2004). Comparison of Kindreds with Parkinsonism and α -Synuclein Genomic Multiplications. *Ann. Neurol.* 55, 174–179.

Ferguson, S., and De Camilli, P. (2012). Dynamin, a membrane remodelling GTPase. *Nat Rev Mol Cell Biol* 13, 75–88.

Filadi, R., Greotti, E., Turacchio, G., Luini, A., Pozzan, T., and Pizzo, P. (2015). Mitofusin 2 ablation increases endoplasmic reticulum-mitochondria coupling. *Proc. Natl. Acad. Sci. U. S. A.* 112, E2174–E2181.

Filadi, R., Theurey, P., and Pizzo, P. (2017). The endoplasmic reticulum-mitochondria coupling in health and disease: Molecules, functions and significance. *Cell Calcium* 62, 1–15.

Di Fonzo, A., Dekker, M.C.J., Montagna, P., Baruzzi, A., Yonova, E.H., Correia Guedes, L., Szczerbinska, A., Zhao, T., Dubbel-Hulsman, L.O.M., Wouters, C.H., et al. (2009). FBXO7 mutations cause autosomal recessive, early-onset parkinsonian-pyramidal syndrome. *Neurology* 72, 240–245.

Forno, L.S. (1996). Neuropathology of Parkinson's Disease. *J. Neuropathol. & Exp. Neurol.* 55, 259 LP-272.

Forrest, S., Chai, A., Sanhueza, M., Marescotti, M., Parry, K., Georgiev, A., Sahota, V., Mendez-castro, R., and Pennetta, G. (2013). Increased levels of phosphoinositides cause neurodegeneration in a Drosophila model of amyotrophic lateral sclerosis. 22, 2689–2704.

Friedman, J.R., Lackner, L.L., West, M., DiBenedetto, J.R., Nunnari, J., and Voeltz, G.K. (2011). ER tubules mark sites of mitochondrial division. *Science* 334, 358–362.

Fuchs, J., Tichopad, A., Golub, Y., Munz, M., Schweitzer, K.J., Wolf, B., Berg, D., Mueller, J.C., and Gasser, T. (2008). Genetic variability in the SNCA gene influences alpha-synuclein levels in the blood and brain. *FASEB J.* 22, 1327–1334.

Gaidarov, I., Chen, Q., John, R., Falck, Reddy, K.K., and Keen, J.H. (1996). A functional phosphatidylinositol 3,4,5-trisphosphate/phosphoinositide binding domain in the clathrin adaptor AP-2 α subunit. Implications for the endocytic pathway. *J. Biol. Chem.* 271, 20922–20929.

Gandre-Babbe, S., and van der Bliek, A.M. (2008). The novel tail-anchored membrane protein Mff controls mitochondrial and peroxisomal fission in mammalian cells. *Mol. Biol. Cell* 19, 2402–2412.

Gao, F., Chen, D., Si, J., Hu, Q., Qin, Z., Fang, M., and Wang, G. (2015). The mitochondrial protein BNIP3L is the substrate of PARK2 and mediates mitophagy in PINK1/PARK2 pathway. *Hum. Mol. Genet.* 24, 2528–2538.

Gasser, T., Müller-Myhsok, B., Wszolek, Z.K., Oehlmann, R., Calne, D.B., Bonifati, V., Bereznoi, B., Fabrizio, E., Vieregge, P., and Horstmann, R.D. (1998). A susceptibility locus for Parkinson's disease maps to chromosome 2p13. *Nat. Genet.* 18, 262–265.

Gautier, C.A., Erpapazoglou, Z., Mouton-Liger, F., Muriel, M.P., Cormier, F., Bigou, S., Duffaure, S., Girard, M., Foret, B., Iannielli, A., et al. (2016). The endoplasmic reticulum-mitochondria interface is perturbed in PARK2 knockout mice and patients with PARK2 mutations. *Hum. Mol. Genet.* 25, 2972–2984.

Geisler, S., Holmström, K.M., Skujat, D., Fiesel, F.C., Rothfuss, O.C., Kahle, P.J., and Springer, W. (2010a). PINK1/Parkin-mediated mitophagy is dependent on VDAC1 and p62/SQSTM1. *Nat. Cell Biol.* 12, 119–131.

Geisler, S., Holmström, K.M., Skujat, D., Fiesel, F.C., Rothfuss, O.C., Kahle, P.J., and Springer, W. (2010b). PINK1/Parkin-mediated mitophagy is dependent on VDAC1 and p62/SQSTM1. *Nat. Cell Biol.* 12, 119–131.

Gelmetti, V., De Rosa, P., Torosantucci, L., Marini, E.S., Romagnoli, A., Di Rienzo, M., Arena, G., Vignone, D., Fimia, G.M., and Valente, E.M. (2017). PINK1 and BECN1 relocalize at mitochondria-associated membranes during mitophagy and promote ER-mitochondria tethering and autophagosome formation. *Autophagy* 13, 654–669.

Geng, J., Wang, L., Lee, J.Y., Chen, C.-K., and Chang, K.T. (2016). Phosphorylation of Synaptojanin Differentially Regulates Endocytosis of Functionally Distinct Synaptic Vesicle Pools. *J. Neurosci.* 36, 8882–8894.

Giacomello, M., Drago, I., Bortolozzi, M., Scorzeto, M., Gianelle, A., Pizzo, P., and Pozzan, T. (2010). Ca²⁺ Hot Spots on the Mitochondrial Surface Are Generated by Ca²⁺ Mobilization from Stores, but Not by Activation of Store-Operated Ca²⁺ Channels. *Mol. Cell* 38, 280–290.

Gincel, D., Zaid, H., and Shoshan-Barnatz, V. (2001). Calcium binding and translocation by the voltage-dependent anion channel: a possible regulatory mechanism in mitochondrial function. *Biochem. J.* 358, 147–155.

Godi, A., Pertile, P., Meyers, R., Marra, P., Di Tullio, G., Iurisci, C., Luini, A., Corda, D., and De Matteis, M.A. (1999). ARF mediates recruitment of PtdIns-4-OH kinase-

beta and stimulates synthesis of PtdIns(4,5)P₂ on the Golgi complex. *Nat. Cell Biol.* *1*, 280–287.

Gomes, L.C., Benedetto, G. Di, and Scorrano, L. (2011). During autophagy mitochondria elongate, are spared from degradation and sustain cell viability. *Nat. Cell Biol.* *13*, 589–598.

Gorell, J.M., Johnson, C.C., Rybicki, B. a, Peterson, E.L., and Richardson, R.J. (1998). The risk of Parkinson's disease with exposure to pesticides, farming, well water, and rural living. *Neurology* *50*, 1346–1350.

Goris, A., Williams-Gray, C.H., Clark, G.R., Foltynie, T., Lewis, S.J.G., Brown, J., Ban, M., Spillantini, M.G., Compston, A., Burn, D.J., et al. (2007). Tau and alpha-synuclein in susceptibility to, and dementia in, Parkinson's disease. *Ann. Neurol.* *62*, 145–153.

Grace, A.A., and Bunney, B.S. (1983). Intracellular and extracellular electrophysiology of nigral dopaminergic neurons-2. Action potential generating mechanisms and morphological correlates. *Neuroscience* *10*.

Greene, A.W., Grenier, K., Aguilera, M. a, Muise, S., Farazifard, R., Haque, M.E., McBride, H.M., Park, D.S., and Fon, E. a (2012). Mitochondrial processing peptidase regulates PINK1 processing, import and Parkin recruitment. *EMBO Rep.* *13*, 378–385.

Greene, J.C., Whitworth, A.J., Kuo, I., Andrews, L.A., Feany, M.B., and Pallanck, L.J. (2003). Mitochondrial pathology and apoptotic muscle degeneration in *Drosophila parkin* mutants. *Proc. Natl. Acad. Sci. U. S. A.* *100*, 4078–4083.

Grenier, K., McLelland, G.L., and Fon, E.A. (2013). Parkin- and PINK1-dependent mitophagy in neurons: Will the real pathway please stand up? *Front. Neurol.* *4 JUL*.

Griffin, E.E., Graumann, J., and Chan, D.C. (2005). The WD40 protein Caf4p is a component of the mitochondrial fission machinery and recruits Dnm1p to mitochondria. *J. Cell Biol.* *170*, 237–248.

Guardia-Laguarta, C., Area-Gomez, E., Rüb, C., Liu, Y., Magrané, J., Becker, D., Voos, W., Schon, E. a, and Przedborski, S. (2014). α -Synuclein Is Localized to Mitochondria-Associated ER Membranes. *J. Neurosci.* *34*, 249–259.

Guo, J., Wenk, M.R., Pellegrini, L., Onofri, F., Benfenati, F., and De Camilli, P. (2003). Phosphatidylinositol 4-kinase type IIalpha is responsible for the phosphatidylinositol 4-kinase activity associated with synaptic vesicles. *Proc. Natl. Acad. Sci. U. S. A.* *100*, 3995–4000.

Hamacher-Brady, A., and Brady, N.R. (2016). Mitophagy programs: Mechanisms and physiological implications of mitochondrial targeting by autophagy. *Cell. Mol. Life Sci.* *73*, 775–795.

Hamasaki, M., Furuta, N., Matsuda, A., Nezu, A., Yamamoto, A., Fujita, N., Oomori, H., Noda, T., Haraguchi, T., Hiraoka, Y., et al. (2013). Autophagosomes form at ER-mitochondria contact sites. *Nature* 495, 389–393.

Han, R., Li, Z., Fan, Y., and Jiang, Y. (2013). Recent Advances in Super-Resolution Fluorescence Imaging and Its Applications in Biology. *J. Genet. Genomics* 40, 583–595.

Hanna, R.A., Quinsay, M.N., Orogo, A.M., Giang, K., Rikka, S., and Gustafsson, Å.B. (2012). Microtubule-associated protein 1 light chain 3 (LC3) interacts with Bnip3 protein to selectively remove endoplasmic reticulum and mitochondria via autophagy. *J. Biol. Chem.* 287, 19094–19104.

Hardy, J. (2010). Genetic analysis of pathways to parkinson disease. *Neuron* 68, 201–206.

Harris, J.J., Jolivet, R., and Attwell, D. (2012). Synaptic Energy Use and Supply. *Neuron* 75, 762–777.

Hatano, Y., Li, Y., Sato, K., Asakawa, S., Yamamura, Y., Tomiyama, H., Yoshino, H., Asahina, M., Kobayashi, S., Hassin-Baer, S., et al. (2004). Novel PINK1 mutations in early-onset parkinsonism. *Ann. Neurol.* 56, 424–427.

Hernandes, M.S., Café-Mendes, C.C., and Britto, L.R.G. (2013). NADPH oxidase and the degeneration of dopaminergic neurons in Parkinsonian mice. *Oxid. Med. Cell. Longev.*

Hichri, H., Rendu, J., Monnier, N., Coutton, C., Dorseuil, O., Poussou, R.V., Baujat, G., Blanchard, A., Nobili, F., Ranchin, B., et al. (2011). From lowe syndrome to Dent disease: Correlations between mutations of the OCRL1 gene and clinical and biochemical phenotypes. *Hum. Mutat.* 32, 379–388.

Hicks, A.A., Pétursson, H., Jónsson, T., Stefánsson, H., Jóhannsdóttir, H.S., Sainz, J., Frigge, M.L., Kong, A., Gulcher, J.R., Stefánsson, K., et al. (2002). A susceptibility gene for late-onset idiopathic Parkinson's disease. *Ann. Neurol.* 52, 549–555.

Hill-Burns, E.M., Wissemann, W.T., Hamza, T.H., Factor, S.A., Zabetian, C.P., and Payami, H. (2014). Identification of a novel Parkinson's disease locus via stratified genome-wide association study. *BMC Genomics* 15, 118.

Holmes, O., Paturi, S., Ye, W., Wolfe, M.S., and Selkoe, D.J. (2012). Effects of membrane lipids on the activity and processivity of purified γ -secretase. *Biochemistry* 51, 3565–3575.

Hsu, N.Y., Ilnytska, O., Belov, G., Santiana, M., Chen, Y.H., Takvorian, P.M., Pau, C., van der Schaar, H., Kaushik-Basu, N., Balla, T., et al. (2010). Viral reorganization of the secretory pathway generates distinct organelles for RNA

replication. *Cell* 141, 799–811.

Hu, Q., and Wang, G. (2016). Mitochondrial dysfunction in Parkinson's disease. *Transl. Neurodegener.* 5, 14.

Hu, C.D., Chinenov, Y., and Kerppola, T.K. (2002). Visualization of interactions among bZIP and Rel family proteins in living cells using bimolecular fluorescence complementation. *Mol. Cell* 9, 789–798.

Van Humbeeck, C., Cornelissen, T., Hofkens, H., Mandemakers, W., Gevaert, K., De Strooper, B., and Vandenberghe, W. (2011). Parkin interacts with Ambra1 to induce mitophagy. *J. Neurosci.* 31, 10249–10261.

Itoh, T., Erdmann, K.S., Roux, A., Habermann, B., Werner, H., and De Camilli, P. (2005). Dynamin and the actin cytoskeleton cooperatively regulate plasma membrane invagination by BAR and F-BAR proteins. *Dev. Cell* 9, 791–804.

Ivatt, R.M., Sanchez-Martinez, A., Godena, V.K., Brown, S., Ziviani, E., and Whitworth, A.J. (2014). Genome-wide RNAi screen identifies the Parkinson disease GWAS risk locus SREBF1 as a regulator of mitophagy. *Proc. Natl. Acad. Sci. U. S. A.* 111, 8494–8499.

Jackson-Lewis, V., and Przedborski, S. (2007). Protocol for the MPTP mouse model of Parkinson's disease. *Nat. Protoc.* 2, 141–151.

Jenner, P. (2003). Oxidative stress in Parkinson's disease. *Ann. Neurol.* 53 Suppl 3, S26-36-8.

Jin, S.M., and Youle, R.J. (2012). PINK1- and Parkin-mediated mitophagy at a glance. *J. Cell Sci.* 125, 795–799.

Jin, S.M., Lazarou, M., Wang, C., Kane, L.A., Narendra, D.P., and Youle, R.J. (2010). Mitochondrial membrane potential regulates PINK1 import and proteolytic destabilization by PARL. *J. Cell Biol.* 191, 933–942.

Jost, M., Simpson, F., Kavran, J.M., Lemmon, M.A., and Schmid, S.L. (1998). Phosphatidylinositol-4,5-bisphosphate is required for endocytic coated vesicle formation. *Curr. Biol.* 8, 1399–1404.

Jung, G., Wang, J., Wlodarski, P., Barylko, B., Binns, D.D., Shu, H., Yin, H.L., and Albanesi, J.P. (2008). Molecular determinants of activation and membrane targeting of phosphoinositol 4-kinase IIbeta. *Biochem. J.* 409, 501–509.

Jung, G., Barylko, B., Lu, D., Shu, H., Yin, H., and Albanesi, J.P. (2011). Stabilization of phosphatidylinositol 4-kinase type IIβ by interaction with Hsp90. *J. Biol. Chem.* 286, 12775–12784.

Kalia, L. V, and Lang, A.E. (2015). Parkinson's disease. *Lancet* 386, 896–912.

Kalinderi, K., Bostantjopoulou, S., and Fidani, L. (2016). The genetic background of Parkinson's disease: Current progress and future prospects. *Acta Neurol. Scand.*

Kane, L.A., Lazarou, M., Fogel, A.I., Li, Y., Yamano, K., Sarraf, S.A., Banerjee, S., and Youle, R.J. (2014). PINK1 phosphorylates ubiquitin to activate parkin E3 ubiquitin ligase activity. *J. Cell Biol.* 205, 143–153.

Kawaguchi, Y., Kovacs, J.J., McLaurin, A., Vance, J.M., Ito, A., and Yao, T.P. (2003). The deacetylase HDAC6 regulates aggresome formation and cell viability in response to misfolded protein stress. *Cell* 115, 727–738.

Kawajiri, S., Saiki, S., Sato, S., and Hattori, N. (2011). Genetic mutations and functions of PINK1. *Trends Pharmacol. Sci.* 32, 573–580.

Kazlauskaitė, A., Kondapalli, C., Gourlay, R., Campbell, D.G., Ritorto, M.S., Hofmann, K., Alessi, D.R., Knebel, A., Trost, M., and Muqit, M.M.K. (2014). Parkin is activated by PINK1-dependent phosphorylation of ubiquitin at Ser⁶⁵. *Biochem. J.* 460, 127–141.

Kempster, P.A., Hurwitz, B., and Lees, A.J. (2007). A new look at James Parkinson's Essay on the Shaking Palsy. *Neurology* 69, 482–485.

Kiely, A.P., Asi, Y.T., Kara, E., Limousin, P., Ling, H., Lewis, P., Proukakis, C., Quinn, N., Lees, A.J., Hardy, J., et al. (2013). A-synucleinopathy associated with G51D SNCA mutation: A link between Parkinson's disease and multiple system atrophy? *Acta Neuropathol.* 125, 753–769.

Kijima, K., Numakura, C., Izumino, H., Umetsu, K., Nezu, A., Shiiki, T., Ogawa, M., Ishizaki, Y., Kitamura, T., Shozawa, Y., et al. (2005). Mitochondrial GTPase mitofusin 2 mutation in Charcot-Marie-Tooth neuropathy type 2A. *Hum. Genet.* 116, 23–27.

Kirkin, V., Lamark, T., Johansen, T., and Dikic, I. (2009). NBR1 cooperates with p62 in selective autophagy of ubiquitinated targets. *Autophagy* 5, 732–733.

Kirola, L., Behari, M., Shishir, C., and Thelma, B.K. (2016). Identification of a novel homozygous mutation Arg459Pro in SYNJ1 gene of an Indian family with autosomal recessive juvenile Parkinsonism. *Park. Relat. Disord.* 31, 124–128.

Kitada, T., Asakawa, S., Hattori, N., Matsumine, H., Yamamura, Y., Minoshima, S., Yokochi, M., Mizuno, Y., and Shimizu, N. (1998a). Mutations in the parkin gene cause autosomal recessive juvenile parkinsonism. *392*, 605–608.

Kitada, T., Asakawa, S., Hattori, N., Matsumine, H., Yamamura, Y., Minoshima, S., Yokochi, M., Mizuno, Y., and Shimizu, N. (1998b). Mutations in the parkin gene cause autosomal recessive juvenile parkinsonism. *Nature* 392, 605–608.

Klein, C., Westenberger, A., Hollingworth, P., Harold, D., Jones, L., Owen, M.J., Williams, J., Marques, S.C.F., Oliveira, C.R., Pereira, C.M.F., et al. (2012). Genetics of Parkinson's Disease. *Int. J. Geriatr. Psychiatry* 26, a008888.

Kodama, Y., and Hu, C.D. (2010). An improved bimolecular fluorescence

complementation assay with a high signal-to-noise ratio. *Biotechniques* 49, 793–803.

Kondapalli, C., Kazlauskaitė, A., Zhang, N., Woodroof, H.I., Campbell, D.G., Gourlay, R., Burchell, L., Walden, H., Macartney, T.J., Deak, M., et al. (2012). PINK1 is activated by mitochondrial membrane potential depolarization and stimulates Parkin E3 ligase activity by phosphorylating Serine 65. *Open Biol.* 2, 120080–120080.

Kononenko, N.L., and Haucke, V. (2015). Molecular mechanisms of presynaptic membrane retrieval and synaptic vesicle reformation. *Neuron* 85, 484–496.

Kornmann, B., Currie, E., Collins, S.R., Schuldiner, M., Nunnari, J., Weissman, J.S., and Walter, P. (2009). An ER-mitochondria tethering complex revealed by a synthetic biology screen. *Science* 325, 477–481.

Koshiba, T., Detmer, S.A., Kaiser, J.T., Chen, H., McCaffery, J.M., and Chan, D.C. (2004). Structural basis of mitochondrial tethering by mitofusin complexes. *Science* (80-). 305, 858–862.

Koyano, F., Okatsu, K., Kosako, H., Tamura, Y., Go, E., Kimura, M., Kimura, Y., Tsuchiya, H., Yoshihara, H., Hirokawa, T., et al. (2014). Ubiquitin is phosphorylated by PINK1 to activate parkin. *Nature* 510, 162–166.

Kozutsumi, Y., Segal, M., Normington, K., Gething, M.-J., and Sambrook, J. (1988). The presence of malfolded proteins in the endoplasmic reticulum signals the induction of glucose-regulated proteins. *Nature* 332, 462–464.

Krebs, C.E., Karkheiran, S., Powell, J.C., Cao, M., Makarov, V., Darvish, H., Di Paolo, G., Walker, R.H., Shahidi, G.A., Buxbaum, J.D., et al. (2013a). The sac1 domain of SYNJ1 identified mutated in a family with early-onset progressive parkinsonism with generalized seizures. *Hum. Mutat.* 34, 1200–1207.

Krebs, C.E., Karkheiran, S., Powell, J.C., Cao, M., Makarov, V., Darvish, H., Di Paolo, G., Walker, R.H., Shahidi, G.A., Buxbaum, J.D., et al. (2013b). The Sac1 domain of SYNJ1 identified mutated in a family with early-onset progressive Parkinsonism with generalized seizures. *Hum. Mutat.* 34, 1200–1207.

Krüger, R., Kuhn, W., Müller, T., Voitalla, D., Graeber, M., Kösel, S., Przuntek, H., Eppelen, J.T., Schöls, L., and Riess, O. (1998). Ala30Pro mutation in the gene encoding alpha-synuclein in Parkinson's disease. *Nat. Genet.* 18, 106–108.

Kumazawa, R., Tomiyama, H., Li, Y., Imamichi, Y., Funayama, M., Yoshino, H., Yokochi, F., Fukusako, T., Takehisa, Y., Kashihara, K., et al. (2008). Mutation Analysis of the PINK1 Gene in 391 Patients With Parkinson Disease. *Arch. Neurol.* 65, 802–808.

Lazarou, M., Jin, S.M., Kane, L.A., and Youle, R.J. (2012). Role of PINK1 Binding to

the TOM Complex and Alternate Intracellular Membranes in Recruitment and Activation of the E3 Ligase Parkin. *Dev. Cell* 22, 320–333.

Leach, M.R., Cohen-Doyle, M.F., Thomas, D.Y., and Williams, D.B. (2002). Localization of the lectin, ERp57 binding, and polypeptide binding sites of calnexin and calreticulin. *J. Biol. Chem.* 277, 29686–29697.

Lee, J.E., and Voeltz, G. (2015). Multiple dynamin family members collaborate to drive mitochondrial division. *Mol. Biol. Cell. Conf. Annu. Meet. Am. Soc. Cell Biol. ASCB* 26, 1–17.

Lemasters, J.J. (2014). Variants of mitochondrial autophagy: Types 1 and 2 mitophagy and micromitophagy (Type 3). *Redox Biol.* 2, 749–754.

Leroy, E., Boyer, R., Auburger, G., Leube, B., Ulm, G., Mezey, E., Harta, G., Brownstein, M.J., Jonnalagada, S., Chernova, T., et al. (1998). The ubiquitin pathway in Parkinson's disease. *Nature* 395, 451–452.

Lesage, S., Anheim, M., Letournel, F., Bousset, L., Honoré, A., Rozas, N., Pieri, L., Madiona, K., Dürr, A., Melki, R., et al. (2013). G51D α -synuclein mutation causes a novel Parkinsonian-pyramidal syndrome. *Ann. Neurol.* 73, 459–471.

Leung, B.O., and Chou, K.C. (2011). Review of super-resolution fluorescence microscopy for biology. *Appl. Spectrosc.* 65, 967–980.

Li, J.-Q., Tan, L., and Yu, J.-T. (2014a). The role of the LRRK2 gene in Parkinsonism. *Mol. Neurodegener.* 9, 47.

Li, J.-Q., Tan, L., and Yu, J.-T. (2014b). The role of the LRRK2 gene in Parkinsonism. *Mol. Neurodegener.* 9, 47.

Li, Y., Tomiyama, H., Sato, K., Hatano, Y., Yoshino, H., Atsumi, M., Kitaguchi, M., Sasaki, S., Kawaguchi, S., Miyajima, H., et al. (2005). Clinicogenetic study of PINK1 mutations in autosomal recessive early-onset parkinsonism. *Neurology* 64, 1955–1957.

Lill, C.M. (2016). Genetics of Parkinson's disease. *Mol. Cell. Probes* 30, 386–396.

Lill, C.M., Roehr, J.T., McQueen, M.B., Kavvoura, F.K., Bagade, S., Schjeide, B.M.M., Schjeide, L.M., Meissner, E., Zauft, U., Allen, N.C., et al. (2012). Comprehensive research synopsis and systematic meta-analyses in Parkinson's disease genetics: The PDgene database. *PLoS Genet.* 8.

van de Linde, S., Löschberger, A., Klein, T., Heidbreder, M., Wolter, S., Heilemann, M., and Sauer, M. (2011). Direct stochastic optical reconstruction microscopy with standard fluorescent probes. *Nat. Protoc.* 6, 991–1009.

Liss, B., Franz, O., Sewing, S., Bruns, R., Neuhoff, H., and Roeper, J. (2001). Tuning pacemaker frequency of individual dopaminergic neurons by Kv4.3L and KChip3.1 transcription. *EMBO J.* 20, 5715–5724.

Liu, L., Sakakibara, K., Chen, Q., and Okamoto, K. (2014). Receptor-mediated mitophagy in yeast and mammalian systems. *Cell Res.* *24*, 787–795.

Liu, S., Sawada, T., Lee, S., Yu, W., Silverio, G., Alapatt, P., Millan, I., Shen, A., Saxton, W., Kanao, T., et al. (2012). Parkinson's disease-associated kinase PINK1 regulates miro protein level and axonal transport of mitochondria. *PLoS Genet.* *8*.

Lv, B.F., Yu, C.F., Chen, Y.Y., Lu, Y., Guo, J.H., Song, Q.S., Ma, D.L., Shi, T.P., and Wang, L. (2006). Protein tyrosine phosphatase interacting protein 51 (PTPIP51) is a novel mitochondria protein with an N-terminal mitochondrial targeting sequence and induces apoptosis. *Apoptosis* *11*, 1489–1501.

Lynes, E.M., Bui, M., Yap, M.C., Benson, M.D., Schneider, B., Ellgaard, L., Berthiaume, L.G., and Simmen, T. (2012). Palmitoylated TMX and calnexin target to the mitochondria-associated membrane. *EMBO J.* *31*, 457–470.

Macvicar, T.D.B., Mannack, L.V.J.C., Lees, R.M., and Lane, J.D. (2015). Targeted siRNA screens identify ER-to-mitochondrial calcium exchange in autophagy and mitophagy responses in RPE1 cells. *Int. J. Mol. Sci.* *16*, 13356–13380.

Magrinelli, F., Picelli, A., Tocco, P., Federico, A., Roncari, L., Smania, N., Zanette, G., and Tamburin, S. (2016). Pathophysiology of Motor Dysfunction in Parkinson's Disease as the Rationale for Drug Treatment and Rehabilitation. *Parkinsons. Dis.* *2016*.

Mallilankaraman, K., Cardenas, C., Doonan, P.J., Chandramoorthy, H.C., Irrinki, K.M., Golenar, T., Csordas, G., Madireddi, P., Yang, J., Muller, M., et al. (2012). MCUR1 is an essential component of mitochondrial Ca(2+) uptake that regulates cellular metabolism. *Nat Cell Biol* *14*, 1336–1343.

Mani, M., Lee, S.Y., Lucast, L., Cremona, O., Di Paolo, G., De Camilli, P., and Ryan, T.A. (2007). The Dual Phosphatase Activity of Synaptojanin1 Is Required for Both Efficient Synaptic Vesicle Endocytosis and Reavailability at Nerve Terminals. *Neuron* *56*, 1004–1018.

Maraganore, D.M., de Andrade, M., Elbaz, A., Farrer, M.J., Ioannidis, J.P., Krüger, R., Rocca, W.A., Schneider, N.K., Lesnick, T.G., Lincoln, S.J., et al. (2006). Collaborative analysis of alpha-synuclein gene promoter variability and Parkinson disease. *JAMA* *296*, 661–670.

Martinez-Vicente, M., Tallozy, Z., Kaushik, S., Massey, A.C., Mazzulli, J., Mosharov, E. V, Hodara, R., Fredenburg, R., Wu, D.-C., Follenzi, A., et al. (2008). Dopamine-modified alpha-synuclein blocks chaperone-mediated autophagy. *J. Clin. Invest.* *118*, 777–788.

Matsuda, N. (2016). Phospho-ubiquitin: Upending the PINK-Parkin-ubiquitin cascade. *J. Biochem.* *159*, 379–385.

Matsuda, N., Sato, S., Shiba, K., Okatsu, K., Saisho, K., Gautier, C.A., Sou, Y.S., Saiki, S., Kawajiri, S., Sato, F., et al. (2010). PINK1 stabilized by mitochondrial depolarization recruits Parkin to damaged mitochondria and activates latent Parkin for mitophagy. *J. Cell Biol.* *189*, 211–221.

Matsumoto, G., Wada, K., Okuno, M., Kurosawa, M., and Nukina, N. (2011). Serine 403 phosphorylation of p62/SQSTM1 regulates selective autophagic clearance of ubiquitinated proteins. *Mol. Cell* *44*, 279–289.

Mayinger, P. (2009). Regulation of Golgi function via phosphoinositide lipids. *Semin. Cell Dev. Biol.* *20*, 793–800.

McLelland, G.L., Soubannier, V., Chen, C.X., McBride, H.M., and Fon, E.A. (2014). Parkin and PINK1 function in a vesicular trafficking pathway regulating mitochondrial quality control. *EMBO J.* *33*, 282–295.

McMahon, H.T.H.T., and Boucrot, E. (2011). Molecular mechanism and physiological functions of clathrin-mediated endocytosis. *Nat. Rev. Mol. Cell Biol.* *12*, 517–533.

McNamara, C.W., Lee, M.C.S., Lim, C.S., Lim, S.H., Roland, J., Nagle, A., Simon, O., Yeung, B.K.S., Chatterjee, A.K., McCormack, S.L., et al. (2013). Targeting Plasmodium PI(4)K to eliminate malaria. *Nature* *504*, 248–253.

Mears, J.A., Lackner, L.L., Fang, S., Ingeman, E., Nunnari, J., and Hinshaw, J.E. (2011). Conformational changes in Dnm1 support a contractile mechanism for mitochondrial fission. *Nat. Struct. Mol. Biol.* *18*, 20–26.

Mejia, E.M., and Hatch, G.M. (2016). Mitochondrial phospholipids: role in mitochondrial function. *J. Bioenerg. Biomembr.* *48*, 99–112.

Michalak, M., Corbett, E.F., Mesaeli, N., Nakamura, K., and Opas, M. (1999). Calreticulin: one protein, one gene, many functions. *Biochem. J.* *344 Pt 2*, 281–292.

Miyazaki, I., and Asanuma, M. (2008). Dopaminergic neuron-specific oxidative stress caused by dopamine itself. *Acta Med. Okayama* *62*.

Mizuno, Y., Hattori, N., Kubo, S. -i., Sato, S., Nishioka, K., Hatano, T., Tomiyama, H., Funayama, M., Machida, Y., and Mochizuki, H. (2008). Progress in the pathogenesis and genetics of Parkinson's disease. *Philos. Trans. R. Soc. B Biol. Sci.* *363*, 2215–2227.

Morais, V.A., Verstreken, P., Roethig, A., Smet, J., Snellinx, A., Vanbrabant, M., Haddad, D., Frezza, C., Mandemakers, W., Vogt-Weisenhorn, D., et al. (2009). Parkinson's disease mutations in PINK1 result in decreased Complex I activity and deficient synaptic function. *EMBO Mol. Med.* *1*, 99–111.

Mouton-Liger, F., Jacoupy, M., Corvol, J.-C., and Corti, O. (2017). PINK1/Parkin-Dependent Mitochondrial Surveillance: From Pleiotropy to Parkinson's Disease.

Front. Mol. Neurosci. 10, 120.

Mozdy, A.D., McCaffery, J.M., and Shaw, J.M. (2000). Dnm1p GTPase-mediated mitochondrial fission is a multi-step process requiring the novel integral membrane component Fis1p. *J. Cell Biol.* 151, 367–379.

Muñoz, J.P., Ivanova, S., Sánchez-Wandelmer, J., Martínez-Cristóbal, P., Noguera, E., Sancho, A., Díaz-Ramos, A., Hernández-Alvarez, M.I., Sebastián, D., Mauvezin, C., et al. (2014). Erratum: Mfn2 modulates the UPR and mitochondrial function via repression of PERK (*EMBO Journal* 32 (2348-2361) DOI 10.1038/emboj.2013.168). *EMBO J.* 33, 171.

Murakawa, T., Yamaguchi, O., Hashimoto, A., Hikoso, S., Takeda, T., Oka, T., Yasui, H., Ueda, H., Akazawa, Y., Nakayama, H., et al. (2015). Bcl-2-like protein 13 is a mammalian Atg32 homologue that mediates mitophagy and mitochondrial fragmentation. *Nat. Commun.* 6, 7527.

Murley, A., Lackner, L.L., Osman, C., West, M., Voeltz, G.K., Walter, P., and Nunnari, J. (2013). ER-associated mitochondrial division links the distribution of mitochondria and mitochondrial DNA in yeast. *Elife* 2013.

Murphy, M.P. (2009). How mitochondria produce reactive oxygen species. *Biochem. J.* 417, 1–13.

Myhill, N., Lynes, E.M., Nanji, J.A., Blagoveshchenskaya, A.D., Fei, H., Simmen, K.C., Cooper, T.J., Thomas, G., and Simmen, T. (2008). The Subcellular Distribution of Calnexin Is Mediated by PACS-2. *Mol. Biol. Cell* 19, 2777–2788.

Nakagawa, C., Nishimura, S., Senda-Murata, K., and Sugimoto, K. (2012). A rapid and simple method of evaluating the dimeric tendency of fluorescent proteins in living cells using a truncated protein of importin α as fusion tag. *Biosci. Biotechnol. Biochem.* 76, 388–390.

Nalls, M.A., Pankratz, N., Lill, C.M., Do, C.B., Hernandez, D.G., Saad, M., DeStefano, A.L., Kara, E., Bras, J., Sharma, M., et al. (2014). Large-scale meta-analysis of genome-wide association data identifies six new risk loci for Parkinson's disease. *Nat. Genet.* 46, 989–993.

Narendra, D., Tanaka, A., Suen, D.-F., and Youle, R.J. (2008a). Parkin is recruited selectively to impaired mitochondria and promotes their autophagy. *J. Cell Biol.* 183, 795–803.

Narendra, D., Tanaka, A., Suen, D.-F., and Youle, R.J. (2008b). Parkin is recruited selectively to impaired mitochondria and promotes their autophagy. *J. Cell Biol.* 183, 795–803.

Narendra, D.P., Jin, S.M., Tanaka, A., Suen, D.F., Gautier, C.A., Shen, J., Cookson, M.R., and Youle, R.J. (2010a). PINK1 is selectively stabilized on impaired

mitochondria to activate Parkin. *PLoS Biol.* 8.

Narendra, D.P., Kane, L.A., Hauser, D.N., Fearnley, I.M., and Youle, R.J. (2010b). p62/SQSTM1 is required for Parkin-induced mitochondrial clustering but not mitophagy; VDAC1 is dispensable for both. *Autophagy* 6, 1090–1106.

Nemoto, Y., and De Camilli, P. (1999a). Recruitment of an alternatively spliced form of synaptojanin 2 to mitochondria by the interaction with the PDZ domain of a mitochondrial outer membrane protein. *EMBO J.* 18, 2991–3006.

Nemoto, Y., and De Camilli, P. (1999b). Recruitment of an alternatively spliced form of synaptojanin 2 to mitochondria by the interaction with the PDZ domain of a mitochondrial outer membrane protein. *EMBO J.* 18, 2991–3006.

Neuspiel, M., Schauss, A.C., Braschi, E., Zunino, R., Rippstein, P., Rachubinski, R. a, Andrade-Navarro, M. a, and McBride, H.M. (2008). Cargo-selected transport from the mitochondria to peroxisomes is mediated by vesicular carriers. *Curr. Biol.* 18, 102–108.

Ng, M.M., Dippold, H.C., Buschman, M.D., Noakes, C.J., and Field, S.J. (2013). GOLPH3L antagonizes GOLPH3 to determine Golgi morphology. *Mol. Biol. Cell* 24, 796–808.

Okatsu, K., Oka, T., Iguchi, M., Imamura, K., Kosako, H., Tani, N., Kimura, M., Go, E., Koyano, F., Funayama, M., et al. (2012). PINK1 autophosphorylation upon membrane potential dissipation is essential for Parkin recruitment to damaged mitochondria. *Nat. Commun.* 3, 1016.

Olanow, C.W., Perl, D.P., DeMartino, G.N., and McNaught, K.S.P. (2004). Lewy-body formation is an aggresome-related process: A hypothesis. *Lancet Neurol.* 3, 496–503.

Olgiate, S., De Rosa, A., Quadri, M., Criscuolo, C., Breedveld, G.J., Picillo, M., Pappatà, S., Quarantelli, M., Barone, P., De Michele, G., et al. (2014). PARK20 caused by SYNJ1 homozygous Arg258Gln mutation in a new Italian family. *Neurogenetics* 15, 183–188.

Ordureau, A., Sarraf, S.A., Duda, D.M., Heo, J.M., Jedrychowski, M.P., Sviderskiy, V.O., Olszewski, J.L., Koerber, J.T., Xie, T., Beausoleil, S.A., et al. (2014). Quantitative proteomics reveal a feedforward mechanism for mitochondrial PARKIN translocation and ubiquitin chain synthesis. *Mol. Cell* 56, 360–375.

Ota, T., Suzuki, Y., Nishikawa, T., Otsuki, T., Sugiyama, T., Irie, R., Wakamatsu, A., Hayashi, K., Sato, H., Nagai, K., et al. (2004). Complete sequencing and characterization of 21,243 full-length human cDNAs. *Nat Genet* 36, 40–45.

Otera, H., Wang, C., Cleland, M.M., Setoguchi, K., Yokota, S., Youle, R.J., and Mihara, K. (2010). Mff is an essential factor for mitochondrial recruitment of Drp1

during mitochondrial fission in mammalian cells. *J. Cell Biol.* 191, 1141–1158.

Otera, H., Ishihara, N., and Mihara, K. (2013). New insights into the function and regulation of mitochondrial fission. *Biochim. Biophys. Acta - Mol. Cell Res.* 1833, 1256–1268.

Paillusson, S., Gomez-Suaga, P., Stoica, R., Little, D., Gissen, P., Devine, M.J., Noble, W., Hanger, D.P., and Miller, C.C.J. (2017). α -Synuclein binds to the ER-mitochondria tethering protein VAPB to disrupt Ca^{2+} homeostasis and mitochondrial ATP production. *Acta Neuropathol.* 134, 129–149.

Paisan-Ruiz, C., Bhatia, K.P., Li, A., Hernandez, D., Davis, M., Wood, N.W., Hardy, J., Houlden, H., Singleton, A., and Schneider, S.A. (2009). Characterization of PLA2G6 as a locus for dystonia-parkinsonism. *Ann. Neurol.* 65, 19–23.

Paisán-Ruiz, C., Jain, S., Evans, E.W., Gilks, W.P., Simón, J., Van Der Brug, M., De Munain, A.L., Aparicio, S., Gil, A.M., Khan, N., et al. (2004). Cloning of the gene containing mutations that cause PARK8-linked Parkinson's disease. *Neuron* 44, 595–600.

Pandey, J.P. (2010). Genomewide association studies and assessment of risk of disease. *N. Engl. J. Med.* 363, 2076–2077; author reply 2077.

Pankratz, N., Nichols, W.C., Uniacke, S.K., Halter, C., Rudolph, A., Shults, C., Conneally, P.M., Foroud, T., and Parkinson Study Group (2003a). Significant linkage of Parkinson disease to chromosome 2q36-37. *Am. J. Hum. Genet.* 72, 1053–1057.

Pankratz, N., Nichols, W.C., Uniacke, S.K., Halter, C., Murrell, J., Rudolph, A., Shults, C.W., Conneally, P.M., Foroud, T., Truong, D., et al. (2003b). Genome-wide linkage analysis and evidence of gene-by-gene interactions in a sample of 362 multiplex Parkinson disease families. *Hum. Mol. Genet.* 12, 2599–2608.

Pankratz, N., Wilk, J.B., Latourelle, J.C., DeStefano, A.L., Halter, C., Pugh, E.W., Doheny, K.F., Gusella, J.F., Nichols, W.C., Foroud, T., et al. (2009). Genomewide association study for susceptibility genes contributing to familial Parkinson disease. *Hum. Genet.* 124, 593–605.

Papapetropoulos, S. (2010). Multicenter Analysis of Glucocerebrosidase Mutations in Parkinson's Disease. *Yearb. Neurol. Neurosurg.* 2010, 104–105.

Park, J., Lee, S.B., Lee, S., Kim, Y., Song, S., Kim, S., Bae, E., Kim, J., Shong, M., Kim, J.-M., et al. (2006). Mitochondrial dysfunction in *Drosophila* PINK1 mutants is complemented by parkin. *Nature* 441, 1157–1161.

Perera, R.M., Zoncu, R., Lucast, L., De Camilli, P., and Toomre, D. (2006). Two synaptojanin 1 isoforms are recruited to clathrin-coated pits at different stages. *Proc. Natl. Acad. Sci. U. S. A.* 103, 19332–19337.

Perfeito, R., Cunha-Oliveira, T., and Rego, A.C. (2012). Revisiting oxidative stress and mitochondrial dysfunction in the pathogenesis of Parkinson disease--resemblance to the effect of amphetamine drugs of abuse. *Free Radic. Biol. Med.* *53*, 1791–1806.

Pesah, Y., Pham, T., Burgess, H., Middlebrooks, B., Verstreken, P., Zhou, Y., Harding, M., Bellen, H., and Mardon, G. (2004). *Drosophila parkin* mutants have decreased mass and cell size and increased sensitivity to oxygen radical stress. *Development* *131*, 2183–2194.

Petko, J. a, Kabani, N., Frey, C., Woll, M., Hickey, K., Craig, M., Canfield, V. a, and Levenson, R. (2009). Proteomic and functional analysis of NCS-1 binding proteins reveals novel signaling pathways required for inner ear development in zebrafish. *BMC Neurosci.* *10*, 27.

Picillo, M., Ranieri, A., Orefice, G., Bonifati, V., and Barone, P. (2014). Clinical progression of SYNJ1-related early onset atypical parkinsonism: 3-year follow up of the original Italian family. *J. Neurol.* *261*, 823–824.

Pogson, J.H., Ivatt, R.M., Sanchez-Martinez, A., Tufi, R., Wilson, E., Mortiboys, H., and Whitworth, A.J. (2014). The Complex I Subunit NDUFA10 Selectively Rescues *Drosophila pink1* Mutants through a Mechanism Independent of Mitophagy. *PLoS Genet.* *10*.

Polevoy, G., Wei, H.-C., Wong, R., Szentpetery, Z., Kim, Y.J., Goldbach, P., Steinbach, S.K., Balla, T., and Brill, J. a (2009). Dual roles for the *Drosophila* PI 4-kinase four wheel drive in localizing Rab11 during cytokinesis. *J. Cell Biol.* *187*, 847–858.

Polymeropoulos, M.H., Lavedan, C., Leroy, E., Ide, S.E., Dehejia, A., Dutra, A., Pike, B., Root, H., Rubenstein, J., Boyer, R., et al. (1997). Mutation in the α -synuclein gene identified in families with Parkinson's disease. *Science* (80-). *276*, 2045–2047.

Pridgeon, J.W., Olzmann, J.A., Chin, L.S., and Li, L. (2007). PINK1 protects against oxidative stress by phosphorylating mitochondrial chaperone TRAP1. *PLoS Biol.* *5*, 1494–1503.

Proukakis, C., Dudzik, C.G., Brier, T., MacKay, D.S., Cooper, J.M., Millhauser, G.L., Houlden, H., and Schapira, A.H. (2013). A novel α -synuclein missense mutation in Parkinson disease. *Neurology* *80*, 1062–1064.

Quadri, M., Fang, M., Picillo, M., Olgiati, S., Breedveld, G.J., Graafland, J., Wu, B., Quarantelli, M., Annesi, G., Quattrone, A., et al. (2013a). Mutation in the SYNJ1 Gene Associated with Autosomal.

Quadri, M., Fang, M., Picillo, M., Olgiati, S., Breedveld, G.J., Graafland, J., Wu, B.,

Xu, F., Erro, R., Amboni, M., et al. (2013b). Mutation in the SYNJ1 gene associated with autosomal recessive, early-onset Parkinsonism. *Hum. Mutat.* 34, 1208–1215.

Quadri, M., Fang, M., Picillo, M., Olgiati, S., Breedveld, G.J., Graafland, J., Wu, B., Xu, F., Erro, R., Amboni, M., et al. (2013c). Mutation in the SYNJ1 gene associated with autosomal recessive, early-onset parkinsonism. *Hum. Mutat.* 34, 1208–1215.

Rakovic, A., Grünewald, A., Seibler, P., Ramirez, A., Kock, N., Orolicki, S., Lohmann, K., and Klein, C. (2010). Effect of endogenous mutant and wild-type PINK1 on Parkin in fibroblasts from Parkinson disease patients. *Hum. Mol. Genet.* 19, 3124–3137.

Rakovic, A., Grünewald, A., Voges, L., Hofmann, S., Orolicki, S., Lohmann, K., and Klein, C. (2011). PINK1-Interacting Proteins: Proteomic Analysis of Overexpressed PINK1. *Parkinsons. Dis.* 2011, 1–9.

Ramachandran, R., and Schmid, S.L. (2008). Real-time detection reveals that effectors couple dynamin's GTP-dependent conformational changes to the membrane. *EMBO J.* 27, 27–37.

Ramirez, A., Heimbach, A., Gründemann, J., Stiller, B., Hampshire, D., Cid, L.P., Goebel, I., Mubaidin, A.F., Wriekat, A.-L., Roeper, J., et al. (2006). Hereditary parkinsonism with dementia is caused by mutations in ATP13A2, encoding a lysosomal type 5 P-type ATPase. *Nat. Genet.* 38, 1184–1191.

Ramjaun, A.R., and McPherson, P.S. (1996). Tissue-specific alternative splicing generates two synaptojanin isoforms with differential membrane binding properties. *J. Biol. Chem.* 271, 24856–24861.

Rapizzi, E., Pinton, P., Szabadkai, G., Wieckowski, M.R., Vandecasteele, G., Baird, G., Tuft, R.A., Fogarty, K.E., and Rizzuto, R. (2002). Recombinant expression of the voltage-dependent anion channel enhances the transfer of Ca²⁺ microdomains to mitochondria. *J. Cell Biol.* 159, 613–624.

Rascol, O., Brooks, D.J., and Korczyn, A.D. (2000a). A five-year study of the incidence of dyskinesia in patients with early Parkinson's disease who were treated with ropinirole or levodopa. ... *Engl. J.*

Rascol, O., Brooks, D.J., and Korczyn, A.D. (2000b). A five-year study of the incidence of dyskinesia in patients with early Parkinson's disease who were treated with ropinirole or levodopa. ... *Engl. J.*

Rego, E.H., Shao, L., Macklin, J.J., Winoto, L., Johansson, G.A., Kamps-Hughes, N., Davidson, M.W., and Gustafsson, M.G.L. (2012). Nonlinear structured-illumination microscopy with a photoswitchable protein reveals cellular structures at 50-nm resolution. *Proc. Natl. Acad. Sci.* 109, E135–E143.

Rizzuto, R., Simpson, A.W.M., Brini, M., and Pozzan, T. (1992). Rapid changes of

mitochondrial Ca²⁺ revealed by specifically targeted recombinant aequorin. *Nature* 358, 325–327.

Roberts, R.F., Tang, M.Y., Fon, E.A., and Durcan, T.M. (2016). Defending the mitochondria: The pathways of mitophagy and mitochondrial-derived vesicles. *Int. J. Biochem. Cell Biol.* 79, 427–436.

Robida, A.M., and Kerppola, T.K. (2009). Bimolecular Fluorescence Complementation Analysis of Inducible Protein Interactions: Effects of Factors Affecting Protein Folding on Fluorescent Protein Fragment Association. *J. Mol. Biol.* 394, 391–409.

Rohé, C.F., Montagna, P., Breedveld, G., Cortelli, P., Oostra, B.A., and Bonifati, V. (2004). Homozygous PINK1 C-terminus mutation causing early-onset parkinsonism. *Ann. Neurol.* 56, 427–431.

Rosivatz, E., and Woscholski, R. (2011). Removal or masking of phosphatidylinositol(4,5)bisphosphate from the outer mitochondrial membrane causes mitochondrial fragmentation. *Cell. Signal.* 23, 478–486.

Rosignol, R., Gilkerson, R., Aggeler, R., Yamagata, K., Remington, S.J., and Capaldi, R.A. (2004). Energy Substrate Modulates Mitochondrial Structure and Oxidative Capacity in Cancer Cells. *Cancer Res.* 64, 985–993.

Rowland, A. a., and Voeltz, G.K. (2012). Endoplasmic reticulum–mitochondria contacts: function of the junction. *Nat. Rev. Mol. Cell Biol.* 13, 607–625.

Rusk, N., Le, P.U., Mariggio, S., Guay, G., Lurisci, C., Nabi, I.R., Corda, D., and Symons, M. (2003). Synaptojanin 2 functions at an early step of clathrin-mediated endocytosis. *Curr. Biol.* 13, 659–663.

Sano, R., Annunziata, I., Patterson, A., Moshich, S., Gomero, E., Opferman, J., Forte, M., and d’Azzo, A. (2009). GM1-Ganglioside Accumulation at the Mitochondria-Associated ER Membranes Links ER Stress to Ca²⁺-Dependent Mitochondrial Apoptosis. *Mol. Cell* 36, 500–511.

Santiago-Tirado, F.H., Legesse-Miller, A., Schott, D., and Bretscher, A. (2011). PI4P and Rab Inputs Collaborate in Myosin-V-Dependent Transport of Secretory Compartments in Yeast. *Dev. Cell* 20, 47–59.

Sarraf, S. a, Raman, M., Guarani-Pereira, V., Sowa, M.E., Huttlin, E.L., Gygi, S.P., and Harper, J.W. (2013). Landscape of the PARKIN-dependent ubiquitylome in response to mitochondrial depolarization. *Nature* 496, 372–376.

Satake, W., Nakabayashi, Y., Mizuta, I., Hirota, Y., Ito, C., Kubo, M., Kawaguchi, T., Tsunoda, T., Watanabe, M., Takeda, A., et al. (2009). Genome-wide association study identifies common variants at four loci as genetic risk factors for Parkinson’s disease. *Nat. Genet.* 41, 1303–1307.

Scarlatti, F., Bauvy, C., Ventruti, A., Sala, G., Cluzeaud, F., Vandewalle, A., Ghidoni, R., and Codogno, P. (2004). Ceramide-mediated Macroautophagy Involves Inhibition of Protein Kinase B and Up-regulation of Beclin 1. *J. Biol. Chem.* 279, 18384–18391.

Schapira, A.H., Cooper, J.M., Dexter, D., Clark, J.B., Jenner, P., and Marsden, C.D. (1990). Mitochondrial complex I deficiency in Parkinson's disease. *J. Neurochem.* 54, 823–827.

Schröder, M., and Kaufman, R.J. (2005). THE MAMMALIAN UNFOLDED PROTEIN RESPONSE. *Annu. Rev. Biochem.* 74, 739–789.

Schwarten, M., Mohrler, J., Ma, P., Stoldt, M., Thielmann, Y., Stangler, T., Hersch, N., Hoffmann, B., Merkel, R., and Willbold, D. (2009). Nix directly binds to GABARAP: A possible crosstalk between apoptosis and autophagy. *Autophagy* 5, 690–698.

Sentelle, R.D., Senkal, C.E., Jiang, W., Ponnusamy, S., Lemasters, J.J., Szulc, Z.M., Bielawski, J., and Ogretmen, B. (2013). Ceramide Targets autophagosomes to mitochondria and induces lethal mitophagy. *Nat. Cell Biol.* 8, 831–838.

Shi, G., Lee, J.R., Grimes, D.A., Racacho, L., Ye, D., Yang, H., Ross, O.A., Farrer, M., McQuibban, G.A., and Bulman, D.E. (2011). Functional alteration of PARL contributes to mitochondrial dysregulation in Parkinson's disease. *Hum. Mol. Genet.* 20, 1966–1974.

Shiba-Fukushima, K., Imai, Y., Yoshida, S., Ishihama, Y., Kanao, T., Sato, S., and Hattori, N. (2012). PINK1-mediated phosphorylation of the Parkin ubiquitin-like domain primes mitochondrial translocation of Parkin and regulates mitophagy. *Sci. Rep.* 2, 1002.

Shrestha, D., Jenei, A., Nagy, P., Vereb, G., and Szöllösi, J. (2015). Understanding FRET as a research tool for cellular studies. *Int. J. Mol. Sci.* 16, 6718–6756.

Shroff, H., Galbraith, C.G., Galbraith, J.A., and Betzig, E. (2008). Live-cell photoactivated localization microscopy of nanoscale adhesion dynamics. *Nat. Methods* 5, 417–423.

Shukla, V., Mishra, S.K., and Pant, H.C. (2011). Oxidative stress in neurodegeneration. *Adv. Pharmacol. Sci.* 2011.

Shyu, Y.J., Liu, H., Deng, X., and Hu, C.D. (2006). Identification of new fluorescent protein fragments for bimolecular fluorescence complementation analysis under physiological conditions. *Biotechniques* 40, 61–66.

Da Silva, F.L., Coelho Cerqueira, E., De Freitas, M.S., Gonçalves, D.L., Costa, L.T., and Follmer, C. (2013). Vitamins K interact with N-terminus α -synuclein and modulate the protein fibrillization in vitro. Exploring the interaction between

quinones and α -synuclein. *Neurochem. Int.* 62, 103–112.

Silvestri, L., Caputo, V., Bellacchio, E., Atorino, L., Dallapiccola, B., Valente, E.M., and Casari, G. (2005). Mitochondrial import and enzymatic activity of PINK1 mutants associated to recessive parkinsonism. *Hum. Mol. Genet.* 14, 3477–3492.

Sim, C.H., Lio, D.S.S., Mok, S.S., Masters, C.L., Hill, A.F., Culvenor, J.G., and Cheng, H.C. (2006). C-terminal truncation and Parkinson's disease-associated mutations down-regulate the protein serine/threonine kinase activity of PTEN-induced kinase-1. *Hum. Mol. Genet.* 15, 3251–3262.

Simmen, T., Aslan, J.E., Blagoveshchenskaya, A.D., Thomas, L., Wan, L., Xiang, Y., Feliciangeli, S.F., Hung, C.-H., Crump, C.M., and Thomas, G. (2005). PACS-2 controls endoplasmic reticulum-mitochondria communication and Bid-mediated apoptosis. *EMBO J.* 24, 717–729.

Sims, K., Haynes, C.A., Kelly, S., Allegood, J.C., Wang, E., Momin, A., Leipelt, M., Reichart, D., Glass, C.K., Cameron Sullards, M., et al. (2010). Kdo2-lipid A, a TLR4-specific agonist, induces de Novo sphingolipid biosynthesis in RAW264.7 macrophages, which is essential for induction of autophagy. *J. Biol. Chem.* 285, 38568–38579.

Singleton, B., Farrer, M., Johnson, J., Singleton, A., Hague, S., Kachergus, J., Hulihan, M., Peuralinna, T., Dutra, A., Nussbaum, R., et al. (2003). α -Synuclein locus triplication causes Parkinson's disease. *Science* 302, 841.

Smith, Y., Wichmann, T., Factor, S.A., and DeLong, M.R. (2012a). Parkinson's Disease Therapeutics: New Developments and Challenges Since the Introduction of Levodopa. *Neuropsychopharmacology* 37, 213–246.

Smith, Y., Wichmann, T., Factor, S.A., and DeLong, M.R. (2012b). Parkinson's Disease Therapeutics: New Developments and Challenges Since the Introduction of Levodopa. *Neuropsychopharmacology* 37, 213–246.

Snyder, C.M., Mardones, G.A., Ladinsky, M.S., and Howell, K.E. (2006). GMx33 associates with the trans-Golgi matrix in a dynamic manner and sorts within tubules exiting the Golgi. *Mol. Biol. Cell* 17, 511–524.

Soman, S., Keatinge, M., Moein, M., Da Costa, M., Mortiboys, H., Skupin, A., Sugunan, S., Bazala, M., Kuznicki, J., and Bandmann, O. (2017). Inhibition of the mitochondrial calcium uniporter rescues dopaminergic neurons in pink1^{-/-} zebrafish. *Eur. J. Neurosci.* 45, 528–535.

Song, W., and Zinsmaier, K.E. (2003). Endophilin and synaptojanin hook up to promote synaptic vesicle endocytosis. *Neuron* 40, 665–667.

Soubannier, V., McLelland, G.-L., Zunino, R., Braschi, E., Rippstein, P., Fon, E. a, and McBride, H.M. (2012). A vesicular transport pathway shuttles cargo from

mitochondria to lysosomes. *Curr. Biol.* 22, 135–141.

De Stefani, D., Raffaello, A., Teardo, E., Szabò, I., and Rizzuto, R. (2011). A forty-kilodalton protein of the inner membrane is the mitochondrial calcium uniporter. *Nature* 476, 336–340.

Stefanis, L. (2012). α -Synuclein in Parkinson's disease. *Cold Spring Harb. Perspect. Med.* 2, 1–23.

Stoica, R., De Vos, K.J., Paillusson, S., Mueller, S., Sancho, R.M., Lau, K.-F., Vizcay-Barrena, G., Lin, W.-L., Xu, Y.-F., Lewis, J., et al. (2014). ER–mitochondria associations are regulated by the VAPB–PTPIP51 interaction and are disrupted by ALS/FTD-associated TDP-43. *Nat. Commun.* 5.

Stoica, R., Paillusson, S., Gomez-suaga, P., Mitchell, J.C., Lau, D.H.W., Gray, E.H., Sancho, R.M., Vizcay-barrena, G., Vos, K.J. De, Shaw, C.E., et al. (2016). ALS / FTD-associated FUS activates GSK-3 β to disrupt the VAPB – PTPIP 51 interaction and ER – mitochondria associations. *EMBO Rep* 17, 1–17.

Stokes, C.E., and Hawthorne, J.N. (1987). Reduced Phosphoinositide Concentrations in Anterior Temporal Cortex of Alzheimer-Diseased Brains. *J. Neurochem.* 48, 1018–1021.

Strack, S., and Cribbs, J.T. (2012). Allosteric modulation of Drp1 mechanoenzyme assembly and mitochondrial fission by the variable domain. *J. Biol. Chem.* 287, 10990–11001.

Strahl, T., Grafelmann, B., Dannenberg, J., Thorner, J., and Pongs, O. (2003). Conservation of regulatory function in calcium-binding proteins: human frequenin (neuronal calcium sensor-1) associates productively with yeast phosphatidylinositol 4-kinase isoform, Pik1. *J. Biol. Chem.* 278, 49589–49599.

Strappazzon, F., Nazio, F., Corrado, M., Cianfanelli, V., Romagnoli, A., Fimia, G.M., Campello, S., Nardacci, R., Piacentini, M., Campanella, M., et al. (2015). AMBRA1 is able to induce mitophagy via LC3 binding, regardless of PARKIN and p62/SQSTM1. *Cell Death Differ.* 22, 419–432.

Strauss, K.M., Martins, L.M., Plun-Favreau, H., Marx, F.P., Kautzmann, S., Berg, D., Gasser, T., Wszolek, Z., Müller, T., Bornemann, A., et al. (2005). Loss of function mutations in the gene encoding Omi/HtrA2 in Parkinson's disease. *Hum. Mol. Genet.* 14, 2099–2111.

Sugiura, A., McLelland, G.-L., Fon, E. a, and McBride, H.M. (2014). A new pathway for mitochondrial quality control: mitochondrial-derived vesicles. *EMBO J.* 33, 1–15.

Sulzer, D., and Zecca, L. (2000). Intra-neuronal Dopamine-Quinone Synthesis: A Review. *Neurotox. Res.* 1, 181–195.

Surmeier, D.J., Guzman, J.N., and Sanchez-Padilla, J. (2010). Calcium, cellular

aging, and selective neuronal vulnerability in Parkinson's disease. *Cell Calcium* 47, 175–182.

Szabadkai, G., Bianchi, K., Várnai, P., De Stefani, D., Wieckowski, M.R., Cavagna, D., Nagy, A.I., Balla, T., and Rizzuto, R. (2006). Chaperone-mediated coupling of endoplasmic reticulum and mitochondrial Ca²⁺ channels. *J. Cell Biol.* 175, 901–911.

Tabara, L.C., and Escalante, R. (2016). VMP1 establishes ER-microdomains that regulate membrane contact sites and autophagy. *PLoS One* 11.

Tabrizi, S.J., Orth, M., Wilkinson, J.M., Taanman, J.W., Warner, T.T., Cooper, J.M., and Schapira, A.H. (2000). Expression of mutant alpha-synuclein causes increased susceptibility to dopamine toxicity. *Hum. Mol. Genet.* 9, 2683–2689.

Taghavi, S., Chaouni, R., Tafakhori, A., Azcona, L.J., Firouzabadi, S.G., Omrani, M.D., Jamshidi, J., Emamalizadeh, B., Shahidi, G.A., Ahmadi, M., et al. (2017). A Clinical and Molecular Genetic Study of 50 Families with Autosomal Recessive Parkinsonism Revealed Known and Novel Gene Mutations. *Mol. Neurobiol.* 1–13.

Tan, J., and Brill, J.A. (2014). Cinderella story: PI4P goes from precursor to key signaling molecule. *Crit. Rev. Biochem. Mol. Biol.* 49, 33–58.

Tanaka, A., Cleland, M.M., Xu, S., Narendra, D.P., Suen, D.-F., Karbowski, M., and Youle, R.J. (2010). Proteasome and p97 mediate mitophagy and degradation of mitofusins induced by Parkin. *J. Cell Biol.* 191, 1367–1380.

Tanner, C.M., Kame, F., Ross, G.W., Hoppin, J.A., Goldman, S.M., Korell, M., Marras, C., Bhudhikanok, G.S., Kasten, M., Chade, A.R., et al. (2011). Rotenone, paraquat, and Parkinson's disease. *Environ. Health Perspect.* 119, 866–872.

Tieu, Q., Okreglak, V., Naylor, K., and Nunnari, J. (2002). The WD repeat protein, Mdv1p, functions as a molecular adaptor by interacting with Dnm1p and Fis1p during mitochondrial fission. *J. Cell Biol.* 158, 445–452.

Trempe, J.-F., Chen, C.X.-Q., Grenier, K., Camacho, E.M., Kozlov, G., McPherson, P.S., Gehring, K., and Fon, E. a (2009a). SH3 domains from a subset of BAR proteins define a Ubl-binding domain and implicate parkin in synaptic ubiquitination. *Mol. Cell* 36, 1034–1047.

Trempe, J.F., Chen, C.X.Q., Grenier, K., Camacho, E.M., Kozlov, G., McPherson, P.S., Gehring, K., and Fon, E.A. (2009b). SH3 Domains from a Subset of BAR Proteins Define a Ubl-Binding Domain and Implicate Parkin in Synaptic Ubiquitination. *Mol. Cell* 36, 1034–1047.

Trinh, R., Gurbaxani, B., Morrison, S.L., and Seyfzadeh, M. (2004). Optimization of codon pair use within the (GGGGS)???3 linker sequence results in enhanced protein expression. *Mol. Immunol.* 40, 717–722.

Twig, G., Elorza, A., Molina, A.J., Mohamed, H., Wikstrom, J.D., and Walzer, G. (2008). Fission and selective fusion govern mitochondrial segregation and elimination by autophagy. *Embo J* 27.

Valente, E.M. (2004). Hereditary Early-Onset Parkinson's Disease Caused by Mutations in PINK1. *Science* (80-). 304, 1158–1160.

Valente, E.M., Abou-Sleiman, P.M., Caputo, V., Muqit, M.M.K., Harvey, K., Gispert, S., Ali, Z., Del Turco, D., Bentivoglio, A.R., Healy, D.G., et al. (2004). Hereditary early-onset Parkinson's disease caused by mutations in PINK1. *Science* 304, 1158–1160.

Verfaillie, T., Rubio, N., Garg, A.D., Bultynck, G., Rizzuto, R., Decuypere, J.-P., Piette, J., Linehan, C., Gupta, S., Samali, A., et al. (2012). PERK is required at the ER-mitochondrial contact sites to convey apoptosis after ROS-based ER stress. *Cell Death Differ.* 19, 1880–1891.

Verstreken, P., Koh, T.-W., Schulze, K.L., Zhai, R.G., Hiesinger, P.R., Zhou, Y., Mehta, S.Q., Cao, Y., Roos, J., and Bellen, H.J. (2003). Synaptojanin is recruited by endophilin to promote synaptic vesicle uncoating. *Neuron* 40, 733–748.

Vicinanza, M., Di Campli, A., Polishchuk, E., Santoro, M., Di Tullio, G., Godi, A., Levchenko, E., De Leo, M.G., Polishchuk, R., Sandoval, L., et al. (2011). OCRL controls trafficking through early endosomes via PtdIns4,5P₂-dependent regulation of endosomal actin. *EMBO J.* 30, 4970–4985.

Vilariño-Güell, C., Rajput, A., Milnerwood, A.J., Shah, B., Szu-Tu, C., Trinh, J., Yu, I., Encarnacion, M., Munsie, L.N., Tapia, L., et al. (2014). DNAJC13 mutations in Parkinson disease. *Hum. Mol. Genet.* 23, 1794–1801.

Vincow, E.S., Merrihew, G., Thomas, R.E., Shulman, N.J., Beyer, R.P., MacCoss, M.J., and Pallanck, L.J. (2013). The PINK1-Parkin pathway promotes both mitophagy and selective respiratory chain turnover in vivo. *Proc. Natl. Acad. Sci.* 110, 6400–6405.

De vos, K.J., Mórotz, G.M., Stoica, R., Tudor, E.L., Lau, K.F., Ackerley, S., Warley, A., Shaw, C.E., and Miller, C.C.J. (2012). VAPB interacts with the mitochondrial protein PTPIP51 to regulate calcium homeostasis. *Hum. Mol. Genet.* 21, 1299–1311.

De Vos, K.J., and Sheetz, M.P. (2007). Visualization and Quantification of Mitochondrial Dynamics in Living Animal Cells. *Methods Cell Biol.* 80, 627–682.

Wakabayashi, K., Tanji, K., Mori, F., and Takahashi, H. (2007a). The Lewy body in Parkinson's disease: Molecules implicated in the formation and degradation of ??-synuclein aggregates. In *Neuropathology*, pp. 494–506.

Wakabayashi, K., Tanji, K., Mori, F., and Takahashi, H. (2007b). The Lewy body in

Parkinson's disease: Molecules implicated in the formation and degradation of α -synuclein aggregates. In *Neuropathology*, pp. 494–506.

Wakabayashi, K., Tanji, K., Odagiri, S., Miki, Y., Mori, F., and Takahashi, H. (2013). The Lewy Body in Parkinson's Disease and Related Neurodegenerative Disorders. *Mol. Neurobiol.* *47*, 495–508.

Wang, J., Sun, H.-Q., Macia, E., Kirchhausen, T., Watson, H., Bonifacino, J.S., and Yin, H.L. (2007). PI4P promotes the recruitment of the GGA adaptor proteins to the trans-Golgi network and regulates their recognition of the ubiquitin sorting signal. *Mol. Biol. Cell* *18*, 2646–2655.

Wang, X., Winter, D., Ashrafi, G., Schlehe, J., Wong, Y.L., Selkoe, D., Rice, S., Steen, J., Lavoie, M.J., and Schwarz, T.L. (2011). PINK1 and Parkin target miro for phosphorylation and degradation to arrest mitochondrial motility. *Cell* *147*, 893–906.

Waterham, H.R., Koster, J., van Roermund, C.W.T., Mooyer, P.A.W., Wanders, R.J.A., Leonard, J. V, Roermund, C.W.T. Van, Mooyer, P.A.W., Wanders, R.J.A., and Leonard, J. V (2007). A Lethal Defect of Mitochondrial and Peroxisomal Fission. *N. Engl. J. Med.* *356*, 1736–1741.

Watt, S.A., Kular, G., Fleming, I.N., Downes, C.P., and Lucocq, J.M. (2002). Subcellular localization of phosphatidylinositol 4,5-bisphosphate using the pleckstrin homology domain of phospholipase C delta1. *Biochem. J.* *363*, 657–666.

Webster, C.P., Smith, E.F., Shaw, P.J., and De Vos, K.J. (2017). Protein Homeostasis in Amyotrophic Lateral Sclerosis: Therapeutic Opportunities? *Front. Mol. Neurosci.* *10*, 123.

Wei, Y.J., Sun, H.Q., Yamamoto, M., Wlodarski, P., Kunii, K., Martinez, M., Barylko, B., Albanesi, J.P., and Yin, H.L. (2002). Type II phosphatidylinositol 4-kinase β is a cytosolic and peripheral membrane protein that is recruited to the plasma membrane and activated by Rac-GTP. *J. Biol. Chem.* *277*, 46586–46593.

Whitworth, A.J., Lee, J.R., Ho, V.M.-W., Flick, R., Chowdhury, R., and McQuibban, G.A. (2008). Rhomboid-7 and HtrA2/Omi act in a common pathway with the Parkinson's disease factors Pink1 and Parkin. *Dis. Model. Mech.* *1*, 168–174.

Winner, B., Jappelli, R., Maji, S.K., Desplats, P.A., Boyer, L., Aigner, S., Hetzer, C., Loher, T., Vilar, M., Campioni, S., et al. (2011). In vivo demonstration that α -synuclein oligomers are toxic. *Proc. Natl. Acad. Sci.* *108*, 4194–4199.

Wong, K. a, and O'Bryan, J.P. (2011). Bimolecular fluorescence complementation. *J. Vis. Exp.* 1–13.

Wong, Y.C., and Holzbaur, E.L.F. (2014). Optineurin is an autophagy receptor for damaged mitochondria in parkin-mediated mitophagy that is disrupted by an ALS-linked mutation. *Proc. Natl. Acad. Sci. U. S. A.* *111*, E4439-48.

Wu, C.C., Taylor, R.S., Lane, D.R., Ladinsky, M.S., Weisz, J. a, and Howell, K.E. (2000). GMx33: a novel family of trans-Golgi proteins identified by proteomics. *Traffic* 1, 963–975.

Wu, W., Tian, W., Hu, Z., Chen, G., Huang, L., Li, W., Zhang, X., Xue, P., Zhou, C., Liu, L., et al. (2014). ULK1 translocates to mitochondria and phosphorylates FUNDC1 to regulate mitophagy. *EMBO Rep.* 15, 566–575.

Xu, J., Kao, S.-Y., Lee, F.J.S., Song, W., Jin, L.-W., and Yankner, B. a (2002). Dopamine-dependent neurotoxicity of alpha-synuclein: a mechanism for selective neurodegeneration in Parkinson disease. *Nat. Med.* 8, 600–606.

Yamanaka, M., Smith, N.I., and Fujita, K. (2014). Introduction to super-resolution microscopy. *Microscopy* 63, 177–192.

Yang, Y., Gehrke, S., Imai, Y., Huang, Z., Ouyang, Y., Wang, J.-W., Yang, L., Beal, M.F., Vogel, H., and Lu, B. (2006). Mitochondrial pathology and muscle and dopaminergic neuron degeneration caused by inactivation of *Drosophila* Pink1 is rescued by Parkin. *Proc. Natl. Acad. Sci. U. S. A.* 103, 10793–10798.

Yim, Y.-I., Sun, T., Wu, L.-G., Raimondi, A., De Camilli, P., Eisenberg, E., and Greene, L.E. (2010). Endocytosis and clathrin-uncoating defects at synapses of auxilin knockout mice. *Proc. Natl. Acad. Sci. U. S. A.* 107, 4412–4417.

Zabetian, C.P., Yamamoto, M., Lopez, A.N., Ujike, H., Mata, I.F., Izumi, Y., Kaji, R., Maruyama, H., Morino, H., Oda, M., et al. (2009). LRRK2 mutations and risk variants in Japanese patients with Parkinson’s disease. *Mov. Disord.* 24, 1034–1041.

Zarranz, J.J., Alegre, J., Gómez-Esteban, J.C., Lezcano, E., Ros, R., Ampuero, I., Vidal, L., Hoenicka, J., Rodriguez, O., Atarés, B., et al. (2004). The new mutation, E46K, of alpha-synuclein causes Parkinson and Lewy body dementia. *Ann. Neurol.* 55, 164–173.

Zhang, H., Bosch-Marce, M., Shimoda, L.A., Yee, S.T., Jin, H.B., Wesley, J.B., Gonzalez, F.J., and Semenza, G.L. (2008). Mitochondrial autophagy is an HIF-1-dependent adaptive metabolic response to hypoxia. *J. Biol. Chem.* 283, 10892–10903.

Zhang, W., Colavita, A., and Ngsee, J.K. (2017). Mitigating Motor Neuronal Loss in *C. elegans* Model of ALS8. *Sci. Rep.* 7, 11582.

Zheng, X., and Hunter, T. (2013). Parkin mitochondrial translocation is achieved through a novel catalytic activity coupled mechanism. *Cell Res.* 23, 886–897.

Zhou, Z.D., Refai, F.S., Xie, S.P., Ng, S.H., Chan, C.H.S., Ho, P.G.H., Zhang, X.D., Lim, T.M., and Tan, E.K. (2014). Mutant PINK1 upregulates tyrosine hydroxylase and dopamine levels, leading to vulnerability of dopaminergic neurons. *Free Radic.*

Biol. Med. 68, 220–233.

Zimprich, A., Biskup, S., Leitner, P., Lichtner, P., Farrer, M., Lincoln, S., Kachergus, J., Hulihan, M., Uitti, R.J., Calne, D.B., et al. (2004). Mutations in LRRK2 cause autosomal-dominant parkinsonism with pleomorphic pathology. *Neuron* 44, 601–607.

Ziviani, E., Tao, R.N., and Whitworth, A.J. (2010). *Drosophila* parkin requires PINK1 for mitochondrial translocation and ubiquitinates mitofusin. *Proc. Natl. Acad. Sci. U. S. A.* 107, 5018–5023.

Zubenko, G.S., Stiffler, J.S., Hughes, H.B., and Martinez, A.J. (1999). Reductions in brain phosphatidylinositol kinase activities in Alzheimer's disease. *Biol. Psychiatry* 45, 731–736.

Züchner, S., Mersiyanova, I. V, Muglia, M., Bissar-Tadmouri, N., Rochelle, J., Dadali, E.L., Zappia, M., Nelis, E., Patitucci, A., Senderek, J., et al. (2004). Mutations in the mitochondrial GTPase mitofusin 2 cause Charcot-Marie-Tooth neuropathy type 2A. *Nat. Genet.* 36, 449–451.